

The background of the slide is a composite of fluorescence microscopy images of Arabidopsis root meristems. The top-left and bottom-right images show a root tip with a grid of cells, where some cells are brightly fluorescent in blue and others in red. The top-right and bottom-left images show a root tip with a grid of cells, where some cells are brightly fluorescent in red and others in blue. The central part of the slide is a dark field with a grid of cells, where some cells are brightly fluorescent in green and others in blue. The text is overlaid on this central image.

Control of cell cycle progression and cell
size in the *Arabidopsis* root meristem

Zaki Ahmad

Royal Holloway,
University of London

Control of cell cycle progression and cell size in the *Arabidopsis* root meristem

Zaki Ahmad




Royal Holloway, University of London

This thesis is submitted for the degree of Doctor of Philosophy

August 2020

Declaration of authorship

I, Zaki Ahmad, hereby declare that this thesis titled “control of cell cycle progression and cell size in the *Arabidopsis* root meristem” and the work presented in it is entirely my own. Where I have consulted the work of others, this is always clearly stated. Original material used in the creation of this thesis has not been previously submitted either in part or whole for a degree of any description from any institution.

Author's signature: 

Date: 28 August 2020

Acknowledgments

I thank Laszlo Bogre for the supervision throughout the course of the PhD and for teaching me not just how to, but also how *not* to do research and science. Thank you for always being so supportive especially during the blues and getting me involved in so many different projects which will hopefully bear fruition in the near future! Thank you so much for giving me the freedom to pursue my own ideas and also being so generous in shaping and developing my own thought process.

I thank other members of my supervisory board for very useful discussions and advice, namely Sena Giovanni (Imperial College London), Gerrit Beemster (University of Antwerp, Belgium) and Enrique Lopez-Juez (RHUL) – Enrique, I will miss the many corridor conversations we have had over the years and I definitely learned something new after each one.

Many thanks to Csaba Papdi (RHUL) for immense technical help, especially during the early days. I am very thankful of Pavla Binarova (Institute of Microbiology of the Czech Academy of Sciences, Czech Republic) and members of her lab, Gabriela Kocarova and Hana Kourova for teaching me the labelling techniques that were essential for the PhD project. Special thanks to Imma Perez-Salamo (RHUL) and Naresh Loudya (RHUL) for their support and many discussions as well as making my time at RHUL fun.

Lots of thanks to Zoltan Magyar (Biological Research Centre, Szeged, Hungary), Masaki Ito (Kanazawa University, Ishikawa, Japan), Alessandra Devoto (RHUL) and Beatrix Horvath (RHUL) for always helping me whenever I needed it, and always promptly replying to my numerous emails. My gratitude further extends to the technical, maintenance, and administrative staff at the Department of Biological Sciences.

To my parents and siblings – thank you so much for all the love, care, and support.

I thank my examiners Walter Dewitte (Cardiff University) and Alessandra Devoto for the invaluable advice and constructive criticism in shaping the current version of the thesis. Lastly, I am ever so grateful to be a recipient of the BBSRC-DTP studentship, without which my PhD would have just been an unfulfilled dream!

Dedicated to K.M. the Fifth

Abstract

Above- and below-ground plant organ growth depends on the cell proliferation-driven shoot and root meristem activities, respectively. Here, I quantitatively characterised cell cycle and cell size dynamics of *Arabidopsis* root meristem using cell cycle phase-specific tools: EdU labelling for S phase and *pCYCB1;1:CYCB1;1-dbGFP* as a mitotic marker under a confocal laser-scanning microscope. Exogenous sucrose transfer experiments under two light intensities and day-night cycles revealed a rapid rheostatic-like adjustment of cell cycle and cell size to different growth conditions.

On possible molecular mechanisms connecting cell cycle to sugar availability, I found that chemical inhibition of nutrient-sensing TARGET OF RAPAMYCIN (TOR) signalling pathway through AZD-8055 suppresses progression through the cell cycle. Importantly, TOR activity is required for passage through both G1-to-S phase and G2-to-M phase transition points, the former involves TOR-mediated phosphorylation of RETINOBLASTOMA-RELATED (RBR) and CYCLIN D2 protein level.

To gain deeper understanding of root meristem control beyond TOR signalling, I studied two well-known protein families involved in cell cycle regulation: the MAPKs and TCPs. Based on EdU time-course experiments in a line that expresses *MKK7*, a MAP kinase kinase, under the control of a β -estradiol-inducible promoter system, I demonstrated that elevated level of *MKK7* inhibits cell cycle in the root meristem. A similar estradiol-inducible system was used to study the effect of *TCP14* overexpression on root growth. Increased *TCP14* level results in accumulation of meristematic-like cells well beyond the meristem region and is accompanied with diminished amount of actively-proliferating cells as measured by EdU labelling. This

suggests that TCP14 might be involved in coordinating cell proliferation with cell elongation during root growth and development

A model is proposed to explain how TOR-, MKK7-, and TCP14- containing protein complexes may act in cooperative and independent ways to regulate cell cycle and cell size in time (i.e. during day and night) and space (root meristem-to-elongation boundary).

Contents

Declaration of authorship	2
Acknowledgments	3
Abstract	6
Contents	8
List of figures.....	12
List of tables	15
List of abbreviations	16
Chapter 1 General introduction: cellular and molecular control of plant organ growth	20
1.1 The cellular basis of plant growth.....	22
1.2 A journey through the plant cell division cycle.....	25
1.2.1 G1-to-S phase transition	27
1.2.2 G2-to-M phase transition	29
1.3 Cell cycle control by inhibitors of CDK activity	31
1.4 Control of cell cycle genes at the transcriptional and translational level	33
1.5 Involvement of MAPKs and TCPs in cell cycle regulation	36
1.6 Nutrient-control of cell cycle by the TOR signalling pathway.....	38
1.7 Size control of cycling cells	41
1.8 <i>Arabidopsis</i> root meristem as a model system to study cell cycle and cell size	45

1.9 Hypotheses, aims and objectives of the thesis	48
Chapter 2 Materials and methods	52
2.1 Plant growth half-strength MS media preparation	53
2.2 <i>Arabidopsis</i> seed surface sterilisation.....	53
2.3 Plant material and growth conditions.....	54
2.4 <i>Arabidopsis</i> primary root growth assay	55
2.5 Standard AZD-8055 experimental set-up	55
2.6 EdU labelling of <i>Arabidopsis</i> root meristem	56
2.7 Confocal laser scanning microscopy	58
2.8 Confocal data processing	59
2.9 Western blotting	59
2.9.1 Protein extraction, quantification, and separation	59
2.9.2 Protein transfer, immunoblotting, and detection.....	60
2.10 Statistical analysis.....	62
Chapter 3 Distinct diel protein accumulation of E2FA and E2FB may differentially control the cell cycle.....	64
3.1 Introduction	66
3.1.1 Aims and objectives	68
3.2 Results.....	69
3.2.1 Cell cycle in the meristem underpins root growth adjustment to the light and sugar availability.	69
3.2.2 Growth conditions dependence of root meristematic cell size.....	73
3.2.3 Cell cycle and cell size in the root meristem changes on an hourly basis	78

3.2.4 Diel pattern of E2FA and E2FB protein accumulation may create temporal changes in S phase	84
3.3 Discussion	87
Chapter 4 TARGET OF RAPAMYCIN signalling pathway regulates sugar-induced progression through the cell cycle.....	92
4.1 Introduction	94
4.1.1 Aims and objectives.....	96
4.2 Results.....	97
4.2.1 Sugar/light-induced increase in mitotic count requires TOR signalling pathway	97
4.2.2 AZD treatment reduces root growth rate, meristem size, cell number and size, but increases cell cycle duration.....	102
4.2.3 Exogenous sucrose suppresses end-of-the-day decline in S phase count in a TOR-dependent manner.....	107
4.2.4 AZD treatment rapidly alters ratio of early/mid-to-late S phase and reduces spatial synchrony of cell cycle	111
4.2.5 CYCD2 protein accumulates diurnally and is sensitive to TOR inhibition	114
4.2.6 TOR regulates G1/S entry through mediating phosphorylation of RBR.	117
4.2.7 Inhibition of TOR activity reduces G2/M cells and meristem size within hours.....	120
4.2.8 Evolution of cell size during TOR inhibition and exogenous sucrose supply	123

4.3 Discussion	125
Chapter 5 MKK7, a MAP kinase kinase, is a negative regulator of the cell cycle	131
5.1 Introduction	133
5.1.1 Aims and objectives	134
5.2 Results.....	135
5.2.1 Overexpression of <i>MKK7</i> dramatically inhibits primary root growth...	135
5.2.2 <i>MKK7</i> overexpression reduces root meristem size and number of cells, but increases meristematic cell size	136
5.2.3 Overexpression of <i>MKK7</i> reduces number of S phase cells in the root meristem.....	138
5.3 Discussion	142
Chapter 6 TCP14 coordinates cell proliferation with cell elongation	144
6.1 Introduction	146
6.1.1 Aims and objectives	147
6.2 Results.....	148
6.2.1 TCP14 is a negative regulator of primary root growth	148
6.2.2 Temporal changes in S phase count upon <i>TCP14</i> overexpression	151
6.2.3 <i>TCP14</i> overexpression increases nuclei count in the transition-to- elongation zone.....	154
6.3 Discussion	156
Chapter 7 General discussion, conclusions, and future perspectives	159
Appendices.....	168
List of references	171

List of figures

Figure 1.1 Cellular basis of plant organ growth.....	23
Figure 1.2 Basics of cell cycle progression and control.....	26
Figure 1.3 TOR signalling and plant growth control.	40
Figure 1.4 Existing models of cell size control.	44
Figure 1.5 <i>Arabidopsis</i> root meristem as a model system.....	46
Figure 1.6 Tools to study cell cycle in the <i>Arabidopsis</i> root meristem.....	47
Figure 2.1 Structural organisation of E2FA and E2FB proteins with position of T- DNA insertion sites	55
Figure 2.2 Step-by-step protocol of EdU labelling of <i>Arabidopsis</i> root tip.....	58
Figure 3.1 Light and sugar set the primary root growth rate.....	71
Figure 3.2 Cell cycle in the root meristem is largely defined by light and sugar availability.....	75
Figure 3.3 Effect of growth conditions on cell size.	77
Figure 3.4 Effect of light-dark cycles on cell cycle in the root meristem.	80
Figure 3.5 Diel changes in G2/M cell size.....	81
Figure 3.6 Diel changes in number of DNA replicating cells in the root meristem.	83
Figure 3.7 Differential accumulation of E2FA and E2FB proteins.	84
Figure 3.8 S phase count in <i>e2fa</i> and <i>e2fb</i> mutants.	86
Figure 3.9 Schematic summary of diel dynamics of cell cycle and E2F protein accumulation.	89
Figure 4.1 Inhibition of TOR suppresses sugar-dependent increase in mitotic activity.....	99

Figure 4.2 AZD treatment blocks light- and sugar-induced cell cycle progression and meristem growth.	101
Figure 4.3 TOR inhibition lowers primary root growth rate.....	103
Figure 4.4 Cellular characterisation of AZD-treated root meristem.	104
Figure 4.5 Inhibition of TOR increases cell cycle duration.	106
Figure 4.6 Sucrose level define activity of TOR-S6K signalling.	108
Figure 4.7 TOR inhibition rapidly reduces number of S phase cells in the root meristem.....	110
Figure 4.8 Spatial and intra-S phase characterisation upon AZD treatment.	113
Figure 4.9 TOR activity drives sugar-dependent increase in CYCD2 protein accumulation.	115
Figure 4.10 AZD reduces CYCD2 protein at the whole-plant level.	117
Figure 4.11 Silencing of RBR reduces sensitivity to AZD.....	118
Figure 4.12 TOR signalling modulates phosphorylation of RBR.....	120
Figure 4.13 TOR inhibition rapidly reduces G2/M entry and meristem length. ...	122
Figure 4.14 Inhibition of TOR differentially affects interphase and G2/M cell size.	124
Figure 4.15 TOR signalling is required for both G1/S and G2/M transitions.....	127
Figure 5.1 Overexpression of <i>MKK7</i> causes a dramatic primary root growth reduction.....	137
Figure 5.2 <i>MKK7</i> overexpression shortens the meristem.....	139
Figure 5.3 Elevated level of MKK7 obscures meristem-to-elongation boundary ..	140
Figure 5.4 S phase count in response to <i>MKK7</i> overexpression.	141
Figure 6.1 Increased primary root growth of <i>tcp14</i> mutant.....	149
Figure 6.2 Cellular phenotypes of <i>tcp14-7 mutant</i> root tip.....	150

Figure 6.3 Overexpression of <i>TCP14</i> causes a dramatic primary root growth reduction.....	151
Figure 6.4 Temporal dynamics of S phase and meristem size in response to <i>TCP14</i> overexpression.....	153
Figure 6.5 Continued overexpression of <i>TCP14</i> delays cell elongation.	155
Figure 7.1 A proposed model of daily control of cell cycle and endocycle.	163
Figure 7.2 A proposed model of cell cycle control by TCP transcription factors and TOR signalling pathway.	166

List of tables

Table 2.1 List of <i>Arabidopsis</i> lines used in the thesis	54
Table 2.2 List of antibodies and their dilutions used in this thesis.....	61
Table 3.1 Averages of cellular parameters measured in light-dark experiments. ..	82
Table 4.1 Average S phase count in AZD experiment in each growth condition...	111
Table 4.2 Average CYCD2 fluorescent intensity in AZD experiment in each growth condition	116

List of abbreviations

%	percent
°C	degree Celsius
µg	microgram
µl	microlitre
µm	micrometre
µM	micromolar
At	<i>Arabidopsis thaliana</i>
au	arbitrary unit
AZD	AZD8055
CDC	cell division cycle
CDK	cyclin-dependent kinase
CKI	CDK inhibitor
Col-0	Columbia-0
CTRL	control
CYC	cyclin
DAPI	4',6-diamidino-2-phenylindole
DAS	day after stratification
DAT	day after transfer
DNA	deoxyribonucleic acid
DP	dimerisation partner
DTT	dithiothreitol
E2F	E2 promoter binding factor
EBP1	erbB3-binding protein 1
EDTA	ethylenediaminetetraacetic acid

EdU	ethynyl deoxyuridine
EMS	ethyl methanesulfonate
EtOH	ethanol
g	gram
G phase	gap phase
GFP	green fluorescent protein
h	hour
kDa	kilodalton
KOH	potassium hydroxide
KRP	kip-related protein
l	litre
LL	low light
M	molar
M phase	mitosis
MAPK	mitogen-activated protein kinase
MCM	minichromosome maintenance
min	minute
MKK	MAP kinase kinase
ml	millilitre
mm	millimetre
mRNA	messenger RNA
MS	Murashige-Skoog
MTSB	microtubule-stabilising buffer
MW	molecular weight
MYB3R	R1R2R3-Myb
n	number of technical replicates

N	number of biological replicates
ns	(statistically) insignificant difference
OIB	Olympus image binary
ORC	origin recognition complex
PBS	phosphate-buffered saline
PCNA	proliferating cell nuclear antigen
PIC	protease inhibitor cocktail
PMSF	phenylmethanesulfonyl fluoride
pNPP	p-nitrophenyl phosphate
QC	quiescent centre
RAM	root apical meristem
RBR	retinoblastoma-related protein
RFP	red fluorescent protein
RNA	ribonucleic acid
RNAi	RNA interference
ROP2	rho-related protein 2
RPS6	ribosomal protein S6
RT	room temperature
S phase	synthesis (DNA) phase
S6K	S6 kinase
SAM	shoot apical meristem
SDS	sodium dodecyl sulfate
SL	standard light
SMR	siamese-related protein
TBS	tris-buffered saline
TBS-T	TBT with Tween-20

TCP	TEOSINTE BRANCHED 1, CYCLOIDEA, PCF1
T-DNA	transfer DNA
TEMED	tetramethyl ethylenediamine
TIFF	tagged image file format
TOR	target of rapamycin
TORC1	TOR complex 1
V	volt
v/v	volume/volume
w/v	weight/volume
WT	wild-type
YFP	yellow fluorescent protein
ZT	zeitgeber

1

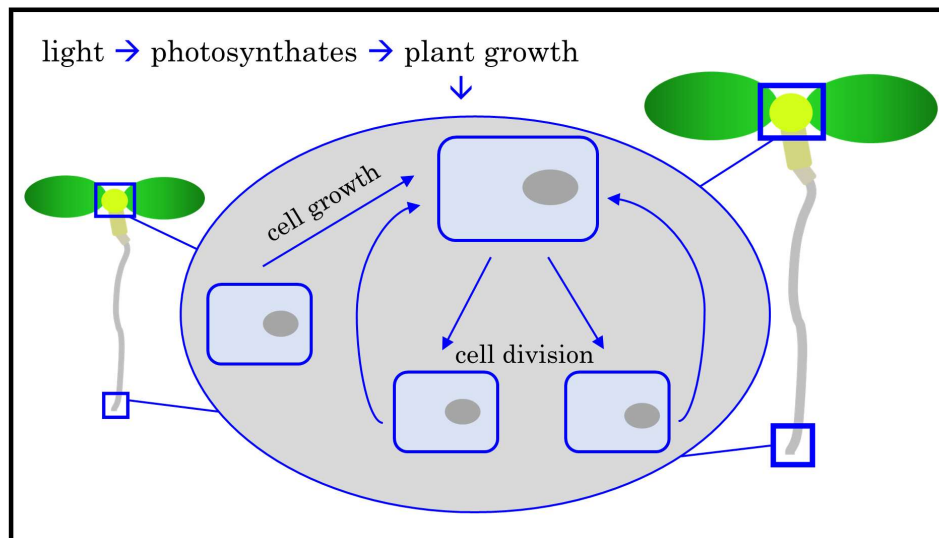
Chapter 1 General introduction: cellular and molecular control of plant organ growth

Declaration – some of the ideas presented in this chapter appear in:

Ahmad Z, Magyar Z, Bogre L, Papdi C (2019) Cell cycle control by the target of rapamycin signalling pathway in plants. *J Exp Bot.* 70: 2275-2284b

General introduction: cellular and molecular control of plant organ growth

In this introductory chapter, I summarise key concepts that define plant organ growth and its relationship with the environment.



Cellular processes driving plant organ growth

In a nutshell

- The bipolar nature of plant growth relies on cell growth- and cell cycle-driven activity within the shoot and root meristems, and is limited by environmental conditions
- Progression through the cell division cycle requires continuous supply of nutrients, and is dependent on nutrient-sensing signalling pathways
- Cell cycle control occurs at the transcriptional, translational, and post-translational levels, and requires coordinative actions between positive and negative regulators
- How different growth conditions (i.e. light and sugar availability) affect cell cycle and cell size is not fully understood
- Due to its cellular organisation, the *Arabidopsis* root meristem is an excellent model system to study cell cycle and cell size control in a multicellular context

What determines organ growth? How does the internal and external environment affect growth? How do individual cells decide when to divide? What intrinsic and extrinsic signals influence cell proliferation? What are the molecular mechanisms that connect a growth signal to the cell cycle machinery? These are some of most fundamental questions in cell and molecular biology that have been a research focus of numerous laboratories around the world for several decades. Through collective efforts, it is only in the recent years that the genetic and cellular control principles of organ growth is becoming better understood. In this introductory chapter, I will present some of the key ideas in relation to underlying cellular basis, signalling pathways, and environmental factors that define plant organ growth.

1.1 The cellular basis of plant growth

Cells make up the basic unit of all known biological life and thus, cellular dynamics define tissue and organ growth dynamics of multi-celled organisms. A cell itself is a makeup of macromolecules and organelles which all need to be duplicated when the cell divides into two daughter cells. At the whole-plant level, tissue or organ growth is as a result of 1) increase in cell number through cell division cycle, 2) cytoplasmic-driven growth of proliferating cells mainly through protein synthesis, and 3) cell wall turgor pressure-driven cell expansion/elongation (Doerner, 2008; Henriques *et al.*, 2014; Barrada *et al.*, 2015; Salvi *et al.*, 2020) as visualised in Figure 1.1. These cellular processes that define final organ size have environmental, developmental, and genetic constraints with specific gene regulatory network at play (Vercruysse *et al.*, 2020). For instance, early post-embryonic root growth (3-7DAS) follows a linear-like increase in number of dividing cells in the meristem that plateaus as root

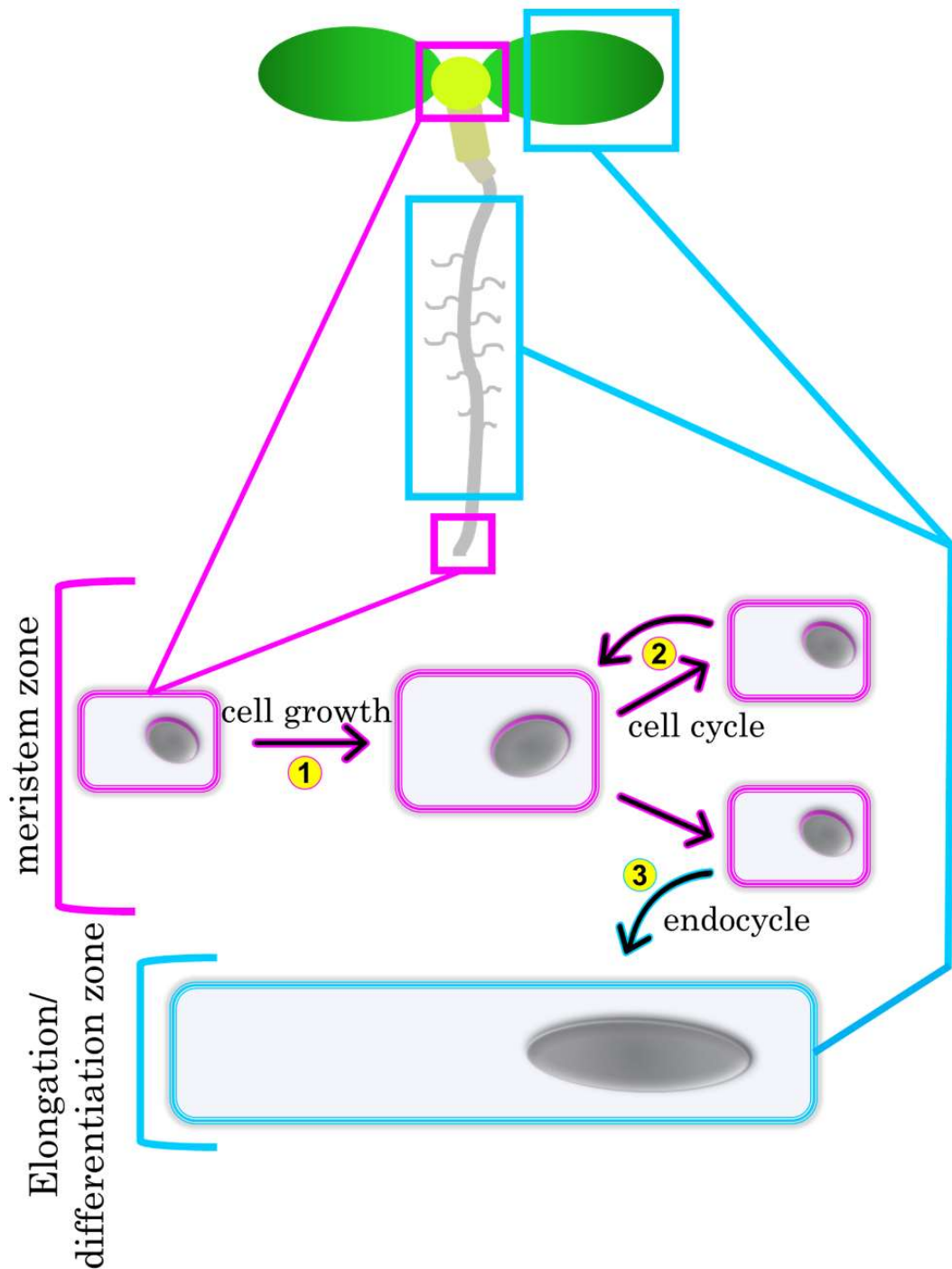


Figure 1.1 Cellular basis of plant organ growth.

Above-ground and below-ground tissue growth is driven by protein synthesis driven-cell growth (1) coupled with cell cycle progression (2) in the meristem. As cells exit the meristem, they start to expand through turgor-driven cell wall extension that is often coupled with increase in ploidy through the endocycle (3), an alternative form of cell cycle with repeated S phase rounds without mitosis. Together, cell proliferation in the meristem and cell expansion in the elongation and differentiation zones underlie plant growth dynamics (Barrada *et al.*, 2015).

progresses through the developmental stages (Dello Ioio *et al.*, 2007). Environmental cues such as light and sugar promote cell cycle in the shoot and root meristems (Li *et al.*, 2017) whilst mild drought, an unfavourable growth condition, rapidly limits cell cycle in young *Arabidopsis* leaves (Dubois *et al.*, 2018).

Post-embryonic plant growth and development can be divided into two major phases: the proliferation phase and expansion phase (Donnelly *et al.*, 1999; Johnson and Lenhard, 2011; Gonzalez *et al.*, 2012). Cell proliferation precedes cell expansion in young organs that is, there is a rapid production of cells in specialised tissues called the meristem which is followed by significant enlargement of cells exiting the mitotic cycle and is associated with increase in DNA ploidy level through endocycle, a modified form of cell cycle in which cells undergo repeated rounds of DNA replication without mitosis/cytokinesis (Beemster *et al.*, 2005; Inzé and De Veylder, 2006; Breuer *et al.*, 2010) as shown in Figure 1.1. In short, cell proliferation provides the material for growth with post-mitotic expansion leading to dramatic enlargement in final organ size. Compensatory mechanisms are activated in response to environmental and/or genetic perturbations of cell cycle to ensure the final organ size remains close to the 'normal' state (Horiguchi and Tsukaya, 2011).

In the next few sections, I will describe the series of events defining cell cycle progression, the underlying molecular control system and the accompanying checkpoints. Proliferating cells are controlled at the transcriptional, translational, and post-translational levels, and I will present recent advances in this field. Besides the intrinsic control system, cell cycle is governed by environmental cues such as light and nutrient availability, both of these growth signals will be discussed. Cells maintain a cell-type specific size upon each round of division implying the existence of an active size-sensing mechanism, I will introduce key ideas and models which explain how cells might sense and maintain their size during cell cycle progression

and upon division. The work introduced here will mostly be from the plant model organism *Arabidopsis thaliana* literature, but wherever necessary research in non-photosynthetic organisms will also be highlighted to reinforce points under discussion or present historical context.

1.2 A journey through the plant cell division cycle

Cell division is a universal feature (Nurse, 1990) of the tree of life, thus in this context cell reproduction ability was arguably one of the greatest evolutionarily milestone. Cell division or mitotic cycle is a series of four ordered events which starts with chromosomal DNA synthesis/replication phase termed S phase and equal segregation of duplicated chromosomes during mitosis or M phase (Norbury and Nurse, 1992). Gap phase 1 (G1) temporally separates S phase from previous M phase and G2 intercedes between S phase and mitosis (Figure 1.2). The unidirectional decision to progress through the cell cycle is determined during the gap phases and forms the basis of the control system (Norbury and Nurse, 1992; Dewitte and Murray, 2003). Thus, the regulatory cell cycle network termed ‘checkpoints’ acts on G1/S and G2/M transitions while the fidelity of chromosome segregation is controlled at the metaphase-to-anaphase checkpoint.

The core cell cycle machinery is centred around CYCLIN-DEPENDENT KINASES (CDK) and CYCLINS (CYC) which form phase-specific complexes that promote the progression from G1 through S phase and mitosis (Figure 1.2). Cyclins are named after their cyclic nature of phase-specific protein accumulation, first identified in sea urchin eggs (Evans *et al.*, 1983). Genome-wide analysis showed that the *Arabidopsis* genome contains over 60 cell cycle genes with 12 *CDK* genes, alphabetically

categorised into A through F; and 32 cyclin genes belonging to A-, B-, D-, and H-types (Vandepoele *et al.*, 2002). Work by Wang and colleagues (2004) identified an additional 18 *Arabidopsis* cyclins grouping them into C-, P-, L, and T-types (Wang *et al.*, 2004). Although the level of redundancy and precise function of each cyclin is far from understood, the high number of cyclins is thought to support the plasticity of post-embryonic development, and the ability of plants to respond adequately to diverse developmental and environmental signals (Inzé and De Veylder, 2006).

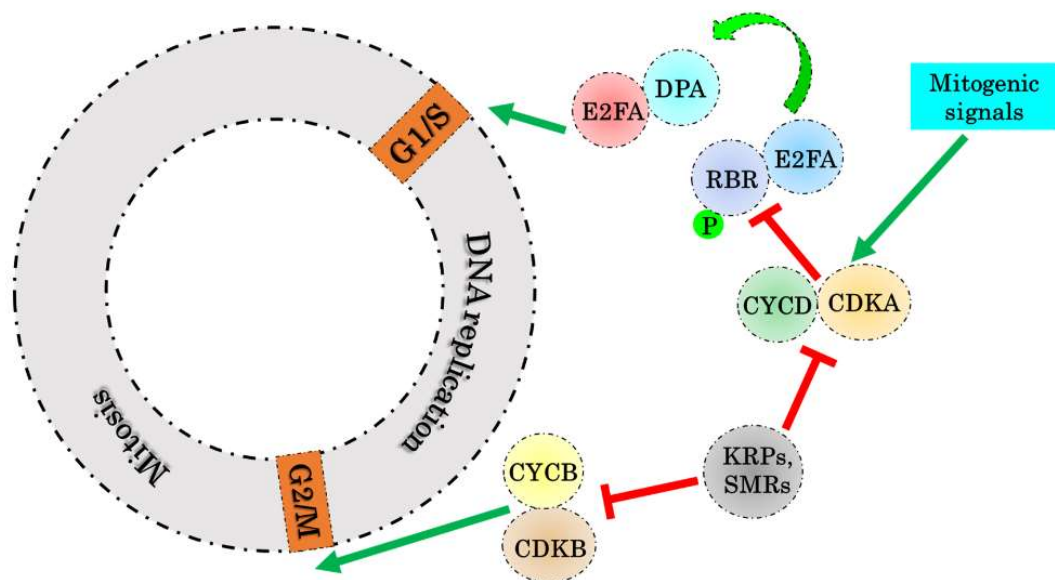


Figure 1.2 Basics of cell cycle progression and control.

The hallmark of G1/S entry to the cell cycle, in response to mitogenic signals such as sugar availability, is the CYCD-CDKA complex dependent phosphorylation of RBR protein which ‘releases’ E2FA transcription factor. Together with its dimerisation partner A (DPA), E2FA initiates transcription of genes required for DNA replication during S phase. Another important cell cycle transition occurs after the entire genome is duplicated, and the cells enter mitosis by passing through G2/M that require CYCB-CDKB complex. Upon environmental or developmental signal, CDK inhibitors such as KRPs and SMRs block CDK activity at G1/S and/or G2/M transition points. The scheme is adapted from Dewitte and Murray, 2003.

CDKs and cyclins form phase-specific functional complexes that drive progression through the cell cycle (Figure 1.2); in *Arabidopsis*, as many as 90 CDK-CYC complex variants were identified (Van Leene *et al.*, 2010). Among the most studied cyclins are types D, A, and B which, in simplistic view, are involved in G1-to-S transition, S-to-G2 progression, and G2-to-M transition, respectively (Menges *et al.*, 2005). In addition to CDKs and CYCs, E2 PROMOTER BINDING FACTOR (E2F) family of transcription factors together with their DIMERISATION PARTNER (DP) and RETINOBLASTOMA-RELATED (RBR) protein form an important regulatory node that is a conserved feature of mammalian and plant cell cycle (Dick and Rubin, 2013; Harashima *et al.*, 2013; Dick *et al.*, 2018).

1.2.1 G1-to-S phase transition

The ‘decision’ to enter the mitotic cycle is made during G1 phase and is influenced by growth signals, mainly sugar availability and hormones such as cytokinin and auxin (Riou-Khamlichi *et al.*, 1999; Gutierrez *et al.*, 2002; Perrot-Rechenmann, 2010). Of the 10 D-type cyclins, CYCD2;1, CYCD3;1, CYCD4;1 were shown to be sensitive to sucrose (Riou-Khamlichi *et al.*, 2000; Menges *et al.*, 2006; Nieuwland *et al.*, 2009). Interestingly, CYCD2 and CYCD3 were shown to rescue the cell cycle-arrested phenotype of *Saccharomyces cerevisiae* G1 cyclin mutant *cln1cln2* and contained the LxCxE RBR-interacting motif (Dahl *et al.*, 1995; Soni *et al.*, 1995), giving an early indication that the basal control mechanism is conserved across the eukaryotic kingdom. Healy and co-workers (2001) showed that CYCD2;1 and CYCD3;1 *in vivo* interacts and forms an active complex with the PSTAIRE-containing CDKA, but not with the plant-specific PPTALRE-containing CDKBs

(Healy *et al.*, 2001). Additionally, a CYCD2/CDKA complex was identified to phosphorylate RBR within the C-terminal domain during late G1 in highly proliferating tissues (Boniotto and Gutierrez, 2001). There is also genetic evidence that RBR is regulated by CDKA;1, Nowack and colleagues (2012) reported that the severely growth-defected *cdka;1* mutant could be partially rescued in *cdka;1 rbr1-2* double homozygous mutant (Nowack *et al.*, 2012).

In its unphosphorylated state, RBR acts as a transcriptional repressor of S phase genes, in part, by binding to and inhibiting E2F transcription factors. *Arabidopsis* has three typical E2Fs that were all shown to form a functional complex with RBR and require DPA or DPB proteins for DNA-binding functions; whereas E2FA and E2FB are considered to be cell cycle activators, E2FC is regarded as a repressor (Magyar *et al.*, 2016; Rossignol *et al.*, 2002). The categoric split of E2Fs is largely based on phenotypic analysis of transgenic lines, where *E2FA* overexpression results in enlarged cotyledon due to extra epidermal cell divisions (De Veylder *et al.*, 2002) as well as increased root meristem size (Magyar *et al.*, 2012). Overexpression of *E2FB* resulted smaller plant with increased cell number and was able to drive cell cycle in auxin-free conditions (Magyar *et al.*, 2005; Sozzani *et al.*, 2006). *E2FC* overexpressing plants showed enlarged epidermal cells of the cotyledons with reduced expression of *CELL DIVISION CYCLE 6 (CDC6)* S phase gene, suggesting E2FC limits cell proliferation further supported by elevated *CYCB1::CYCB1-GUS* activity in the RNAi-induced *E2FC* silencing line (Del Pozo *et al.*, 2002, 2006).

At the protein level, E2FA accumulates in proliferating cells and peaks during S phase whilst E2FB maintains a constant level throughout the cell cycle (Magyar *et al.*, 2005). In terms of cellular spatial distribution, *E2FA* is expressed predominantly in proliferating tissues such as the root meristem and the shoot apex with a weak detection in differentiating tissues whilst E2FB maintains a strong presence in fully

differentiated cells such pavement cells and stomatal guard cells and root columella cells (De Veylder *et al.*, 2002; Magyar *et al.*, 2012; Oszki *et al.*, 2020). The E2FB spatial pattern closely resembles that of RBR protein indicating a cooperative cell cycle repressive role (Oszki *et al.*, 2020) that will be discussed later.

Genome-wide microarray analysis of *E2FA-DPA* overexpression *Arabidopsis* line identified 181 putative target genes that are overwhelmingly expressed during G1 and S phase (Vandepoele *et al.*, 2005). DNA replication machinery is largely conserved between animals and plants (Shultz *et al.*, 2007) which involve proteins establishing multiple sites of replication origins, subsequent unwinding of DNA followed by DNA synthesis that is catalysed by DNA polymerases (Shultz *et al.*, 2007). Thus, the core DNA replication machinery include DNA polymerases, proliferating cell nuclear antigen (PCNA), DNA replication licensing factors, origin recognition complexes (ORCs), minichromosome maintenance proteins (MCMs), most of which were identified as E2FA targets (Vandepoele *et al.*, 2005).

1.2.2 G2-to-M phase transition

Sugar-induced increase in D-type cyclins which form a functional complex with CYCLIN-DEPENDENT KINASE A (CDKA) that phosphorylates RBR during G1 allowing transcriptional role of activator-type E2Fs. With correctly doubled chromosomes, proliferating cells are able to move onto to the next cell cycle stage. G2-to-M phase transition follows a similar mode to G1-to-S in that a CYC-CDK complex and activator E2F together with another family of transcription factor called MYB3Rs drive cells into mitosis; transition to both stages is dependent on cell size and level of CDK activity (Jones *et al.*, 2017). Plants have mitotic-specific PPTALRE-

or PPTTLRE-containing CYCLIN-DEPENDENT KINASE B (CDKBs), *Arabidopsis* contains at least four *CDKB* genes: *CDKB1;1*, *CDKB1;2*, *CDK2;1*, *CDKB2;2* (Vandepoele *et al.*, 2002). Transcript of *B1*-type *CDKs* accumulate during S-to-G2 whilst *B2*-type peaks at the G2/M transition (Menges *et al.*, 2005). Transcript and protein level of *CDKB1;1* are elevated in *E2FA* and *E2FB* overexpression lines, (Boudolf *et al.*, 2004; Magyar *et al.*, 2012; Oszl *et al.*, 2020), but overexpression of *E2FB* shows a stronger and developmentally prolonged *CDKB1;1* induction (Oszl *et al.*, 2020), suggesting that E2FB may have a superior role in *CDKB1* regulation.

Transcriptionally, *CYCA2;3* peaks at G2/M transition (Menges *et al.*, 2005) and was shown as the cyclin binding partner of *CDKB1;1* that negatively regulates endocycle transition (Boudolf *et al.*, 2009). *CDKB1;1* could partially rescue the root meristem developmental defects in the *cdka;1* mutant, suggesting CDKBs can compensate for the loss of CDKA (Nowack *et al.*, 2012). Furthermore, all four CDKBs were found in a complex with A- and/or B-type cyclins at the G2/M transition point (Van Leene *et al.*, 2010), the precise biological role of each *CDKB1/2-CYCA/B* function is far from understood – they are likely to have cell cycle independent roles. In this regard, *CDKB1;1-CYCB1;1* complex was shown to specifically phosphorylate RAD51, a well-known DNA repair protein, presumably preventing onset of mitosis and allowing time for DNA repair (Weimer *et al.*, 2016). Interestingly, *CDKB1;1*, but not *CDKA;1*, was reported to co-purify with RBR (Van Leene *et al.*, 2010), given that *CDKB1-CYCB1* complex was shown to recruit RBR to DNA damage sites (Biedermann *et al.*, 2017), the RBR-CDKB interaction is likely to be activated upon genome damage.

Whilst E2Fs mostly regulate genes for the G1-to-S phase transition with some exceptions like *CDKB1;1*, the family of transcription factors that specifically regulates G2/M genes is the R1R2R3-Myb or MYB3R proteins. *Arabidopsis* has five *MYB3R* genes, numerically named *MYB3R1* to *MYB3R5* that have overlapping

activating and repressive transcriptional functions that bind to mitosis-specific activator (MSA) elements in the promoters of G2/M genes (Kobayashi et al., 2015; Magyar et al., 2016). MYB3R1 and MYB3R4 are regarded as transcriptional activators of G2/M genes such as *CYCB1;2* and *KNOLLE (KN)*; correspondingly, mitotic genes are among the over-represented down-regulated genes in the *myb3r1myb3r4* double mutant (Haga et al., 2007, 2011). The cooperative transcriptional control of cell cycle by E2Fs and MYB3Rs will be discussed later. Whilst positive regulators drive cells through each phase of the cell cycle, the proper phase-specific execution also requires timely inhibition of CDK activity.

1.3 Cell cycle control by inhibitors of CDK activity

Cell cycle transitions including the mitotic cycle-to-endocycle switch are primarily driven by CYC-CDK activity and CDK itself is subjected to regulation by its inhibitors and activators. Plants have two distinct families of CDK inhibitors (CKIs): KIP-RELATED PROTEIN (KRPs) and SIAMESE (SIM)/SIAMESE-RELATED (SIM/SMR) proteins. *Arabidopsis* genome contains seven *KRP (1-7)* and 17 putative *SIM/SMR (SIM, SMR1-16)* genes (De Veylder et al., 2001; Vandepoele et al., 2002; Kumar et al., 2015), the unusually high number of CDK inhibitors is thought to fine-tune cell cycle to various environmental and developmental signals (Kumar and Larkin, 2017).

Transcriptionally, *KRP3*, *KRP4* and *KRP5* peak during S phase, *KRP1* peaks at the G2/M boundary and *KRP6* in G1/S; additionally, *KRP2* accumulates in sugar-starved cells (Menges et al., 2005). KRP2-7 could co-purify preferentially with CDKA;1-CYCD complex (Van Leene et al., 2010) and have been shown in vitro to inhibit the

kinase activity of CYCD2-CDKB and CYCD2/CDKA (Nakai *et al.*, 2006). *KRP1* is expressed mostly in non-dividing tissues and was demonstrated to interact with CDKA;1 and CYCD2;1 in planta and thus has a key role in G1/S regulation (Ren *et al.*, 2008). Strong over-expression of *KRP2* led to inhibition of CDK activity in both dividing and endocycling leaf tissues, but weak overexpression line only limits G2/M progression and allows S phase rounds leading to increase in ploidy (Verkest *et al.*, 2005).

KRP3 is expressed in meristematic tissues and its overexpression leads to low cell count but enhanced cell size which is followed by increased ploidy (Jun *et al.*, 2013). Similarly, *KRP5* is strongly expressed in the root meristem and mature stele tissue, the *krp5* mutant showed a slow growth rate which was explained by reduced rounds of endocycles and lowered cell elongation rate (Wen *et al.*, 2013). The quintuple mutant *krp1/2/3/4/7* has increased number of root meristematic cells and shows more phosphorylated form of RBR and higher expression of E2F target genes such as *MCMs* and *PCNA* (Cheng *et al.*, 2013, 2015). A similar conclusion was made in the triple *krp4/6/7* mutant that showed enhanced leaf growth with high cell count and ploidy level and increased expression of core DNA replication machinery (Sizani *et al.*, 2019). In short, studies on knock-out mutants and overexpression lines of different KRPs show that they predominantly have an inhibitory role on regulators of G1/S, such that there is an inverse relationship between KRP protein level and CDKA activity.

The plant-specific family of CKIs, the SIM/SMRs play key regulatory roles in adjusting CDK activity in response to environmental stress. SIM, SMR1, SMR2 were found to be associated with CDKB1;1 and SMR11 interacted with CYCB2;4 whilst SMR3, SMR4, SMR5, SMR6 and SMR8 co-purified with CDKA;1 and CYCDs (Van Leene *et al.*, 2010). SIM, SMR1 and SMR2 were proposed to work cooperatively to

inhibit G2/M progression and promote onset of endocycle during early leaf development (Kumar *et al.*, 2015). Of all KRPs and SMRs, *SMR1* and *SMR5* are transcriptionally induced in response to drought and SMR1 protein was shown to be a short-lived that is post-translationally stabilised under drought, presumably functioning to inhibit cell division via CDKA/B (Dubois *et al.*, 2018). SMR4, SMR5, and SMR7 were identified to be strongly induced by DNA damage in ATM and SOG1-dependent manner and was proposed to be an integral part of DNA damaged-induced checkpoint (Yi *et al.*, 2014).

In summary, KRPs and SMRs are overwhelmingly involved in proliferation-to-endocycle switch and play critical roles in blocking cell cycle progression under stress conditions.

1.4 Control of cell cycle genes at the transcriptional and translational level

Besides tuning of CDK activity by CKIs, core S phase and mitotic genes are controlled at the transcriptional level as evident from their peak expression level at specific points of the cell cycle (Menges *et al.*, 2005); indeed, there are two bursts of transcription during G1-to-S and G2-to-M transitions (Breyne *et al.*, 2002; Berckmans and De Veylder, 2009). In addition to transcriptional activation of cell cycle phase-specific genes, transcription of genes outside their phase need to be actively switched off as well as during cell cycle exit, quiescence and/or differentiation (Kobayashi, T. Suzuki, *et al.*, 2015; Magyar *et al.*, 2016). A landmark paper by Kobayashi, Suzuki and co-workers (2015) found that specific E2Fs and MYB3Rs together with RBR and other cell cycle proteins are components of a same

multi-protein complex called DREAM (dimerization partner, RB-like, E2F and multi-vulval class B) that is conserved in other eukaryotes such as worm, fly and human (Sadasivam and DeCaprio, 2013; Kobayashi, T. T. Suzuki, *et al.*, 2015; Fischer and Müller, 2017).

ChIP-seq analysis of MYB3R3-bound genes revealed not only G2/M-specific genes but surprisingly also E2F targets and further co-immunoprecipitation experiments found MYB3R3 in complex with RBR and E2FC, but not E2FB, during later stages of leaf development (Kobayashi, T. T. Suzuki, *et al.*, 2015). Furthermore, MYB3R4 was found in complex with RBR1 and E2FB but not E2FC during early leaf development. Additionally, CDKA;1 was found to be associated with MYB3R4 and MYB3R3 during early and late leaf development, respectively (Kobayashi, T. T. Suzuki, *et al.*, 2015). Components of the MuvB core were also identified as TCX5, ALY2, ALY3 among other proteins (Kobayashi, T. T. Suzuki, *et al.*, 2015). The E2FB-MYB3R4 association is described as an activator-type DREAM complex that promotes transcription of G2/M genes in proliferating cells whilst E2FC-MYB3R4 association forms the repressor-type DREAM complex that represses G2/M transcription both during interphase and in post-mitotic cells such as differentiated cells (Kobayashi, T. T. Suzuki, *et al.*, 2015; Magyar *et al.*, 2016).

Whilst DREAM complexes are involved in transcriptional regulation of cell cycle genes, translational regulation provides another layer of cell cycle control. Indeed, cell cycle genes are translationally repressed upon sucrose starvation in *Arabidopsis* cell culture (Nicolai *et al.*, 2006). Another study based on ribosome profiling in human cells arrested at G1/S and G2 phases highlighted an extensive translational control of numerous mRNAs that are periodically translated and formed functional clusters such as regulators of the mitotic spindle checkpoint (Stumpf *et al.*, 2013). Components of the translation machinery are also implicated in cell cycle control, for

instance eIF3h, which is part of the translation initiation complex. The *Arabidopsis eif3h* mutant showed enhanced expression of regulators of shoot development such as *WUSCHEL* and *CLAVATA3* in the apical shoot meristem, resulting in over-proliferation and enlarged meristem, suggesting that eif3h could provide a translational control in meristem maintenance (Zhou *et al.*, 2014).

Another candidate for regulating cell cycle at the translational level is ERBB3-BINDING PROTEIN 1 (EBP1) that is, in part, functionally conserved between mammals and plants and is involved in ribosome biogenesis (Stegmann, 2018; Lokdarshi *et al.*, 2020). In potato leaves, silencing of *EBP1* led to fewer epidermal cells whilst its overexpression resulted in higher cell count (Horváth *et al.*, 2006). It was further shown that EBP1 is required for the expression of cell cycle regulators such as RIBONUCLEOTIDE REDUCTASE 1 (*RNR1*), *CDKB1;1* and *CYCD3;1*, and negatively regulates the abundance of RBR protein (Horváth *et al.*, 2006). Consistent with its cell cycle role, EBP1 protein is mostly present in the meristem where it is predominantly localised in the cytoplasm with mild presence in the nucleolus (Lokdarshi *et al.*, 2020). Furthermore, *EBP1* promoter and protein was significantly reduced upon induced overexpression of *RBR*, and *EBP1* overexpression partially rescues severely shortened meristem phenotype of *RBR* overexpression line suggesting that EBP1 and RBR have counteracting cell cycle functions in the meristem (Lokdarshi *et al.*, 2020). However, given the timeframe during which EBP1 level is lowered upon *RBR* overexpression i.e. EBP1 reduction is only apparent at 2d after *RBR* overexpression (Lokdarshi *et al.*, 2020) when the meristem has almost disappeared, I think it is likely to be an indirect effect of RBR on EBP1.

In short, transcriptional control by DREAM complexes and possible translational control by eIF3h and EBP1 show the significance of cell cycle regulation on multiple levels.

1.5 Involvement of MAPKs and TCPs in cell cycle regulation

The eukaryotic mitogen-activated protein kinase (MAPK) signalling pathways are partially involved in shaping a specific cell cycle response to various developmental and environmental stress signals. For instance, the animal p38 MAPK is activated in response to UV radiation and inhibits the CDK1 phosphatase CDC25B which initiates G2/M DNA damage checkpoint and thus delays onset of mitosis (Bulavin *et al.*, 2001). The general cascade of events starts when a stimulus is sensed via a plasma membrane receptor that results in the activation of MAP kinase kinase kinases (MAPKKKs) that activate MAP kinase kinases (MKKs) which, in turn, results in the activation of MAPKs (Cristina *et al.*, 2010). MAPKs then activate or inhibit other kinases and/or transcription factors among other proteins to regulate numerous cellular responses. The *Arabidopsis* genome contains at least 60 *MAPKKKs*, 10 *MKKs*, and 20 *MAPKs* (Ichimura *et al.*, 2002).

Several MAP kinases are implicated in cell cycle regulation, for instance MPK6 shows cell cycle progression-dependent subcellular localisation in the root meristem where it is both nuclear and cytoplasmic-localised during interphase but moves to the mitotic spindle during mitosis (Smékalová *et al.*, 2014). Therefore, MPK6 was suggested to be involved in microtubule organisation. MPK4 activity is high in actively-dividing tissues such as the shoot apex and root tip and the protein is localised to the cell division plane where it regulates cytokinesis (Kosetsu *et al.*, 2010). One possible mechanism proposed by Sasabe and co-workers (2011) for metaphase-to-anaphase transition and subsequent progression to cytokinesis centres on MAPKKK1 (also known as NPK1) and NPK1-ACTIVATING KINESIN-

LIKE PROTEIN 1 (NACK1), a key regulator of cytokinesis (Sasabe *et al.*, 2011). Phosphorylation of NACK1 and NPK1 by CDKB prevents their complex formation that is lifted after metaphase when CDKB is inactivated and NACK1 and NPK1 are subsequently dephosphorylated (Sasabe *et al.*, 2011). Activated NACK1-NPK1 results in the cascade of events that proposedly results in phosphorylation of MAP65, a microtubule-associated protein, that allows cytokinesis to occur (Sasabe *et al.*, 2011). In addition to cell proliferation, MAPKs play key roles in cell fate decision during stomatal development (Lampard *et al.*, 2009; Umbrasaitė *et al.*, 2010).

Another family of proteins involved in meristem functions and cell cycle regulation in response to various environmental and developmental cues is the TEOSINTE BRANCHED 1, CYCLOIDEA, PCF1 (TCP) transcription factor family. The *Arabidopsis* genome contains at least 24 TCP genes that are categorised into two classes, I and II, which have antagonistic roles with class I considered as growth activators and class II as growth repressors, but some TCP proteins have overlapping functions (Martín-Trillo and Cubas, 2010; Li, 2015; Danisman, 2016). Several TCPs have been shown in cell cycle regulation, for example, TCP15 overexpression reduces *CYCB1:GUS* level in root tips, ploidy level, and *E2FB* transcript level, but increases and binds to *RBR* and *CYCA2;3* promoter region implying that TCP15 may function in balancing proliferation and endocycle (Li *et al.*, 2012). TCP20 was shown to bind to *CYCB1;1* and *PCNA2*, suggesting TCP20 involvement in cell cycle progression (Li *et al.*, 2005).

Single *tcp* mutants have little-to-no physiological phenotypes suggesting functional redundancy and/or compensation, but cumulative loss/reduction of *TCP8*, *TCP14*, *TCP15*, and *TCP22* results in progressive reduction of plant stature and expression of cell cycle genes (Davière *et al.*, 2014). TCP5, TCP13, and TCP17 were shown to redundantly repress mitotic cell cycle in developed petal and in young petal

primordia, these TCPs are transcriptionally repressed by a C2H2 zinc finger transcription factor called RABBIT EARS or RBE (Huang and Irish, 2015). TCP4 was shown to bind to KRP1 promoter and *KRP1* transcript level is increased in *TCP4* overexpression line, implying repressive cell cycle role of TCP4 (Schommer *et al.*, 2014). In summary, TCP transcription factors are involved in promoting or repressing cell cycle progression in multiple plant organs during growth and development.

1.6 Nutrient-control of cell cycle by the TOR signalling pathway

Whilst core and upstream control of cell cycle is central for plant growth, progression through the cell cycle is dependent on cellular nutrient status and nutrient-sensing signalling pathways. One such pathway that is remarkably conserved between plants and animals is the TARGET OF RAPAMYCIN (TOR) signalling (Wullschleger *et al.*, 2006; Dobrenel, Caldana, *et al.*, 2016). Heitman and colleagues (1991) carried out a mutant screen in budding yeast to look for strains that were resistant to rapamycin treatment that had initially been identified as an anti-fungal agent, these strains lacked *FK506 BINDING PROTEIN (FKBP)* which narrowed the search to two gene products which the authors named *TOR1* and *TOR2* (Heitman *et al.*, 1991). Moreover, the authors reported that the FKBP-rapamycin complex causes growth arrest at G1 phase of the cell cycle.

In *Arabidopsis*, a single *TOR* gene was identified that was shown to be highly expressed in actively dividing meristematic tissues and was not detected in differentiated cells (Menand *et al.*, 2002). Inducible silencing of *TOR* through artificial microRNA (amiR) showed a positive correlation between level of *TOR* and

overall plant growth (Deprost *et al.*, 2007) as depicted in Figure 1.3A. Additionally, some of the Gene Ontology (GO) categories among the down-regulated genes in the *amiR-tor* line were “regulation of mitotic cell cycle” and “cell growth” (Deprost *et al.*, 2007), suggesting a direct involvement of TOR signalling in control of cell proliferation.

Normal TOR function in mammals is known to be essential to allow progression through the cell cycle as the early studies showed that rapamycin blocks cell at G1 phase. Rapamycin-resistant *tor* mutants were shown to rescue rapamycin-inhibited cells by promoting G1-to-S transition through its downstream effectors S6 KINASE 1 (S6K1), 4E-BINDING PROTEIN 1 (4E-BP1), and EUKARYOTIC TRANSLATION INITIATION FACTOR 4E or eIF4E (Fingar *et al.*, 2004). However, the authors did not identify which cyclin-CDK complex is involved or targeted by mTOR signalling. In yeast, it is known that G1 blockade occurs due to decreased cyclin CLN3 translation, in other words TOR activates core cell cycle players required to drive G1 progression in response to nutrients, therefore preventing early entry into cell cycle (Barbet *et al.*, 1996).

Xiong and colleagues (2013) developed an experimental system to study TOR signalling pathway in relation to sugar availability and root meristem activation (Xiong *et al.*, 2013). The set-up involves germinating *Arabidopsis* seeds in photosynthesis-limiting sugar-free liquid growth medium which leads to mitotically quiescent root meristem at the photoautotrophic transition. Seedlings are then transferred to glucose with or without rapamycin and observations are made. It was shown that glucose-induced meristem activation strictly depends on active-TOR signalling, and that TOR directly targets E2FA for phosphorylation (Xiong *et al.*, 2013; Figure 1.3B). The same experimental system was used to propose that E2FB is another target of TOR phosphorylation (Li *et al.*, 2017).

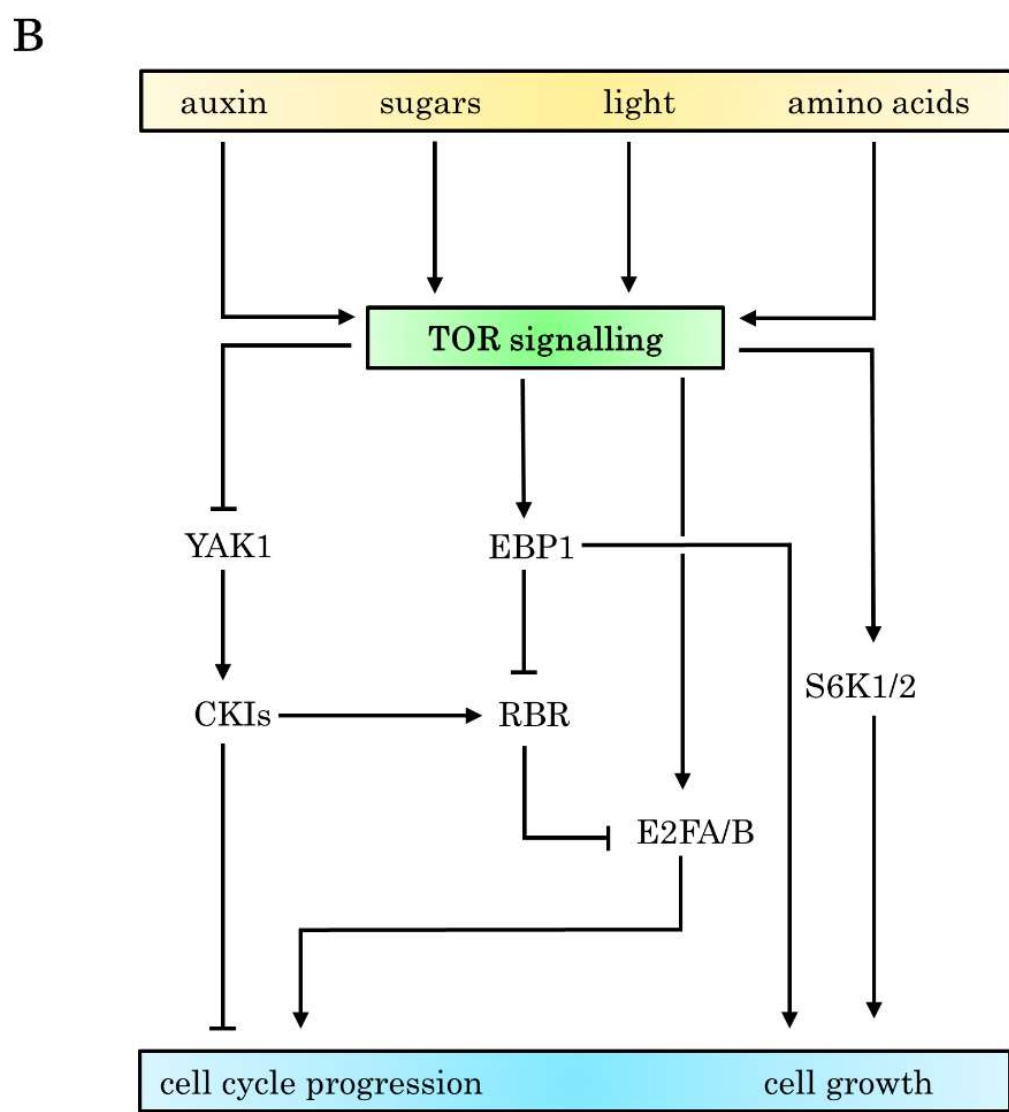
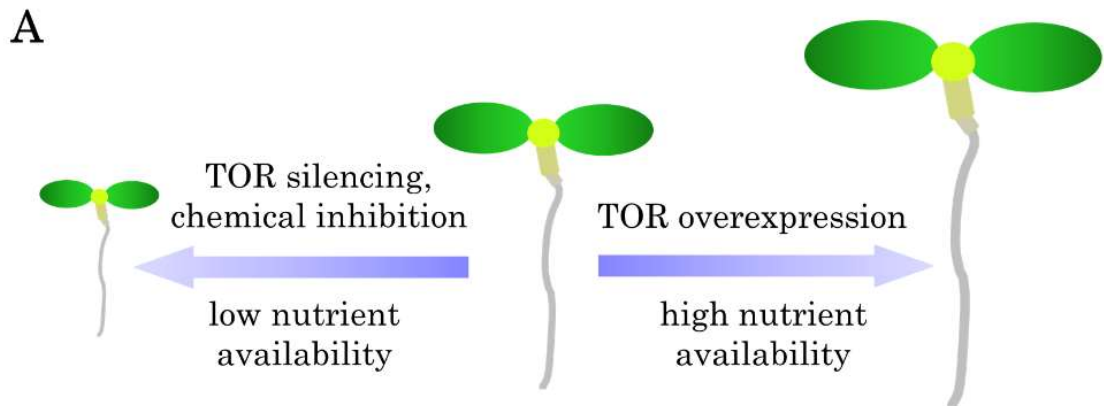


Figure 1.3 TOR signalling and plant growth control.
A. Transgenic lines with reduced or increased TOR protein amount lead to smaller and larger plants, respectively, reminiscent of effects on nutrient level on plant growth.
B. Positive growth signals such as light and sugar promote TOR activity which, in turn,

leads to phosphorylation of S6Ks and proposedly EBP1 that acts antagonistically to RBR. S6K1 and EBP1 are positive regulators of mRNA translation that could enhanced protein synthesis-driven cell growth. TOR phosphorylates E2Fs to allow transcription of cell cycle genes and inhibits YAK1 which is an activator of CDK inhibitors (CKIs). Through these side-by-side branches, TOR signalling connects growth signals to growth processes. Information and figure provided here are adapted from Ahmad *et al.*, 2019.

Light-induced cell cycle activation is also dependent on active TOR signalling (Mohammed *et al.*, 2018). Small GTPase RHO-RELATED PROTEIN 2 (ROP2) was suggested to relay auxin-light signalling to the TOR pathway which in turn phosphorylates E2FB and activates cell cycle (Li *et al.*, 2017). ROP2 has been shown to work upstream of ROP2-TOR axis (Cai *et al.*, 2017). Although the studies discussed above provide compelling evidence that light and sugar through TOR signalling promote cell cycle activation; cell cycle events under unperturbed conditions has not been fully characterised (Ahmad *et al.*, 2019). In short, sugar and light availability is connected to cell cycle through TOR-E2F signalling (Figure 1.3B). TOR signalling is counteracted by SUCROSE NON-FERMENTING-1-RELATED KINASE (SnRK) pathway which is activated in response nutrient deprivation and/or stress signals (Halford and Hey, 2009).

1.7 Size control of cycling cells

Whilst cell proliferation underpins organ size regulation, size of individual cells at which they divide is actively controlled as evident from low size variation among the same cell-type population (Amodeo and Skotheim, 2016). Thus, to maintain size homeostasis requires a tight coordination between cell cycle and cell growth which can occur through size-dependent progression through the cell cycle and/or size-dependent adjustment of cell growth rate (Ginzberg *et al.*, 2015). As shown in Figure

1.4, at least three distinct models, namely sizer, adder, and timer have been proposed to explain how cells can maintain size homeostasis, summarised by Jones and colleagues (Jones *et al.*, 2019). Below we provide a brief overview of the three models with examples in yeast studies since most of the current understanding of cell size control has cemented from it, relevant literature on plant cell size control will be covered in the chapter-specific introduction.

According to the sizer model, small cells accumulate more mass by prolonging cell cycle whilst larger cells spend less time in the cell cycle (Figure 1.4A). Thus, sizer cells have an inverse relationship between size at division and growth rate (Figure 1.4A). In the adder model, cells add the same mass irrespective of size at birth and optimal size homeostasis is achieved over several cell division rounds (Figure 1.4B). In the timer model, cells show temporal cell cycle synchrony and thus have the same period for growth (Figure 1.4C). Homeostatic state of timer cells can be achieved over multiple divisions or if cell growth shows a linear relationship between size at birth and growth rate. In short, sizer cells require threshold size to divide, adder cells add a fixed growth amount, and timer cells grow within a fixed time window (Figure 1.4).

One possible mechanistic explanation for the sizer model based on budding yeast and animal studies involves dilution of the G1/S repressor, Whi5 in yeast (Schmoller *et al.*, 2015) and Retinoblastoma (Rb) protein in humans (Zatulovskiy *et al.*, 2018). According to this model, Rb (and whi5) is size-independently produced during S-G2 phases and being a stable protein, it is diluted as the cell grows during G1. Accordingly, *RB*-overexpressing cells are large since it takes longer to reach a threshold RB concentration, and *RB* deletion results in smaller cells (Zatulovskiy *et al.*, 2018). Thus, dilution of Rb serves as proxy for sensing cell size and allows homeostasis to occur over successive division rounds. Interestingly, deletion *METHIONINE ADENOSYLTRANSFERASE 3* (*MAT3*) also leads to smaller cells,

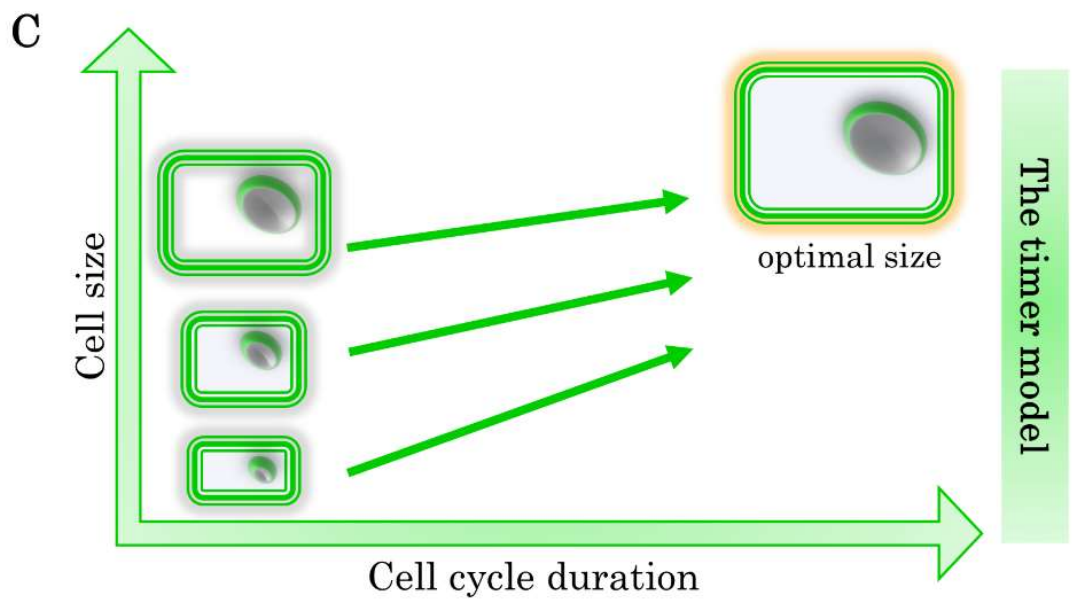
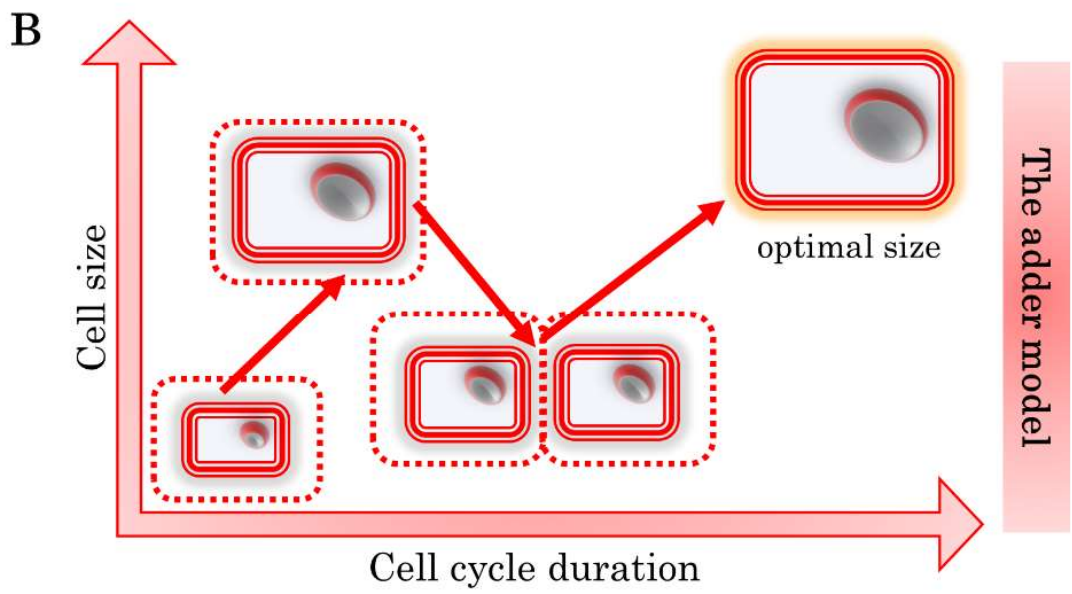
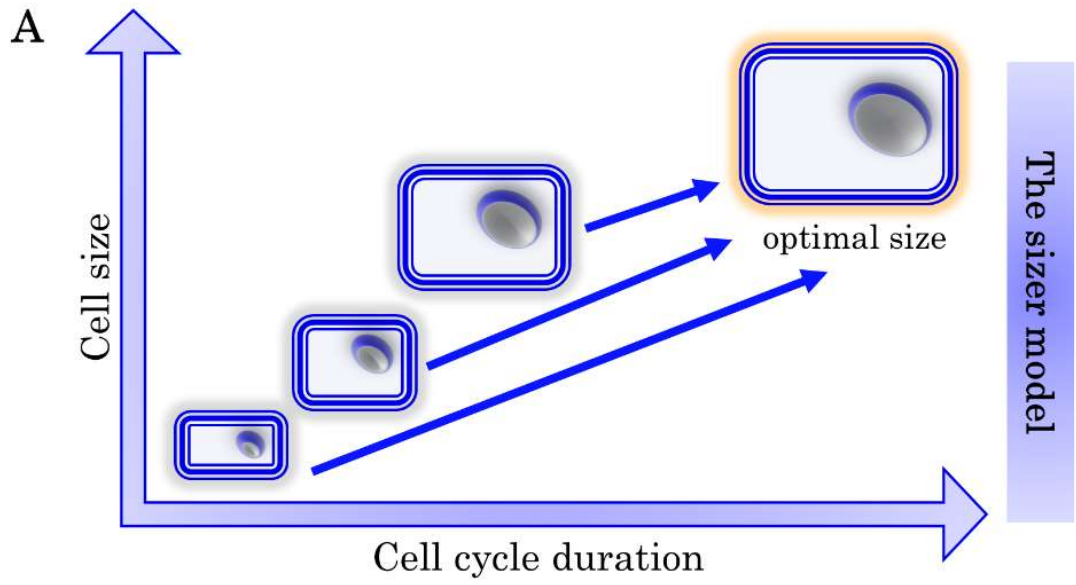


Figure 1.4 Existing models of cell size control.

A. Sizer cells achieve cell size homeostasis by inversely correlating cell cycle duration with size at birth. This leads to smaller cells with longer period of cell cycle and larger cells divide quickly, representing length of blue arrows. Optimal size can be achieved within one cycle given cells strictly couple cell growth and cell cycle progression.

B. Adder cells add a fixed volume or growth unit per cell cycle round, represented by dashed lines. Optimal size required for cell homeostasis can be achieved over successive division rounds.

C. Timer cells progress through the cell cycle within a fixed time window, irrespective of size at birth as represented by equal lengths of green arrows. Cell size homeostasis can be achieved if small cells grow faster than large cells during cell cycle.

Information and figure provided here are adapted from Jones *et al.*, 2019.

MAT3 is a Rb homologue in *Chlamydomonas reinhardtii* (Umen and Goodenough, 2001), suggesting the size-sensing logic between yeast, humans and green alga may be conserved. An identical mechanism may exist in *Arabidopsis*, we noted a similar small cell size phenotype in the root meristem of *RBR* silencing line (not shown in this thesis).

Experimental evidence for the adder model (Figure 1.4B) is most convincing in bacterial studies where it was shown that two evolutionary distant species *Escherichia coli* and *Caulobacter crescentus* cells add a fixed volume, irrespective of length at birth (Campos *et al.*, 2014). In another study, *E. coli* cells were shown to fit sizer and adder models under slow- and fast-growing conditions, respectively (Wallden *et al.*, 2016). Further complicating the size control mechanism budding yeast cells, *whi5*-dilution model alone does not explain mutants with altered ploidy and *Whi5* gene copy number (Heldt *et al.*, 2018). Simulations showed that during S/G2/M phases, cells use the timer mode to keep the *Whi5* level constant per cell cycle and when combined with G1 sizer, it produces an overall adder outcome during the whole cell cycle (Heldt *et al.*, 2018).

Mechanistic understanding of plant cell size control is extremely poor, and largely focuses on phenotypic observation of increased or reduced cell size of several mutants

and overexpression lines. For example, overexpression of *CYCD3;1* and *E2FB* decreases cell size whilst *KRPI* expression driven by epidermis-specific promoter increases size of epidermal cells, phenocopied when *REGULATORY PARTICLE AAA-ATPASE 2A* (*RPT2A*) gene, a 26S proteasome subunit, is mutated (Marshall *et al.*, 2012). In conclusion, our understanding of cell size control is far from completed and it is becoming apparent that a single model cannot explain size homeostasis within a cell population and all phases of the cell cycle. Additionally, how cell-to-cell communication and daily environmental changes affect size of dividing cells is not explored much.

1.8 *Arabidopsis* root meristem as a model system to study cell cycle and cell size

Arabidopsis thaliana, commonly known as thale cress or rock cress, belongs to the Brassicaceae (mustard) family of flowering plants that is native to Europe and Asia, but has colonised all major parts of the world (Hoffmann, 2002; Alonso-Blanco *et al.*, 2016). Factors that make *Arabidopsis* an ideal model species (Koornneef and Meinke, 2010) to study plant biology include: 1) short generation time; for example, it takes approximately a month from germination to flowering 2) small size, wild-type plants height is ~30cm and thus makes easy to handle in confined space of laboratories 3) high seed yield through self-pollination means ample availability of plant material at low cost 4) ease of genetic manipulation for forward and reverse genetic studies 5) well-characterised genome and availability of thousands of knock-out mutants.

Besides these qualities that make *Arabidopsis* a popular choice to study plant growth responses under normal and stress conditions at the molecular and cellular level,

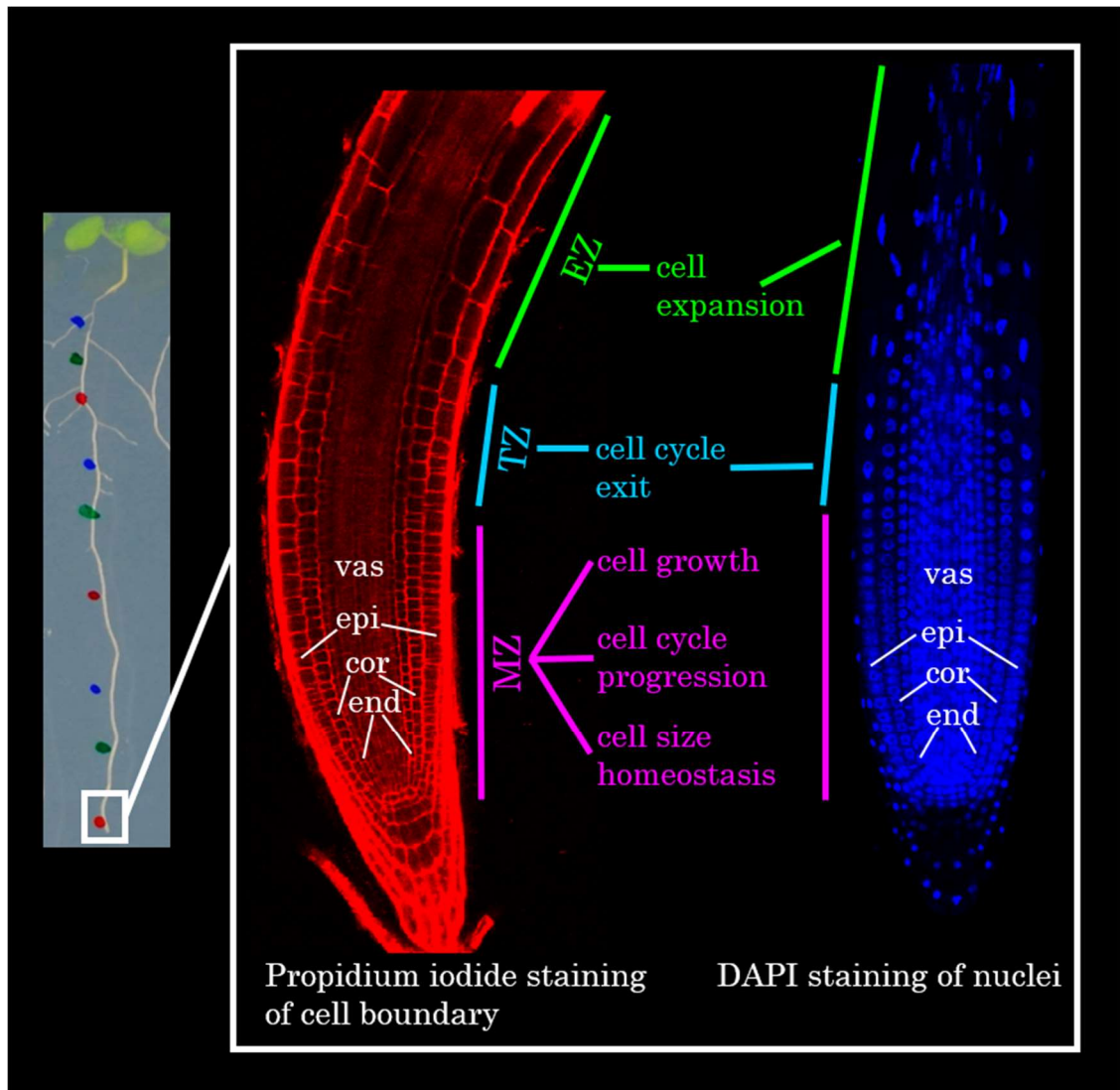


Figure 1.5 *Arabidopsis* root meristem as a model system.

Primary root growth can easily be tracked by marking position of the growing root tip which hosts the meristem zone (MZ) where cells grow and divide. Cells exit the cycle in the transition zone (TZ) and start to dramatically expand through cell wall extension in the elongation zone (EZ). Nuclei size and morphology also changes along the root, with elongated nucleus appearing in the EZ. In most experiments, counting of S-phase cells (EdU labelling, see Figure 1.6) and mitotic cells (*CYCB1;1-GFP*, see Figure 1.6) was done in the epidermis (epi), cortex (cor), endodermis (end), and the vasculature (vas) cell files. Confocal images presented here were taken by the author.

the root meristem is an excellent model system (Figure 1.5) to investigate cell cycle regulation and cell size control for the following reasons:

- I. cell cycle occurs in specific region called the meristem located in the root tip that is spatially separated from other tissues (Dolan *et al.*, 1993)

- II. transparent nature of the root means easy microscopic observation and efficient cell staining (Choe and Lee, 2017)
- III. availability of phase-specific tools allows visualisation and quantitative characterisation of cell cycle in a multi-cellular context (Yin *et al.*, 2014)
- IV. cell cycle is primarily driven by shoot-derived sugars and thus allows investigation into nutrient control of cell proliferation (Li *et al.*, 2017)
- V. cell size can be measured easily and reliably in multi-cellular context (Pavelescu *et al.*, 2018)

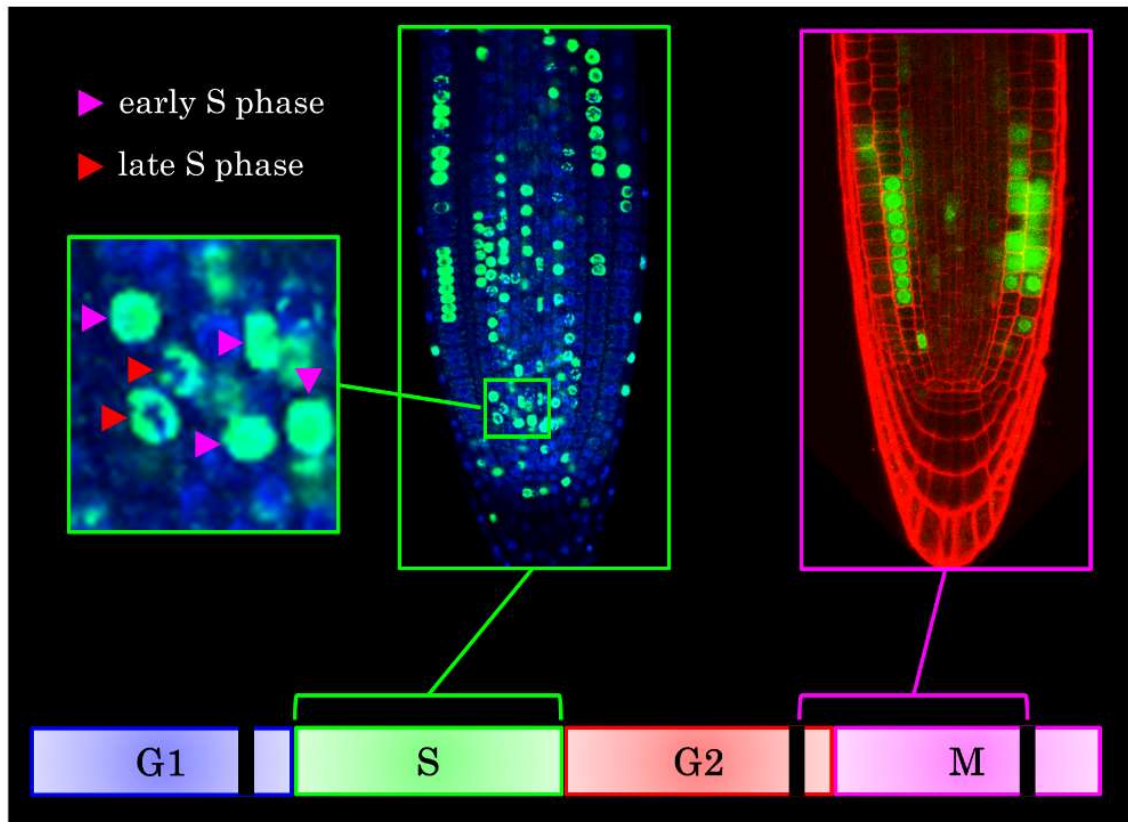


Figure 1.6 Tools to study cell cycle in the *Arabidopsis* root meristem.

S phase progression in the root meristem can be visualised by EdU labelling that has two distinct signals. Whole EdU signal corresponds to early-S phase cells whereas speckled localisation of EdU corresponds to late-S phase cells (Hayashi *et al.*, 2013). Onset of mitosis can be visualised by *CYCB1;1-GFP* marker (Meng and Feldman, 2010) that is active at G2/M to metaphase-anaphase transition, represented by black lines. In most experiments, EdU-positive and mitotic cells were counted in all cell layers of the root meristem.

Confocal images presented here were taken by the author.

At the basic experimental level, studying cell cycle requires measurement and/or visualisation of different cell cycle phases. One of the common and traditional methods is flow cytometry which involves measurement of DNA content or ploidy level of the cell by staining DNA with a fluorochrome (Darzynkiewicz *et al.*, 2010). Another method commonly used to study cell cycle involves fluorescence microscopy-based observation of proliferating cells, which relies on use of fluorochromes and/or unique intra-cellular features such as DNA/nucleus (and other organelles) morphology and visualisation of proteins with phase-specific expression, such as cyclins, to identify different cell cycle stages and their dynamics in response to environmental and developmental cues (Roukos *et al.*, 2015).

1.9 Hypotheses, aims and objectives of the thesis

In the present thesis, we mainly use two tools, EdU labelling for S phase and *CYCB1;1-GFP* as a mitotic marker (Figure 1.6). 5-Ethynyl-2'-deoxyuridine or EdU, preceded by antibody-based BrdU labelling, is a nucleoside analogue of thymidine that is incorporated into DNA when it is undergoing replication in a population of proliferating cells (Buck *et al.*, 2008). DNA-incorporated EdU is then detected with a fluorescent azide which forms a covalent bond via so-called "click" chemistry reaction and is observed under a fluorescence microscope. EdU method of S phase detection has also been applied in *Arabidopsis* root (Hayashi *et al.*, 2013).

For mitotic cells, we used an engineered GFP containing *CYCB1;1* destruction box sequence driven under the control of *CYCB1;1* promoter (Meng and Feldman, 2010) thus the GFP marker is switched on at G2/M to metaphase-anaphase transition (Figure 1.6). Furthermore, cell length measurements of *CYCB1*-positive cells

determine size of actively-dividing cells as compared with the whole of meristematic tissue.

The overarching aim of the thesis is to better understand the effects of genetic and environmental perturbation on cell cycle and cell size driven root meristem growth. More specifically, we aim to achieve the following:

Aim 1: Cellular-level characterisation of primary root and meristem growth under different growth conditions

Accompanying objectives: Measure a) primary root growth, b) meristem length, c) number of mitotic cells, d) size of mitotic cells under two constant light intensities and exogenous sucrose concentrations for a 6d period. Seedlings will be transferred from sucrose-containing to sucrose-free media.

Hypothesis 1: This will reveal the cellular re-organisation that takes place when roots are exposed to different growth conditions. I hypothesise that standard light supplemented with sucrose will score the highest in cellular measurements whereas low-light sucrose-free will score the lowest and sucrose-supplemented low-light will score at an intermediate level. This is consistent with current understanding on widespread control of plant growth by sugar availability (Wingler, 2017).

Aim 2: Determine whether cell cycle and cell size change on a diel basis and dissect possible molecular basis.

Accompanying objectives: Carry out time-course experiments under 12h light 12h dark cycle using the mitotic marker and EdU labelling in Col-0 background. Carry out EdU labelling in selected timepoints (based from the timecourse experiment) in mutants of different cell cycle proteins.

Hypothesis 2: Temporal changes in cell cycle and size will be better classified. I hypothesise that cell cycle will mostly occur during the light hours consistent with the rapid cell cycle activation in response to light availability (Mohammed *et al.*, 2018)

Aim 3: Dissect the role of TOR signalling pathway in cell cycle control.

Accompanying objectives: Follow cell cycle using the mitotic marker and EdU labelling upon chemical inhibition of TOR activity. Investigate whether RBR is part of the TOR-cell cycle network by carrying out EdU labelling in RBR silencing line.

Hypothesis 3: This will reveal novel insights into TOR control of entry into S phase (G1/S) and mitosis (G2/M). I hypothesise that TOR signalling will be involved in RBR regulation as TOR is known to regulate components of the RBR network such as E2FA and E2FB (Wu *et al.*, 2019). Additionally, I hypothesise that TOR activity will be required for G2/M transition, previous reports have shown the requirement of metabolic signals in promoting G2/M progression (Skylar *et al.*, 2011; Peng *et al.*, 2014).

Aim 4: Investigate involvement of known cell cycle regulators such as components of MAPK signalling cascade and TCP transcription factor family.

Accompanying objectives: Determine the effect of elevated levels of MKK7 and TCP14 using lines which express these genes under the control of a β -estradiol-inducible promoter system.

Hypothesis 4: This will show how different signalling pathways converge to regulate cell proliferation in the root meristem. Based on current understanding of MAPK signalling in limiting plant growth in response to various stress signals (Dóczi and Bögre, 2018), I hypothesise that under normal growth condition, increased MKK7 level will result in inhibition of root growth and cell cycle in the root meristem. TCPs

play key role during plant growth and development through regulation of cell proliferation and endoreduplication (Li *et al.*, 2012; Huang and Irish, 2015; Danisman, 2016), thus I hypothesise that overexpression of *TCP14* will perturb the balance between cell cycle and endocycle in the primary root.

The thesis has 7 chapters with 4 chapters of results. Each chapter has a cover page with a brief graphical and written summary of main findings as well as its own specific introduction and discussion sections. Chapter-specific aims and objectives are provided at the end of the introduction section, General discussion and conclusions are made in chapter 7.

A large, bold, black serif numeral '2' is centered within a light gray rectangular background.

Chapter 2 Materials and methods

2.1 Plant growth half-strength MS media preparation

Half-strength Murashige-Skoog (Murashige and Skoog, 1962) basal salt mixture (0.22% w/v, Duchefa Biochemie) was prepared with 1% w/v phytoagar (Melford Laboratories Ltd) and experiment-specific sucrose concentration of either 0%, 1%, 2%, 3% w/v. Morpholineethanesulfonic acid (MES) solution was used as a buffering agent and the final pH was set to 5.7 by 1N potassium hydroxide (KOH) solution. Media was sterilised by autoclavation at 121°C for 20min. The media was subsequently let to be cooled to ~60°C before being poured into petri dishes. ~20ml MS media was added to 90mm round petri dishes and ~40ml MS media was added to 120mm x 120mm square petri dishes.

2.2 *Arabidopsis* seed surface sterilisation

Seed surface sterilisation was carried out using the liquid-phase method as previously described (Rivero *et al.*, 2014) with altered concentration and incubation periods. Seeds were washed with 70% v/v ethanol (EtOH) by inverting 3-5 times for 1min. EtOH was then removed, and the seeds were incubated in sodium hypochlorite solution (5% v/v Domestos) for 5min on a vertical rotator (Rotator Grant Bio PTR-60). Sodium hypochlorite solution was discarded, and seeds were subsequently washed four times with sterilised distilled water. Finally, the sterilised seeds were kept in water after the final wash and cold stratified at 4°C for at least 2-3 days before sowing.

2.3 Plant material and growth conditions

Seeds were sown on petri dishes placed vertically in the growth chamber (PHcbi, MLR-352) with $\sim 80 \mu\text{mol m}^{-2} \text{s}^{-1}$ photon flux of cool white fluorescent light under 12h day-night cycles at day temperature of 21°C and night temperature of 18°C, which is considered as standard growth regime in this thesis. Other growth conditions include continuous standard light ($\sim 80 \mu\text{mol m}^{-2} \text{s}^{-1}$) and continuous low light ($\sim 20 \mu\text{mol m}^{-2} \text{s}^{-1}$) at 21°C. For molecular work, seeds were sown on mesh for easy harvesting. Specific growth conditions for some experiments are described in the results chapter.

A list of *Arabidopsis* lines used is provided in Table 2.1 below which are all that the ecotype Columbia 0 (Col-0) background. Additional details on T-DNA insertion sites of *e2fa* and *e2fb* mutants is provided in Figure 2.1.

Table 2.1 List of *Arabidopsis* lines used in the thesis

Seed line	Identifier	Reference
<i>amiRBR</i>	NA	(Cruz-Ramírez <i>et al.</i> , 2013)
<i>e2fa-1</i>	MPIZ_244	(Berckmans, Vassileva, <i>et al.</i> , 2011)
<i>e2fa-2</i>	GABI-348E09	(Berckmans, Vassileva, <i>et al.</i> , 2011)
<i>e2fa-3</i>	Not listed	(Xiong <i>et al.</i> , 2013; Horvath <i>et al.</i> , 2017)
<i>e2fb-1</i>	SALK_103138	(Berckmans, Lammens, <i>et al.</i> , 2011)
<i>e2fb-2</i>	SALK_120959	(Horvath <i>et al.</i> , 2017)
<i>pCYCB1:1-GFP</i>	NA	(Meng and Feldman, 2010)
<i>pCYCD2:1:CYCD2:1-GFP</i>	NA	(Sanz <i>et al.</i> , 2011)
<i>pER8GW:myc:MKK7</i>	NA	(Dory <i>et al.</i> , 2018)
<i>tcp14-7</i>	GABI611_C04	Unpublished (Ben Scheres collection)
<i>TCP14-iOE</i>	NA	Unpublished (Ben Scheres collection)
<i>TOR-RNAi</i>	NA	(Deprost <i>et al.</i> , 2007)

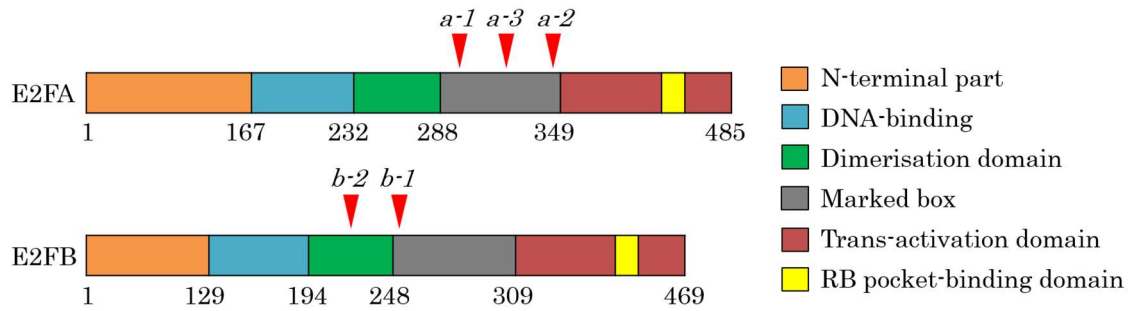


Figure 2.1 Structural organisation of E2FA and E2FB proteins with position of T-DNA insertion sites

Schematic showing different regions of E2FA and E2FB protein, red arrowheads show location of T-DNA insertions corresponding to different alleles of *e2fa* (*a-1*, *a-2*, *a-3*) and *e2fb* (*b-1*, *b-2*) mutants. The schematic is adapted from Leviczky and co-workers (2019) and was originally designed by Zoltan Magyar.

2.4 *Arabidopsis* primary root growth assay

Primary root growth was tracked by marking the position of the growing tip at the ‘backside’ of the petri dish at 24h intervals using different colour markers. At the end of the experiment, photographs of the petri dish with a ruler (as means of a scale reference) were taken. Using the freehand tool on ImageJ software (<https://imagej.nih.gov/ij/>), root growth was measured between two intervals which is the growth rate per day (growth over 24h period) and plotted as a function of time.

2.5 Standard AZD-8055 experimental set-up

To inhibit *in vivo* activity of TOR signalling, AZD-8055 (AZD) was used. For most AZD experiments the following regime was used. Seeds were sown on sucrose-free media under 12h light-dark cycles for one week. At 7DAS (day after stratification),

seedlings were transferred to either fresh sucrose-free or sucrose-containing media supplemented with 1 μ M AZD just before the growth chamber lights are switched on (timepoint = 0h). For maximum efficacy of AZD, AZD-containing media plates were prepared the day before the experiment and the drug was added after the media was cooled to 40-50 °C.

2.6 EdU labelling of *Arabidopsis* root meristem

To detect S phase cells, commercially available 5-ethynyl-2'-deoxyuridine (EdU) kit was used (ThermoFisher, Click-iT™ EdU Alexa Fluor™ 488 Imaging Kit). The following protocol is adapted from Hayashi and colleagues (2013) was designed and tested for 4d to 10d old *Arabidopsis* roots (Figure 2.1). Stocks of EdU and reaction mixture components are prepared in accordance with manufacturer's instructions.

Following experiment-specific treatment, seedlings were transferred to six-well plates and incubated in 10 μ M EdU-containing liquid MS media. For some experiments, EdU solution was directly added on the root tip on plates. The most common EdU incorporation period was 15min unless otherwise stated.

After incubation period, seedlings were placed on a glass microscope slide containing a drop of 3.7% v/v formaldehyde and shoots were excised for easy handling. The cut-roots were then transferred to a 1.5ml microcentrifuge tube containing 1ml of fixation solution consisting of 3.7% v/v formaldehyde + 0.1% v/v Triton X100 (Sigma) in 1X microtubule-stabilising buffer[a] (MTSB) for 1h under vacuum at RT. The fixation solution was removed, and the roots were washed 3 times with 1X MTSB, 5min per wash. At this stage, samples were either stored at 4°C or the following

steps were subsequently followed. Note, fixed root samples can be safely stored at 4°C for ~6 months.

Next, cut-roots were permeabilised in 1ml 0.5% v/v Triton-X100 PBS[b] for 15 min at RT. Permeabilisation solution is then discarded and roots were washed 3 times with 1X PBS, 5min per wash. Samples were then incubated in 100µl Click-iT reaction mixture[c] for 40 min at RT, protected from light. Samples were washed 3 times with 1X PBS, 5 min per wash.

For nuclei counter-staining, samples were incubated in 500µl 25% v/v Sysmex CyStain UV Precise P staining buffer (contains DAPI[d]) in 1X PBS for 15min at RT, protected from light. Samples were then washed 3 times with 1X PBS, 5min each. Samples were kept in 1X PBS after the final wash. EdU-labelled and DAPI-stained roots were then observed under a confocal microscope or stored at 4°C and protected from light.

[a] 10X MTSB stock preparation: 1.5% w/v of PIPES, 0.19% w/v of EGTA, 0.132% w/v of MgSO₄·7H₂O and 0.5% w/v of KOH were added in distilled water. pH was adjusted to pH 7.0 with KOH. The solution was sterilised by autoclavation at 120°C for 20min. 1X working MTSB solution (in distilled water) was filtered using a 50ml syringe with 0.2µm sterile filter. Protocol was taken from <http://biowww.net/know/1/301.html> [Last accessed: 16 December 2020]

[b] 10X PBS stock preparation: 8% w/v of NaCl, 0.2% w/v of KCl, 1.44% w/v of Na₂HPO₄ and 0.24% w/v of KH₂PO₄ were added in distilled water. pH was adjusted to pH 7.4 with HCl. The solution was sterilised by autoclavation at 120°C for 20min. 1X working PBX solution (in distilled water) was filtered using a 50ml syringe with 0.2µm filter. Protocol was taken from <http://cshprotocols.cshlp.org/> (doi:10.1101/pdb.rec8247).

[c] Click-iT reaction mixture: 80.5% v/v distilled water, 11% v/v EdU reaction buffer + 6% v/v CuSO₄ + 2% v/v EdU buffer additive + 0.5% v/v Alexa Fluor 488 were added.

[d] Alternatively, roots were incubated in 1µg/ml DAPI in 1X PBS solution for 20-25min, protected from light.

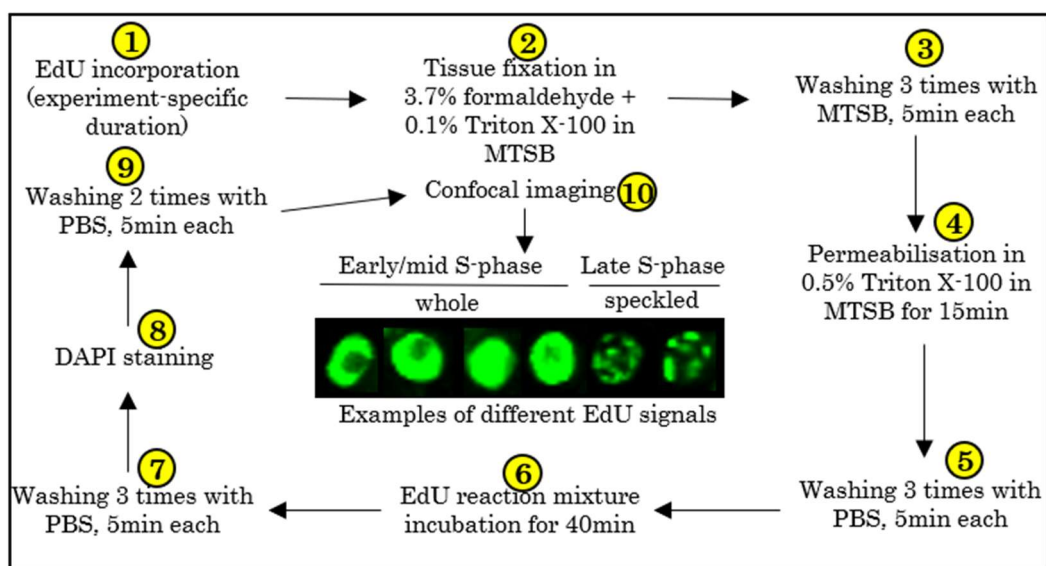


Figure 2.2 Step-by-step protocol of EdU labelling of *Arabidopsis* root tip.

For additional information, see section 2.6 above. The protocol is adapted from Hayashi and colleagues (2013).

2.7 Confocal laser scanning microscopy

An Olympus IX-81 FluoView FV-1000 inverted microscope equipped with multiple laser lines was used. The following lasers were used for fluorescent dyes/proteins: 405nm for DAPI, 488nm for GFP and Alexa Fluor 488, 543nm for propidium iodide. The parameters including high voltage (HV), gain, and offset settings once set were

unchanged for fluorescence-of-interest but were modified for counter-staining dyes such as DAPI and propidium iodide.

2.8 Confocal data processing

The confocal images were processed and analysed using the Olympus FV10-ASW 4.2 and/or ImageJ. Confocal OIB files were converted to TIFF files and processed in ImageJ software. Using the straight-line tool on ImageJ, cell length was measured in longitudinal direction from middle of the cell in the cortex layer. Meristem was defined as region of cells smaller than 10µm in length or the boundary of cells becoming gradually enlarged which defines the transition zone.

2.9 Western blotting

2.9.1 Protein extraction, quantification, and separation

Whole-plant material was harvested and snap-frozen in liquid nitrogen and stored in 80°C or used immediately. Samples were ground to fine powder form using liquid nitrogen-cooled mortar and pestle and transferred to pre-chilled 1.5ml microcentrifuge tube. Lacus protein extraction buffer[a] (Magyar *et al.*, 1997) consisting of PIC, DTT, PMSF, pNPP was added by following 1:1 v/v ratio and mixed by vortex. The samples were centrifuged at 14,000rpm at 4°C for 10min. Supernatant was transferred to a new microcentrifuge tube and SDS was added by following 1:4 v/v ratio i.e. 20µl SDS to 80µl lysate. The SDS samples were then

heated at 100°C for 5min and kept on ice afterwards for immediate use or stored at -20°C for later use.

Protein concentration was determined by performing a Bradford assay. Briefly, 800µl distilled water, 200µl Bradford solution, and 2µl protein sample were sequentially added to a microcentrifuge tube and mixed by vortex. For blank, 2µl Lacus protein extraction solution was added. The protein solution was then transferred to a glass cuvette and absorbance at 595nm was detected using a spectrophotometer. The recordings were entered on an Excel spreadsheet to interpolate the protein concentration of the given sample.

Proteins were separated in 10% SDS-polyacrylamide gels which were composed of approximately 4/5 separating solution[b] and 1/5 stacking solution[c]. The separating gel was let to polymerise under a layer of isopropanol. Gel electrophoresis apparatus was filled with 1X SDS running buffer and 20µg or 30µg protein was loaded onto each well. PageRuler protein ladder (ThermoFisher) was used as a marker. The gel was run at 50V for 4-5h or until the running bands entered the buffer solution. Gel region-of-interest was cut and subsequently rinsed with distilled water on a rocking platform for 2min. The gel was kept in 1X transfer buffer with gentle agitation till the next step.

2.9.2 Protein transfer, immunoblotting, and detection

Proteins were transferred by performing a wet electroblotting. Nitrocellulose transfer membrane was soaked in absolute methanol for 30sec and rinsed with 1X transfer buffer. The transfer sandwich was assembled in the following order: cushion pad-Whatman paper-gel-membrane-Whatman paper-cushion pad. All components

were pre-wetted with transfer buffer. The gel and membrane were marked at the top left corner that the order of protein samples on the membrane could be determined. The assembled sandwich was then placed at a vertical position in a tank and ran overnight at 14V in the cold room.

Following day, the membrane was washed once with 1x TBS-T (containing 1% v/v Tween-20 in 1X TBS) for 5min and subsequently incubated in blocking solution containing 5% w/v milk powder in TBS-T for 2h with gentle agitation. The membrane was then washed once with TBS-T and subsequently incubated in primary antibody overnight in the cold room. The membrane was then washed 4 times with TBS-T, 10min per wash on a rocking platform. Secondary antibodies were diluted in 5% w/v milk powder in TBS-T and incubated for 30min at RT followed by washing with TBS-T 4 times, 10min per wash on a rocking platform. Antibody dilutions are provided below.

Table 2.2 List of antibodies and their dilutions used in this thesis.

Antigen	Host	Source	Dilution
E2FA	rat	(Leviczky <i>et al.</i> , 2019)	1:500
E2FB	rabbit	(Magyar <i>et al.</i> , 2005)	1:500
GFP	mouse	Roche, 11814460001	1:1000
phospho-Rb(Ser807/811)	rabbit	Cell Signaling, 9308	1:500
phospho-S6K1/2	rabbit	Agrisera, AS132664	1:500
RBR1	chicken	Agrisera, AS111627	1:1000
S6K1/2	rabbit	Agrisera, AS121855	1:1000
chicken-IgG	goat	Sigma, 12-349	1:20000
mouse-IgG	rabbit	Sigma, 12-341	1:10000
rabbit-IgG	goat	Sigma, A0545	1:10000
rat-IgG	goat	Sigma, A9037	1:10000

The membrane was developed using Immobilon chemiluminescent HRP (Merck Milipore) substrate by following 1:1 ratio of luminol reagent and peroxide reagent. Substrate solution was poured onto the membrane and incubated for 2min. The membrane was then fixed in an X-ray film cassette, exposure period depended on the antibody and the experiment. After development, membrane was stained with 0.1% w/v Coomassie Brilliant Blue (dissolved in 50% v/v methanol) for 5min, and de-stained with 50% v/v methanol. Membrane and X-ray film were scanned for analysis.

[a] Lacus protein extraction buffer: 1% v/v of PIC (Sigma, PhosSTOP™), 0.1% v/v of 1mM DTT, 1% v/v of 1mM PMSF, 1.5% v/v of PNPP are added to Lacus solution. Protocol is taken from Magyar and colleagues (1997).

[b] 10% separating gel: 39.4% v/v of H₂O, 33% v/v of 30% v/v acrylamide mix, 25% v/v of 1.5M Tris (pH 8.8), 1% v/v of 10% SDS, 1% v/v 10% w/v APS, 0.6% v/v of TEMED were added. Protocol is taken from Bio-Rad Laboratories, Inc.

[c] For 5ml of stacking gel: 68.7% v/v of H₂O, 16.6% v/v of 30% v/v acrylamide mix, 12.6% v/v of 1M Tris (pH 6.8), 1% v/v of 10% SDS, 1% v/v of APS, 0.1% v/v of TEMED were added. Protocol is taken from Bio-Rad Laboratories, Inc.

2.10 Statistical analysis

Information on number of technical and biological replicates is provided in the figure legend corresponding to the experiment. Since most of the experimental work involved comparing two groups i.e. comparison between 0% and 1% sucrose, between two timepoints, light versus dark, or control versus AZD samples, I carried out two-sample assuming unequal variance (heteroscedastic) t-test on Microsoft Excel 2019

to statistically determine significant differences. A p -value of less than 0.05 was considered to be a statistically significant difference.

Unless otherwise stated, error bars in all figures of the thesis and in textual parentheses represent standard deviation.

3

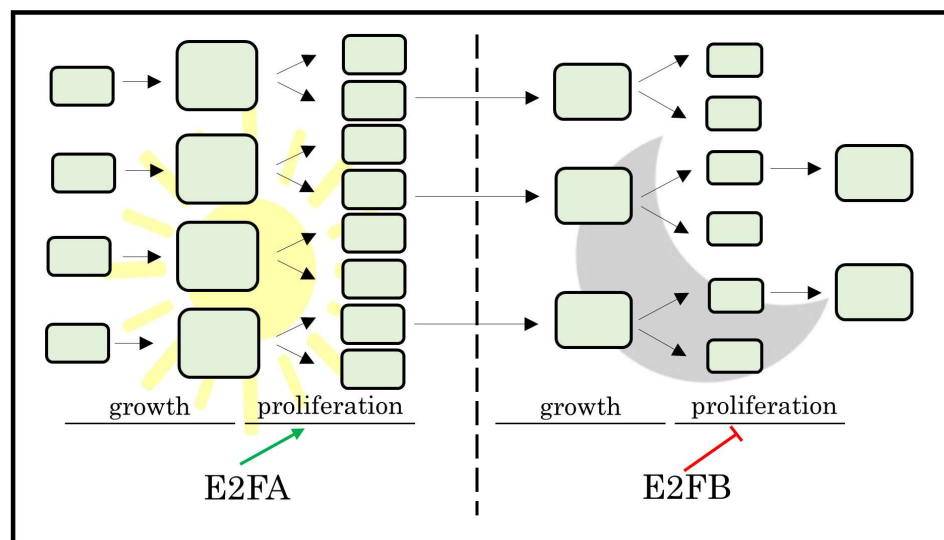
Chapter 3 Distinct diel protein accumulation of E2FA and E2FB may differentially control the cell cycle

Declaration – Western blot in Figure 7 was performed by Csaba Papdi with a biological repeat done by the author.

Zaki Ahmad, Csaba Papdi, Zoltan Magyar, Laszlo Bogre. Diurnal rhythm of cell cycle and size in the *Arabidopsis* root meristem. Manuscript in preparation.

Distinct diel protein accumulation of E2FA and E2FB may differentially control the cell cycle

In this chapter, cell cycle- and cell size-driven root meristem growth dynamics and its relationship with the environment are investigated.



E2FA and E2FB may have distinct roles in governing diel changes in cell cycle

In a nutshell

- Meristematic cells dividing under standard light growth conditions divide more frequently, but at a reduced size compared with low-light growth conditions
- Exogenous sucrose supply does not interfere with size of dividing cells
- Cells preferentially divide more frequently and at larger size during the day than during the night, suggesting a diurnal rhythm of cell cycle
- Cell cycle transcriptional factors, E2FA and E2FB, have anti-phasic protein accumulation
- Analysis of *e2f* mutants suggest E2FA is required in the morning to stimulate cell cycle, whereas E2FB limits S phase at end-of-day and night

3.1 Introduction

Cell cycle and protein synthesis-driven cell growth processes underlie meristem growth, which in turn are limited by internal and external cellular environmental factors, namely light and sugar availability (Lastdrager *et al.*, 2014). Consistent with this idea, transcripts of several cell cycle and translation regulators are coordinatively upregulated during the day (light period) and decrease during the night (dark period; Usadel *et al.*, 2008). Transfer of dark-grown seedlings to light also promotes expression of genes involved in translation (Ma *et al.*, 2001). Some of the cell cycle proteins are also post-translationally modified in a diurnal manner (Uhrig *et al.*, 2019). Furthermore, sugar promotes accumulation of cyclins and could partially derepress growth in transgenic seedlings where growth is otherwise compromised (Gutzat *et al.*, 2011; Wang and Ruan, 2013; Lokdarshi *et al.*, 2020). Additionally, exogenous sucrose supply leads to cell-type specific increase in cell cycle gene expression in the root meristem (Shulse *et al.*, 2019) whilst nutrient-deficiency reduces cell cycle progression (Buckner *et al.*, 2019). Collectively, these findings suggest that light-dark cycles and nutrient availability level may jointly contribute to the increase in cell number and size to promote tissue growth at the whole-plant level.

Phenomenologically, cell size and division can be coupled through size-dependent progression through cell cycle phases and/or size-dependent growth of small and large cycling cells (Schmoller, 2017). Time-course imaging of *Arabidopsis* shoot apical meristem (SAM) revealed that variations in cell size at birth are largely corrected by adjusting cell cycle duration such that large cells cycle faster, and small cells spend longer period in the cell cycle; in extreme cases, cell cycle length of daughter cells can differ by up to 48h (Jones *et al.*, 2017). Transfer of plants from

normal light to low-light led to reversible reduction in cell size that could also be restored by exogenous sucrose (Jones *et al.*, 2017). This suggests that size of dividing cells is fundamentally limited by environmental conditions, whether similar changes occur in the root meristem is not known. Computer simulations backed up by cell size measurements of mutants with altered CDK production revealed that reduced CDK amount results in larger cells whilst high CDK level leads to smaller cells without influencing cell cycle length (Jones *et al.*, 2017). Furthermore, cell growth continues beyond G1 phase and it was implied that progression through both G1/S and G2/M transitions are size dependent that is primarily determined by CDK activity (Jones *et al.*, 2017).

One main target of CDK is to lift RBR repression on E2F transcription factors to drive transcription of genes required for S phase and mitosis. The classical view of E2FA and E2FB as cell cycle activators is being challenged such that E2FB, depending on its protein interactors, can act to limit cell proliferation (Magyar *et al.*, 2016). E2FA and E2FB have non-overlapping biological roles; for example, E2FA in complex with RBR represses endocycle genes in the meristem and is part of the DNA damage response (Magyar *et al.*, 2012; Horvath *et al.*, 2017). In developing leaves, RBR-bound E2FB represses cell proliferation, and is a component of the multi-protein DREAM complex (Kobayashi, T. T. Suzuki, *et al.*, 2015; Oszl *et al.*, 2020).

Minimal overlap in temporal and spatial transcript and protein accumulation of E2FA and E2FB further strengthens the view that these two transcription factors are not redundant. For example, in developing siliques *E2FA* expression was highest in proliferation phase and nearly disappeared during maturation phase when *E2FB* expression peaked (Leviczky *et al.*, 2019). Confocal imaging of Yellow Fluorescent Protein-tagged E2F lines showed E2FA protein accumulated during globular to late-heart stages and disappeared in mature embryo whilst E2FB was mostly present at

the torpedo stage and remained detectable in mature embryo (Leviczky *et al.*, 2019). Whereas E2FA is predominantly found in proliferating tissues such as young leaves, E2FB could also be detected in fully-differentiated cells (Oszi *et al.*, 2020). During SAM growth and development, *E2FB* trough corresponds with peak expression of *E2FA* and S phase genes as well as *A*- and *B*-type *CDKs* (Klepikova *et al.*, 2015). Additionally, *E2FA* and *E2FB* expression patterns are anti-phasic in most timepoints with *E2FB* and *RBR* level closely resembling each other (Klepikova *et al.*, 2015). Lastly, spatial pattern and intensity of *E2FA* and *E2FB* expression appear in distinct cell clusters of root tip (T. Q. Zhang *et al.*, 2019). Whilst these studies convincingly distinguish between E2FA and E2FB functions, daily accumulation of E2Fs, on hourly basis, has not been determined.

Light-dark cycles are arguably the most extreme change plants face on daily basis, indeed, transfer of dark-grown seedlings to light rapidly activates cell cycle in the shoot apex (López-Juez *et al.*, 2008). Whilst the effect of light intensity on plant biomass and several other growth traits has been explored (Schumann *et al.*, 2017; Poorter *et al.*, 2019), there is still a lack of detailed investigation into cell cycle and cell size adjustment to light and sugar availability in the *Arabidopsis* root meristem over a long time-period and under light-dark cycles.

3.1.1 Aims and objectives

The overarching aim of this chapter is to define temporal changes in cell cycle and cell size in response to different growth conditions.

Aim 1. quantitatively characterise dynamics of cell cycle and cell size under standard light and low light growth conditions as well as sucrose supplementation.

Accompanying objective: Utilise *pCYCB1;1:CYCB1;1-db-GFP* marker line to measure number of mitotic cells in different growth conditions.

Aim 2. determine diel hourly changes in cell cycle and G2/M cell size under light-dark cycles.

Accompanying objective: Carry out timecourse experiment with EdU labelling and the mitotic marker under 24h light-dark cycles. Measure length of *CYCB1;1*-positive cells as a proxy for G2/M size.

Aim 3. explore whether protein accumulation of E2F transcription factors have time-of-the-day dependent pattern

Accompanying objective: carry out Western blot with E2FA- and E2FB-specific antibodies as well as with GFP antibody in GFP-fusion lines of E2FA and E2FB.

Aim 4. determine whether diel dynamics in cell cycle is altered in the *e2f* mutants.

Accompanying objective: selected timepoints from Aim 2 to measure number of S phase cells in different *e2fa* and *e2fb* mutants.

3.2 Results

3.2.1 Cell cycle in the meristem underpins root growth adjustment to the light and sugar availability.

Availability of photosynthates is one of the limiting factors for plant organ growth, in particular cell production in the root meristem exclusively depends on available sugars (Li *et al.*, 2017). To understand cell cycle dynamics of root growth and how it is shaped by growth conditions, primary root growth and number of mitotic cells

were followed over time under constant standard light (SL; light intensity $\sim 80 \mu\text{mol m}^{-2} \text{s}^{-1}$) and constant low light (LL; $\sim 20 \mu\text{mol m}^{-2} \text{s}^{-1}$) conditions of the G2/M marker line *pCYCB1;1:CYCB1;1-db-GFP* (hereafter referred to as mitotic marker or *CYCB1;1-GFP*; Meng and Feldman, 2010). A similar range of light intensity for our LL condition has been used by others that show light intensity-dependent increase in *Arabidopsis* growth (Bailey *et al.*, 2001; Mishra *et al.*, 2012). To ensure equal seedling establishment ratio, seeds were sown on 1% sucrose MS media and transferred to sucrose-free media or fresh 1% media at 4d after stratification (DAS; Figure 3.1A).

Transfer of seedlings from 1% to 0% sucrose reduces root growth rate in both light conditions within 1d after transfer (DAT) and the lowered growth was maintained throughout the course of the experiment (Figure 3.1B,C). Under SL, a modest but statistically significant reduction of $\sim 12\%$ and under LL a significant reduction of $\sim 43\%$ was observed at 1DAT and a similar separation of growth rate is observed between sucrose and sucrose-free condition over 6DAT in the two light conditions. During 6DAT, an average difference of $\sim 39\%$ between SL 1% and LL 1% was observed. The total root growth after transfer was clearly distinguishable between each of the four conditions with $\sim 52\text{mm}$ ($\pm 3.7\text{mm}$) growth under SL 1%, $\sim 47\text{mm}$ ($\pm 3.9\text{mm}$) under SL 0%, $\sim 32\text{mm}$ ($\pm 3.8\text{mm}$) under LL 1% and $\sim 24\text{mm}$ ($\pm 3.7\text{mm}$) under LL 0% (Figure 3.1D).

We next checked the occurrence of cell division events using the mitotic marker and found a similar trend as the primary root growth. *CYCB1;1-GFP* positive cells were counted in all cell layers of the root tip, and meristem length was determined by measuring the average distance from quiescent centre (QC) to the last GFP-positive cell in both sides of the cortex layer (Figure 3.2A). At 0DAT, number of mitotic cells

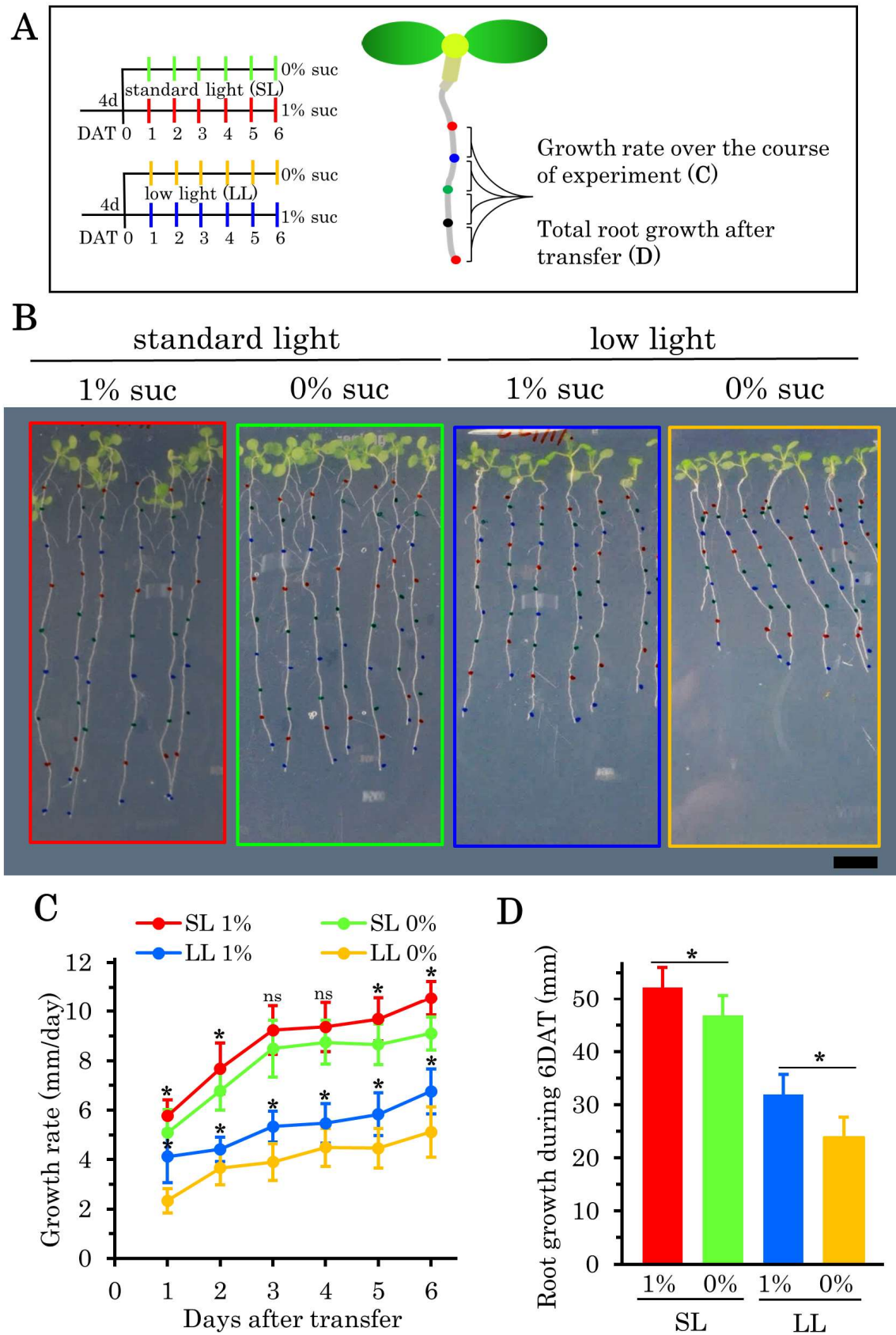


Figure 3.1 Light and sugar set the primary root growth rate.

A. Schematic of experimental design. *CYCB1;1-GFP* seeds were sown on 1% suc under two light intensities and transferred to 0% and 1% at 4d. Position of the primary root tip was marked daily for a 6d period and used to plot growth rate and cumulative root growth

after transfer.

B. Representative whole-plant photograph of *CYCB1;1-GFP* in each growth condition. Scale bar = 10mm

C. Measurements of primary root growth rate, determined as distance between two marks along the root.

D. Sum total of root growth after transfer to +/- sucrose at each growth condition.

Data presented as mean, error bars represent standard deviation. Number of roots (n) > 15, number of biological repeats (N) = 2. Statistical differences between 1% and 0% within SL and LL were determined using Student's t-test. Asterisk represents a significant difference, "ns" represents a difference that is not significant.

under both light conditions was around 15 (\pm 5.2 for SL and \pm 4.2 for LL) which increased to 28 cells (\pm 8.7) and 19 (\pm 5.0) cells 1DAT under SL 1% and SL 0%, respectively (Figure 3.2B,F). Mitotic count at 1DAT under LL 1% and LL 0% was 17 (\pm 5.7) cells and 12 cells (\pm 4.4), respectively (Figure 3.2B,F). At all timepoints, mitotic cell frequency was clearly distinguishable between 0% and 1% within LL, but a large overlap in mitotic count was observed in most timepoints between SL 0% and LL 1% whereas LL 0% showed the lowest count at all timepoints (Figure 3.2B). During all timepoints, under SL 1%, and SL 0%, 28 (\pm 5.9) and 24 (\pm 4.2) mitotic cells were observed on average (Figure 3.2C). Under LL 1% and LL 0%, 21 (\pm 3.7) and 12 (\pm 2.3) cells were observed on average of all time points, respectively (Figure 3.2C).

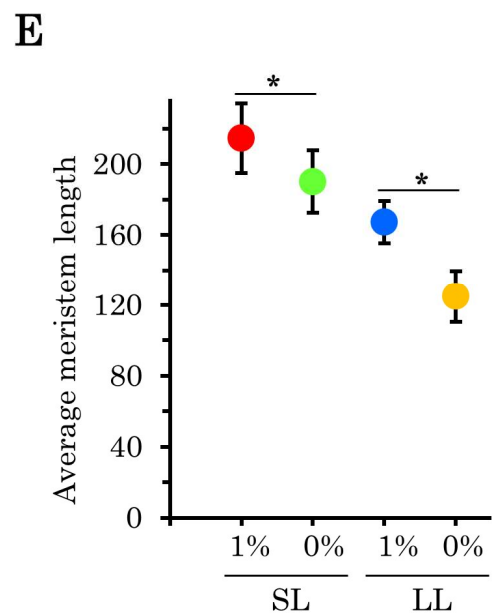
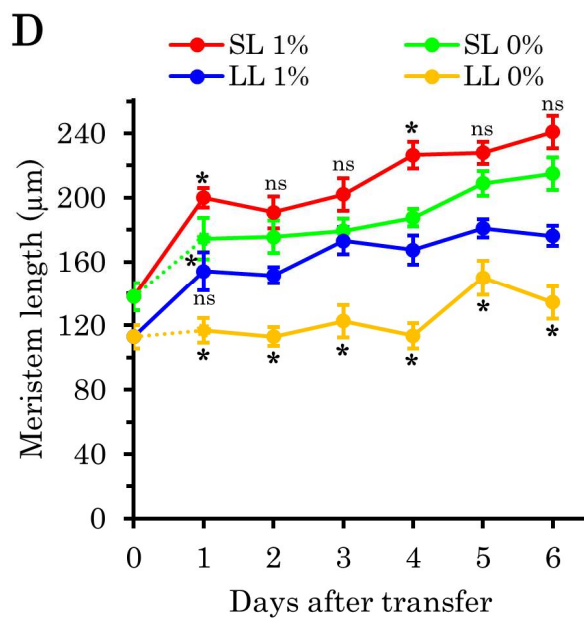
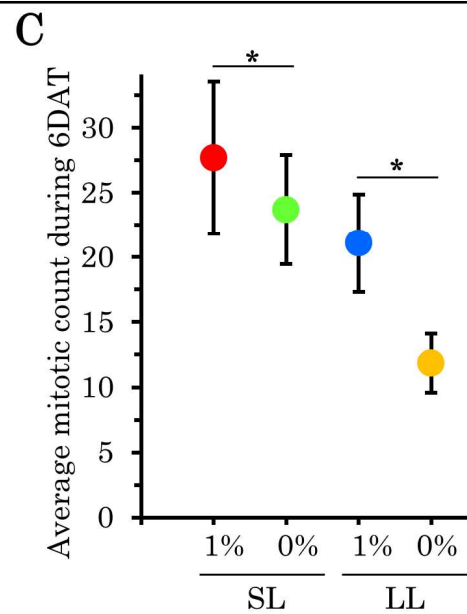
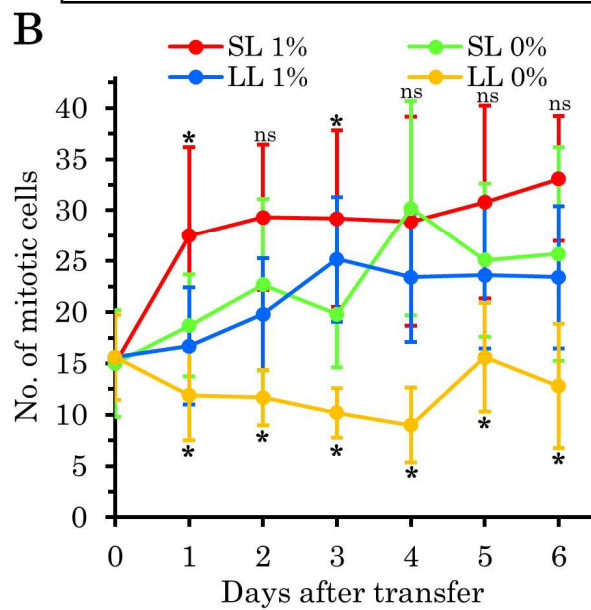
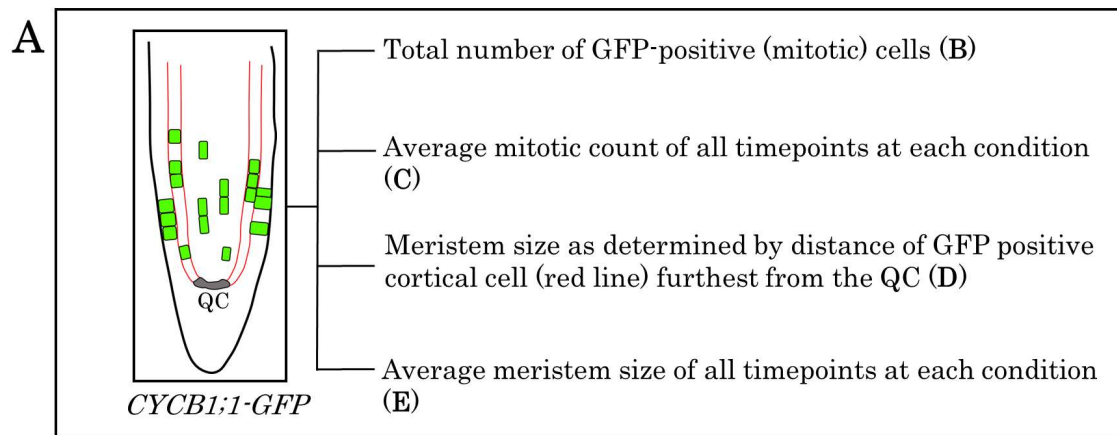
Meristem is defined as a region with the highest proliferation capacity (Dolan *et al.*, 1993; Otero *et al.*, 2016), and thus we defined the size of the meristem as the distance from QC cells to the last GFP-positive cortical cell. Under SL 1% at 1DAT, meristem size was \sim 200 μ m (SEM \pm 6.2 μ m), and under SL 0% it was \sim 175 μ m (SEM \pm 13.0 μ m), a reduction of 12.5% (Figure 3.2D,F). Under LL 1% at 1DAT, meristem size was \sim 155 μ m (SEM \pm 11.8 μ m), and under SL 0% it was \sim 115 μ m (SEM \pm 7.8 μ m), a reduction of \sim 25% (Figure 3.2D,F). At all timepoints, a clear difference in meristem size was observed when comparing 0% and 1% samples within SL and LL, whilst there was an overlap between SL 0% and LL 1% in some timepoints (Figure 3.2D)

During the course of experiment, the average meristem size under SL 1% was 215 μm (\pm 19.7 μm), 190 μm (\pm 17.6 μm) under SL 0%, 165 μm (\pm 12.0 μm) under LL 1% and 125 μm (\pm 14.6 μm) under LL 0% (Figure 3.2E).

To summarise, the root growth assay revealed a dynamic adjustment of growth rate from sucrose-containing to sucrose-free growth media, and a clear separation of growth between the two light intensities. This suggests an active monitoring of root growth even under constant growth conditions and implies an involvement nutrient-sensing signalling pathway. The shift from 1% to 0% sucrose media under LL causes a higher reduction in growth rate, cell cycle occurrence and meristem size implying that exogenous sucrose supply has an overall greater positive effect on the aforementioned growth parameters under LL as compared to SL. Additionally, the size of meristem almost mirrors the primary root growth implying that the tuning of growth to the environment occurs in the meristem through regulation of cell cycle. This is consistent with the view that cell division events in the root meristem is a key determinant of root growth rate (Bennett and Scheres, 2010; Street *et al.*, 2015; Gázquez and Beemster, 2017).

3.2.2 Growth conditions dependence of root meristematic cell size

Meristem regulation occurs through both rate of cell division and cell size at division (Ahmad *et al.*, 2019), so we next asked whether cell size is affected by various growth conditions as we observed for primary root growth and root meristem mitotic count. To this end, we used the same SL/LL mitotic marker confocal data and measured only the size of *CYCB1;1*-positive cells (hereafter referred to as G2/M cell length/size) in the cortex layer of both sides of the root (Figure 3.3A). G2/M cell length at 4d (OD-



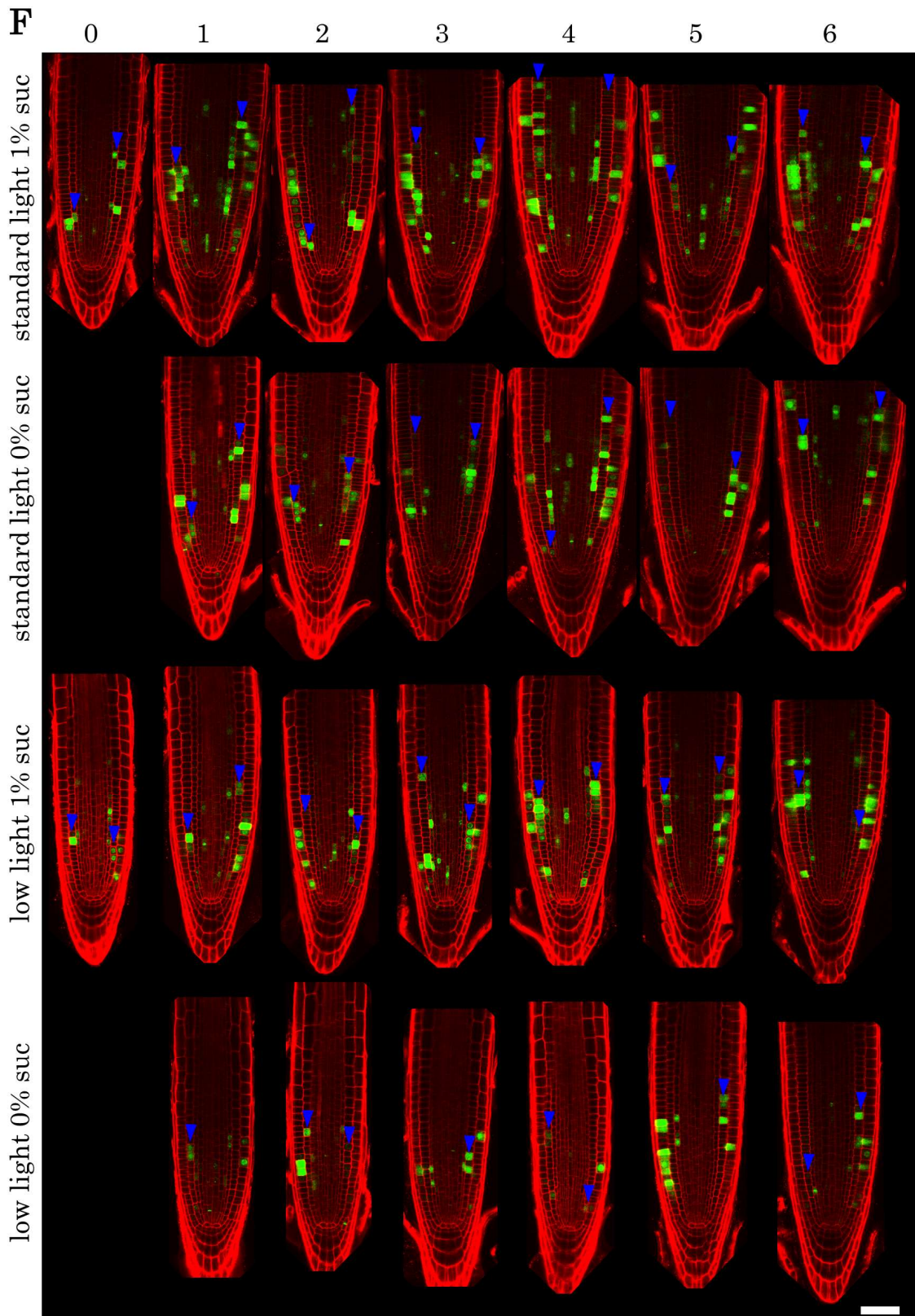


Figure 3.2 Cell cycle in the root meristem is largely defined by light and sugar availability

- A.** Schematic of measurements made. All *CYCB1;1-GFP* positive cells were manually counted, and meristem size was determined as length between the QC and last GFP-positive in the cortex layer.
- B.** Number of *CYCB1;1-GFP* positive (mitotic) cells in the four growth conditions.
- C.** Average number of mitotic cells of all timepoints in the four growth conditions.

D. Root meristem length in the four growth conditions during the course of experiment.
E. Average size of root meristem of all timepoints in the four growth conditions.
F. Representative confocal micrograph of PI-stained (red) *CYCB1;1-GFP* (green) root tip at each timepoint of four growth conditions. Blue arrowheads point meristem boundary.

Data presented as mean, error bars in panels B,C,E represent standard deviation, error bars in panel D represent standard error of mean (SEM). Number of roots (n) > 15, a biological repeat was performed independently yielding identical conclusions. Statistical differences between 1% and 0% within SL and LL were determined using Student's t-test. 1DAT data of 1% and 0% were compared with 1% 0DAT data for both light conditions. For other subsequent timepoints, 1% was compared with corresponding 0% in each light condition. Asterisk represents a significant difference, "ns" represents a difference that is not significant.

AT) under both light conditions was $\sim 10\mu\text{m}$ ($\pm 0.8\mu\text{m}$ for SL and $\pm 0.7\mu\text{m}$ for LL) and significantly reduced to $8.7\mu\text{m}$ ($\pm 0.8\mu\text{m}$) and $9.3\mu\text{m}$ ($\pm 0.5\mu\text{m}$) on 1% suc and 0% suc under SL 1DAT, respectively (Figure 3.3B). At later timepoints, SL 1% G2/M cell size fluctuated between $9.4\mu\text{m}$ ($\pm 1.2\mu\text{m}$) at 2DAT to $7.7\mu\text{m}$ ($\pm 0.5\mu\text{m}$) at 4DAT and $8.4\mu\text{m}$ ($\pm 0.7\mu\text{m}$) at 5DAT, whilst SL 0% showed a gradual reduction and appeared to become less variant at $\sim 7.7\mu\text{m}$ ($\pm 0.3\mu\text{m}$) during 5 to 6 DAT (Figure 3.3B). G2/M cell size under LL 1% at 2DAT was $10.1\mu\text{m}$ ($\pm 0.7\mu\text{m}$) and plateaued at $\sim 9.3\mu\text{m}$ ($\pm 0.7\mu\text{m}$) during 3 to 5 DAT and reduced to $8.5\mu\text{m}$ ($\pm 0.6\mu\text{m}$) at 6DAT, whilst LL 0% G2/M size remained unaltered during 2DAT and reduced to $9.5\mu\text{m}$ ($\pm 0.2\mu\text{m}$) and did not show any significant difference till 6DAT (Figure 3.3B). The most extreme difference in cell size under SL 1% occurred at 4DAT in which cells were 25% smaller than the starting point (0DAT) and the same percentage difference occurred at 5DAT under SL 0%. In case of LL 1% and LL 0%, the highest percentage reduction was 16% and 8% at 6DAT, respectively.

Additionally, we did not observe any apparent difference between 0% and 1% sugar within the same light condition in size of cycling cells, but a clear difference between the two light intensities was observed (Figure 3.3C). The average cell size of all 1% LL timepoints was $\sim 9.6\mu\text{m}$ ($\pm 0.7\mu\text{m}$) and average 1% SL cell size was $8.7\mu\text{m}$ ($\pm 0.9\mu\text{m}$), a significant difference of $\sim 10\%$; 0% LL cell size was $9.6\mu\text{m}$ ($\pm 0.4\mu\text{m}$) and

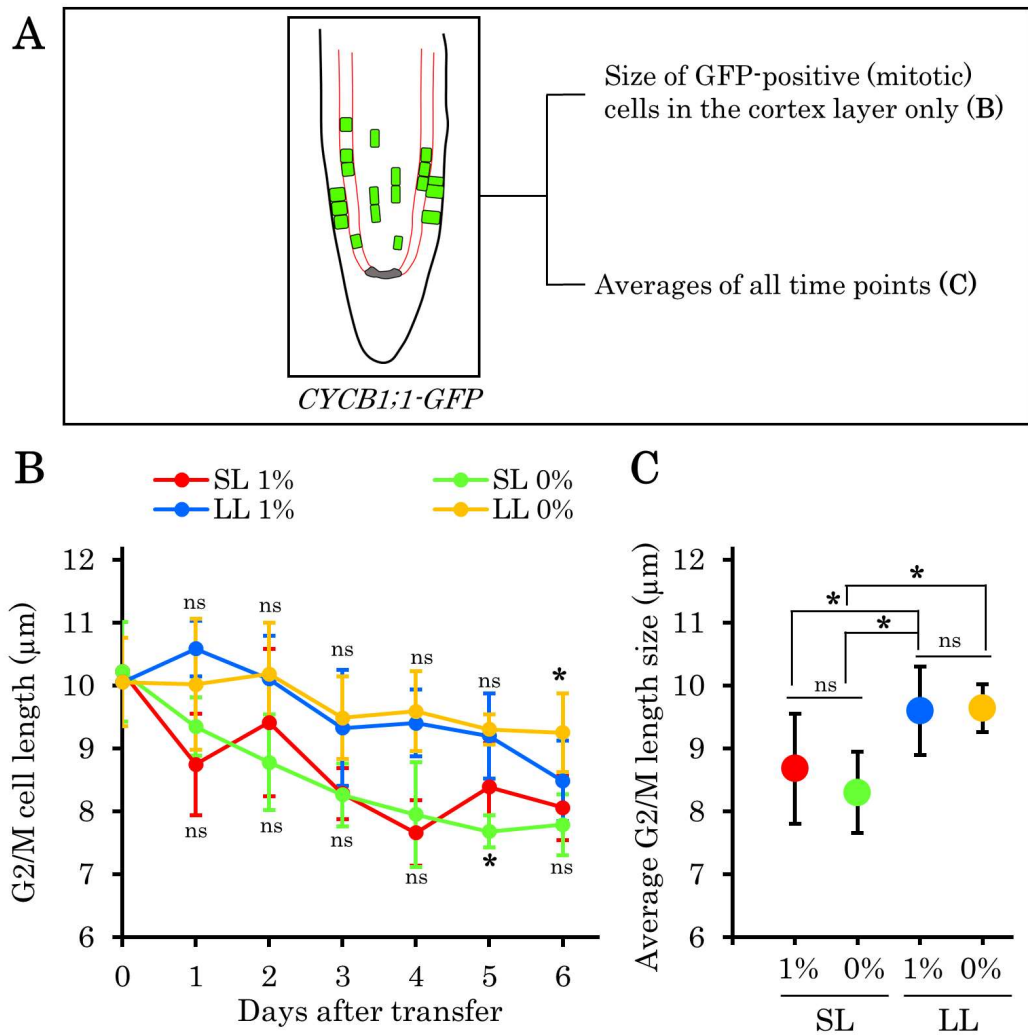


Figure 3.3 Effect of growth conditions on cell size.

A. Schematic of cell length measurements made. Size of *CYCB1;1-GFP* positive cells, representing size at G2/M, was measured in the cortex layer of both sides of the root and averaged for each timepoint.

B. Cortical cell length at G2/M transition in the four growth conditions during the course of experiment.

C. Average G2/M cortical cell length of all timepoints in the four growth conditions.

Data presented as mean, $n > 15$, error bars represent standard deviation. Data used here is from Figure 3.2. a biological repeat was performed independently yielding identical conclusions. Statistical differences between 1% and 0% within SL and within LL were determined using Student's t-test. Asterisk represents a significant difference, "ns" represents a difference that is not significant.

0% SL was $8.3\mu\text{m}$ ($\pm 0.6\mu\text{m}$), a significant difference of $\sim 14\%$ (Figure 3.3C). In summary, exogenous sucrose does not cause an overall change in final size at division, but by comparing size differences between the two light intensities, we found that under low light cells divided at bigger size than under standard light

conditions. This suggests under low light which may reflect nutrient-poor endogenous conditions, cells compensate for reduced cell cycle by increasing division size. Supposedly, this allows the maximum meristem length to be achieved in a cell population with low proliferative capacity which would subsequently maximise growth of primary root. Additionally, the gradual reduction or plateauing of cell size during the course of experiment irrespective of growth conditions suggest that size threshold at division changes during root growth and development and is partially set by light signalling and/or photosynthetic capacity as we saw a clear separation of size distribution between standard light and low light growth conditions.

3.2.3 Cell cycle and cell size in the root meristem changes on an hourly basis

The sucrose transfer experiment in Figure 3.2 showed that the re-adjustment of cell cycle occurs within a period of 24h with low light and standard light having a low and high mitotic count, respectively. This led us to investigate how cell cycle might be altered under light-dark cycles without exogenous sucrose supply since dark in this photoperiod may resemble the sucrose-free LL condition in Figure 3.2. To test this, we followed cell cycle using the mitotic marker without exogenous sucrose supply under 12h light (day) 12h dark (night) cycles with day temperature of 21°C and night temperature of 18°C. The temperature cycle was used to mimic warm days and cool nights plants experience in nature; however, I acknowledge the effect temperature cycles may have on interpreting the effect of light-dark cycles on cell cycle count in the root meristem.

Confocal imaging was carried out every 4h for a 48h period when the seedlings were 6d old, we used the 0h timepoint as the reference point to compare changes at other

timepoints (Figure 3.4A). Number of mitotic cells at 0h (growth chamber lights off) was 15 (\pm 3.1) which increased to 26 (\pm 6.0) cells within 4h after lights are switched on (Figure 3.4B,C). After the 4h peak, there was a gradual decrease in mitotic count from 8h to 20h with a moderate increase afterwards followed by a sharp increase of \sim 45% between 28h and 32h, with 16 (\pm 4.6) cells and 29 (\pm 5.0) cells, respectively (Figures 3.4C, S3.1 – see appendix). The second 32h peak followed another decline but fluctuated at 40h. Overall, average mitotic count during the light period was 22 (\pm 4.9) cells and 16 (\pm 3.6) cells during the dark period, a significant difference of \sim 25% (Table 3.1).

Since SL/LL experiment showed light intensity- and root growth -dependent cell size differences, we next checked whether cell size changes within and/or between light and dark periods and measured length of *CYCB1;1-GFP* positive cells from the same confocal data as in Figure 3.4. At 0h, cell size was 8.3 μ m (\pm 0.7) and increased by \sim 15% to 9.7 μ m (\pm 0.8) at 4h and stayed the same size at 8h and 12h (Figure 3.5A). At 16h and 20h, cell size was 9.1 μ m (\pm 0.5 for 16h and \pm 0.6 for 20h), a modest but significant difference of \sim 7% from the preceding light hours (Figure 3.5A). At 24h, cell size increased to 9.7 μ m (\pm 0.6) and further to 10.1 μ m (\pm 0.7) at 28h; at 32h and 36h cell size was determined to be 9.5 μ m (\pm 0.6 for 32h and \pm 0.7 for 36h) and reduced to 8.8 μ m during the dark hours (Figure 3.5A). Although we noted significant differences from 0h to light-hours and dark-hours, the percentage difference was mostly greater during light-hours. Thus, night-cycling cells divide with a slight, but statistically significant smaller size (9.0 μ m) than cells dividing during the day (9.7 μ m; Table 3.1).

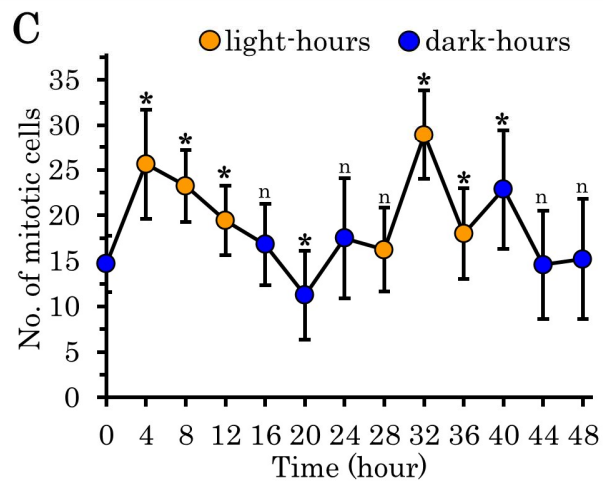
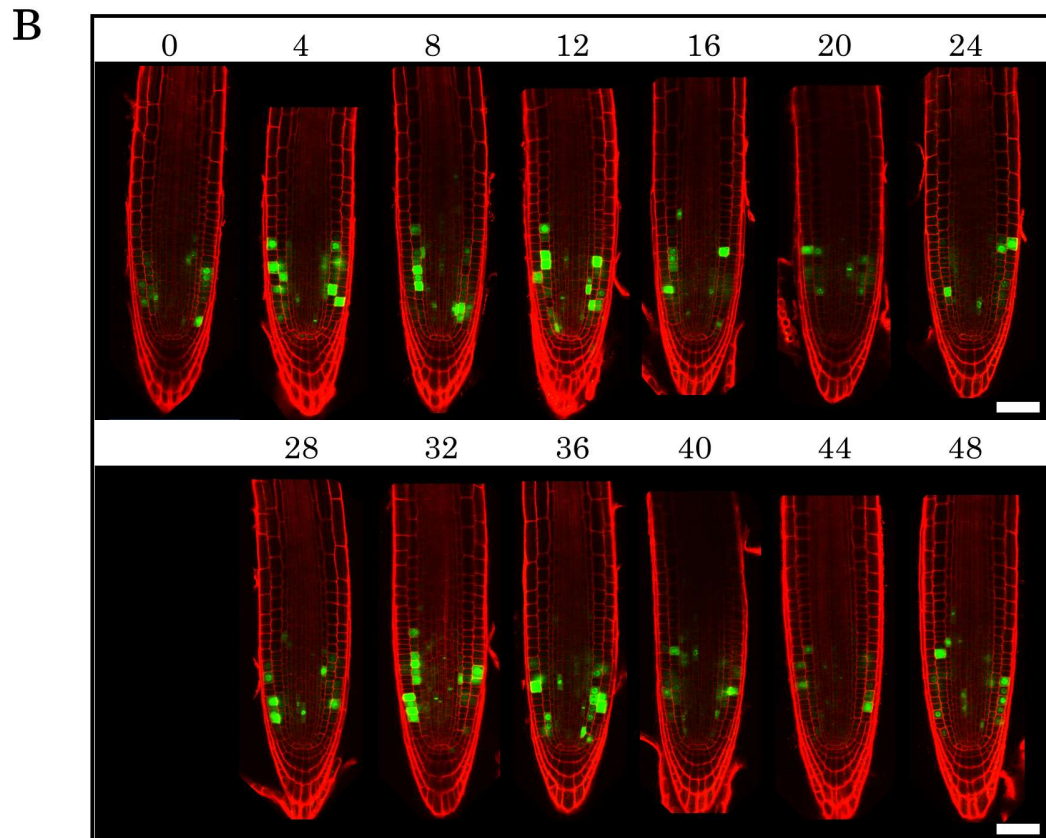
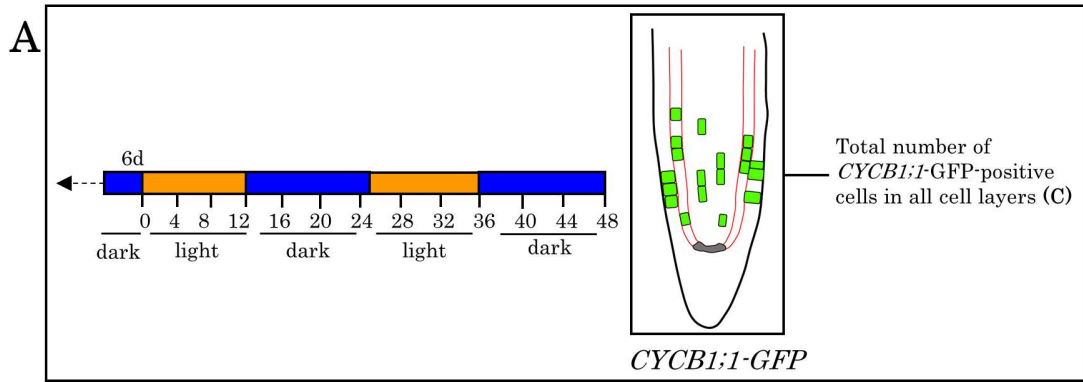


Figure 3.4 Effect of light-dark cycles on cell cycle in the root meristem.

A. Schematic of experimental design. Seeds were sown on sucrose-free MS media under 12h light-dark cycles. All *CYCB1;1-GFP* positive cells were manually counted and the co-

unt for all roots in each timepoint was averaged.

B. Representative confocal micrograph of PI-stained (red) *CYCB1;1-GFP* (green) root tip of each timepoint.

C. Number of mitotic cells at each timepoint during the course of experiment.

Data presented as mean, error bars represent standard deviation. Number of roots (n) > 9. Number of biological repeats (N) = 2. A biological repeat is presented in Figure S3.1. All three repeats yield identical conclusions. Statistical differences between 0h and all other timepoints were determined using Student's t-test. Asterisk represents a significant difference, "ns" represents a difference that is not significant.

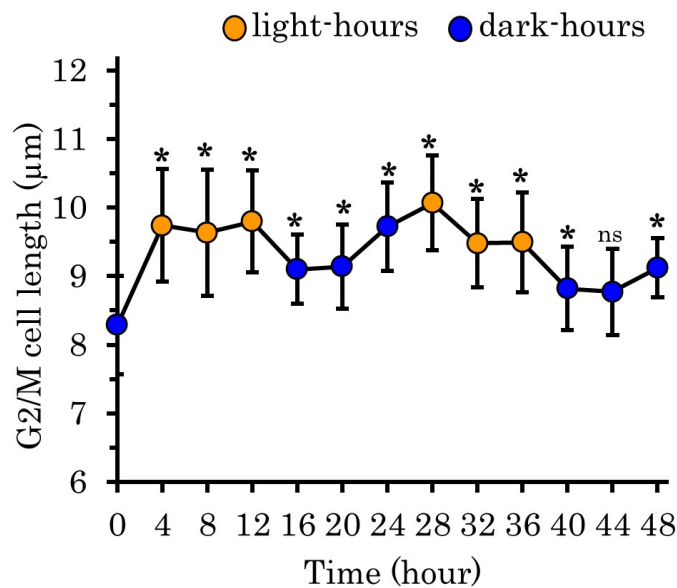


Figure 3.5 Diel changes in G2/M cell size.

Cortical cell length at G2/M transition during diel cycles. Size of *CYCB1;1-GFP* positive cells, representing size at G2/M, was measured in the cortex layer of both sides of the root and averaged for each timepoint.

Data presented as mean, error bars represent standard deviation. Number of roots (n) > 13. Confocal data used here is from Figure 3.4. Statistical differences between 0h and all other timepoints were determined using Student's t-test. Asterisk represents a significant difference, "ns" represents a difference that is not significant.

Since onset of mitosis shows time-of-the-day dependent changes, we asked whether S phase count in the root meristem will behave in the same way. For this, we used 5-ethynyl-2'-deoxy-uridine (EdU) labelling technique under the same experimental system as for the mitotic marker. EdU is a thymidine analogue and incorporates into DNA during replication and is visualised with a fluorescent probe (Buck *et al.*, 2008).

EdU is a versatile cell cycle tool and can be used to label DNA replicating cells in any plant tissue and genotypes (Hayashi *et al.*, 2013).

At 0h, the number of S phase (EdU-positive) cells were 14 (+/- 4.5) which increased by over two-fold to 35 (+/- 6.2) within 4h after growth chamber lights are switched on (Figure 3.6A,B). A similar number of S phase cells were observed at 8h followed by a gradual decline till EdU count reached a similar level as 0h at 20h. A similar pattern of rise and fall in number in EdU cells was observed between 24h and 48h (Figure 3.6B). The average S phase count of all light hours was determined to be 34 (+/- 5.6) cells and an average of 18 cells (+/- 5.5) during dark hours, a significant decrease of 45% (Table 3.1).

Table 3.1 Averages of cellular parameters measured in light-dark experiments.

Parameter	Light-hours (L)	Dark-hours (D)	p-value (L vs D)
S phase count ¹	33.5 (+/- 5.6)	18.4 (+/- 5.5)	0.000549
Mitotic count ²	21.9 (+/- 4.9)	16.1 (+/- 3.6)	0.039285
G2/M cell length ³ (µm)	9.7 (+/- 0.2)	9.0 (+/- 0.4)	0.004500

1. Mean S phase count of all light-hours and all dark-hours in Figure 3.6 were averaged, standard deviation is presented in the parenthesis.

2. Mean mitotic count of all light-hours and all dark-hours in Figure 3.4 were averaged, standard deviation is presented in the parenthesis.

3. Mean G2/M cell length of all light-hours and all dark-hours in Figure 3.5 were averaged, standard deviation is presented in the parenthesis.

In summary, the daily oscillation of cell cycle with peak count during the day and trough during the night suggests a functional diurnal rhythm of cell cycle. This is implied from the observation that the starting point (0h and 24h in Figure 3.6B) of S phase cells reaches after a 20h cycle (0h to 20h and 24h to 44h in Figure 3.6B) in a gradual way coupled with the observation that most of the S phase and mitotic events (Figures 3.4 and 3.6) occur during the light part of the light-dark cycles. Furt-

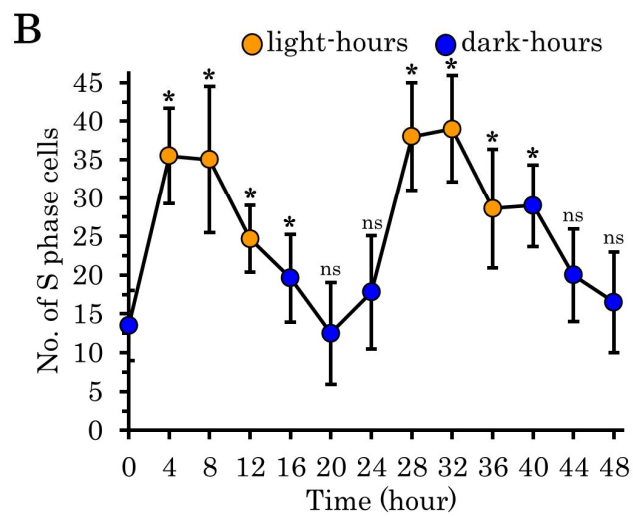
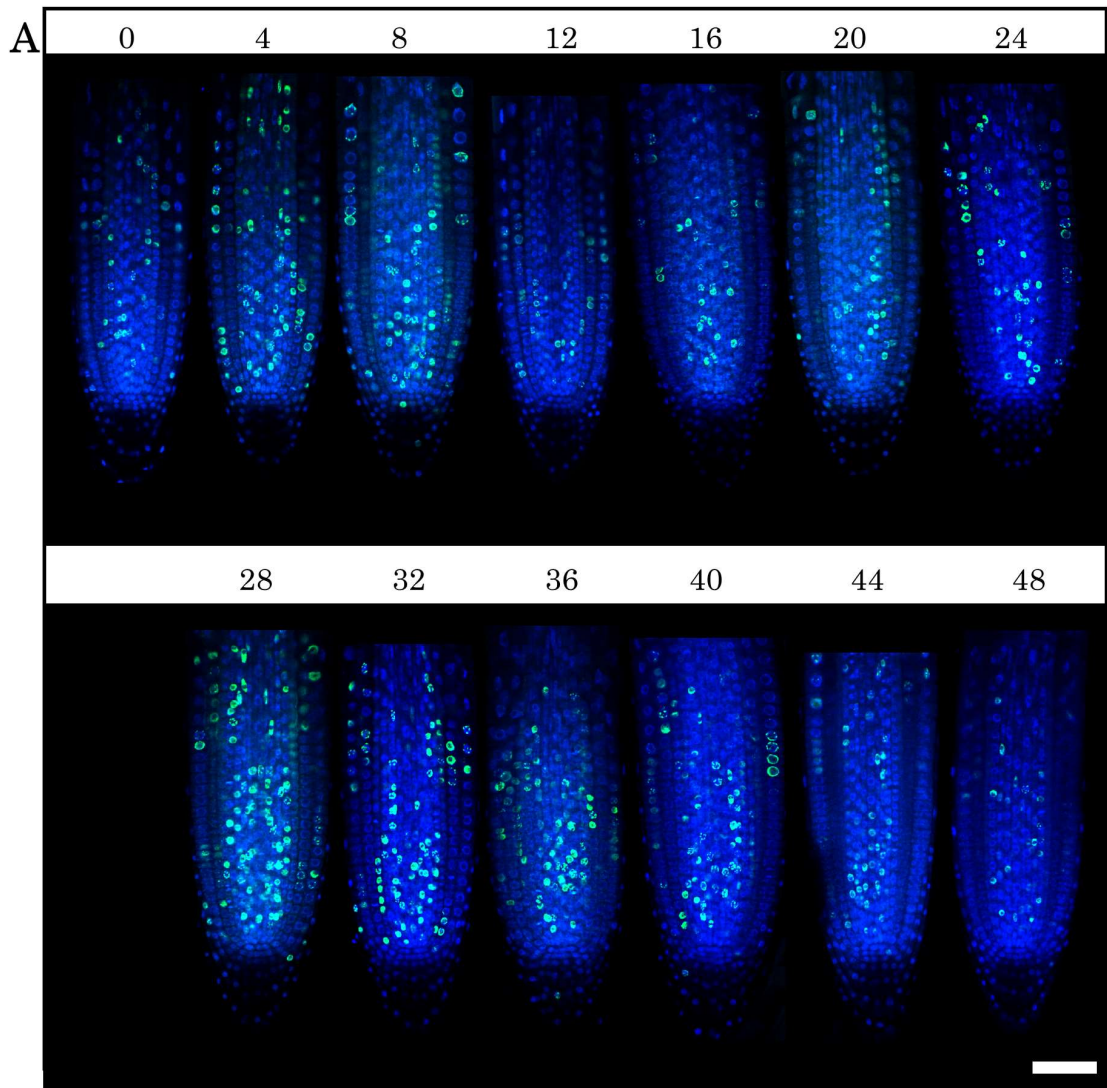


Figure 3.6 Diel changes in number of DNA replicating cells in the root meristem.

A. Representative confocal micrograph of DAPI-stained (blue) EdU-labelled (green) root tip of each timepoint.

B. Number of S phase (EdU-positive) cells at each timepoint during the course of experiment. EdU-positive cells were counted in all layers of the root meristem. Data presented as mean, error bars represent standard deviation. Average number of roots (n) > 7. Statistical differences between 0h and all other timepoints were determined using Student's t-test. Asterisk represents a significant difference, "ns" represents a difference that is not significant.

her investigation into duration of cell cycle during the day and the night should reveal cellular mechanistic insight into diel control of root meristem.

3.2.4 Diel pattern of E2FA and E2FB protein accumulation may create temporal changes in S phase

E2FA and E2FB have different regulatory roles throughout the cell cycle and so we next explored their protein levels during a day-night cycle. To this end, we collected 7d- old seedlings every 4h for a 24h period under 12h light-dark cycles and measured endogenous E2F protein amount using E2FA- (Leviczky *et al.*, 2019) and E2FB-specific antibodies (Magyar *et al.*, 2005). E2FA accumulated early in the morning with maximal level at 4h and followed a gradual decline till 16h and started to rise at 20h whilst E2FB showed low amount from 0h to 8h, with an increased level at 12h to 20h and a decrease afterwards (Figures 3.7, S3.2 – see appendix).

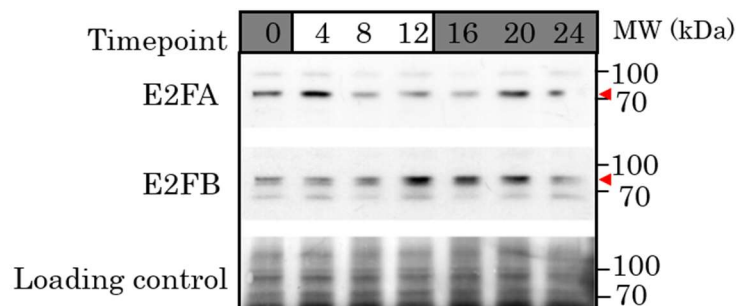


Figure 3.7 Differential accumulation of E2FA and E2FB proteins.

Endogenous E2FA and E2FB protein abundance in whole-seedlings during light-dark cycle was determined using specific antibodies against the two E2Fs. Number of biological repeats (N) = 2. A Western blot with E2F-GFP lines using GFP antibody is presented in Figure S3.2. For antibody dilution, see Table 2.2.

In short, E2FA and E2FB protein abundance show an almost anti-phasic pattern with E2FA peaking during “morning” hours and end-of-night corresponding to high cell cycle count and E2FB peaking towards the end-of-day and night corresponding to decline in cell cycle count. A similar anti-phasic pattern was observed with mRNA level of *E2FA* and *E2FB* obtained from an online data repository (Figure S3.3 – see appendix). We theorised that E2FA is needed in the morning to stimulate light/sugar-driven cell cycle induction and E2FB acts to limit cell cycle entry during end-of-day/dark hours. To test this idea, we carried out EdU labelling in different T-DNA insertion mutants of *e2fa* and *e2fb* described in detail by Leviczky and colleagues (2019; also see Figure 2.1). Since in wild-type we observed a low S phase count at 0h with a two-fold increase at 4h and then a significant decrease at 12h (Figure 3.6B), we only focused on an early timepoint of 3h and a later one of 12h to examine EdU frequency in the *e2f* mutants.

As expected, wild-type Col-0 EdU count increased by nearly three-fold from 17 (+/- 4.7) cells at 0h to 49 (+/- 8.7) cells at 3h and subsequently reduced by ~40% to 26 (+/- 11.0) cells at 12h (Figure 3.8A, B). At 0h, S phase count of *e2fa-1*, *e2fa-2*, *e2fa-3* was 22 (+/- 7.6), 24 (+/- 10.7), and 32 (+/- 10.0) cells, respectively. *e2fa-1* showed a moderate increase at 3h and reduction at 12h, whilst *e2fa-2* and *e2fa-3* did not show any significant change at 3h but decreased at 12h (Figure 3.8A, B). S phase count of *e2fb-1* and *e2fb-2* at 0h was 46 (+/- 8.4) and 53 (+/- 8.7) cells, respectively and *e2fb-1* did not show any change at 3h and 12h whilst *e2fb-2* increased to 69 (+/- 10.9) cells at 3h and reduced to 56 (+/- 11.2) cells at 12h (Figure 3.8A, B). Overall, *e2fa* mutants have a low S phase count when WT count is high and *e2fb* mutants have higher number of S phase cells when WT count is less. Considering matching time window of E2FB accumulation and high S phase count in the *e2fb* mutants, we propose that

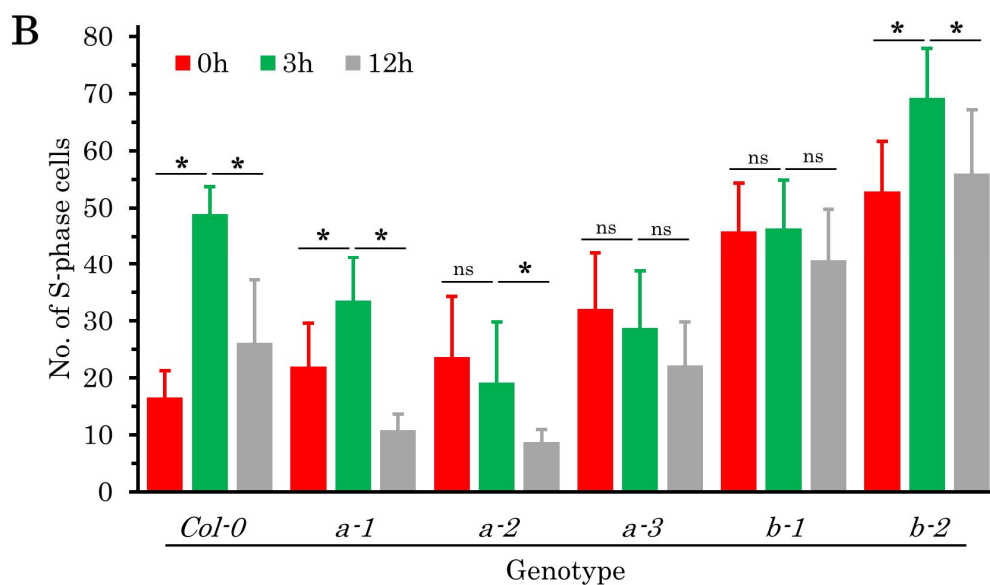
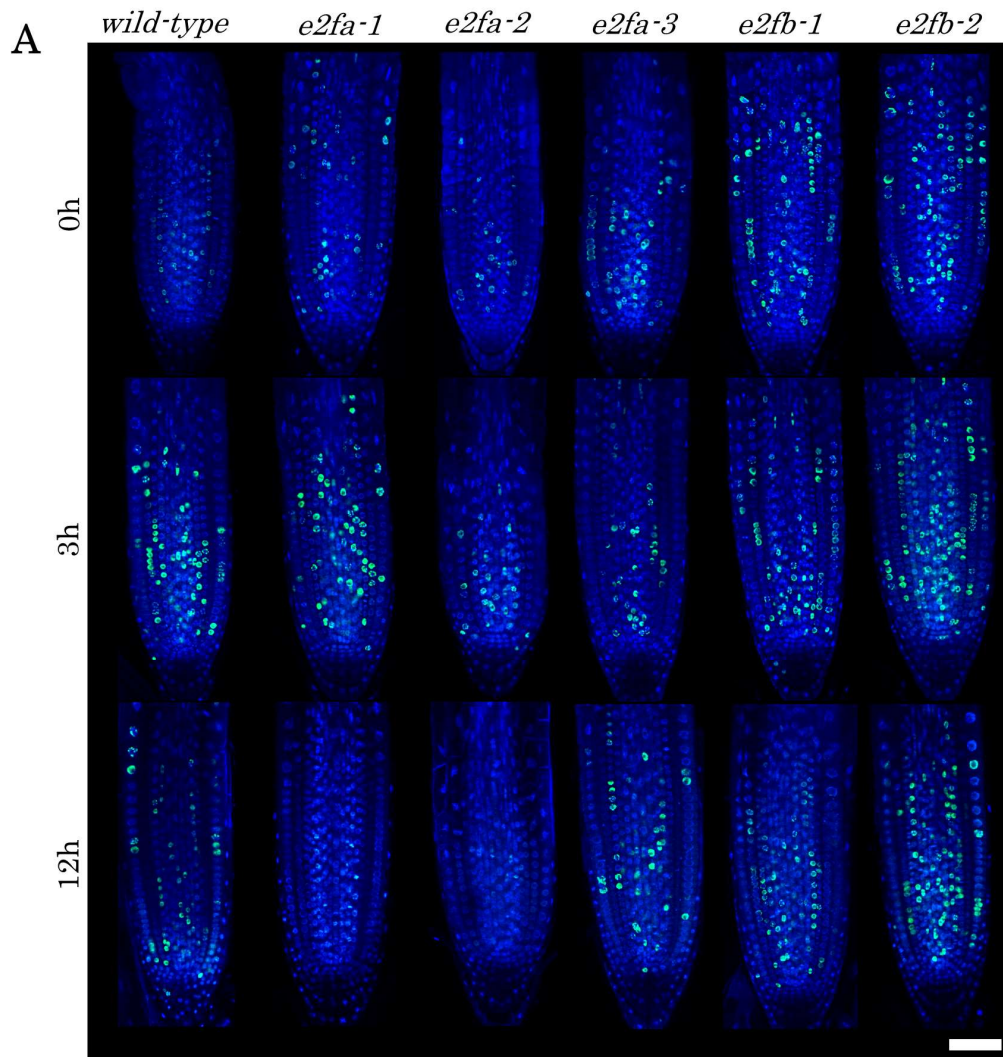


Figure 3.8 S phase count in *e2fa* and *e2fb* mutants.

A. Representative confocal micrographs of DAPI-stained (blue) EdU-labelled (green)

root tip of each timepoint and mutant.

B. Number of S phase (EdU-positive) cells of each *e2fa* and *e2fb* mutant at the three time points. EdU-positive cells were counted in all layers of the root meristem.

Data presented as mean, error bars represent standard deviation. Average number of roots ($n > 10$). A biological repeat was performed with *e2fa-1* and *e2fb-2* yielding identical conclusions. Statistical differences were determined using Student's t-test. Asterisk represents a significant difference, "ns" represents a difference that is not significant.

E2FB acts to limit cell cycle entry at the end-of-day whilst E2FA is required in the morning to trigger light/sucrose-dependent cell cycle.

Consistent with Hypotheses 1 and 2 stated in section 1.9, I showed that cell cycle in the root meristem is dynamic such that cell cycle is tuned to sucrose, light intensity and light-dark cycles.

3.3 Discussion

Quantitative characterisation of cell cycle in the *Arabidopsis* root meristem using S phase EdU labelling and *CYCB1;1-GFP* mitotic marker revealed a remarkable rheostatic-like tuning of cell cycle to light, sugar availability, and day-light cycles such that high sugar availability (standard light, 1% sucrose, light part of the light-dark cycle) results in high mitotic count compared to low mitotic count observed in low-light sucrose-free and dark part of the light-dark cycles.

Of noteworthy, the average cell length of both light-hours and dark-hours (Figure 3.4D) resembles that of averaged low-light cell length as supposed to averaged cell length of standard-light timepoints (Figure 3.3C). Whilst it is clear that exogenous sucrose supply had no clear affect on length of *CYCB1*-positive cells (Figure 3.3C), the similarity between light-dark cycle and low-light suggests that total luminous

flux might play a role in determining cell growth rate. It would be of interest to pursue this experimentally by carrying out cell length measurements under different light intensities of under constant light and 12h photoperiod.

Interestingly, under continuous light regime, exogenous sucrose supply had no clear effect on cell size. Rather, the differences were more pronounced between standard light and low light conditions such that G2/M cells were larger under LL than under SL. Coupling this observation with the mitotic count under LL suggests that root meristem compensates for reduced mitotic count by increasing size at which cells divide. This is different to observations made in yeast and mammalian cells where poor nutrient conditions lead to smaller cells (Petersen and Nurse, 2007; Lloyd, 2013).

Conceptually, a similar compensatory phenomenon has been observed in *an3-4* mutant leaves where decrease in cell proliferation results in increased post-mitotic cell expansion (Kawade *et al.*, 2010), and in petals of *rbe-1* mutant (Huang and Irish, 2015). Primary roots also exhibit compensatory behaviour as seen in the *aak6* mutant where reduced meristematic cell division increases mature cell length (Slovak *et al.*, 2020). Whilst these studies show a remarkable similarity of cellular responses between different plant organs, we specifically focused on size of *CYCB1*-positive cells within the meristem region and found an inverse-like relationship under constant light between number and size of mitotic cells suggesting the compensation mechanism may be active at both inter- and intra-tissue level. For example, Slovak and colleagues (2020) focused on relationship between meristematic cell number and cell length of mature cells and found an inverse relationship in the *aak6* mutant that has fewer meristematic cells which is accompanied with increased cell mature cells (Slovak *et al.*, 2020). Whilst this is a different cellular approach as we focused on comparison between size and number of cells within the same tissue

(root meristem), this suggests that cellular principles in shaping final organ size (primary root) work coherently across different root tissues.

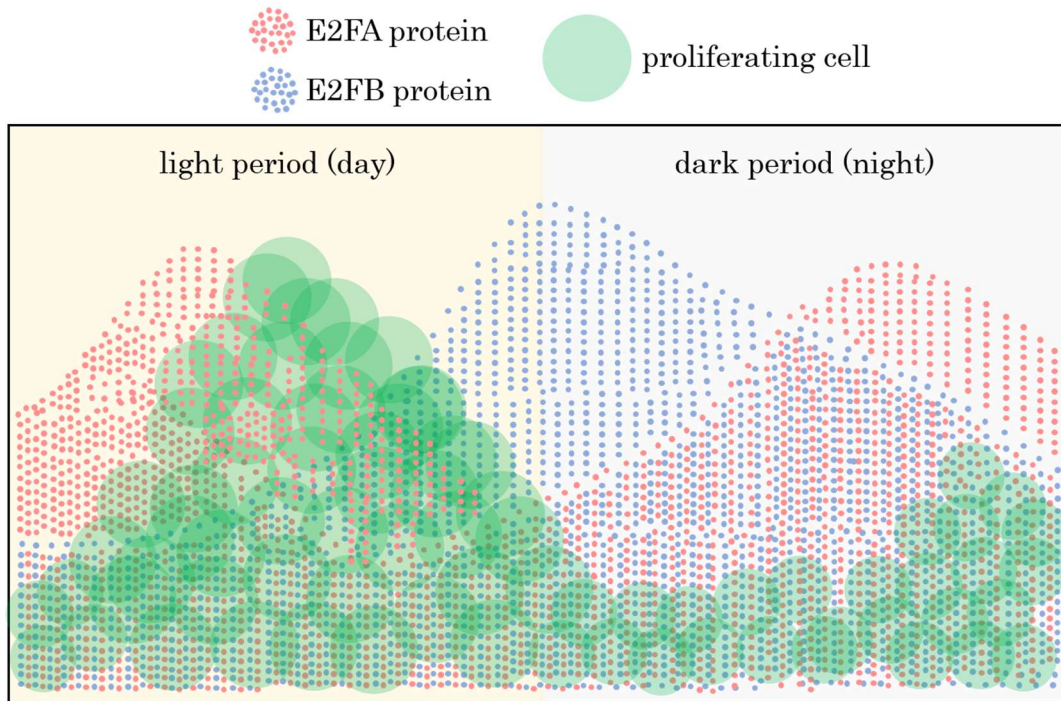


Figure 3.9 Schematic summary of diel dynamics of cell cycle and E2F protein accumulation.

Cell cycle (green circle) predominantly occurs during the day with mild occurrence towards the end-of-night. Cells dividing during the light hours are considered larger than cells dividing during the dark hours as depicted by relative size of green circle. The high cell cycle count corresponds with high protein accumulation of E2FA (red circle) whereas low cell cycle count corresponds with high E2FB (blue circle) levels. Taken together, we proposed that E2FA is required during the light period to trigger cell cycle whilst E2FB limits cell cycle at the end-of-day and during the night.

Time-course analysis of cell size determined that size threshold at G2/M is not fixed, but changes during root growth and development, irrespective of growth condition. For example, we found a general downward trend such that 10d old dividing cells are much smaller than 5d old dividing cells. The reduced cell size phenotype of old roots compared with younger roots can be explained by CDK threshold amount required to progress through mitosis. Mutants with supposedly low CDK activity, such as *cyd3;1-3* triple and *cdkb1;1/1;2* double, have larger SAM cells compared

with *CYCD3;1*-overexpressing line that has smaller cells (Jones *et al.*, 2017). As young seedlings grow and develop leaves, photosynthate availability is presumably higher, leading to increased CYCD production and the resultant enhanced CDK activity. Thus, older roots have smaller cells due to less time it takes to meet the required CDK activity to progress through G1/S and G2/M transitions.

Whilst 12h light-dark cycles are a popular choice to study diurnal and circadian rhythms (McClung, 2006), a high temporal resolution of cell division and cell size dynamics is missing. Both of these cellular events are key determinants of final organ size (Gázquez and Beemster, 2017) and a better understanding of these events are likely to improve crop yield in the future (Gonzalez *et al.*, 2009). To fill this gap in knowledge, we investigated diel changes of cell cycle under 12h light-dark cycles without sucrose supplementation, and found cells predominantly enter S phase and mitosis during light (day) hours. The spike in cell cycle events in the meristem during the day could be due to photosynthesis-derived sugars being transported to the root, and reduced sugar availability at night through starch metabolism leading to suppression of cell cycle. In support of this view, the sugar transporter SWEET2 shows a high expression in the root and the *sweet2* mutants have a smaller meristem (Chen *et al.*, 2015). Additionally, the starchless mutant *pgm* has little-to-no cell cycle events in the root meristem during the night (personal observation, unpublished).

To elucidate possible molecular basis of diel dynamics of cell cycle, we focused on E2F transcription factors and found that *e2fa* mutants do not show increase in S phase count during light hours whereas *e2fb* mutants lose end-of-day dependent decrease in S phase count. Coupling this finding with the observation that E2FA protein accumulates most during the day whilst E2FB peaks during the night suggest that these two E2Fs act antagonistically to create a diurnal rhythm of cell cycle. Thus, according to this model, E2FA would be required in the morning to

trigger S phase gene expression, and E2FB limits cell cycle progression in the evening (Figure 3.9). Whilst E2FB is traditionally viewed as a positive regulator of cell cycle, when bound to RBR, E2FB acts as negative regulator as evident from decreased leaf epidermal cell count (Oszi *et al.*, 2020). Future Co-IP studies are likely to shed light on differential complex formation between E2FA and E2FB during day-night cycles.

The diurnal rhythm of cell cycle is coupled with hourly changes in G2/M size, such that day-dividing cells are considerably larger than night-dividing cells. Whilst we unexpectedly found that the *Arabidopsis* root meristem undergoes these diel changes in cell size, a similar observation was made in the *Synechococcus elongatus* photosynthetic bacterial cells (Martins *et al.*, 2018). A hallmark of the timer model of size-homeostasis is that cell growth occurs for a fixed period and a sizer model suggests that cells 'wait' till a certain size is reached before progressing through the cell cycle (Facchetti *et al.*, 2017; Jones *et al.*, 2019). Coupling this to our observation that G2/M size remains constant during the day (Figure 3.5A) and most of cell cycle events occur within a short time-window of the light period (Figures 3.4 and 3.6), we think root meristematic cells likely coordinate cell cycle progression and cell growth through a sizer that works at G1/S, followed by a G2/M timer mechanism to achieve cell size homeostasis.

4

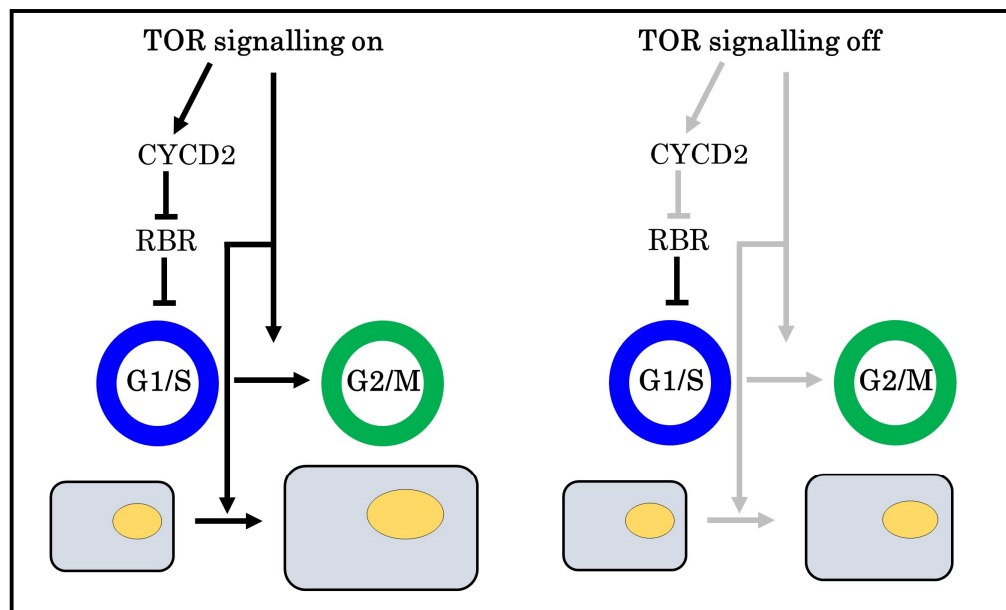
Chapter 4 TARGET OF RAPAMYCIN signalling pathway regulates sugar-induced progression through the cell cycle

Declaration – Western blots in Figures 4.6, 4.10, and 4.12 were performed by Csaba Papdi.

Zaki Ahmad*, Csaba Papdi*, Zoltan Magyar, Laszlo Bogre. TOR signalling pathway regulates cell cycle by mediating phosphorylation of RBR. Manuscript in preparation.

TARGET OF RAPAMYCIN signalling pathway regulates sugar-induced progression through the cell cycle

In this chapter, I investigated the role of TOR signalling in context of cell growth and cell cycle progression under 12h day-night cycles.



TOR activity is required for cell cycle progression and cell growth

In a nutshell

- Chemical inhibition of TOR signalling by AZD8055 leads to dramatic lowering of primary root growth rate and meristem size
- AZD8055 treatment lengthens cell cycle period and reduces the size of dividing cells
- TOR inhibition rapidly decreases S phase count and onset of mitosis, implying TOR activity is required for both G1/S and G2/M transitions
- TOR activity promotes protein accumulation of CYCD2
- TOR regulates G1-to-S phase transition by regulating phosphorylation of RBR

4.1 Introduction

TOR signalling pathway is the principle regulator connecting growth signals with growth processes such as cell proliferation and protein synthesis-driven cell growth and thus ensuring cell size homeostasis. In *Arabidopsis*, signals that increase TOR kinase activity, as measured *in vivo* from phosphorylation of its prime target S6K1, include sucrose and glucose availability, light, auxin, amino acids (Xiong and Sheen, 2014; Dobrenel, Caldana, *et al.*, 2016; Wu *et al.*, 2019; O'Leary *et al.*, 2020). Sugar production through photosynthesis reflects energy status, indeed a large proportion of *Arabidopsis* transcriptome responds to changing sugar levels (Bläsing *et al.*, 2005; Smith and Stitt, 2007; Usadel *et al.*, 2008). Additionally, sugar-starved seedlings rapidly trigger cell cycle gene expression and progress through the cell cycle when treated with sucrose and/or light (López-Juez *et al.*, 2008; Mohammed *et al.*, 2018).

Although the precise series of molecular events connecting sugar availability to cell cycle entry are not fully delineated, D-type cyclins were shown to be positively regulated by sugar availability suggesting that sugar-sensing signalling pathways may be involved in CYCD regulation. mRNA and protein level of *CYCD2* and *CYCD3* respond rapidly to sucrose supply and dramatically reduce upon sucrose removal (Riou-Khamlichi *et al.*, 2000; Healy *et al.*, 2001). Furthermore, *CYCD2;1* and *CYCD3;1* were shown as binding partners and activators of PSTAIRE-containing CDKA, but not of the mitotic CDKB, and the CYCD-CDKA complex was shown to phosphorylate RBR (Healy *et al.*, 2001; Nakagami *et al.*, 2002). Additionally, *CYCD2;1-GFP* translational fusion line showed that the CYCD2 protein is strongly present in all cell-types of the root meristem and is sensitive to sucrose availability (Sanz *et al.*, 2011), whether CYCD2 accumulation shows diel changes is not known. In a brief simplistic view, G1/S entry is strongly dependent on sugar availability

which promote the accumulation of D-type cyclins that result in the inhibition of RBR cell cycle repressor function, and thus allows S phase gene expression through E2FA transcription factor. The upstream signalling pathway involved in the CDKA-CYCD-RBR linear model is not fully delineated.

Due to embryo lethality of *tor* mutant and limited use of transgenic *TOR* lines with altered expression level, deeper understanding of the inputs and outputs TOR signalling network has largely relied on ATP-competitive chemical inhibitors such as AZD-8055 and TORIN (Montané and Menand, 2019). Although these TOR inhibitors were designed to target the mammalian TOR, they have been shown to be specific for inhibiting *Arabidopsis* TOR function (Montané and Menand, 2013). For instance, AZD led to inhibition of primary root growth and meristem shortening in a dose-dependent manner (Montané and Menand, 2013). Due to absence of critical amino acids in the *Arabidopsis* FKBP12, rapamycin does not have an inhibitory effect on TOR activity in most commonly used experimental conditions (Menand *et al.*, 2002; Mahfouz *et al.*, 2006; Sormani *et al.*, 2007). However, rapamycin was shown to inhibit TOR activity as detected from Thr-449 S6K1 phosphorylation under extreme growth conditions at a very high concentration (Xiong and Sheen, 2012).

A CYC-CDK-RBR independent pathway was proposed where TOR kinase was identified to phosphorylate E2FA and E2FB directly, connecting glucose availability to transcriptional changes which trigger S phase entry (Xiong *et al.*, 2013). Whether CYC-CDK and RBR are involved in TOR signalling is not explored. A recent phosphoproteomics study identified RBR phospho peptides that were sensitive to AZD, but not rapamycin, suggesting RBR involvement in TOR dependent control of cell cycle (Van Leene *et al.*, 2019). Thus, it appears that TOR-E2FA/B model is probably specific to the experimental system used. Whilst the E2FA connection puts TOR as a G1/S regulator, whether TOR signalling is required for G2-to-M phase

transition is not known. In this regard, some mitotic genes such as *B1*-type *CYC* and *B2*-type *CDK* are among the down-regulated genes in *amiR-tor* silencing lines (Caldana *et al.*, 2013), however, direct cellular evidence for TOR-G2/M connection is missing.

Whilst the role of TOR signalling in cell cycle regulation has been explored widely, no study to date has investigated whether TOR is involved in G2/M transition as well as quantitative temporal changes on cell cycle progression upon chemical inhibition of TOR under light-dark cycles. In this chapter, we aim to more precisely dissect the involvement of TOR signalling in S phase progression and onset of mitosis. We also did experiments to understand how TOR affects cell cycle duration. Additionally, we checked whether *CYCD2*, a major sugar-responsive cyclin, protein accumulation requires TOR activity as well as effect of TOR inhibition on phosphorylation of RBR. An alternative model is proposed to explain TOR regulation of G1/S transition and G2/M connection, as well as how TOR signalling may be involved in cell size homeostasis.

4.1.1 Aims and objectives

The overarching aim of this chapter is to elucidate cellular and molecular control of the root meristem by the TOR signalling pathway.

Aim 1. characterise effect of TOR inhibition, through AZD-8055 treatment, on cell cycle under different growth conditions

Accompanying objective: Utilise *pCYCB1;1:CYCB1;1-db-GFP* marker line to measure number of mitotic cells in different light intensities and concentrations of exogenous sucrose upon AZD-8055 treatment

Aim 2. determine whether cell cycle length is altered in response to TOR inhibition

Accompanying objective: Carry out EdU labelling with different incubation periods of EdU as described by Hayashi and colleagues (2013)

Aim 3. determine whether diurnal rhythm of cell cycle (shown in chapter 3) is altered by exogenous sucrose supply and/or TOR inhibition

Accompanying objective: carry out timecourse experiment with EdU labelling and the mitotic marker under the same experimental system as Figure 3.4 and transfer seedlings to different sucrose concentrations supplemented with/without AZD

Aim 4. determine whether RBR protein is part of the TOR-cell cycle network

Accompanying objective: measure sensitivity of the RBR silencing line (*amiRBR*) to AZD at the level of S phase count and determine whether RBR phosphorylation amount changes in response to TOR inhibition

4.2 Results

4.2.1 Sugar/light-induced increase in mitotic count requires TOR signalling pathway

The tuning of cell cycle in the root meristem to light intensity and sugar availability (Figure 3.2) implies an active control of cycle control in response to growth cues. Indeed, work by others have revealed TARGET OF RAPAMYCIN (TOR), a Ser/Thr protein kinase, as a master regulator which functions to connect growth signals to cellular processes. As the *tor* null mutant is embryo lethal, ATP-competitive inhibitors such as AZD-8055 (hereafter referred to as AZD) designed as anti-cancer

drugs for mammalian TOR have been shown to specifically inhibit the activity of *Arabidopsis* TOR (Montané and Menand, 2013, 2019; Dobrenel, Mancera-Martínez, *et al.*, 2016). AZD is commonly used to study diverse plant TOR functions at a concentration of 1 μ M (Montané and Menand, 2013).

To show TOR signalling is required for sugar-dependent increase in mitotic cells, we studied the effect of different exogenous sucrose concentrations on cell cycle as visualised by *CYCB1;1GFP* mitotic marker in the root meristem and TOR inhibition through 1 μ M AZD. Mitotic marker seeds were sown on sucrose-free media under continuous low light and at 7d, transferred similar sized seedlings to different sucrose concentrations (0%, 0.5%, 1%, 2%, 3%) and 1 μ M AZD in each sucrose concentration for 1d (Figure 4.1A). Within 0% samples, the number of mitotic cells at 7d and 8d on average increase from 6 to 10 cells (Figure 4.1B,C), this may be due to natural kinetics of root growth as seen in Figures 3.1, 3.2 or as a result of the transfer to fresh plates. We then examined whether exogenous sucrose supply causes a further increase in the number of mitotic cells and thus we compared 0% 8d samples to the four sucrose concentrations. We did not see a significant difference between 0% to 0.5% or 1% sucrose samples, implying that exogenous sucrose supply at those concentrations do not enhance proliferative potential of the root meristem. However, there was a significant increase of 32% in mitotic cell count between 0% and 2% sucrose, and no further significant increase at 3% sucrose (Figure 4.1B,C). This identifies 2% as an ideal sucrose concentration under low nutrient growth conditions which enhances cell cycle count and can be used to study sugar-sensing signalling pathways.

As expected, the TOR inhibitor AZD causes a significant reduction in the number of mitotic cells at all sucrose concentrations (panels 1B,C). We found a ~70% reduction

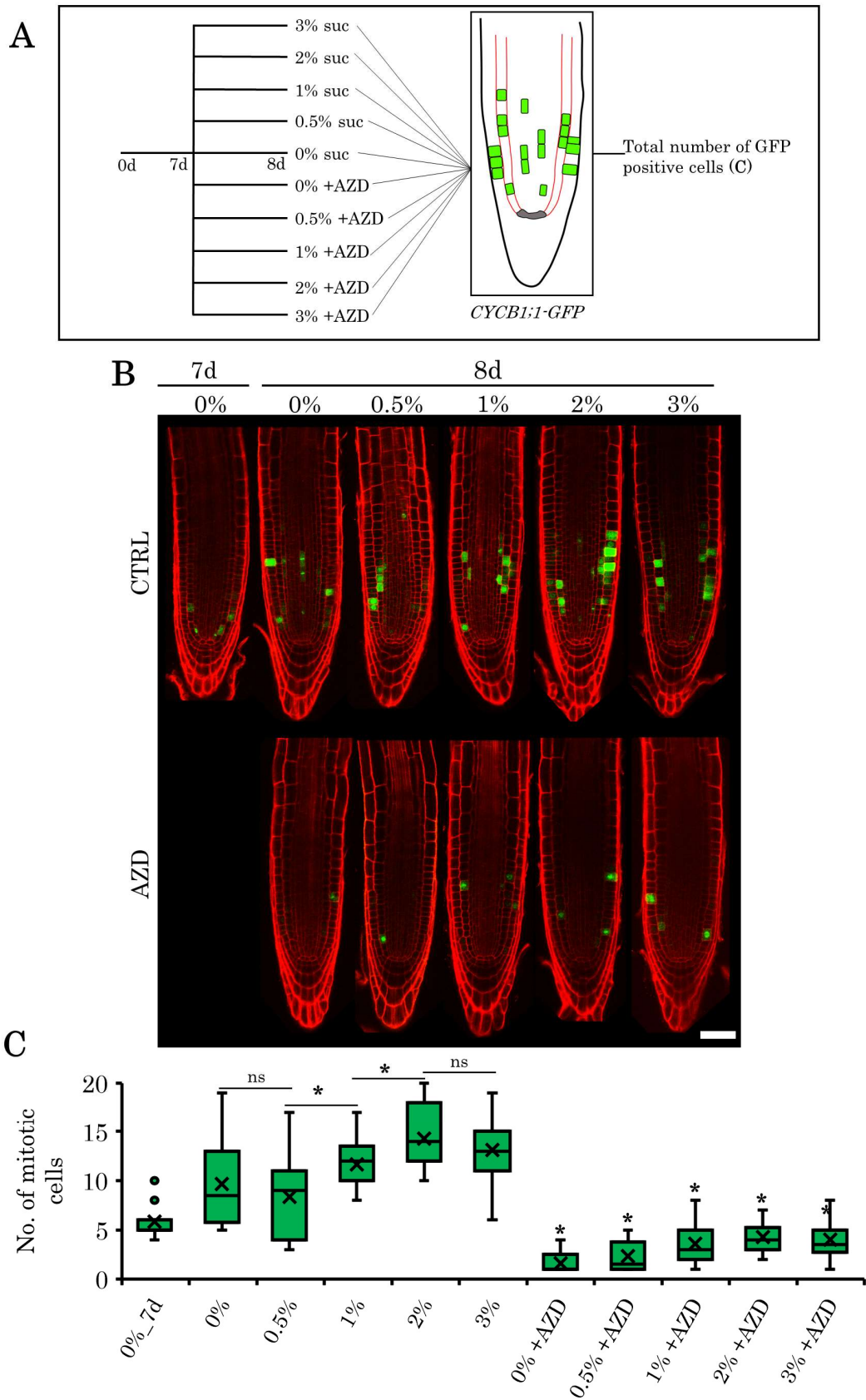


Figure 4.1 Inhibition of TOR suppresses sugar-dependent increase in mitotic activity.

A. Schematic of experimental design. *CYCB1:1-GFP* seeds were sown on sucrose-free

media under low light growth condition and transferred to different sucrose concentrations with or without 1 μ M AZD at 7d. Confocal images were taken 1d after transfer and total number of *CYCB1;1-GFP*-positive cells were counted.

B. Representative confocal micrograph of PI-stained (red) *CYCB1;1-GFP* (green) root tip of each growth condition. Scale bar = 50 μ m

C. Box plots of mitotic count for each sucrose and AZD treatment.

Average number of roots (n) = 13. Number of biological repeats (N) = 1. Statistical differences between sucrose and sucrose + AZD were determined using Student's t-test. Asterisk represents a significant difference, "ns" represents a difference that is not significant.

in the number of mitotic cells at all sucrose concentrations upon 1 μ M AZD treatment, suggesting TOR activity is required for sucrose-induced promotion of cell cycle. This led us to ask 1) whether light intensity dependent effect on cell cycle (Figure 3.2) also requires TOR activity and 2) whether cell cycle under low light could be increased by exogenous sucrose and 3) to what extent this requires activity of TOR signalling. To answer these scenarios, we used the same experimental system as in Figure 3.2 and counted number of mitotic cells 1d after transfer at 7d (Figure 4.2A). Under standard light, exogenous sucrose supply did not cause any significant change in number of mitotic cells, but interestingly increased the meristem boundary by 25% whilst AZD reduced both the mitotic count and meristem size ~50% and 35%, respectively (Figure 4.2B-D). Under low light, exogenous sucrose doubled the number of mitotic cells and increased meristem size by 35% whilst this increase was largely blocked by AZD (Figure 4.2B-D). This was expected as we showed in Figure 4.1 that any sucrose-dependent increase in mitotic count requires TOR activity.

Taken together, the dramatic cell cycle response to the sucrose-free and sucrose-containing media irrespective of growth condition implies that endogenous and exogenous sugar-induced enhancement of cell cycle requires the activity of TOR signalling pathway.

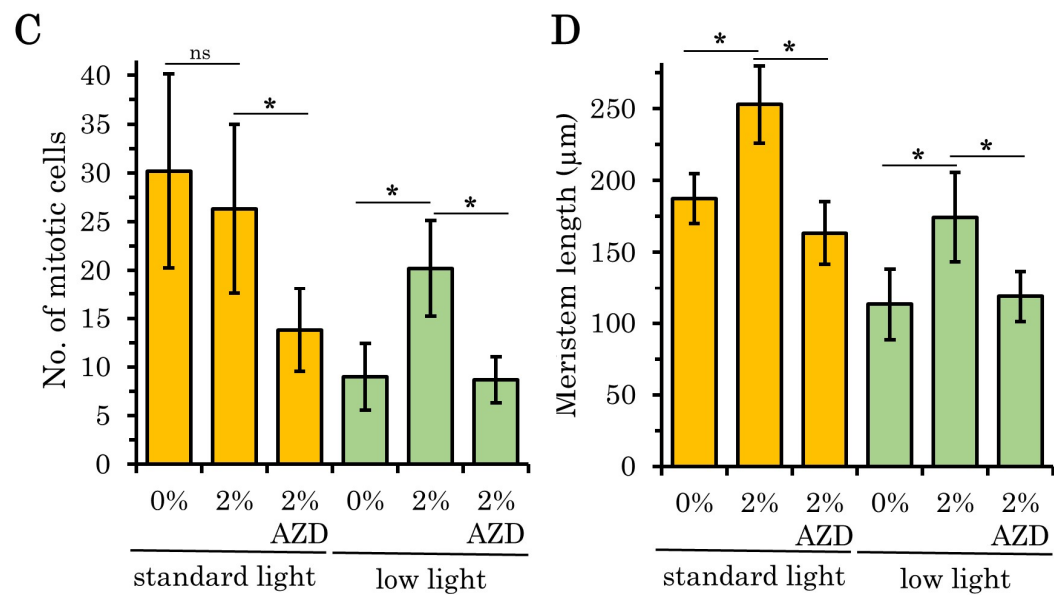
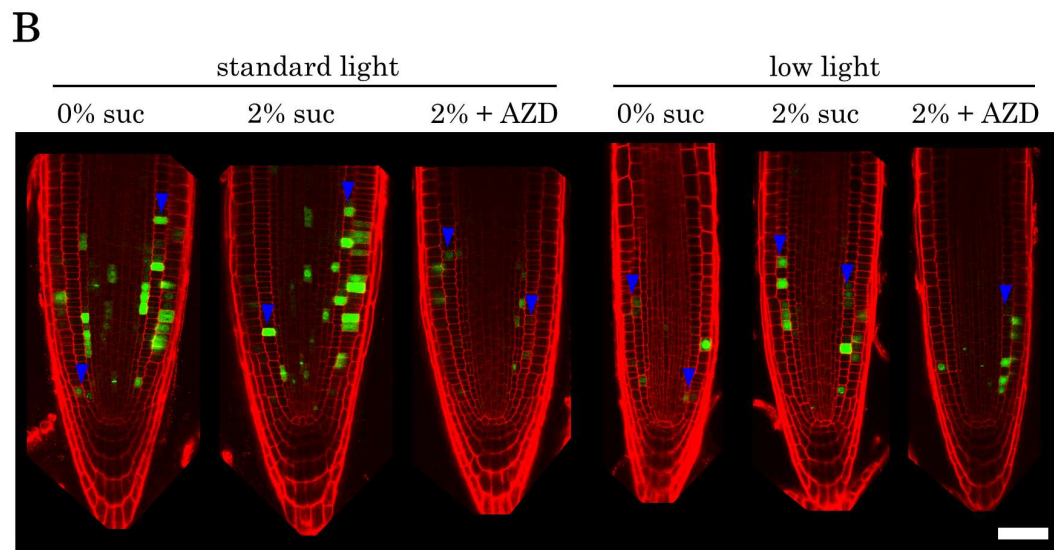
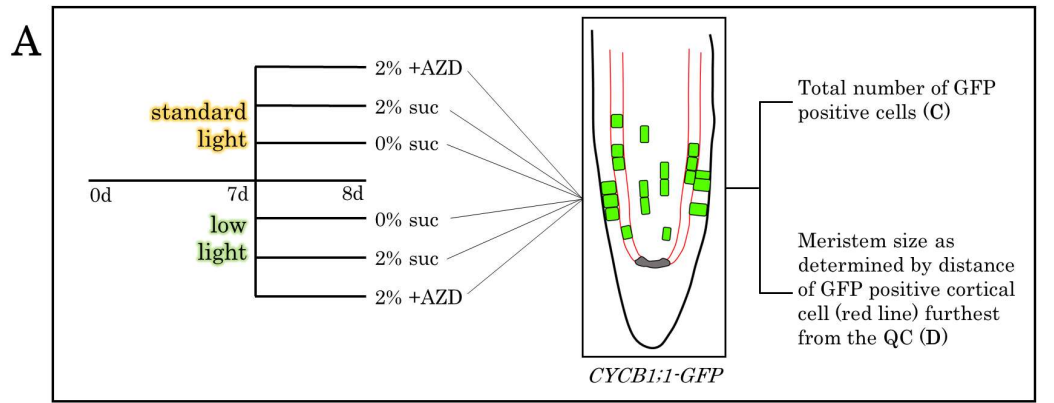


Figure 4.2 AZD treatment blocks light- and sugar-induced cell cycle progression and meristem growth.

A. Schematic of measurements made. *CYCB1;1-GFP* seeds were sown on sucrose-free media under low and standard light growth conditions, and transferred to different 2% sucrose with or without 1 μ M AZD at 7d. Confocal images were taken 1d after transfer and total number of *CYCB1;1-GFP*-positive cells were counted. Meristem size was determined as average length between the QC and last GFP-positive cells in both sides of the cortex layer

B. Representative confocal micrograph of PI-stained (red) *CYCB1;1-GFP* (green) root tip of each growth condition. Scale bar = 50 μ m

C. Number of *CYCB1;1-GFP*-positive (mitotic) cells in 0%, 2%, and 2% + AZD under two light intensities.

D. Meristem length in 0%, 2%, and 2% + AZD under two light intensities.

Data presented as mean, error bars represent standard deviation. Average number of roots (n) = 10. Number of biological repeats (N) = 1. Statistical differences were determined using Student's t-test. Asterisk represents a significant difference, "ns" represents a difference that is not significant. Note: 0% data in panels B, C and D is same as chapter 3 Figure 2B,D 4DAT timepoint.

4.2.2 AZD treatment reduces root growth rate, meristem size, cell number and size, but increases cell cycle duration

To support the observations in Figures 4.1 and 4.2 and to further characterise how TOR inhibition by AZD affects root meristem activities, we transferred similar sized over a one-week period and observed cellular phenotypes using propidium iodide-stained root meristem 1d after transfer under a confocal microscope (Figures 4.3A, 4.4A). Transfer to AZD causes a dramatic shift to a much lower root growth rate within 1DAT that is maintained throughout the course of the experiment (Figure 4.3B,C). At 1DAT, the control root growth was \sim 5.6mm (+/- 0.6) and AZD-treated growth was \sim 2.4mm (+/- 0.5), a reduction of \sim 57%. At later timepoints, the percentage difference of growth rate between controlled and AZD-treated roots is further increased by \sim 10%.

At the tissue level, TOR-inhibition within 1d leads to shortening of meristem zone (Figure 4.4B, D) as evident from the early exit to the elongation in the cell length profile (Figure 4.4C). Meristem size is reduced by \sim 25%, from \sim 205 μ m (+/- 23.1 μ m) profile (Figure 4.4C). Meristem size is reduced by \sim 25%, from \sim 205 μ m (+/- 23.1 μ m) to \sim 150 μ m (+/- 16.8 μ m) upon AZD treatment (Figure 4.4D). Meristem shortening is

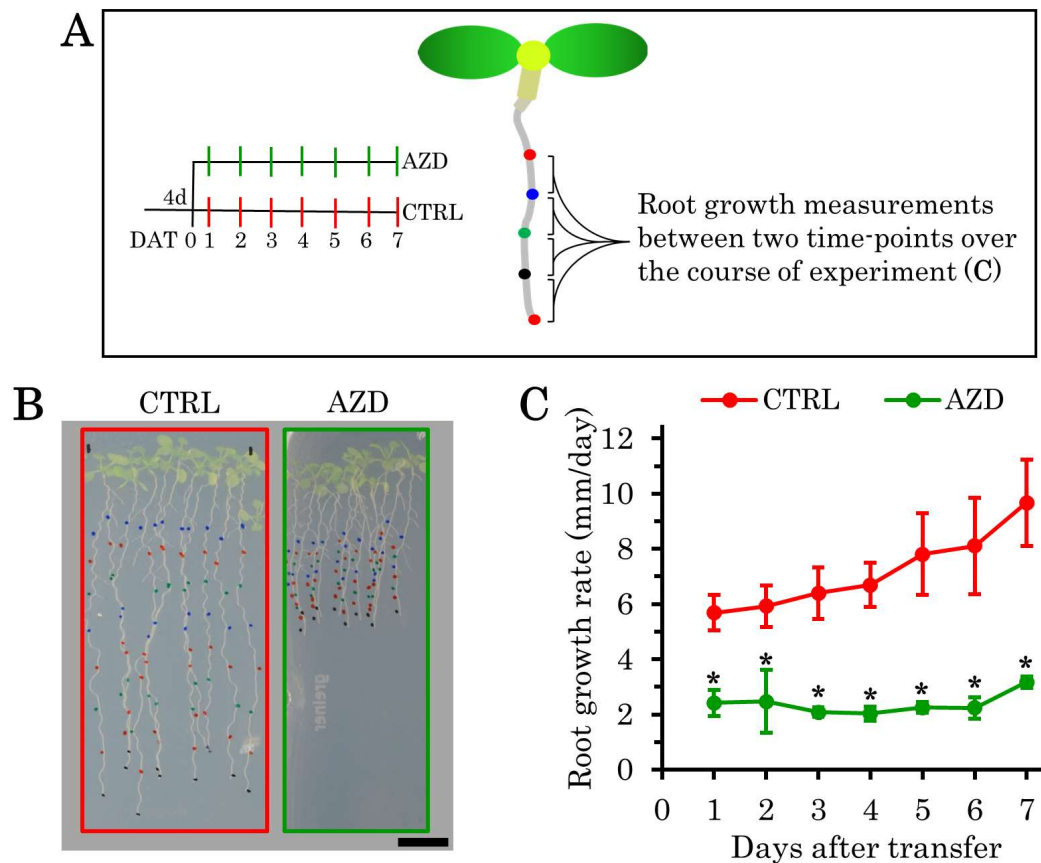


Figure 4.3 TOR inhibition lowers primary root growth rate.

A. Schematic of experimental design. Wild-type Col-0 seeds were sown on 1% sucrose under standard growth conditions and transferred to 1% sucrose with or without 1 μ M AZD. Position of the primary root tip was marked daily for a 6d period and used to plot growth rate.

B. Whole-plant photograph of Col-0 with or without 1 μ M AZD. Scale bar = 10mm

C. Primary root growth rate measurements, determined as distance between two marks along the root.

Data presented as mean, error bars represent standard deviation. Average number of roots (n) = 9. Number of biological repeats (N) = 2. Statistical differences were determined using Student's t -test. Asterisk represents a significant difference. CTRL = control (without AZD).

accompanied with fewer cells, from 28 (+/- 2.8) cells in the control to 22 (+/- 3.0) cells in the AZD-treated roots (Figure 4.4E). Moreover, we noted a statistically significant ~12% reduced size of first 15 cells from the QC in AZD samples (Figure 4.4F).

We next asked whether the reduced meristematic cell count is due to slowing down of cell cycle or accelerated cell cycle exit or both. To address the former scenario, we

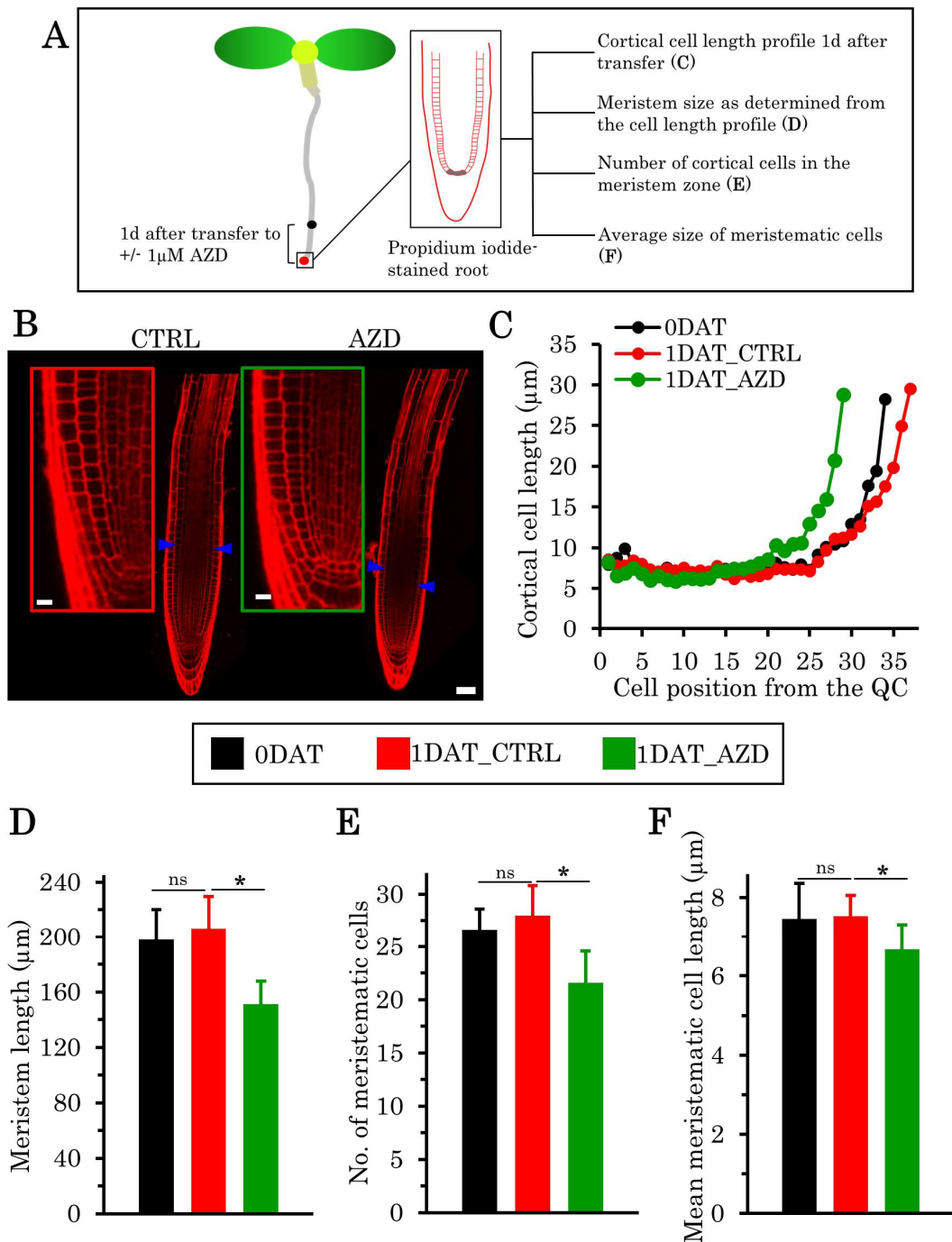


Figure 4.4 Cellular characterisation of AZD-treated root meristem.

A. Schematic of measurements made. Profile of cortical cell lengths were used to determine meristem size, number and size of meristematic cells.

B. Representative confocal micrographs of PI-stained (red) Col-0 root tip with or without 1µM AZD. Blue arrowheads point meristem boundary. Scale bar = 50µm, inset scale bar = 10µm.

C. Cortical cell length profiles of control at 4d (0DAT) and 1DAT with or without 1µM AZD.

D. Meristem length of 0DAT and with or without AZD 1DAT.

E. Number of cells in the meristem 0DAT and with or without AZD 1DAT.

F. Mean size of meristematic cells at 0DAT and with or without AZD 1DAT.

Data presented as mean, error bars represent standard deviation. Average number of roots (n) = 9. Number of biological repeats (N) = 2. Statistical differences were determined using Student's t-test. Asterisk represents a significant difference, "ns" represents a difference that is not significant. DAT = day(s) after transfer, CTRL= control (without AZD).

measured the duration of cell cycle in the root meristem by 5-ethynyl-2'-deoxyuridine (EdU) incorporation as previously described (Hayashi *et al.*, 2013). The rate of S phase entry can be determined by carrying out a time-course experiment of multiple EdU incubation periods and quantifying the percentage EdU-positive cells from the total population of meristematic cell (Figure 4.5A). As duration of EdU incubation increases, more proliferating cells take up EdU and thus percentage of EdU-positive increases over time. To calculate cell cycle duration i.e. time taken to achieve 100% EdU-positive in the meristematic cell population, percentage of EdU-positive cells is plotted against EdU incubation period and a line of best fit can then be used to determine equation for the linear regression line (Hayashi *et al.*, 2013).

In the early time-points of 0.5h, 1h and 2h, the percentage of EdU-positive cells do not show a clear difference between control and AZD samples (Figure 4.5B,C). However, a clear separation starts to emerge after 4h of EdU incubation between AZD-free and AZD-containing samples. At 8h, 80% (+/- 8.4%) of meristematic cells are positive for EdU, whereas only 50% (+/- 7.7%) cells, on average, are EdU-positive in the AZD-treated roots. From the linear equations, cell cycle duration in the control root meristem is determined to be ~21h with a predicted S phase length of 4.6h (Figure 4.5D). In the AZD-treated root meristem, duration of the cell cycle is ~30h with a predicted S phase length of 5.5h (Figure 4.5D). Whereas inhibition of TOR signalling increases cell cycle period, AZD treatment does not proportionally increase the duration of DNA synthesis. A similar observation was reported for rapamycin-treated mammalian cell line (Fingar *et al.*, 2004).

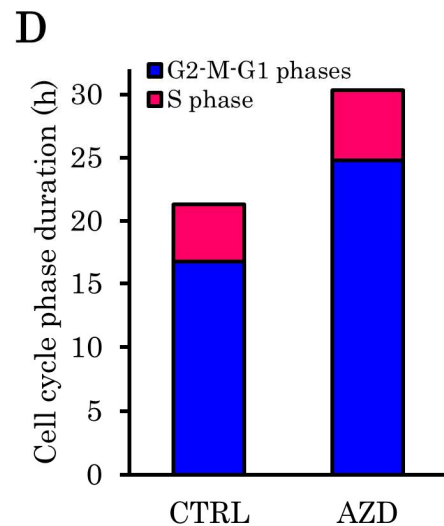
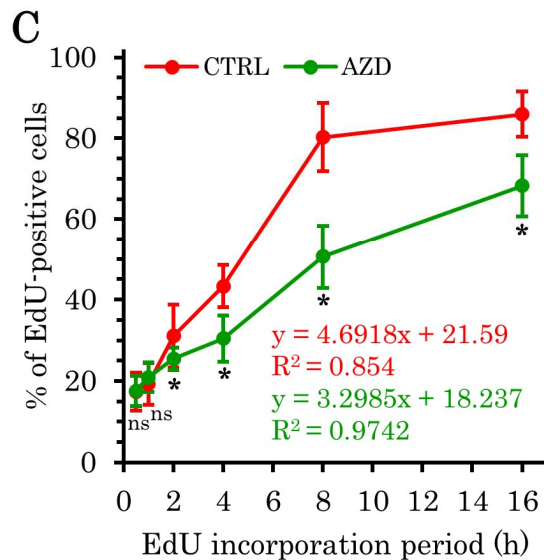
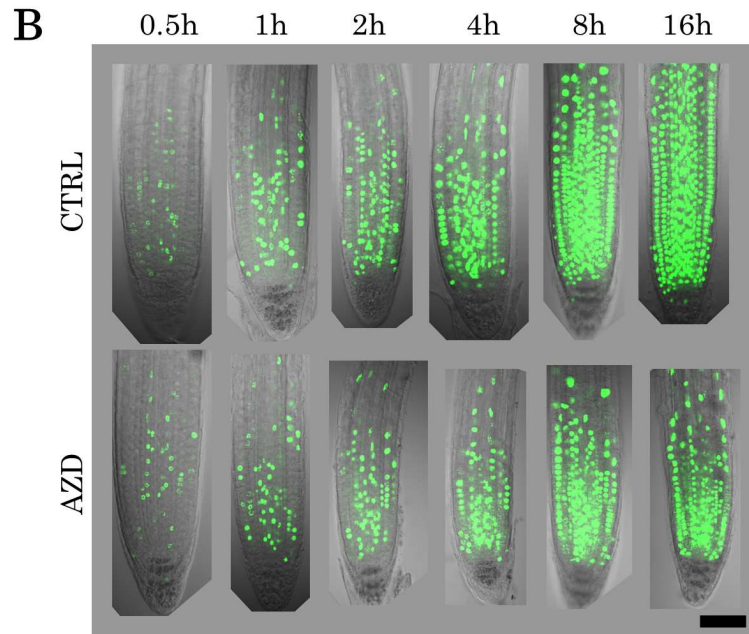
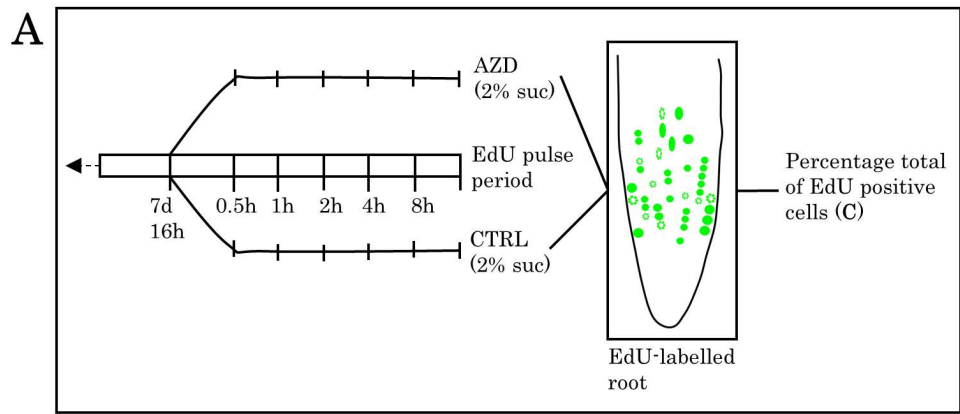


Figure 4.5 Inhibition of TOR increases cell cycle duration.

A. Schematic of experimental design. 7d Col-0 seedlings grown under standard conditions was transferred to 2% sucrose liquid EdU-containing media with or without AZD. EdU pulse period was doubled each time from 0.5h till 16h. EdU count is expressed as percentage total, and used to predict S phase and cell cycle length from the linear equation.

B. Representative confocal micrographs of EdU-labelled (green) root tip of each timepoint. Scale bar = 50µm.

C. Percentage of S phase EdU-positive cells in 2% (CTRL) and 2% + AZD.

D. Bar plot of predicted S phase length and cell cycle duration of 2% with or without AZD.

Data presented as mean, error bars represent standard deviation. Average number of roots (n) = 16. Number of biological repeats (N) = 1. Statistical differences between CTRL and AZD were determined using Student's t-test. Asterisk represents a significant difference, "n" represents a difference that is not significant. CTRL= control (without AZD).

Taken together, the reduced root growth rate can be explained from the shortening of meristem which is due to fewer cells as a result of slowing of cell cycle as well as reduced size of dividing cells. Thus, the cellular basis of AZD-induced suppression of primary root growth as a result of meristem shortening caused by cells spending a longer period in the cell cycle.

4.2.3 Exogenous sucrose suppresses end-of-the-day decline in S phase count in a TOR-dependent manner

Prior to further experiments, we first set out to confirm whether TOR activity changes in response to different sucrose concentrations. To this end, we carried out Western blotting with TOR-targeted phospho-specific S6K1/2 antibody and collected whole-seedlings at 3h treated with AZD and 0% to 3% sucrose under 12h photoperiod (Figure 4.6A). Without sucrose and AZD, we detected a low amount of phosphorylated S6K form which increased substantially at 1% and even more at 2% but reduced at 3% (Figure 4.6B). AZD caused a visible reduction of phosphorylated S6K in 1% and 2% sucrose samples; although slight changes were observed, in proportion to phosphorylated form, the non-phosphorylated S6K did not show any apparent change (Figure 4.6B). Why AZD led to an increased S6K phosphorylation at sucrose-free conditions and why at 3% sucrose the S6K phosphorylation is insensi-

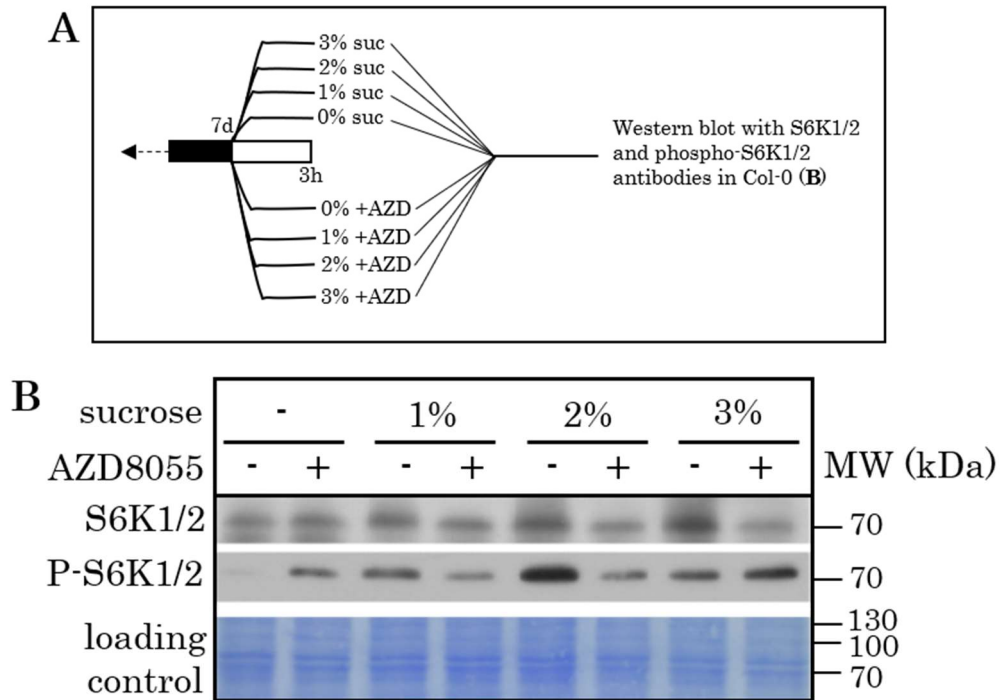


Figure 4.6 Sucrose level define activity of TOR-S6K signalling.

A. Schematic of experimental design. Col-0 seeds were sown on sucrose-free MS plates and grown under 12h light-dark cycles. At 7DAS, seedlings were transferred to different sucrose concentrations containing either DMSO (mock) or 1 μ M AZD for a 3h period after which samples were snap-frozen for Western blot.

B. Western blot image of S6K1/2 and phospho-S6K1/2 antibodies. Coomassie Brilliant Blue was used as a loading control. For antibody dilution, see Table 2.2.

tive to AZD is not clear but might indicate that multiple signals may lead to S6K phosphorylation at different conditions, and some of these are TOR independent. Consistently, we did not observe any further increase in mitotic count between 2% and 3% sucrose (Figure 4.1C). Altogether, this confirms previous reports (Schepetilnikov *et al.*, 2013; Dong *et al.*, 2015; Dobrenel, Mancera-Martínez, *et al.*, 2016; Enganti *et al.*, 2018) on specificity of AZD-8055 in inhibiting *Arabidopsis* TOR kinase activity.

To understand how rapidly AZD inhibits cell cycle, we carried out a timecourse experiment using the same experimental system of light-dark cycles as in chapter 3 (Figures 3.4 and 3.6) with the mitotic marker and EdU labelling. Since we observed a rapid S phase response within 4h and a reduction towards the end-of-day, we only

focused within this timeframe of 0h to 12h and collected samples every 3h and used 1% and 2% sucrose supplemented with 1 μ M AZD (Figure 4.7A).

We observed a 3.5-fold increase in number of S phase cells in the root meristem, from averaged 10 (+/- 5.2) cells at 0h to 35 (+/- 12.6) cells at 3h after light period (Figure 4.7B,C). A greater increase of ~50 cells was seen for both sucrose concentrations at 3h. A similar EdU count was observed for 0%, 1% and 2% sucrose at 6h. Whereas sucrose-free roots showed a decline at 9h and to a similar 0h level at 12, exogenous sucrose supply suppressed this fall in S phase count. The higher positive effect on cell cycle of 2% over 1% becomes apparent at 9h and 12h, where S phase count was 59 (+/- 8.9) and 52 (+/- 12.3), respectively (Figure 4.7B,C). On 1% sucrose, the S phase count was 47 at 9h (+/- 6.5) and 39 (+/- 13.4) at 12h. In short, exogenous supply of sucrose leads to an enhanced entry into the cell cycle early in the day that is not lowered at the same level as the sucrose-free roots.

The addition of AZD in the 1% and 2% sucrose media causes a significant reduction of 60% and 52%, respectively in S phase count within 3h and inhibits the diurnal rhythm of cell cycle (Figures 4.7B,C). This implies that the daily sugar-induced tuning of S phase is regulated by TOR signalling. Although within the AZD samples we observed a marginal but statistically significant difference between 3h and 6h for both sucrose concentrations, the amplitude between AZD and AZD-free samples is visibly lower. Overall, the average number of S phase cells across all timepoints is 32 (+/- 21.7), 48 (+/- 7.7), and 56 (+/- 5.7) cells in 0%, 1%, and 2% sucrose, respectively (Table 4.1). The high standard deviation of sucrose-free timepoints (~70% of mean value) is due to fluctuating EdU count from 0h towards end-of-day, the low standard deviation at both sucrose concentrations suggest that sucrose uncouples temporal concentration is around 25 cells (+/- 7.1 for 1% +AZD and +/- 4.8 for 2% +AZD; Table 4.1). The high standard deviation in sucrose-free timepoints signifies the diurnal

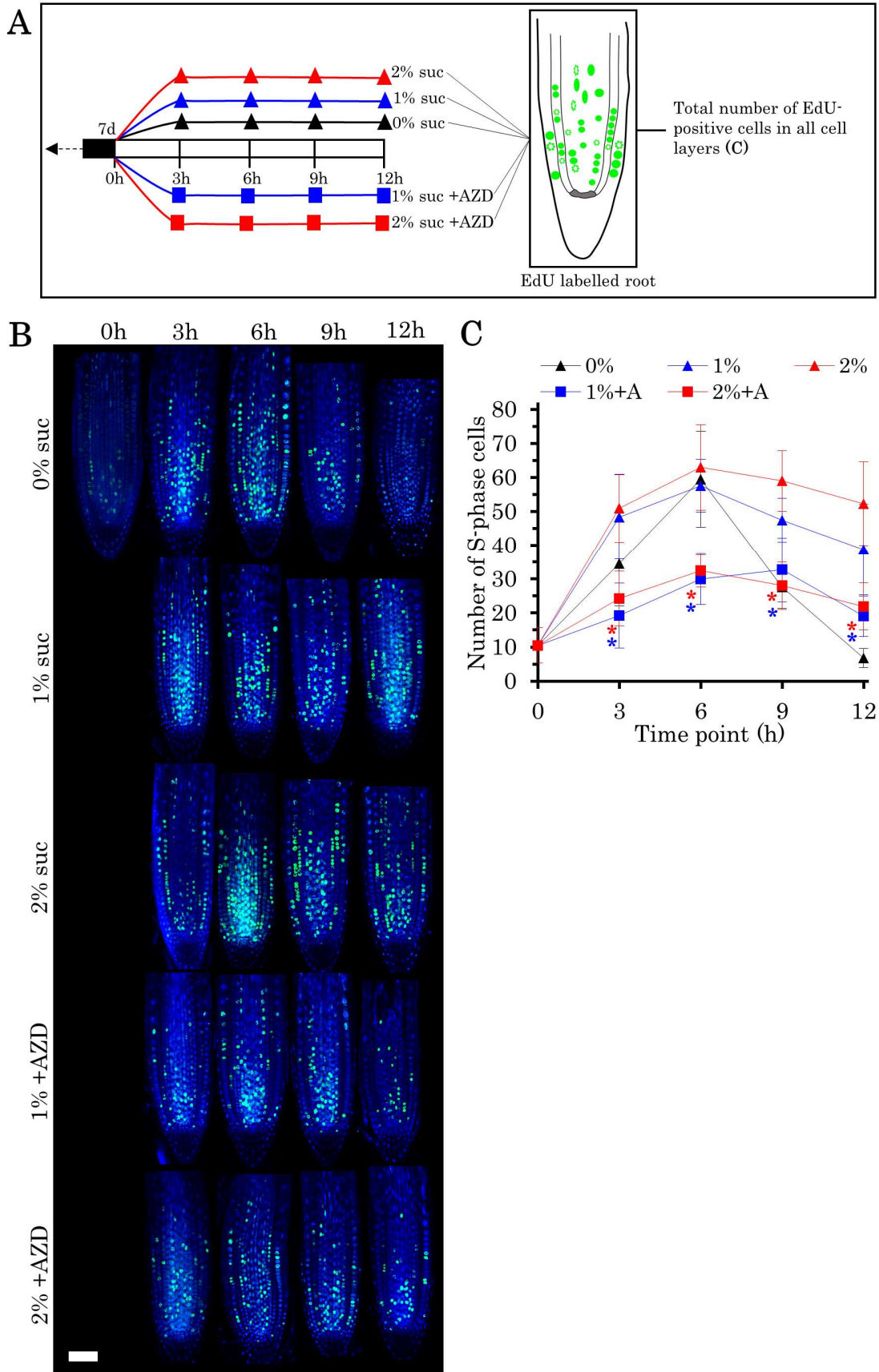


Figure 4.7 TOR inhibition rapidly reduces number of S phase cells in the root meristem.

A. Schematic of experimental design. Col-0 Seeds were sown on sucrose-free MS media under 12h light-dark cycles. All EdU positive S phase cells were manually counted and averaged for each timepoint.

B. Representative confocal micrograph of DAPI-stained (blue) EdU-labelled (green) root tip of each timepoint and growth condition. Scale bar = 50µm.

C. Number of S phase (Edu) cells for each sucrose and AZD condition during the course of experiment.

D. Average number of S phase cells of all timepoints for each sucrose and AZD condition. Data presented as mean, error bars represent standard deviation. Average number of roots (n) = 14. Experiments with similar set-up were performed twice. Statistical differences between sucrose and corresponding sucrose + AZD for each timepoint were determined using Student's t-test. Asterisk represents a significant difference, "ns" represents a difference that is not significant.

rhythm of S phase (Table 4.1).

Table 4.1 Average S phase count in AZD experiment in each growth condition.

Condition	Mean value	Standard deviation	p-value (suc vs AZD)
0% suc.	32.1	21.7	-
1% suc.	48.0	7.7	-
1% suc. +AZD	56.3	5.7	0.00493
2% suc.	25.3	7.1	-
1% suc. +AZD	26.6	4.6	0.00023

Mean valued presented here is an average of all timepoints in Figure 4.7.

Taken together, inhibition of S phase within hours of AZD treatment suggests that cell cycle entry i.e. G1/S transition requires TOR signalling. Furthermore, the level of sucrose defines the level of cell cycle count which becomes apparent at the end of the day. That is, at 12h 2% sucrose has ~25% higher number of S phase compared to 1% sucrose whereas there was no statistically significant difference between the AZD-treated roots at the two concentrations (Figure 4.7C).

4.2.4 AZD treatment rapidly alters ratio of early/mid-to-late S phase and reduces spatial synchrony of cell cycle

EdU signals have two distinct patterns, a signal evenly distributed within the nucleus corresponding to early-to-mid S phase and speckled signal corresponding to late S phase (Dvořáčková *et al.*, 2018). This is due to early replication firing of euchromatin which uniformly diffused in the nucleus giving a whole EdU fluorescent signal, and late firing of heterochromatin which occurs in compact structures in the nucleus and thus gives a speckled-appearing EdU signal (Feng and Michaels, 2015). Giving that total S phase count was rapidly reduced upon TOR inhibition, we asked whether AZD perturbs S phase progression. To test this, we counted whole and speckled EdU signals at 3h only (Figure 4.8A). On average, we observed approximately 3 to 1 ratio of early/mid to late S phase cells for 0%, 1% and 2% sucrose (Figure 4.8B). However, this ratio reduced to 1.5 to 1 (or 3:2) upon AZD treatment at both sucrose concentrations. Thus, inhibition of TOR activity disturbs intra-S phase progression.

Besides entry into S phase, the change in the ratio between early and late EdU pattern hints to the involvement of TOR signalling post G1/S. In another scenario, the change of ratio suggests the slowing down of cell cycle as a longer S phase would result in increased probability of capturing cells in late S phase. This is consistent with our observation that TOR inhibition increases cell cycle duration as well as predicted S phase length (Figure 4.5).

We noticed the occurrence of EdU positives cells in clusters within cell files, suggesting a spatial synchrony among neighbour cells. We decided to quantify this at the time point of 6h during the diurnal cycle, since these show a similar EdU count for all three sucrose conditions. We counted clusters of 2,3 or 4 neighbouring EdU-positive cells in epidermis, cortex and endodermis layers on both sides of the root meristem since individual nuclei could be clearly distinguished in these layers. There was no apparent difference in clusters of 2 or 3 cells in all conditions, but we noted

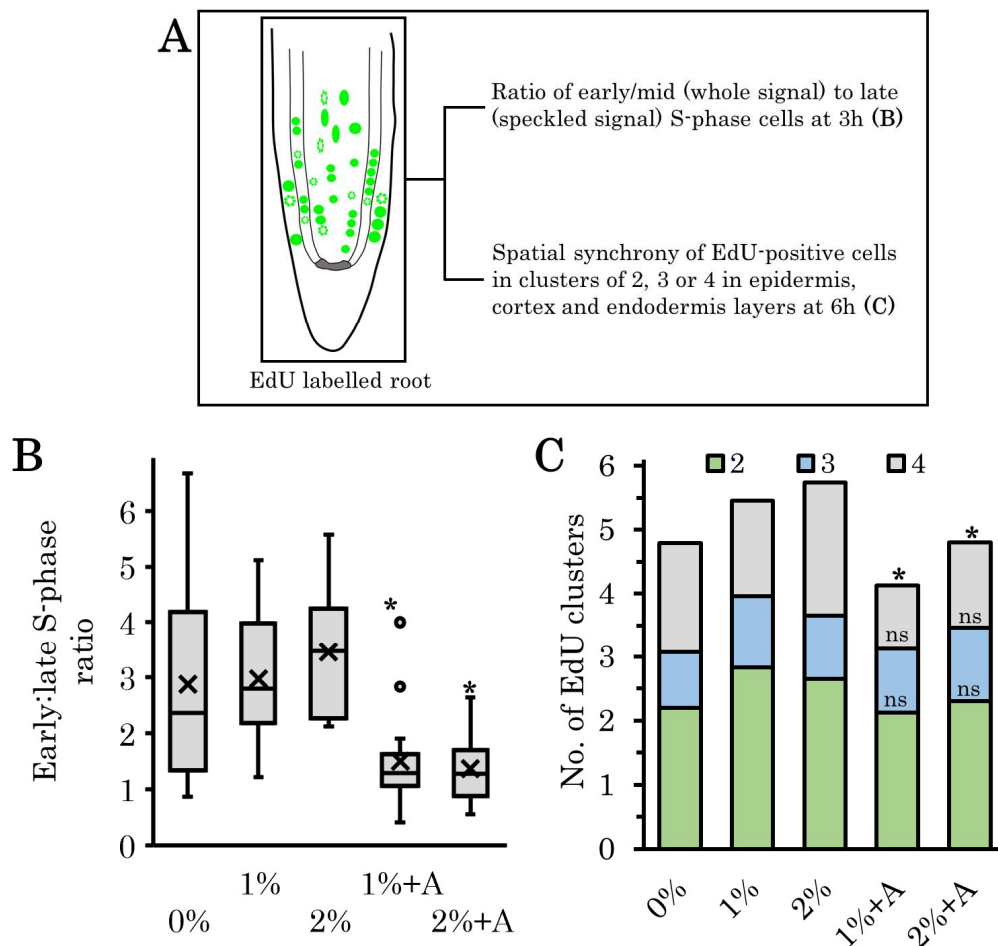


Figure 4.8 Spatial and intra-S phase characterisation upon AZD treatment.

A. Schematic of measurements made. EdU signal was categorised into whole-type, corresponding to early/mid S phase and speckled-type, corresponding to late S phase. Clusters of 2, 3, and 4 EdU-positive cells were quantified in three outward cell layers of the root meristem.

B. AZD favours accumulation of late S phase cells. Box plots of early/mid to late S phase ratio at 3h under different sucrose and AZD conditions.

C. TOR inhibition reduces spatial synchrony of S phase. Number of spatial clusters of EdU-positive cells at 6h under different sucrose and AZD conditions.

Data presented as mean, error bars represent standard deviation. Average number of roots (n) = 14. Data used here is from Figure 4.7. Statistical differences between sucrose and corresponding sucrose + AZD were determined using Student's t-test. Asterisk represents a significant difference, "ns" represents a difference that is not significant. 1% or 2% = 1% or 2% sucrose, A = AZD.

a significant difference in the occurrence of clusters of 4 S phase cells between AZD-free and AZD-containing 2% samples (Figure 4.8C), suggesting TOR signalling promotes cell cycle entry at the local cell-level in the meristem.

4.2.5 CYCD2 protein accumulates diurnally and is sensitive to TOR inhibition

A conserved hallmark of cell cycle entry is the accumulation of D-type cyclins during G1 (Healy *et al.*, 2001); in particular, *CYCD2* mRNA and protein levels have been shown to be regulated by sucrose level (Riou-Khamlichi *et al.*, 2000). Thus, we asked whether CYCD2 protein level is sensitive to AZD treatment. To this end, we used a translational GFP fusion line *proCYCD2;1:CYCD2;1-GFP* (Sanz *et al.*, 2011) and followed the same time-points and conditions as for the EdU experiment (Figure 4.9A). To maintain consistency within different samples and timepoints, we measured fluorescent intensity (grey value) of GFP in 100µm meristem region from the QC (Figure 4.9A). In the sucrose-free samples, we observed a 40% increase in fluorescent intensity of *CYCD2;1-GFP* line from ~21 (+/- 5.5) arbitrary unit (au) at 0h to ~35 (+/- 6.1) au at 3h which was not statistically different from 1% sucrose (Figure 4.9B, C). There was a further 6% increase in CYCD2;1 protein abundance with 2% sucrose (Figure 4.9B,C). These CYCD inductions are blocked by AZD at 3h and remain low throughout the timecourse (Figure 4.9B,C).

Interestingly, without sucrose CYCD2 protein level follows a diurnal rhythm with a peak at 3h and then a gradual decline afterwards such that the starting level at 0h is within the 10% range to the end-of-day level at 12h (Figure 4.9C). The intrinsic mechanism that drives the decline in CYCD2 after the 3h peak was not explored here but given the observation that exogenous sucrose suppresses the end-of-day reduced CYCD2 protein amount suggests that sugar availability might play a critical role in regulating CYCD2 levels. Although we observed a significantly higher grey value for 2% over 1% at 3h, there was no significant difference at other timepoints between the two sucrose concentrations and the basal level remained unaltered between 6h and 12h for each concentration (Figure 4.9C).

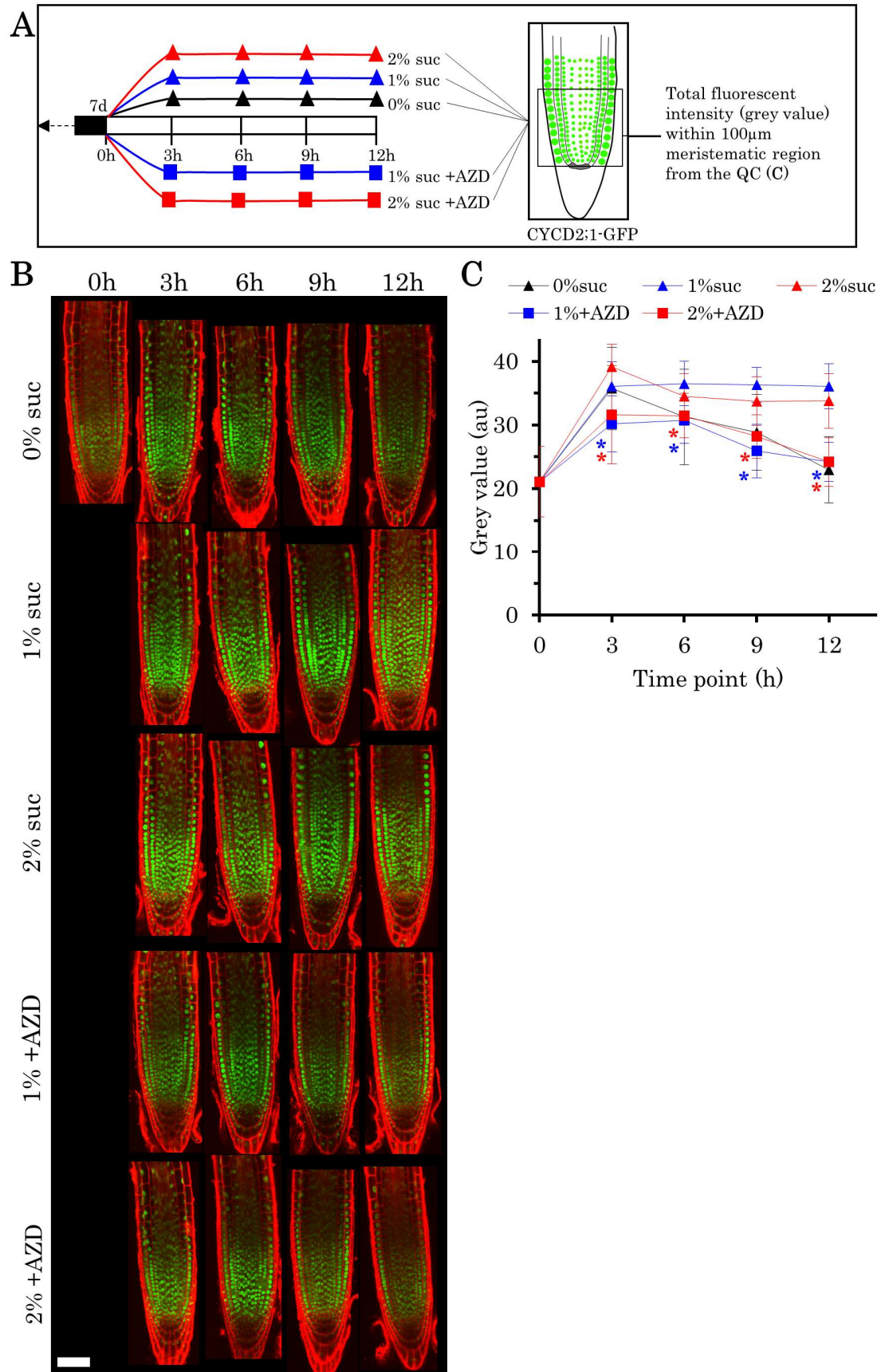


Figure 4.9 TOR activity drives sugar-dependent increase in CYCD2 protein accumulation.

A. Schematic of experimental design. CYCD2-GFP seeds were sown on sucrose-free MS

media under 12h light-dark cycles. GFP fluorescent intensity (grey value) of 100µm meristematic region from the QC was quantified.

B. Representative confocal micrographs of PI-stained (red) CYCD2-GFP (green) root tip of each timepoint and growth condition. Scale bar = 50µm.

C. Fluorescent intensity CYCD2-GFP for each sucrose and AZD condition during the course of experiment.

Data presented as mean, error bars represent standard deviation. Average number of roots (n) = 15. A similar timecourse experiment was performed under different growth condition, an identical conclusion was made in regards to effect of sucrose and AZD on CYCD2 protein accumulation. Statistical differences between sucrose and corresponding sucrose + AZD for each timepoint were determined using Student's t-test.

Asterisk represents a significant difference, "ns" represents a difference that is not significant. 1% or 2% = 1% or 2% sucrose, A = AZD.

Overall, the average CYCD2 protein amount of all timepoints is 29au (+/- 5.1) in 0%, around 35au (+/- 0.2 for 1% and +/- 2.5 for 2%) in 1%, and 2% sucrose, and around 28au (+/- 3.2 for 1% +AZD and +/- 3.5 for 2% +AZD) with AZD at both sucrose concentration (Table 4.2). We could also show the elevation of CYCD2;1 protein amount when seedlings were treated with 2% sucrose for 3h on a Western blot with GFP antibody, which was inhibited by AZD (Figure 4.10).

Table 4.2 Average CYCD2 fluorescent intensity in AZD experiment in each growth condition

Condition	Mean value	Standard deviation	p-value (suc vs AZD)
0% suc.	29.5	5.1	-
1% suc.	36.2	0.2	-
1% suc. +AZD	35.3	2.6	0.01281
2% suc.	27.8	3.2	-
1% suc. +AZD	28.9	3.5	0.02818

Mean valued presented here is an average of all timepoints in Figure 4.9.

Whereas we noted a significant reduction in CYCD2 level upon AZD treatment within 3h, the down-tuning is similar to the sucrose-free samples at other timepoints suggesting that CYCD2 protein dynamics may be regulated in TOR-dependent and TOR-independent signalling pathways. This is consistent with the observation that

light without exogenous sucrose leads to stronger accumulation of CYCD2 protein as compared with sucrose under dark (Sanz *et al.*, 2011). CYCD2 might be behind the diurnal rhythm of cell cycle as detected by EdU labelling, but this needs to be further studied genetically using mutants.

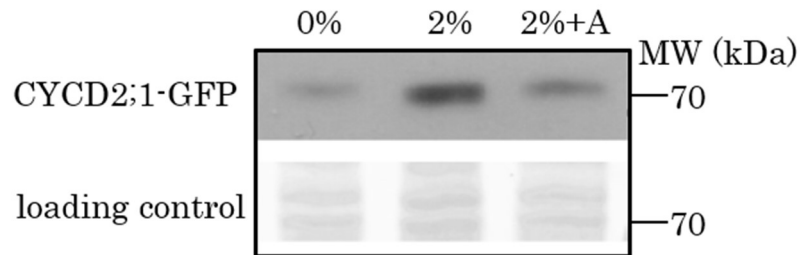


Figure 4.10 AZD reduces CYCD2 protein at the whole-plant level.

Western blot image of CYCD2 using GFP antibody. CYCD2-GFP seeds were sown on sucrose-free MS plates and grown under 12h light-dark cycles. At 7DAS, seedlings were transferred to 2% sucrose containing either DMSO (mock) or 1 μ M AZD for a 3h period after which samples were snap-frozen for Western blot. Coomassie Brilliant Blue was used as a loading control. Number of biological repeats = 1. For antibody dilution, see Table 2.2.

4.2.6 TOR regulates G1/S entry through mediating phosphorylation of RBR.

To gain further insight into the molecular mechanism behind TOR-dependent G1/S regulation, we tested the involvement of RETINOBLASTOMA-RELATED (RBR) protein, a master repressor of cell cycle which is inhibited by CYC-CDK phosphorylation event (Nowack *et al.*, 2012). To this end, we used the 12h light 12h dark experimental set-up and only focused on a single timepoint and selected 3h since we saw a clear elevation in S phase and CYCD2 level, both of which were inhibited by AZD. As knockout of *rbr* leads to embryo lethality, we used an artificial microRNA induced silencing line of RBR, hereafter referred to as *amiRBR* (Cruz-Ramírez *et al.*, 2013). Additionally, we studied phosphorylation of RBR using phospho-specific antibody for human Rb phospho-site Ser807/811 that was shown to

recognise serine 911 position in *Arabidopsis* (Magyar *et al.*, 2012) (Figure 4.12A). This phosphorylation site is targeted by CDK and the specificity of this antibody was further shown by mutating serine 911 to alanine which resulted in the absence of the band-of-interest on a Western blot (Wang *et al.*, 2014).

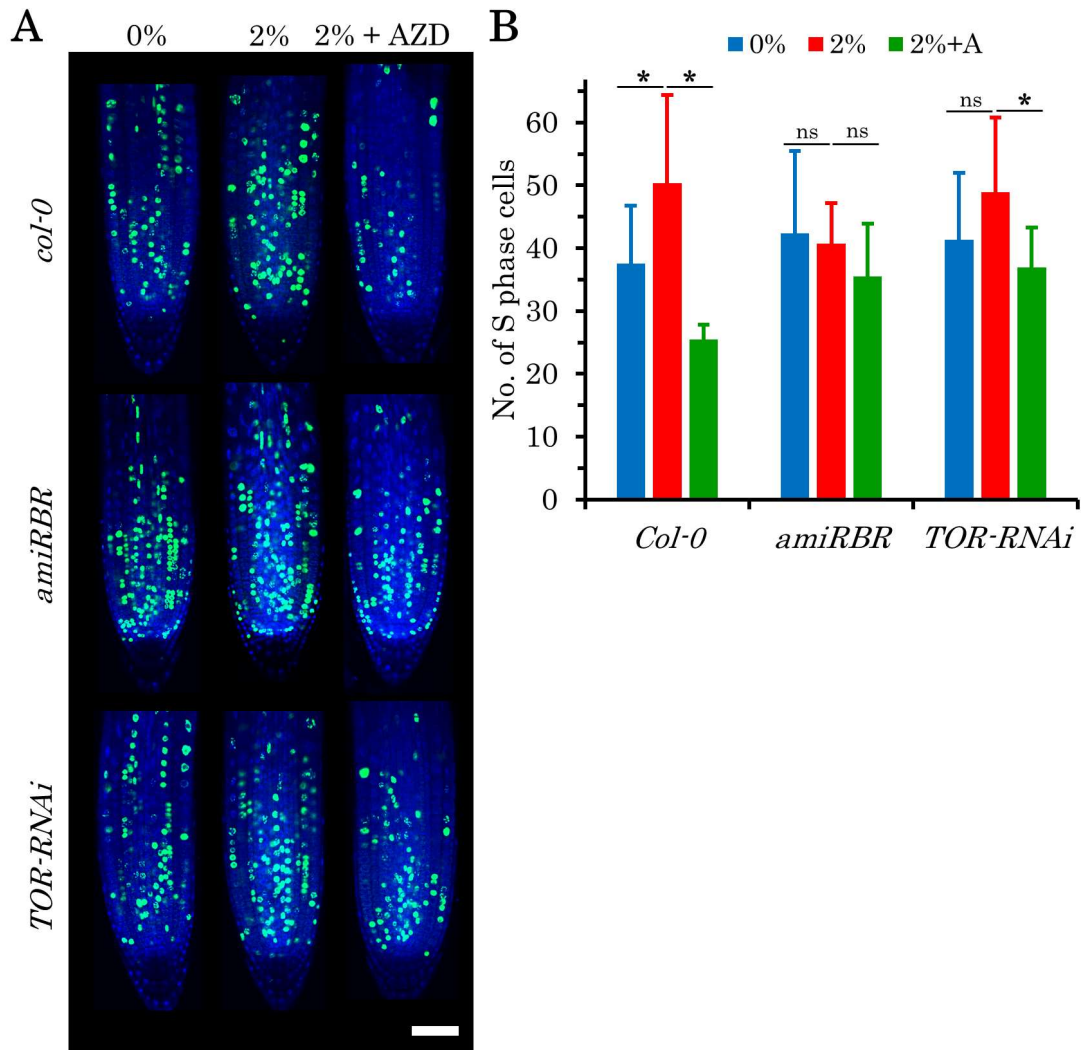


Figure 4.11 Silencing of RBR reduces sensitivity to AZD.

A. Representative confocal micrograph of DAPI-stained (blue) EdU-labelled (green) *Col-0*, *amiRBR*, and *TOR-RNAi* root tip of each growth condition. Scale bar = 50 μ m.

B. Number of EdU-positive S phase cells 3h after transfer to 0% sucrose and 2% sucrose with or without 1 μ M AZD.

Data presented as mean, error bars represent standard deviation. Average number of roots for each line (n) = 10. Number of biological repeats (N) = 2. Statistical differences were determined using Student's t-test. Asterisk represents a significant difference, "ns" represents a difference that is not significant. 2% = 2% sucrose, A = AZD.

Whereas at 3h there was a significant increase in the number of S phase cells upon exogenous sucrose supply which showed a 50% reduction in response to AZD treatment in wild-type, but there was no significant change in S phase count to both sucrose and AZD in the *amiRBR* line (Figure 4.11A, B). In the RNAi-induced *TOR* silencing line, number of S phase cells reduced by 25%, reduced sensitivity to AZD provides further evidence for AZD specificity. Without sucrose and AZD, we detected a low amount of phosphorylated RBR which increased substantially at 1% and even more at 2% but reduced at 3% (Figure 4.12B), corresponding to the EdU labelling at these sucrose levels. AZD caused a visible reduction of phosphorylated form of RBR at all sucrose concentrations. Interestingly, without the addition of external sucrose the RBR phosphorylation is low, but it was increased by the addition of AZD. This suggest a cross talk between a sucrose and TOR-dependent pathway leading to RBR phosphorylation, which inhibits a TOR independent and possibly light regulated pathway, both leading to RBR phosphorylation. While the loading control shows equal protein amounts, we also observed an increase in RBR amounts upon sucrose treatment, but the inhibition by AZD was less pronounced (Figure 4.12B). This is in agreement with previous reports that RBR amount is most abundant in proliferating cells (Oszi *et al.*, 2020).

Taken together, the AZD insensitivity at the level of S phase in the RBR silencing line and AZD-induced lowering of RBR phosphorylation implies that TOR signalling promotes S phase entry through RBR phosphorylation that lifts the RBR repression on E2Fs and cell cycle progression. Additionally, the use of anti-phospho-Rb that is a target site for CDK phosphorylation (Magyar *et al.*, 2012) and the observation that AZD reduces CYCD2 protein level strongly suggests that TOR pathway is involved in CDK-CYCD dependent phosphorylation of RBR. This could be experimentally tested through identifying and mutating TOR phosho-site on RBR protein, this

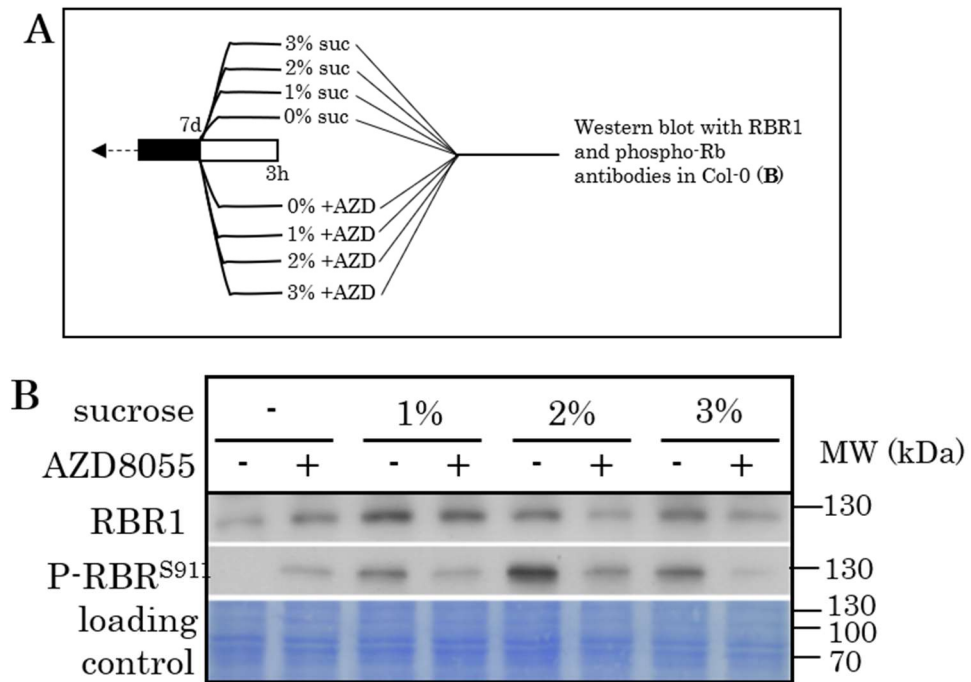


Figure 4.12 TOR signalling modulates phosphorylation of RBR.

A. Schematic of experimental design. 7d old Col-0 seedlings grown without sucrose under 12h light-dark cycles were transferred to different sucrose concentration with or without 1 μ M AZD at 0h (lights off) for a 3h period.

B. Western blot image of RBR and phospho-RBR antibodies. Coomassie Brilliant Blue was used as a loading control. N.B. Loading control used here is the same as in Figure 4.6.

should diminish the sensitivity of AZD at the level of RBR phosphorylation.

4.2.7 Inhibition of TOR activity reduces G2/M cells and meristem size within hours

Previous reports (Xiong *et al.*, 2013; Li *et al.*, 2017; Wu *et al.*, 2019) and our EdU experiments with high temporal resolution (Figures 4.7 and 4.8) conclusively show that TOR activity is essential for G1-to-S phase transition. This led us to ask whether G2-to-M phase transition also requires TOR activity. To test the hypothesis that TOR is required for G2/M entry, we made use of the *CYCB1;1* mitotic marker and carried out the same time-course experiment as for EdU labelling and *CYCD2-GFP* line (Figure 4.13A). At 0h, there were 18 (+/- 6.2) mitotic cells which increased by

~33% to 27 (+/- 5.5) at 3h without exogenous sucrose (Figure 4.13B,C). 1% sucrose supply caused an additional ~18% rise in mitotic count whereas 2% did not cause any significant change to 0% (Figure 4.13B,C). There was a gradual decline in number of mitotic cells after 3h with a significant decrease at 9h and to a level below 0h at 12h (Figure 4.13C). This down-tuning was lost with exogenous sucrose, interestingly the 1% sucrose causes a greater mitotic count than 2% (Figure 4.13C). Surprisingly, AZD leads to inhibition of sucrose-induced increase in mitotic count within 3h and no significant change is observed at other timepoints (Figure 4.13B,C).

We then asked whether size of the meristem is altered within the same timeframe as the inhibition of mitotic cells. Meristem is defined as a region of actively-proliferating tissue with the highest proliferative (Dolan *et al.*, 1993; Otero *et al.*, 2016) and so we defined it as the distance of the last *CYCB1;1-GFP* positive cortical cell from the QC. Meristem length at 0h was ~110 μ m (+/- 19.1 μ m) which increased by 13% to 128 μ m (+/- 14.2 μ m) at 3h without sucrose (Figure 4.13D). There was a marginal increase with 1% and 2% exogenous sucrose that resulted in ~134 μ m (+/- 14.4 μ m) and ~137 μ m (+/- 12.8 μ m) meristem length, respectively (Figure 4.13D). However, the difference in meristem size becomes visibly apparent at 6h with 0% meristem size of ~120 μ m (+/- 21.5 μ m) and 1% and 2% meristem length at a similar value of 150 μ m (+/- 10.2 μ m for 1% and +/- 17.5 μ m for 2%; Figure 4.13D). At later timepoints, without sugar there was a gradual decrease in meristem size that is suppressed with exogenous sucrose supply. AZD treatment completely inhibited the sugar-induced increase in meristem size within 3h and to a similar level as sucrose-free samples at all other timepoints (Figure 4.13D). In short, sucrose availability pushes the meristem boundary shootward whereas TOR inhibition rapidly represses cell proliferation-driven meristem growth. This implies that the initial TOR-dependent organ growth through promotion of cell cycle is due to an increased

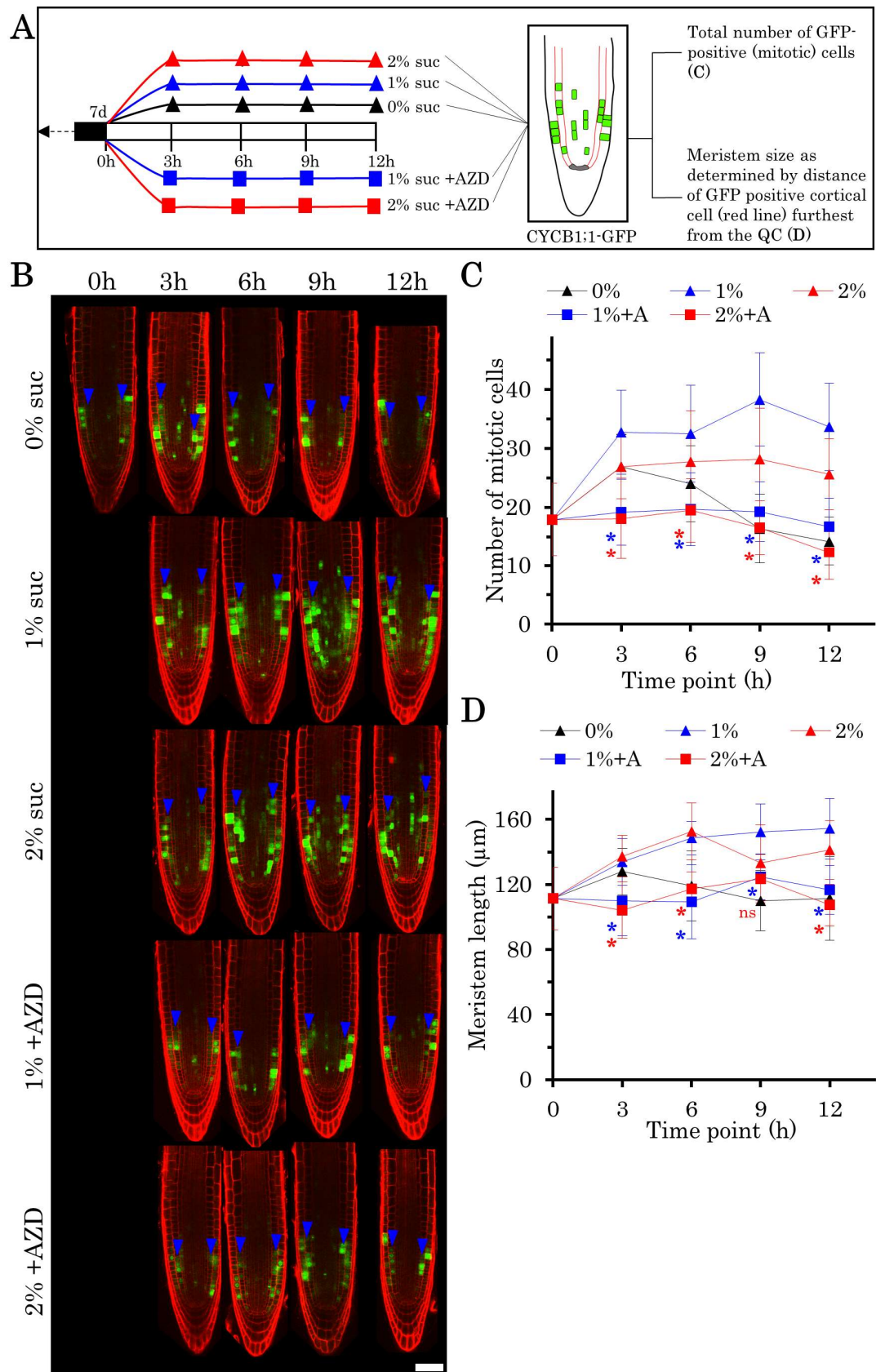


Figure 4.13 TOR inhibition rapidly reduces G2/M entry and meristem length.

A. Schematic of experimental design. *CYCB1:1-GFP* seeds were sown on sucrose-free MS

media under 12h light-dark cycles. All *CYCB1;1-GFP*-positive mitotic cells were manually counted and averaged for each timepoint.

B. Representative confocal micrograph of PI-stained (red) *CYCB1;1-GFP* (green) root tip of each timepoint and growth condition. Blue arrowheads point meristem boundary. Scale bar = 50 μ m.

C. Number of mitotic cells for each sucrose and AZD condition during the course of experiment.

D. Meristem length for each sucrose and AZD condition during the course of experiment.

Data presented as mean, error bars represent standard deviation. Average number of roots (n) = 14. Statistical differences between sucrose and corresponding sucrose + AZD for each timepoint were determined using Student's t-test. Asterisk represents a significant difference, "ns" represents a difference that is not significant. 1% or 2% = 1% or 2% suc, A = AZD

proliferative capacity of the meristem.

4.2.8 Evolution of cell size during TOR inhibition and exogenous sucrose supply

In chapter 3, G2/M cell size was shown to change on an hourly basis under light-dark cycles (Figure 3.5), given the observation that AZD treatment reduces number of mitotic cells within 3h (4.13C) and size of meristematic cells within 1d (Figure 4.4F), we asked how quickly does the effect of AZD on cell size becomes apparent. To this end, we used the same mitotic marker confocal data as in Figure 4.13 and measured the size of GFP-positive and non-GFP cells separately (Figure 4.14A). As a mitotic cyclin, *CYCB1* expression is well-defined and accumulates at the G2-to-M phase transition and degrades at metaphase-to-anaphase transition (Doerner *et al.*, 1996; Gutierrez, 2009). Thus, we reasoned that *CYCB1;1-GFP* positive cells are those in late G2 or early mitosis, and non-*CYCB1;1-GFP* cells are in G1,S, or early G2 phases. Thereby, it is reasonable to state *CYCB1;1*-positive cell length as proxy for G2/M size and *CYCB1;1*-negative cell length as a proxy for interphase cell size. At 0h, interphase and G2/M cell sizes were 6.1 μ m (+/- 0.4 μ m) and 8 μ m (+/- 0.6 μ m), respectively, whereas G2/M size increased by ~14% to 9.3 μ m (+/- 0.7 μ m) at 6h and

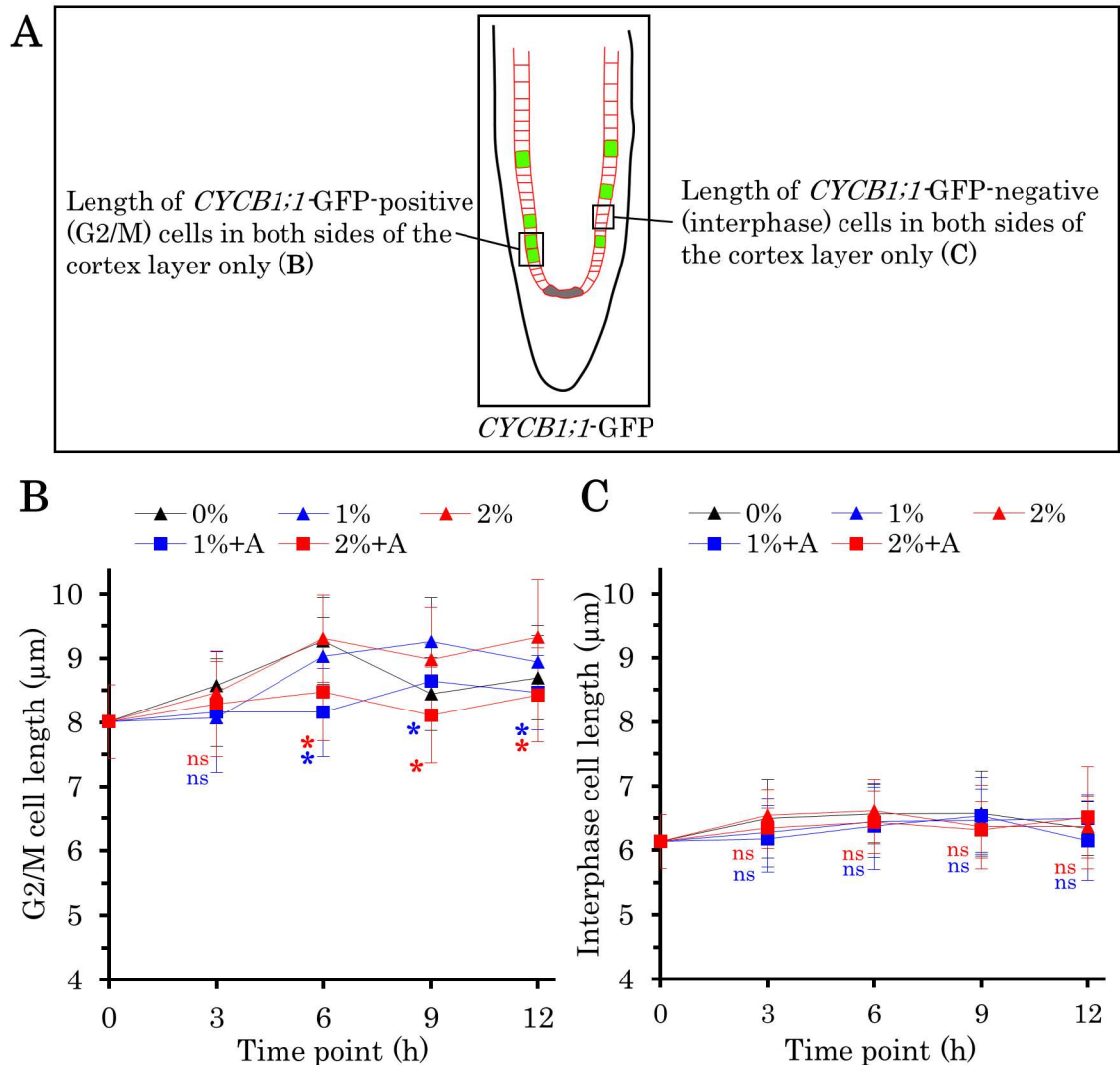


Figure 4.14 Inhibition of TOR differentially affects interphase and G2/M cell size.

A. Schematic of cell size measurement methodology. Size of *CYCB1:1*-GFP positive and negative cells, respectively representing size at G2/M and G1/S, was measured in the cortex layer of both sides of the root and averaged for each timepoint.

B. G2/M cell length for each sucrose and AZD condition.

C. Interphase cell length for each sucrose and AZD condition.

Data presented as mean, error bars represent standard deviation. Average number of roots (n) = 14. Data used here is from Figure 4.13. Statistical differences between sucrose and corresponding sucrose + AZD for each timepoint were determined using Student's *t*-test. Asterisk represents a significant difference, "ns" represents a difference that is not significant. 1% or 2% = 1% or 2% sucrose, A = AZD.

reduced to $8.7\mu\text{m}$ ($\pm 0.7\mu\text{m}$) at 12h, interphase cell size did not fluctuate proportionally as much (Figure 4.14B,C). Exogenous 1% and 2% sucrose supply does not cause any difference in G2/M size during early timepoints but leads to larger cells than sucrose-free at 9h and 12h. At 9h, G2/M size were $8.4\mu\text{m}$ ($\pm 0.6\mu\text{m}$)

without sucrose, $9.3\mu\text{m}$ ($\pm 0.7\mu\text{m}$) and $9\mu\text{m}$ ($\pm 0.8\mu\text{m}$) with 1% and 2% sucrose, respectively (Figure 4.14B). Cells in interphase did not show any apparent time-of-the-day or sucrose concentration-dependent changes in cell size (Figure 4.14C).

TOR inhibition prevents sucrose-induced G2/M size increase and significantly reduces G2/M size at 6h which is $8.2\mu\text{m}$ ($\pm 0.7\mu\text{m}$) with 1% + AZD and $8.5\mu\text{m}$ ($\pm 0.8\mu\text{m}$) with 2% + AZD (Figure 4.14B). A similar G2/M size was measured at both sucrose concentrations with AZD. Interestingly, interphase cell size did not show a clear effect of AZD treatment at all timepoints and show similar minor fluctuations to AZD-free samples (Figure 4.14C). In summary, inhibition of TOR activity rapidly lowers cell size at the G2-to-M phase transition without having any visible effect on interphase cells. This could be due to cell growth occurring predominantly during G1 in a TOR-independent way and cell size being “checked” by TOR pathway at the G2/M transition.

Consistent with Hypothesis 3 stated in section 1.9, I showed TOR activity is required for G2-to-M phase transition. Additionally, I showed RBR to be part of the TOR-cell cycle regulatory network.

4.3 Discussion

Progression through the cell cycle requires continuous supply of energy and is limited by nutrient-sensing signalling pathways. Time-course experiments with S phase EdU labelling and *CYC1;1-GFP* mitotic marker showed a significant AZD-dependent reduction of both phases within the same time window, suggesting that TOR signalling is required for light/sugar induced cell cycle, and regulates both G1-to-S and G2-to-M transition points (Figure 4.15A,B). Contradictory to the direct

TOR-E2F G1/S control model proposed by Xiong and co-workers (2013), we found that RBR is part of the TOR regulatory network. This conclusion is based on AZD-induced reduction in phosphorylated form of RBR and reduced AZD sensitivity of the *RBR* silencing line at the level of S phase. Consistent with our view of RBR as part of TOR network, AZD-sensitive RBR phosphopeptides, but not E2Fs, were recently identified (Van Leene *et al.*, 2019) suggesting that TOR kinase may coordinate phosphorylation of RBR on multiple sites which would result in “release” of E2FA to allow S phase gene expression.

Although we did not dissect the molecular basis of G2/M control, we identified TOR as a putative upstream signalling pathway connecting sugar availability with the onset of mitosis. A recent transcriptome analysis of synchronised tobacco BY2 cells showed TOR was differentially expressed throughout the cell cycle with peak expression at the G2/M transition (Trolet *et al.*, 2019). This suggests that TOR is required beyond triggering cell cycle entry, consistent with our TOR-G2/M model. On possible molecular mechanism of TOR control on G2-to-M phase transition, RBR could be co-purified with CDKB1;1 (Van Leene *et al.*, 2019) and a CDKB-CYCD6;1 complex could *in vitro* phosphorylate RBR pocket domain (Cruz-Ramírez *et al.*, 2012) suggesting its involvement in G2/M transition. Thus, continued TOR activity throughout the cell cycle may maintain RBR in its phosphorylated form which would ensure progression from G1/S through G2/M. Precise cell cycle role of these TOR phospho-sites on RBR protein could be experimentally tested through mutating them and measuring S phase and mitotic frequency with and without AZD-8055.

What could be a target of TOR kinase to allow progression through G2/M? A recent genetic screen to identify mutants resistant to AZD-8055 identified YET ANOTHER KINASE 1 (YAK1) as a downstream target of TOR signalling that transcriptionally

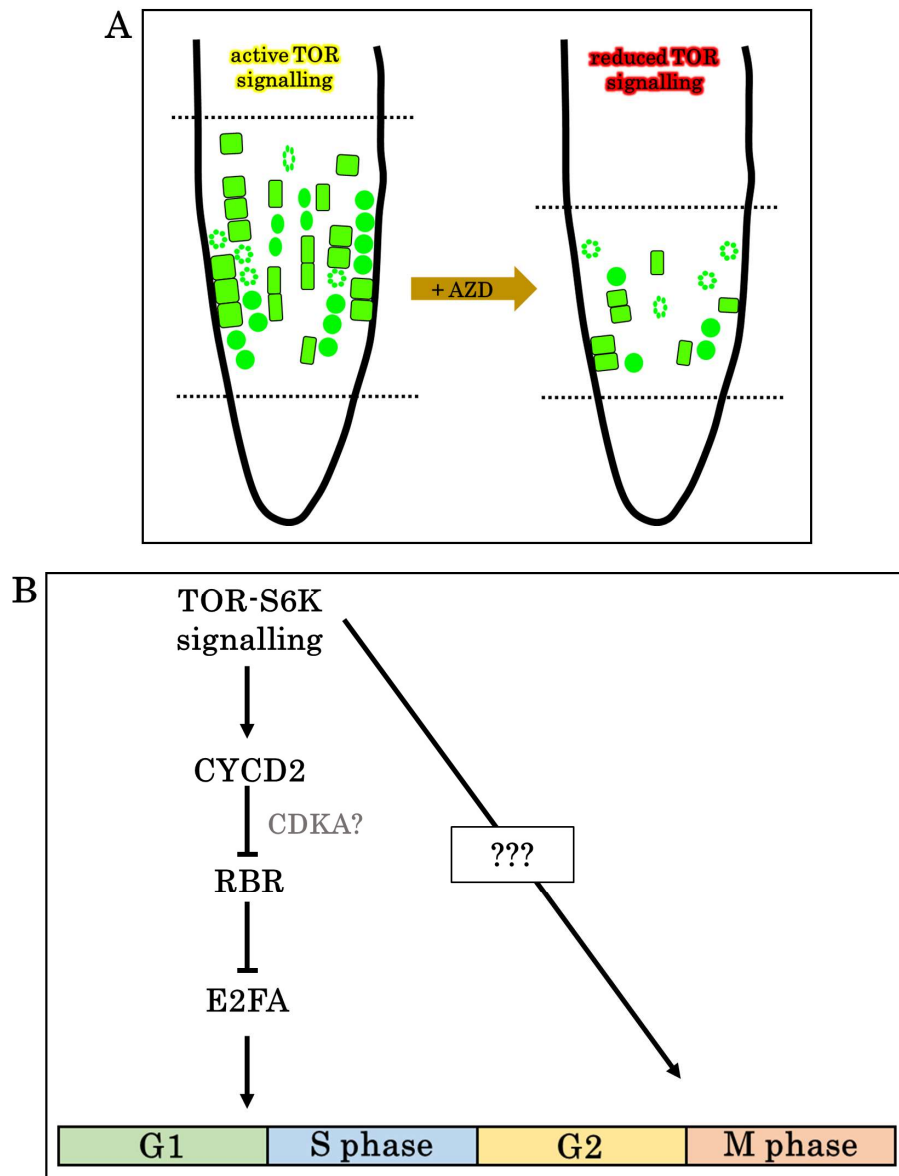


Figure 4.15 TOR signalling is required for both G1/S and G2/M transitions.

A. Schematic summary of cellular phenotypes of TOR-inhibited root tips. AZD treatment results in a smaller meristem (dashed lines) due to reduced S phase progression (whole and speckled circles representing early and late S phase, respectively) and mitotic onset (rectangles). Additionally, inhibition of TOR reduces size of cycling cells.

B. A proposed model for TOR control of G1/S transition. TOR signalling promotes accumulation of CYCD2 protein which presumably increases formation of CYCD-CDKA complex which phosphorylates RBR and thus liberating E2FA to carry out S phase transcription. TOR activity is also required for G2-to-M phase transition, but the molecular mechanism was not investigated.

promotes SMR activity (Barrada *et al.*, 2019). YAK1 belongs to the family of dual-specificity tyrosine (Y) phosphorylation-regulated kinase (DYRK) that have been

shown to be conserved in all studied model organisms and have been strongly implicated to have negative regulatory roles in cell cycle (Aranda *et al.*, 2011; Soppa and Becker, 2015). In *Arabidopsis*, TOR complex was shown to phosphorylate YAK1 (Forzani *et al.*, 2019), which likely inhibits its negative cell cycle role. YAK1 specifically promotes transcription of *SIM*, *SMR4*, *SMR5*, and *SMR7* (Barrada *et al.*, 2019). *SMR4* and *SMR6* proteins could be co-purified with CDKA;1 and CYCDs whilst *SIM* was found to interact with CDKB1;1-CYCB2 and CDKB1;1-CYCA2 complexes (Van Leene *et al.*, 2019) suggesting that the *SIM/SMRs* which are targeted by TOR, are involved in both G1/S and G2/M transitions. RBR phosphorylation level is increased in *simsmr1* mutant (Wang *et al.*, 2014), supporting the view that phosphorylated RBR form exists beyond G1 and S phase. Taken together, a TOR-E2F independent pathway is likely to exist that is centred on TOR-YAK1-SMR-CDK-RBR. The former pathway may act throughout the cell cycle as supposed to transcriptional control of cell cycle entry executed by TOR-E2F node at the G1/S transition point (Ahmad *et al.*, 2019).

Progression through all phases of the cell cycle is connected with cell growth rate to achieve size homeostasis over successive division rounds, our quantitative characterisation of cell size changes in response to TOR inhibition showed reduced *CYCB1;1-GFP* size within hours but not that of non-*CYCB1;1-GFP* cells. Given that size sensing occurs at both G1-to-S and G2-to-M phase transition points (Jones *et al.*, 2017) and our observation of decrease in S phase and mitotic cells as well rapid cell size reduction suggests that TOR signalling coordinates cell growth rate with cell cycle progression preferentially at G2/M as supposed to G1/S. This conclusion is based on the observation that only the *CYCB1;1* cell size is sensitive to AZD, and since growth in *CYCB1;1*-positive cells likely occurs before i.e. during G1, S to G2 phases, it follows that TOR signalling acts at G2/M to couple cell cycle entry to

growth rate. Since the DREAM complex, which target mitotic genes, includes RBR and E2FB, it is possible that the TOR pathway could regulate mitosis and cell size through DREAM.

More broadly, our cell size observation implies that more than one size-sensing mechanisms may act to maintain size homeostasis. In fission yeast, a major proposed mechanism involved spatial dilution of Pom1, a DYRK family kinase (Martin and Berthelot-Grosjean, 2009; Moseley *et al.*, 2009). At the protein level, Pom1 is enriched at cell tips and forms a gradient along the cell. Pom1 in shorter cells phosphorylate and inhibit *cdr2*, as yeast cell grows during G2 phase, *cdr2* is liberated from Pom1-inhibition which results in the activation of downstream events involving CDK activity and entry into mitosis (Martin and Berthelot-Grosjean, 2009; Moseley *et al.*, 2009). Although this places Pom1 to be a sole size-sensor in fission yeast, a later study found that cell size homeostasis could still be achieved in the absence of Pom1 (Wood and Nurse, 2013), suggesting independent and/or multiple pathways involved in size homeostasis. Although the role of DYRKs in plant cell size control has not yet been investigated, we note that *Arabidopsis* YAK1 which is a DYRK protein, may play functionally equivalent role in meristematic tissues.

Like yeast cells, in *Arabidopsis*, CDK activity mainly drives passage through different cell cycle stages and cell growth (Jones *et al.*, 2017, 2019); here we have identified TOR signalling, which partially promotes CYCD2 protein accumulation that correlates with cell size diel changes, as an upstream pathway involved in maintaining size homeostasis that likely acts on the G1-to-S phase transition. Additionally, exogenous sugar supply could suppress the end-of-day reduction in cell size and CYCD2 level, suggesting that TOR is central to coupling nutritional control of cell size and cell cycle, and likely drives CDK activity. However, it cannot be ruled out whether sucrose increases protein stability of CYCD2, which would result in

increased CYCD2 detected at the end-of-day. In this regard, sucrose has been shown to increase stabilisation of DELLA (aspartic acid (D)-glutamic acid(E)-leucine(L)-leucine(L)-alanine(A)) proteins that function as negative regulators of gibberellin signalling (Li *et al.*, 2014). Whether exogenous sucrose promotes CYCD2 stabilisation can be experimentally tested by treating CYCD2-GFP seedlings with cycloheximide (CHX; an inhibitor of protein synthesis) and detecting CYCD2 level by GFP antibody over time.

Our cell cycle and size measurements with high temporal resolution identified a previously unknown role of TOR signalling in G2/M regulation as well as mediating RBR phosphorylation and provided strong cellular evidence for direct role in cell size control. Future work will likely shed light on the precise molecular mechanisms involved in separating roles of TOR signalling in cell cycle and cell growth control to maintain size homeostasis in meristematic tissues.

5

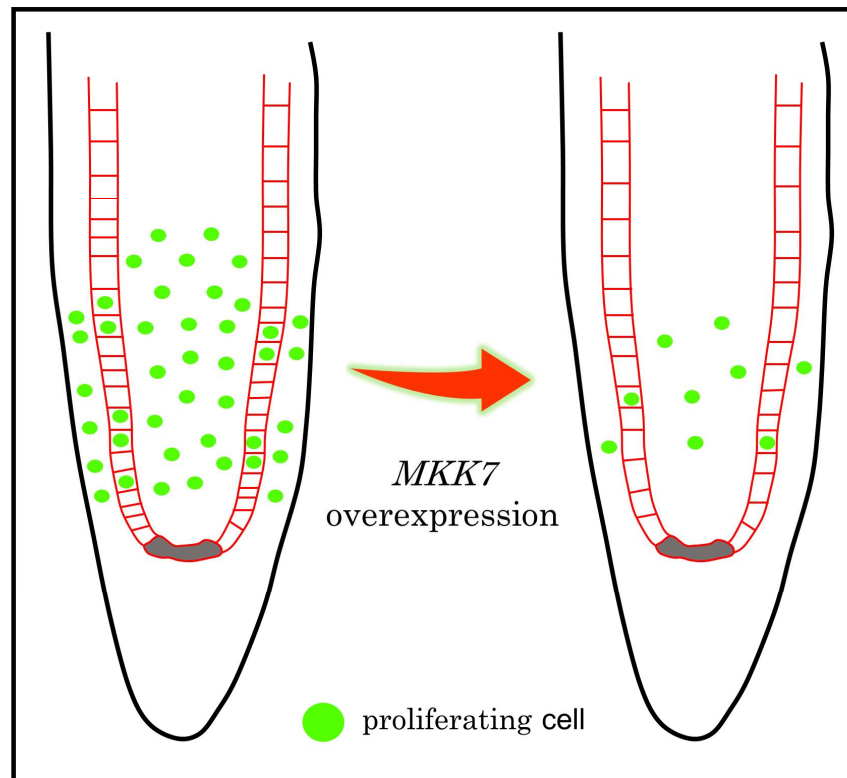
Chapter 5 MKK7, a MAP kinase kinase, is a negative regulator of the cell cycle

Declaration – Work presented in this chapter appears in:

Róbert Dóczi, Elizabeth Hatzimasoura, Sara Farahi Bilooei, Zaki Ahmad, Franck Anicet Ditengou, Enrique Lopez Juez, Klaus Palme and László Bögre (2019). The MKK7-MPK6 MAP Kinase Module is a Regulator of Meristem Quiescence and Outgrowth in *Arabidopsis*. *Frontiers in Plant Science*. <https://doi.org/10.3389/fpls.2019.00202>

MKK7, a MAP kinase kinase, is a negative regulator of the cell cycle

In this chapter, I set out to characterise meristem in the root tip of an inducible overexpression line of *MKK7* (Dory *et al.*, 2018).



MKK7 overexpression reduces meristem size by inhibiting cell cycle

In a nutshell

- Induced overexpression of *MKK7* leads to dramatic lowering of primary root growth rate in a dose-dependent manner
- Elevated level of *MKK7* leads to meristem shortening and reduced number of cells, but increased cell length
- Elevated *MKK7* levels result in a dramatic reduction in S phase count

5.1 Introduction

MAP KINASE KINASE 7 (MKK7) belongs to the MKK family of MAPKs that is positioned in the middle of the three-tiered MAPK module and function to converge and diversify signalling events (Cardinale *et al.*, 2002). Elevated *MKK7* expression in the gain-of-function *bushy and dwarf 1 (bud1)* mutant leads to strong phenotypes such as ~80% reduction in plant height with smaller cells in rosette leaves and over halved the number of lateral roots than wild-type (Dai *et al.*, 2006). Conversely, the *mkk7* mutant plants are bigger with increased number of lateral roots (Jia *et al.*, 2016), whether *MKK7* expression alters cellular dynamics in the primary root has not yet been explored.

MPK6 was shown to be a downstream phospho-target of MKK7, and together the MKK7-MPK6 cascade regulates shoot branching through phosphorylating PIN1 on Ser337 which influences its polar localisation and auxin flow (Jia *et al.*, 2016). MPK6 and MPK4 were also shown to phosphorylate PIN-FORMED 1 (PIN1) within the hydrophilic loop at multiple conserved sites adjacent to sites phosphorylated by AGC kinases, such as PINOID (Dory *et al.*, 2018). MPK6 and PINOID oppositely regulate PIN1 localisation, the former leads to PIN1 plasma membrane dissociation while the later to enhance PM attachment and polarity (Dory *et al.*, 2018). In the *bud1* mutant, continued activation of MKK7-MPK6 nodules results in prolonged PIN1 polarity which ultimately translates into increased branch number (Jia *et al.*, 2016). Induced overexpression of *MKK7* was shown to also disturb PIN1 polarity in young root tips, where plasma membrane localisation of PIN1 is significantly compromised (Dory *et al.*, 2018).

MKK7 is among the four MKKs that is mitochondrial-localised and has a regulatory role in enhancing stomatal clustering (Lampard *et al.*, 2014). Salt stress promotes kinase activity of MKK7 through phosphatidic acid which subsequently promotes MPK6 activity (Shen *et al.*, 2019). NaCl addition to growth media rapidly reduces primary root growth through reduced cell production rate in the meristem (West *et al.*, 2004). The precise molecular mechanism of salt stress-induced cell cycle repression is unknown, but it likely involves MKK7-MPK6 as it is the predominant MAPK cascade that participates in the cellular response. Additionally, MKK7 is required for systemic acquired resistance to bacterial diseases (Zhang *et al.*, 2007). Lastly, RPS6A was identified as a downstream target of MKK7-MPK3/6, the functional relevance of this is unknown (Huck *et al.*, 2017). RPS6A is a direct target of TOR kinase phosphorylation (Dobrenel, Mancera-Martínez, *et al.*, 2016) which is well-documented as a positive regulator of cell cycle and cell growth (see Chapter 4). Thus, MKK7 likely counteracts TOR signalling.

In summary, the studies summarised above demonstrate involvement of MKK7 in several growth and developmental processes in both shoots and roots. In this brief chapter, we examine how the level of *MKK7* alters primary root growth as well as cell cycle-driven root meristem growth. We find a dramatic reduction in S phase count but increased meristematic cell size upon *MKK7* overexpression. A model is proposed to explain the MKK7 connection to cell cycle with cell growth to maintain cell size homeostasis.

5.1.1 Aims and objectives

The central aim of this chapter is to characterise *Arabidopsis* root phenotypes upon elevated levels of MKK7 by utilising the line of *MKK7* expression driven under the control of a β -estradiol-inducible promoter system (Dory *et al.*, 2018).

Aim 1. determine the effect of different elevated levels of MKK7 on primary root growth

Accompanying objective: Carry out root growth assay with different estradiol concentrations to induce varying levels of MKK7 and measure root length after transfer to +/- estradiol MS media

Aim 2. characterise short-term effect of MKK7 overexpression on the root meristem using propidium iodide staining

Accompanying objective: measure meristem size, number and size of meristematic cells upon MKK7 induction

Aim 3. characterise short-term effect of MKK7 overexpression on cell cycle using EdU labelling

Accompanying objective: Carry out EdU labelling with different estradiol concentrations and count number of S phase cells as a proxy for cell cycle 'state' of the root meristem

5.2 Results

5.2.1 Overexpression of *MKK7* dramatically inhibits primary root growth

As a first step to understand the relationship between mitogen-activated protein (MAP) kinase kinase 7 (MKK7) and plant growth, we made use of an estradiol-inducible overexpression line (*pER8:MKK7*) which has been previously described (Dory *et al.*, 2018) and carried out a root growth assay. Six-day old seedlings grown under standard growth conditions of 1% sucrose under long-day were transferred to three different β -estradiol concentrations of 0.01 μ M, 0.1 μ M, 1 μ M. The position of the growing root tip was marked every day for three days (Figure 5.1A).

In the empty vector, there was no significant difference within the three β -estradiol concentrations during the course of the experiment (Figure 5.1B,C). Without β -estradiol, the average root growth rate of *pER8:MKK7* was around 7mm (+/- 1.2mm) and at 0.01 μ M the average growth rate was around 3mm (+/- 0.8mm; Figure 5.1C), with a 60% root inhibition at 1d after transfer (DAT). At 0.1 μ M and 1 μ M, the average growth rate was around 0.31mm (+/- 0.1mm) and 0.24mm (+/- 0.1mm), respectively (Figure 5.1C). Surprisingly, within 1DAT, 0.1 μ M and 1 μ M led to a 95% and 97% root inhibition, respectively (Figure 5.1C). There was no apparent difference in MKK7 root growth between 0.1 μ M and 1 μ M during the three days of experiment, suggesting a set threshold of MKK7 protein level is reached between 0.01 μ M and 0.1 μ M. Further, the rapid near-complete inhibition of growth implies that MKK7 is a negative regulator of root growth.

5.2.2 *MKK7* overexpression reduces root meristem size and number of cells, but increases meristematic cell size

Since root growth is dependent on cell cycle in the meristem (Gázquez and Beemster, 2017), we next characterised different parameters 16h after transfer to 0.1 μ M β -estradiol (Figure 5.2A). We selected 16h as a sole time-point as we observed a

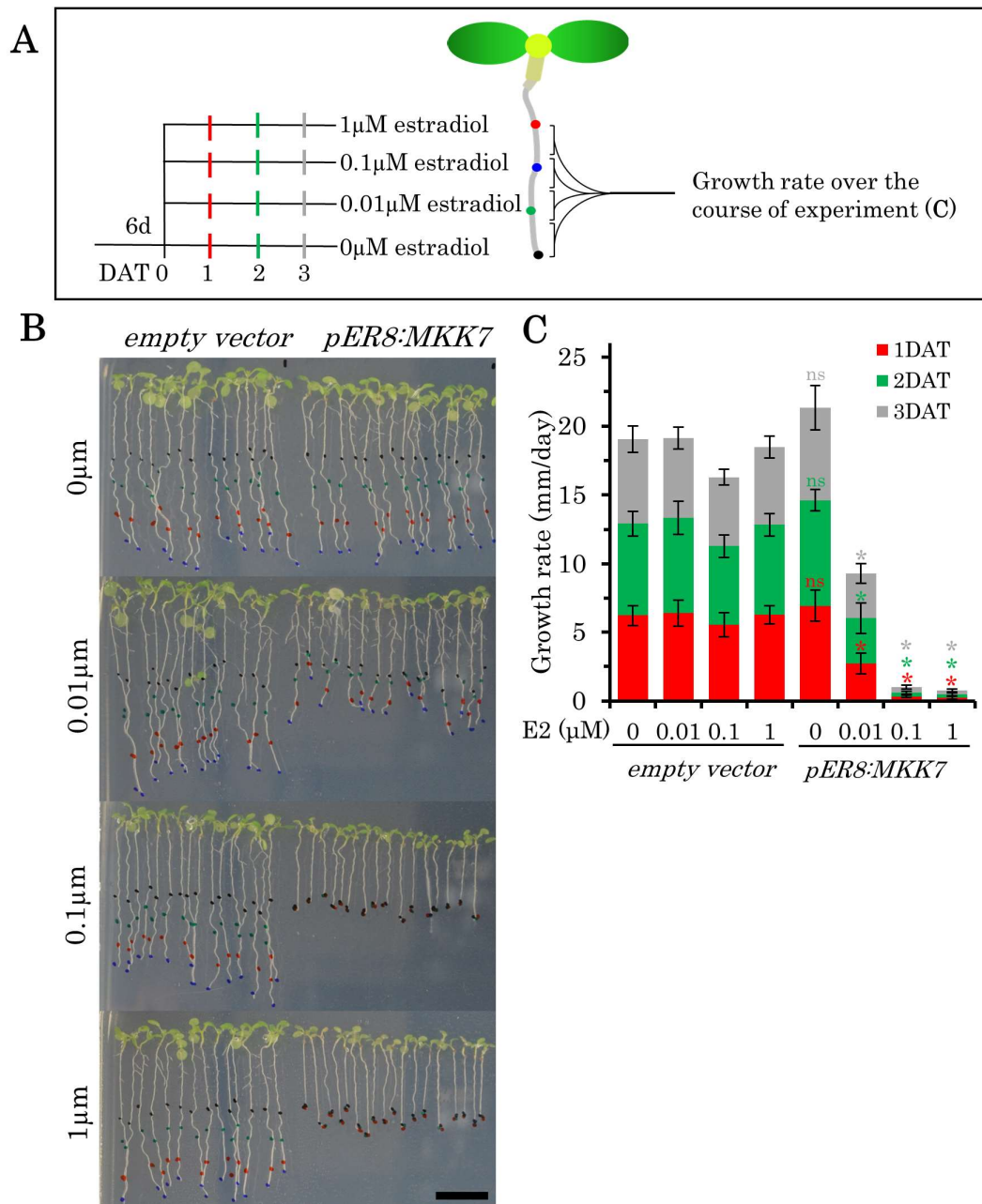


Figure 5.1 Overexpression of *MKK7* causes a dramatic primary root growth reduction.

A. Schematic of experimental design. Seeds of empty vector and *pER8:MKK7* estradiol inducible line were sown on 1% suc under long-day growth condition. At 6d, seedlings were transferred to different β -estradiol concentrations and position of the primary root tip was marked daily for a 3d period which was used to plot growth rate.

B. Representative whole-plant photographs of empty vector and *pER8:MKK7* with or without 0.1 μ M estradiol. Scale bar = 10mm

C. Primary root growth rate measurements of empty vector and *pER8:MKK7*, determined as distance between two marks along the root.

Data presented as mean, error bars represent standard deviation. Number of biological repeats (N) = 3. Average number of roots (n) = 14. Statistical differences between empty vector and *pER8:MKK7* with or without estradiol were determined using Student's t-test. Asterisk represents a significant difference, "ns" represents a difference that is not significant. DAT= days after transfer, E2 = β -estradiol.

dramatic inhibition of primary root within 24h. In the same experimental batch as the growth assay, we checked the root meristem under a confocal microscope using propidium iodide staining (Figure 5.2A). Cell length profile was measured in the cortex layer and used to determine size of meristem, number of cells, and average meristematic cell size (Figure 5.2A).

There was no apparent difference between estradiol-free and 0.1 μ M in the cell length profiles of the empty vector and steady-state of cell size (Figure 5.2B,C). *MKK7* overexpression shifts the curve to the left implying an early transition to elongation (Figure 5.2B,C). Additionally, upon *MKK7 overexpression*, cells appear to accumulate in the transition zone for longer compared with the mock and empty vector controls (Figure 5.3). From the cell profile, meristem size was determined to be around 230 μ m for estradiol-free (+/- 19.1 μ m) and 0.1 μ M empty vector (+/- 8.8 μ m), and estradiol-free (+/- 18.5 μ m) *MKK7* roots (Figure 5.2D). Induction of *MKK7* overexpression with 0.1 μ M β -estradiol shortened the meristem to ~150 μ m (+/- 16.4 μ m), a reduction of around 30% (Figure 5.2D). Additionally, *MKK7* overexpression decreased number of meristematic cells by ~50%, from 35 (+/- 3.5 μ m) to 18 (+/- 1.3 μ m) on average (Figure 5.2E). Interestingly, the average cell size in the meristem increased by 20% upon *MKK7* overexpression (Figure 5.2F) suggesting an early transition to cell cycle exit or uncoupling of cell cycle progression from cell growth.

5.2.3 Overexpression of *MKK7* reduces number of S phase cells in the root meristem

To confirm *MKK7* involvement in cell cycle as indicated by reduced meristematic cell count, we carried out EdU labelling to visualise cells in S phase. Six-day old seedlings

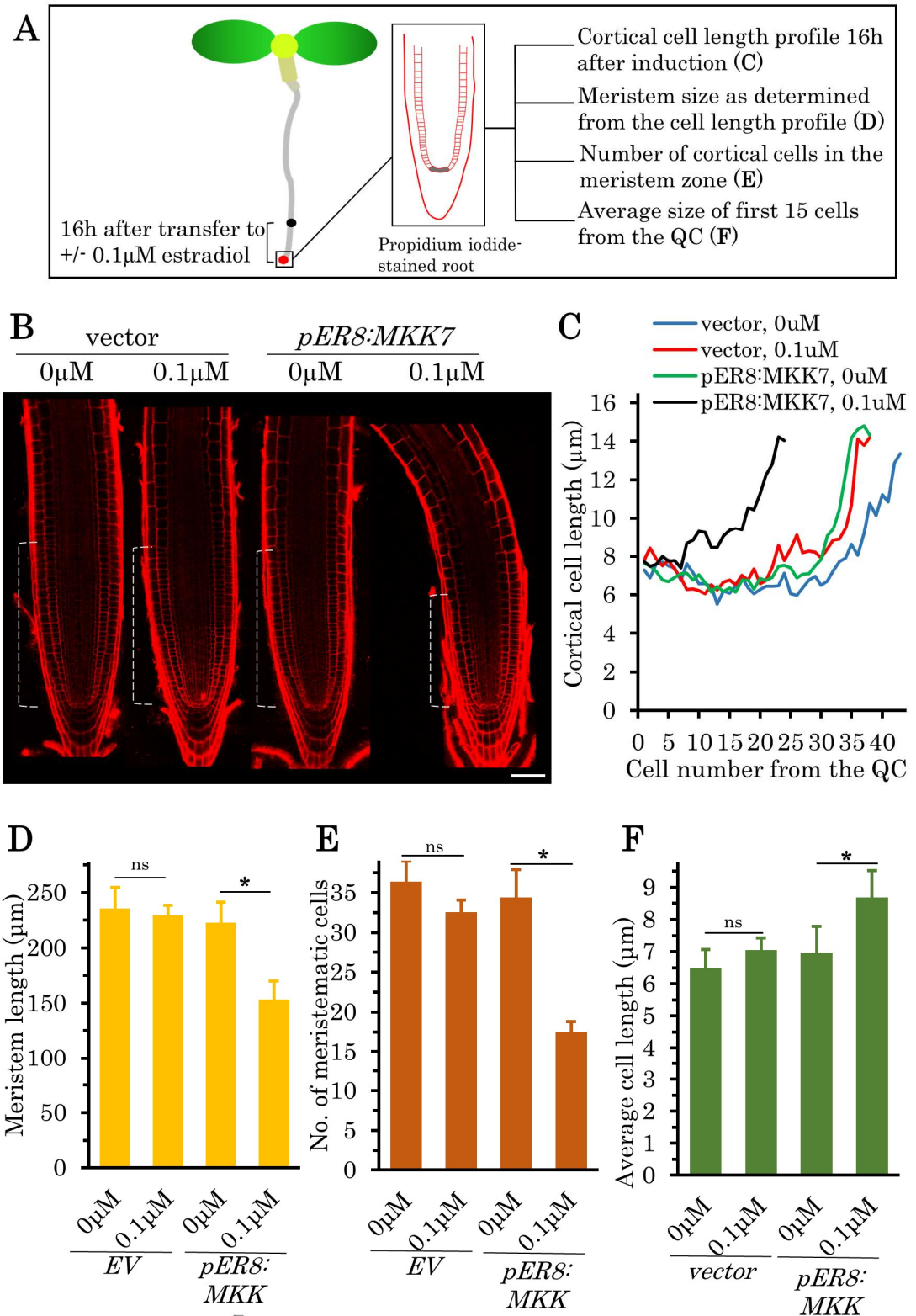


Figure 5.2 *MKK7* overexpression shortens the meristem.

A. Schematic of measurements made. At 6d, empty vector and *pER8:MKK* seedlings were transferred to +/- 0.1µM estradiol and confocal images were taken 16h after transfer.

B. Representative confocal micrographs of PI-stained (red) empty vector and *pER8:MKK7* root tip with or without 0.1µM estradiol. Dashed lines represent meristem length. Scale bar = 50µm.

C. Cortical cell length profiles of empty vector and *pER8:MKK7*.

D. Root meristem length of empty vector and *pER8:MKK7*.

E. Number of cells in the meristem of empty vector and *pER8:MKK7*.

F. Average length of meristematic cells of empty vector and *pER8:MKK7*.

Data presented as mean, error bars represent standard deviation. Average number of roots (n) = 11. Number of biological repeats (N) = 1. Statistical differences between empty vector and *pER8:MKK7* with or without 0.1 μ M estradiol were determined using Student's t-test. Asterisk represents a significant difference, "ns" represents a difference that is not significant.

Note: Panels D-F are derived from the cell length profile in Panel C.

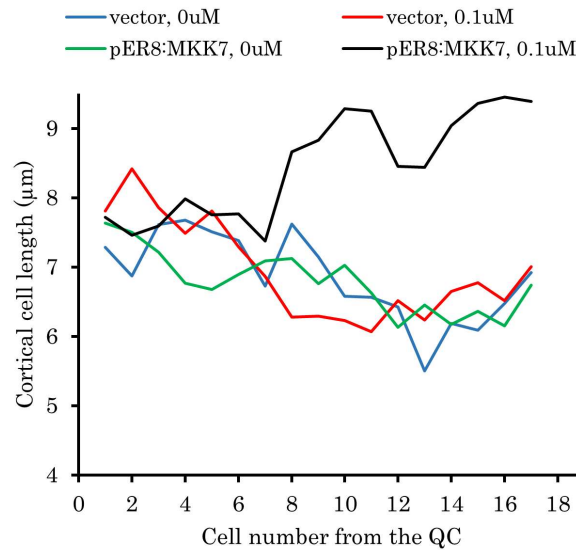


Figure 5.3 Elevated level of MKK7 obscures meristem-to-elongation boundary

A closed-up view of plot in Figure 5.2C.

grown under standard growth conditions were transferred to three different β -estradiol concentrations of 0.01 μ M, 0.1 μ M, 1 μ M for 16h and number of S phase cells were counted in six 50 μ m sections from the QC (Figure 5.4A).

There was no significant difference between estradiol-free and all other β -estradiol concentrations in the empty vector in all measured 50 μ m sections along the root tip (Figure 5.4B,C). We also did not note any significant difference between 0 μ M and 0.01 μ M β -estradiol in all 50 μ m sections of the *MKK7* root. Induction of *MKK7* overexpression with 0.1 μ M reduced number of EdU-positive cells by ~70%, from a total count of 63 (+/- 9.1) S phase cells to 17 cells (+/- 11.5; Figure 5.4C). A further 20% reduction was observed with 1 μ M β -estradiol (Figure 5.4C). In short, *MKK7*

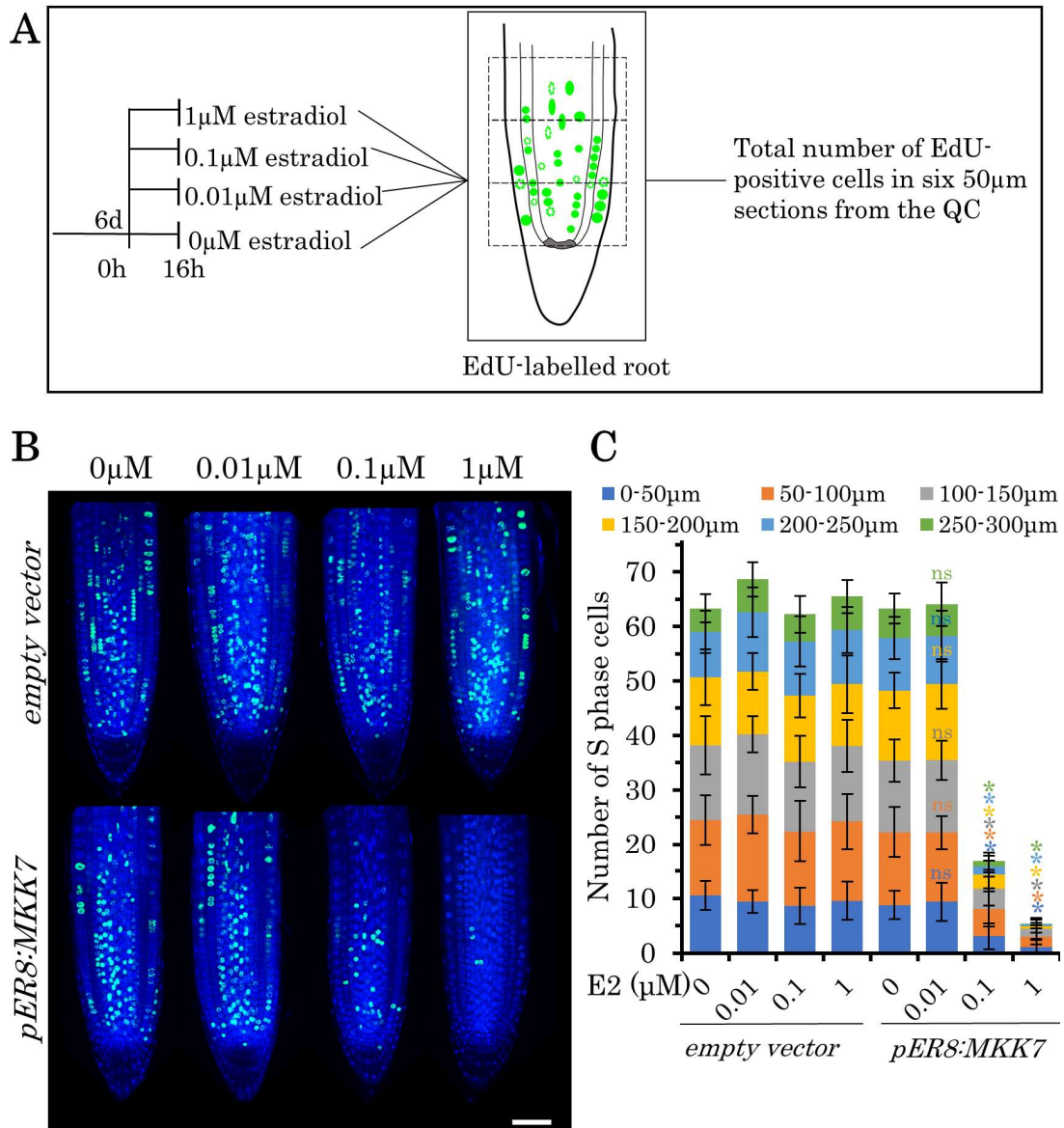


Figure 5.4 S phase count in response to *MKK7* overexpression.

A. Schematic of experimental design. Seeds of empty vector and *pER8:MKK7* estradiol inducible line were sown on 1% suc under long-day growth condition. At 6d, seedlings were transferred to different estradiol concentrations for 16h. All EdU positive S phase cells were manually counted.

B. Representative confocal micrographs of DAPI-stained (blue) EdU-labelled (green) root tip of empty vector and *pER8:MKK7* for each estradiol concentration. Scale bar = 50µm.

C. Number of S phase (Edu) cells of empty vector and *pER8:MKK7* in each estradiol concentration.

Data presented as mean, error bars represent standard deviation. Average number of roots (n) = 21. Number of biological repeats (N) = 1. Statistical differences between empty vector and *pER8:MKK7* with or without corresponding estradiol concentration at each 50µm region (colour-coded) were determined using Student's t-test Asterisk represents a significant difference, "ns" represents a difference that is not significant. E2 = β -estradiol.

overexpression drastically lowered S phase count implying a negative regulatory role of cell cycle.

Consistent with Hypothesis 4 stated in section 1.9, I showed induced overexpression of *MKK7* inhibits cell cycle as measured by EdU labelling.

5.3 Discussion

MKK7 is induced by both abiotic and biotic stresses and likely re-organises plant growth and developmental processes. In this chapter, we examined how changing the expression level of *MKK7* affects primary root growth and meristem under standard growth conditions without any stress. We found a near-complete inhibition of root growth and a dramatic reduction in meristem size and number of cycling cells within one day after induced overexpression of *MKK7*. This places *MKK7* to have a negative regulatory role in cell cycle. Based on the *mpk6* mutant analysis, a similar conclusion was made for *MPK6* which is a *MKK7* phospho-target (López-Bucio *et al.*, 2014). In synchronised BY2 cells, *MPK6* transcript accumulates during G2 and peaks during mitosis (Trolet *et al.*, 2019). Thus, the *MKK7*-*MPK6* signalling may act on the G2-to-M phase transition and the effect on S phase might be a secondary effect. This is consistent with the timing of 16h required for the pronounced reduction in EdU labelling, although a time-course with higher temporal resolution should resolve how long it takes for S phase reduction upon *MKK7* overexpression.

Some of the phosphorylation substrates of *MPK6*, include RBR, MYB3R5, and TESMIN/TSO1-LIKE CXC 2, also known as TCX2 (Popescu *et al.*, 2009). MYB3R5 have redundant G2/M transcriptional repressor functions with MYB3R3, and together with RBR among other cell cycle proteins, form the DREAM complex

(Kobayashi, T. T. Suzuki, *et al.*, 2015). TCX2 is likely homologue of the animal DNA-binding LIN54 that is also a DREAM member (Kobayashi, T. Suzuki, *et al.*, 2015). Given our EdU data indicates a rapid inhibition of cell cycle upon *MKK7* overexpression, it is reasonable to speculate that the continued MKK7-MPK6 cascade activation potentiates the repressive function of DREAM complex through RBR and/or MYB3R5 phosphorylation.

Interestingly, despite reduced cell cycle in the root meristem, the average meristematic cell length is increased in response to *MKK7* overexpression. This suggests a possible dual role MKK7 may play in coordinating cell cycle with cell growth to maintain cell size homeostasis. In animal cells, the p38 MAPK was shown to coordinate length of G1 phase with cell growth such that small cells have increased p38 activity and thus have a prolonged G1 and allowing more time to accumulate mass (Liu *et al.*, 2018). A similar size-sensing mechanism may exist in *Arabidopsis*; indeed, it was reported that meristematic cells measure size at both G1/S and G2/M transitions (Jones *et al.*, 2017). The G2/M cell size checkpoint may involve MAPK signalling. In short, we identified MKK7 as a possible upstream regulator of cell proliferation that likely coordinates with other signalling pathways.

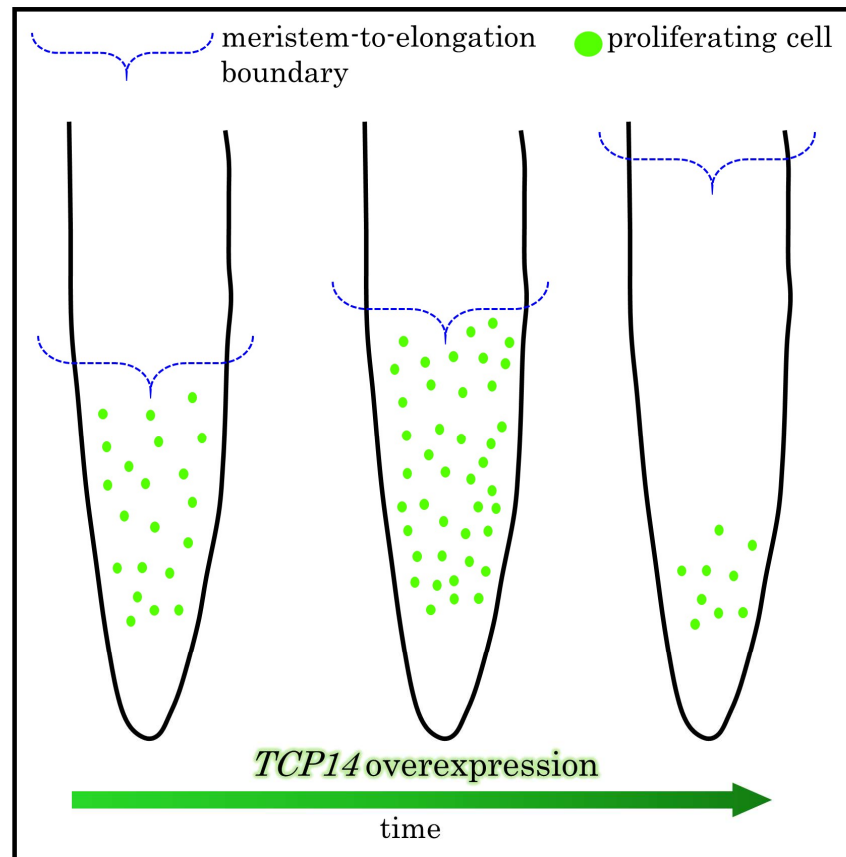


Chapter 6 TCP14 coordinates cell proliferation with cell elongation

Declaration – Data presented here is part of a collaboration and was originally performed and interpreted by Ruy Kortbeek, Maaïke Krijnen and Beatrix Horvath (Utrecht University, The Netherlands). A biological repeat presented here was performed by the author. Manuscript in preparation.

TCP14 coordinates cell proliferation with cell elongation

In this chapter, I set out to characterise cell cycle dynamics in the root meristem of inducible overexpression line and knock-out mutant of *TCP14* transcription factor.



Elevated level of TCP14 disturbs the transition zone

In a nutshell

- Primary root of *tcp14* mutant grows slightly faster with increased number of meristematic cells
- Induced overexpression of *TCP14* leads to dramatic reduction in root growth
- Short-term *TCP14* overexpression leads to increased S phase cells and increased meristem size
- Prolonged overexpression of *TCP14* leads to near-complete inhibition of cell proliferation and an increase of meristem-to-elongation zone boundary

6.1 Introduction

TCP14 belongs to class I TEOSINTE BRANCHED1/CYCLOIDEA/PROLIFERATING CELL FACTOR1 family of transcription factors, whose members include TCP20 that is known to be a negative regulator of endocycle onset or cell elongation (Li *et al.*, 2005). Phylogenetic analysis showed that *TCP14* together with *TCP7*, *TCP8*, *TCP15*, *TCP21*, *TCP22*, and *TCP23* form a distinct clade (Aguilar-Martinez and Sinha, 2013). The quadruple mutant *tcp8 tcp14 tcp15 tcp22* plants are extremely small and show a reduced response to gibberellins (Davière *et al.*, 2014), a phytohormone that promotes cell proliferation (Takatsuka and Umeda, 2014). Of all the TCPs, *TCP14* was found to be most strongly expressed during seed germination which is tightly coupled with cell cycle and protein synthesis (Tatematsu *et al.*, 2008). Additionally, the *TCP14* is highly expressed during the proliferation phase of leaf growth, especially in the shoot apex (Kieffer *et al.*, 2011). From the *Arabidopsis* Root Cell Atlas, *TCP14* transcript is also detectable in the root meristematic region (T. Q. Zhang *et al.*, 2019). In the *tcp14-4 tcp15-3* double mutant and *tcp8 tcp14 tcp15 tcp22* quadruple mutant, expression level of *A*- and *B*-type *CYCs* is significantly reduced (Kieffer *et al.*, 2011; Davière *et al.*, 2014).

Interestingly, overexpression *Chrysanthemum TCP14* in *Arabidopsis* resulted in reduced expression of *CYCs* and *CDKs* that corresponding with reduced organ size (Zhang *et al.*, 2017). Induced overexpression of *Gossypium TCP14* in *Arabidopsis* advances formation of trichomes and root hairs and promotes responsiveness to auxin in roots (Wang *et al.*, 2013). Chemical inhibition of proteasomal activity by MG132 increases intensity and spatial distribution of TCP14 and TCP15 and the protein stability of these two TCPs was shown to be regulated by ubiquitin receptors DA1, DAR1, and DAR2 (Peng *et al.*, 2015). Genetic analysis of double, triple, and

pentuple mutants placed *TCP14/15* downstream of DA proteins that promote protein degradation of TCP14/15 and therefore down-tunes the expression of endocycle repressors such as *RBR* and *CYCA2;3* (Peng *et al.*, 2015). Taken together, these heterologous expression and mutant studies suggest that a critical threshold of TCP14 (and other TCP proteins) abundance maintains normal plant growth and development through regulation of cell proliferation and endoreduplication.

In this brief chapter, we investigated the role of TCP14 in root meristem growth. We found that whilst the number of meristematic cells and root length in the *tcp14* mutant are significantly greater than wild-type, prolonged induced *TCP14* overexpression causes a dramatic reduction in cell proliferation as measured by EdU labelling. We propose a model whereby TCP14 level may define when cells enter cell elongation which feeds back to cell proliferation.

6.1.1 Aims and objectives

The central aim of this chapter is to define the cellular consequence of loss and elevated level of *TCP14* in the root tip.

Aim 1. determine the effect of loss and overexpression of *TCP14* on primary root growth

Accompanying objective: Carry out root growth assay with *tcp14* mutant and estradiol-inducible overexpression line of *TCP14* and measure root length after transfer to +/- estradiol MS media

Aim 2. characterise root phenotypes of *tcp14* mutant

Accompanying objective: use propidium iodide staining and measure meristem size, number and size of meristematic cells of wild-type and *tcp14* mutant

Aim 3. characterises short-term effect of *TCP14* overexpression on cell cycle using EdU labelling

Accompanying objective: Carry out EdU timecourse experiment and count number of S phase cells as a proxy for cell cycle ‘state’ of the root meristem

6.2 Results

6.2.1 TCP14 is a negative regulator of primary root growth

As a first step towards understanding the role of TCP14 in root growth, we characterised several cellular parameters including size and number of cells of the cortex layer in the root meristem of 7d old *tcp14-7 GABI611_C04* mutant, hereafter referred to as ‘*tcp14*’ (Figure 6.2A). Primary roots of *tcp14* were longer than wild-type Col-0 (Figure 6.1A) and on average, *tcp14* roots grew 20% more than Col-0 during 6d to 7d (Figure 6.1B). Propidium iodide-stained confocal imaging and cell length profile of *tcp14* root tips suggested that proliferation-to-elongation transition was further away in terms of cell position from the QC (Figure 6.2B,C). There was no significant difference between meristem size of Col-0 and *tcp14* (Figure 6.2D), however *tcp14* mutant had significantly more cells than Col-0 in the cortex layer (Figure 6.2E). Additionally, *tcp14* meristematic cortical cells were ~12% smaller than wild-type (Figure 6.2F). In summary, the increased root length of *tcp14* can be

explained by increased cell count in the meristem which does not affect meristem size due to the smaller size of dividing cells.

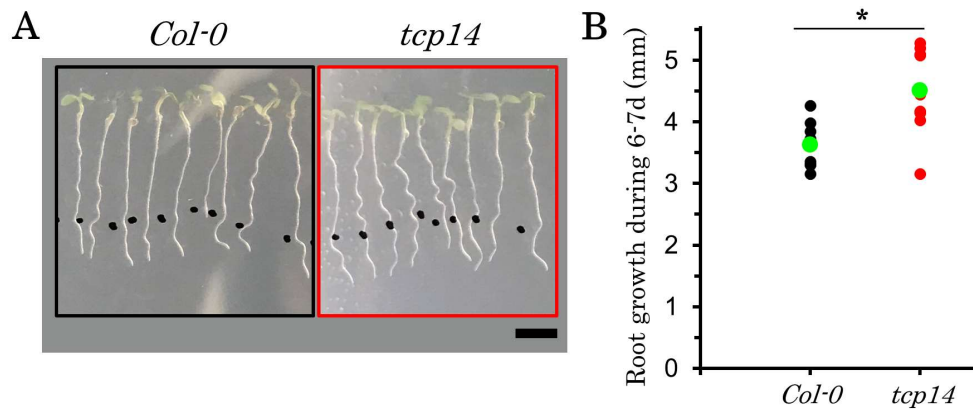


Figure 6.1 Increased primary root growth of *tcp14* mutant.

A. Whole-plant photographs of Col-0 and *tcp14*. Seeds were sown on 1% sucrose under long-day conditions. Root growth was measured between 6d and 7d. Scale bar = 4mm.

B. Measurements of primary root growth between 6d and 7d for both Col-0 and *tcp14* seedlings. Green circle represents the mean value.

Average number of roots (n) = 9. Statistical difference between Col-0 and *tcp14* using Student's t-test. Asterisk represents a significant difference. This is a biological repeat of collaborative work, conclusions made here are consistent with previous observations.

We next investigated the effect of elevated level of *TCP14* and measured root growth of estradiol-inducible overexpression line of *TCP14* (hereafter referred to as *TCP14-iOE*) and transferred 5d old seedlings of *TCP14-iOE* and Col-0 (*pERS*), hereafter referred to as empty vector or EV (Zuo *et al.*, 2000) as a control to 5 μ M β -estradiol containing media. There was no difference in root growth rate between *TCP14-iOE* and EV at 6h and 12h after transfer to estradiol, however, a 40% reduction was observed at 24h after transfer (Figure 6.3A,B). At 36h and 48h, EV roots grew by 2mm/day (+/- 0.7mm for 36h and +/- 0.6mm for 48h) whereas *TCP14-iOE* growth rate was 0.9mm/day (+/- 0.4mm for both timepoints; Figure 6.3A,B). In summary, the *tcp14* mutant shows increased primary root length and meristematic cells whilst prolonged overexpression of *TCP14* lowers root growth rate.

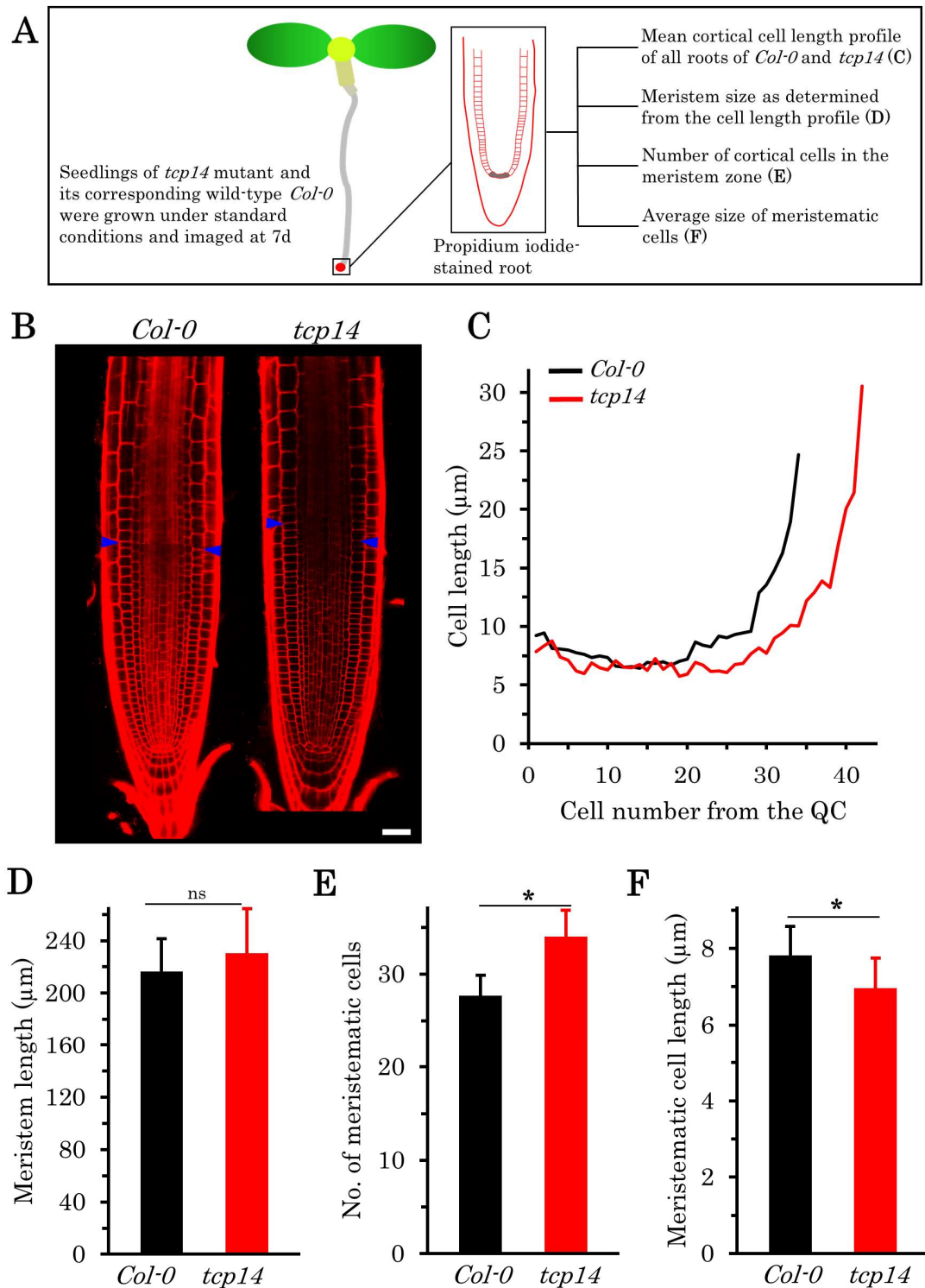


Figure 6.2 Cellular phenotypes of *tcp14-7* mutant root tip.

A. Schematic of measurements made. Confocal images of 7d old root tip of *Col-0* and *tcp14-7* mutant. Profile of cortical cell length was used to determine meristem size, number and average cell size cells.

B. Representative confocal micrograph of PI-stained (red) *Col-0* and *tcp14*. Blue arrowheads point meristem boundary. Scale bar = 30 μm

- C. Cortical cell length profiles of Col-0 and *tcp14*.
- D. Root meristem length of empty Col-0 and *tcp14*.
- E. Number of cells in the meristem in the cortex layer of Col-0 and *tcp14*.
- F. Average length of meristematic cells of Col-0 and *tcp14*.

Data presented as mean, error bars represent standard deviation. Average number of roots (n) = 9. Statistical differences between Col-0 and *tcp14* were determined using Student's t-test. Asterisk represents a significant difference, "ns" represents a difference that is not significant. This is a biological repeat of collaborative work, conclusions made here are consistent with previous observations.

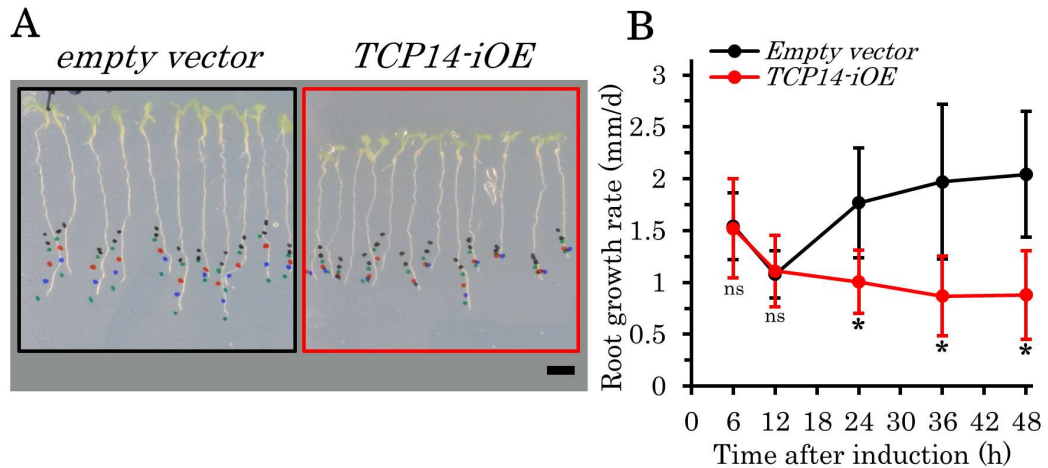


Figure 6.3 Overexpression of *TCP14* causes a dramatic primary root growth reduction.

A. Whole-plant photographs of empty vector and *TCP14-iOE* estradiol inducible line. Seeds were sown on 1% sucrose under long-day conditions. At 5d, seedlings were transferred to +/- β -estradiol, and position of root tip was marked for 48h after transfer. Scale bar = 4mm.

B. Primary root growth rate measurements of empty vector and *TCP-iOE*, determined as distance between two marks along the growing root.

Data presented as mean, error bars represent standard deviation. Average number of roots (n) = 12. Statistical differences between empty vector and *TCP14-iOE* estradiol inducible line for each timepoint were determined using Student's t-test. Asterisk represents a significant difference, "ns" represents a difference that is not significant. This is a biological repeat of collaborative work, conclusions made here are consistent with previous observations.

6.2.2 Temporal changes in S phase count upon *TCP14* overexpression

To better understand root inhibition of *TCP14-iOE*, we carried out EdU labelling to visualise DNA replication in proliferating cells of the root tip. *TCP14-iOE* and EV

roots were collected at 0, 3, 6, 12, 24, and 48h after β -estradiol induction and the number of EdU-positive cells were recorded in 200 μ m region from the QC (Figure 6.4A). At 0h, the number of S phase cells in EV were 75 (\pm 12.0) which reduced to 58 (\pm 12.4) and 51 cells (\pm 9.3) at 3h and 6h, respectively and increased to 66 (\pm 7.9) cells at 12h and 24h and 77 (\pm 22.7) cells at 48h (Figure 6.4B,C). Whereas EV showed an initial drop in S phase count at 3h and 6h, number of S phase cells in *TCP14-iOE* did not change from 0h to 3h, but increased by 15% to 72 (\pm 17.9) cells at 6h which was 30% more than EV at the same timepoint. The 6h peak was followed by a decrease to 54 (\pm 10.4) cells and 44 (\pm 14.8) cells at 12h and 24h, respectively (Figure 6.4B,C). At 48h, only 16 (\pm 8.2) S phase cells were observed which mostly concentrated around the QC region, a \sim 75% reduction from the 6h peak of *TCP14-iOE* and EV count at 48h (Figure 6.4C).

We next measured meristem size which we defined as the distance from the QC to the last EdU-positive cell in the epidermis, cortex and endodermis layers of both sides of the root. To ensure accurate measurements of meristem length, we did not consider EdU-positive cell where the nuclei was visible large and the space between two nuclei increased as this indicates occurrence of endoreduplicating cells in the elongation zone. Although at 0h, meristem size of *TCP14-iOE* was significantly smaller than EV, comparing 144 μ m (\pm 24.4 μ m) with 199 μ m (\pm 40.0 μ m), *TCP14-iOE* meristem size at 3h increased by 20% whereas EV did not show any change (Figure 6.4D). At 6h and 12h, meristem size was statistically indifferent and *TCP14-iOE* showed a 15% and 40% reduction at 24h and 48h, respectively (Figure 6.4D).

To summarise, overexpression of *TCP14* leads to a short-term increase in S phase cell count and meristem length which is followed by a dramatic reduction in number of proliferating cells.

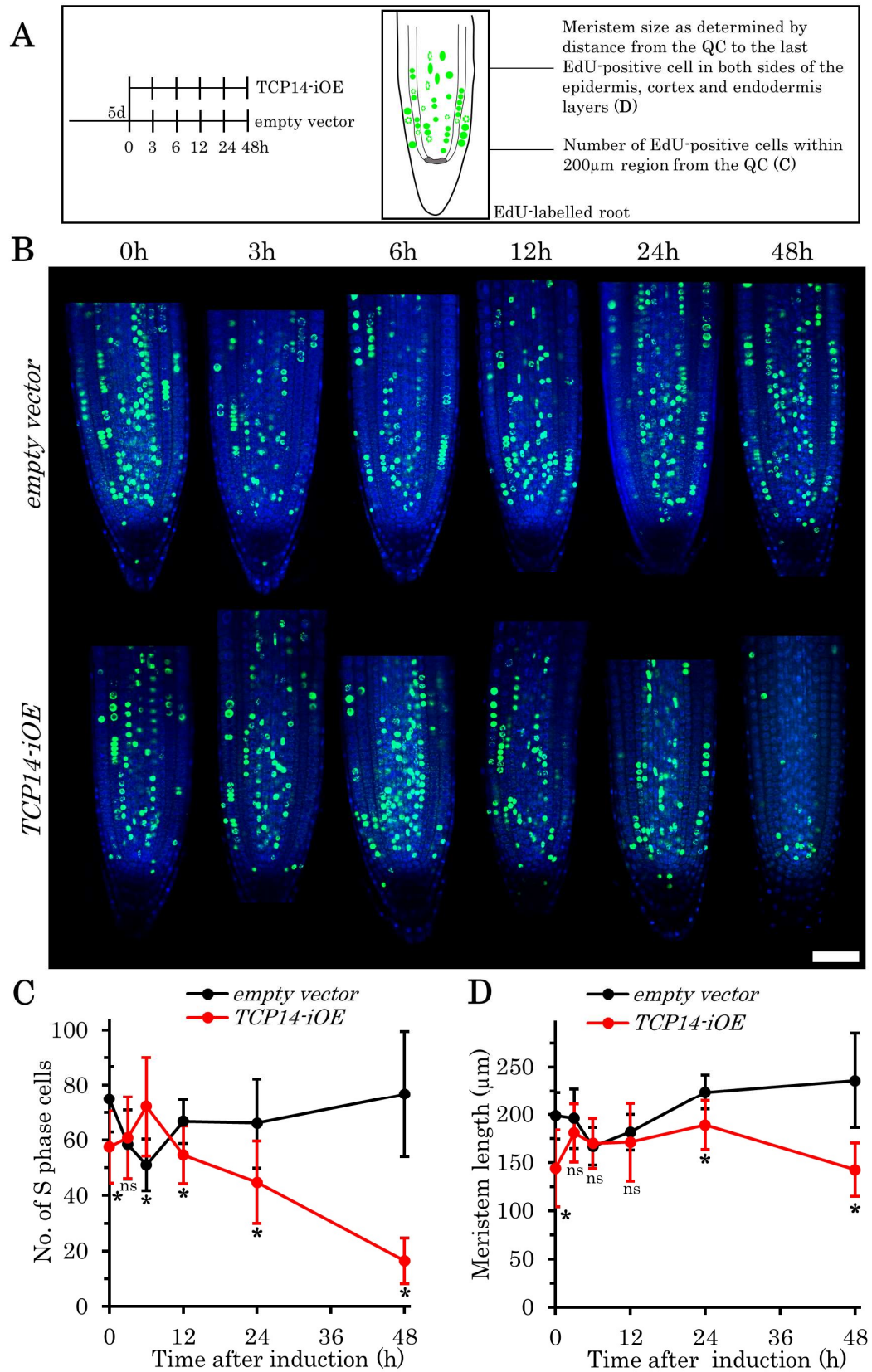


Figure 6.4 Temporal dynamics of S phase and meristem size in response to *TCP14* overexpression.

A. Schematic of experimental design. At 5d, seedlings of empty vector and *TCP14-iOE* estradiol inducible line were transferred to +/- β -estradiol. EdU-positive S phase cells within 200 μ m measured from the QC in all layers of the meristem were manually counted. Meristem size was defined as the average distance between the QC and the last EdU-positive cells in three outermost layers.

B. Representative confocal micrographs of DAPI-stained (blue) EdU-labelled (green) root tip of empty vector and *TCP14-iOE* for each timepoint. Scale bar = 50 μ m.

C. Number of S phase (EdU) cells of empty vector and *TCP14-iOE* in each timepoint.

D. Root meristem length of empty vector and *TCP14-iOE* in each timepoint.

Data presented as mean, error bars represent standard deviation. Average number of roots (n) = 8. Statistical differences between empty vector and *TCP14-iOE* at each timepoint were determined using Student's t-test. Asterisk represents a significant difference, "ns" represents a difference that is not significant. This is a biological repeat of collaborative work, conclusions made here are consistent with previous observations.

6.2.3 *TCP14* overexpression increases nuclei count in the transition-to-elongation zone

During the course of counting EdU-positive cells, we observed increased occurrence of DAPI-stained nuclei beyond the meristematic region at 48h after induction in the *TCP14-iOE* line. Thus, we quantified the number of nuclei within 500 μ m to 600 μ m region from the QC (Figure 6.5A). Number of nuclei in empty vector roots ranged from 25 to 42 and in *TCP14-iOE* the range was from 35 to 55 (Figure 6.5B,C). On average, *TCP14-iOE* and EV respectively had 45 (+/- 7.6) and 29 nuclei (+/- 5.2) within the 500-600 μ m region, a significant difference of 35%.

Morphological features of the nucleus, such as size and shape, varies along the primary root with elongated rod-like nuclei associated in the elongation/differentiation zone (Tamura and Hara-Nishimura, 2011). Compared with the empty vector, prolonged elevated level of TCP14 results in delayed spatial occurrence of elongated rod-like nuclei in the epidermal and cortex layers of the primary root (Figure 6.5C). Taken together, the significant reduction of S phase cells and high nuclei count beyond the meristem coupled with absence of rod-like nuclei strongly suggests that long-term overexpression of *TCP14* prevents cell from

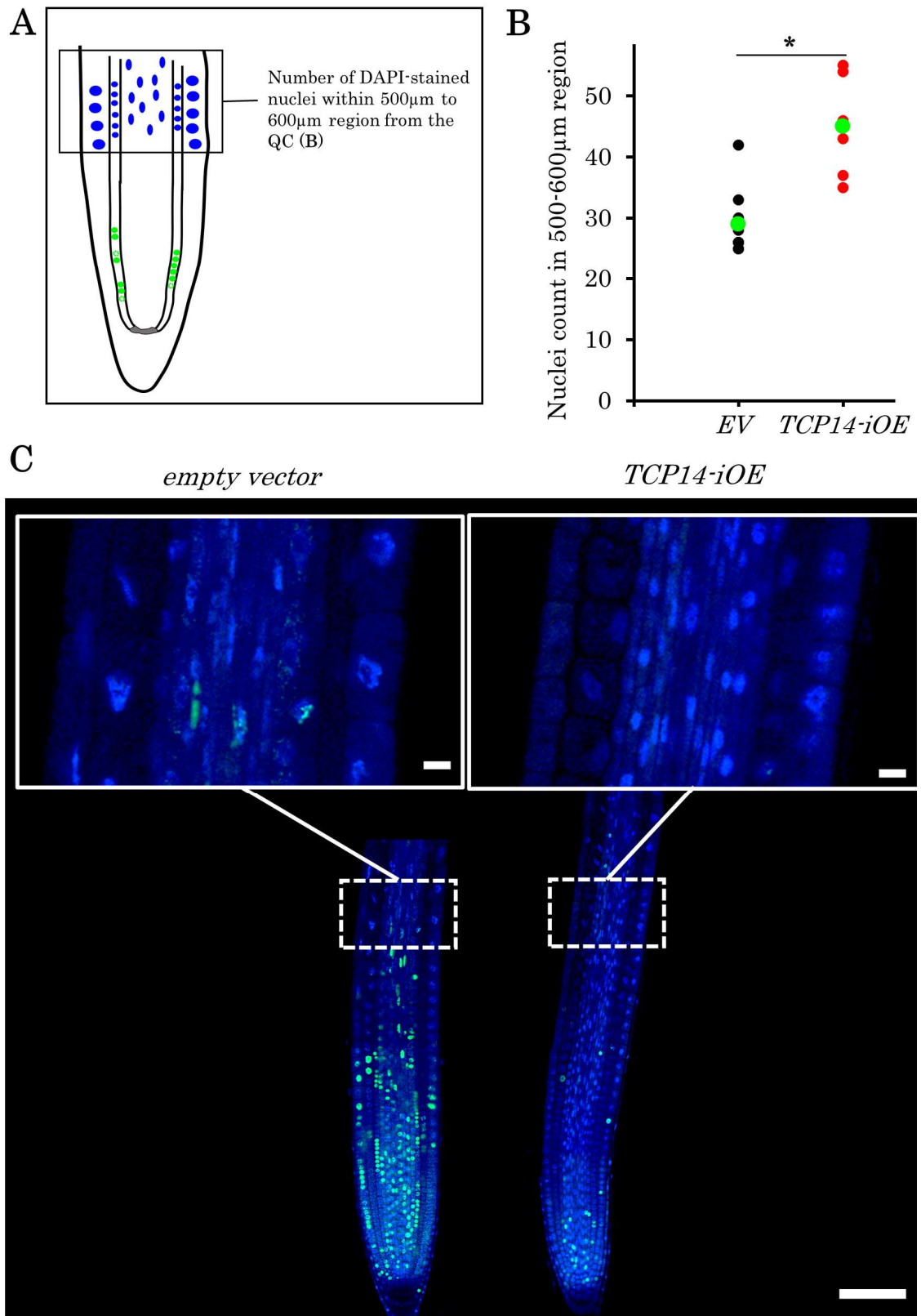


Figure 6.5 Continued overexpression of *TCP14* delays cell elongation.

A. Schematic of measurements made. Number of DAPI-stained nuclei within 500 μ m to 600 μ m region were counted 48h after estradiol induction.

B. Number of nuclei within 500-600 μ m region from the QC of empty vector and *TCP14-iOE* root. Green circle represents the mean value.

C. Representative confocal micrographs of DAPI-stained (blue) root tip of empty vector and *TCP14-iOE*, inset shows the 500 μ m to 600 μ m root region. Scale bar = 100 μ m. Inset scale bar = 10 μ m.

Data presented as mean, error bars represent standard deviation. Average number of roots (n) = 8. Statistical differences between empty vector and *TCP14-iOE* were determined using Student's t-test. Asterisk represents a significant difference. This is a biological repeat of collaborative work, conclusions made here are consistent with previous observations.

entering the elongation zone.

Consistent with Hypothesis 4 stated in section 1.9, I showed that induced overexpression of *TCP14* disturbs proliferation-to-elongation boundary such that cells struggle to exit the meristem/transitions regions as observed with occurrence of increased small-sized nuclei well-beyond the meristem zone.

6.3 Discussion

Long-term organ growth sustainability requires cells to timely enter, progress, and exit the cell division cycle. *tcp14* mutant has increased number of cells in the root meristem with reduced size. However, induced overexpression of *TCP14* has a two-stage phenotype. First, in the early hours of induction, S phase count increased; second, prolonged overexpression led to a dramatic near-complete inhibition of cell cycle suggesting that an increased protein level of TCP14 inhibits cell cycle. Quantification of spatial dynamics in response to prolonged *TCP14* overexpression revealed a build-up of small meristem/transition-like nuclei in 500 μ m to 600 μ m root region, considering that meristem size in the empty vector was around 230 μ m, the presence of small round-shaped nuclei without EdU signals shootward in *TCP14-iOE* suggests an inhibition or delay of cell elongation.

From the root ‘endoploidy map’ published by Bhosale and co-workers (2018), it appears that in endocycling cells of cortex layer, *TCP14* is differentially expressed with highest expression in 2C cells, intermediate expression in 4C and 16C cells, and lowest expression level in 8C cells (Bhosale *et al.*, 2018). The spatial down-tuning of *TCP14* transcript from 4C to 8C suggests that exit from mitotic cycle (4C cells) and switch to endocycle (8C cells) requires reduction of TCP14. Induced overexpression causes an early burst of S phase cells (Figure 6.4C), but presumably fails to meet the low threshold level of TCP14 to exit the meristem zone and start to elongate. Genes that show a similar expression pattern include several ribosomal proteins (Bhosale *et al.*, 2018) suggesting TCP14 transcriptional regulation may be involved in distinct spatial dynamics of protein synthesis-driven cell growth. TCP20 was proposed to couple cell growth with cell proliferation (Li *et al.*, 2005), and here we suggest that TCP14 may be involved on coupling cell proliferation with cell elongation and coordinatively tuning cell growth.

Exogenous supply of Root Growth Factor 1 (RGF1), a peptide hormone, greatly increases number of meristematic cells but does not proportionally increases primary root length (Matsuzaki *et al.*, 2010; An *et al.*, 2018). RGF1 sustains root meristem growth through stabilising PLETHORA (PLT) 1 and PLT2 transcription factors which form gradient along the root with highest level in the stem cell niche and gradually decreasing shootward (Galinha *et al.*, 2007; Matsuzaki *et al.*, 2010). Whether TCP14 is part of the RGF1-PLT signalling is not known, in this regard, PLT1 was shown to interact with TCP8, TCP20, and TCP21 proteins which function in the same pathway to control primary root formation and other root developmental contexts (Shimotohno *et al.*, 2018).

To summarise, in this short chapter we uncovered a new role of TCP14 in regulating meristem-to-elongation transition. The precise molecular mechanism of TCP14

action is yet to be discovered, but likely involves well-known regulators of cell cycle and/or endocycle. Plausible connections to TOR signalling and MAPK signalling cascade are made in the next chapter.



Chapter 7 General discussion, conclusions, and future perspectives

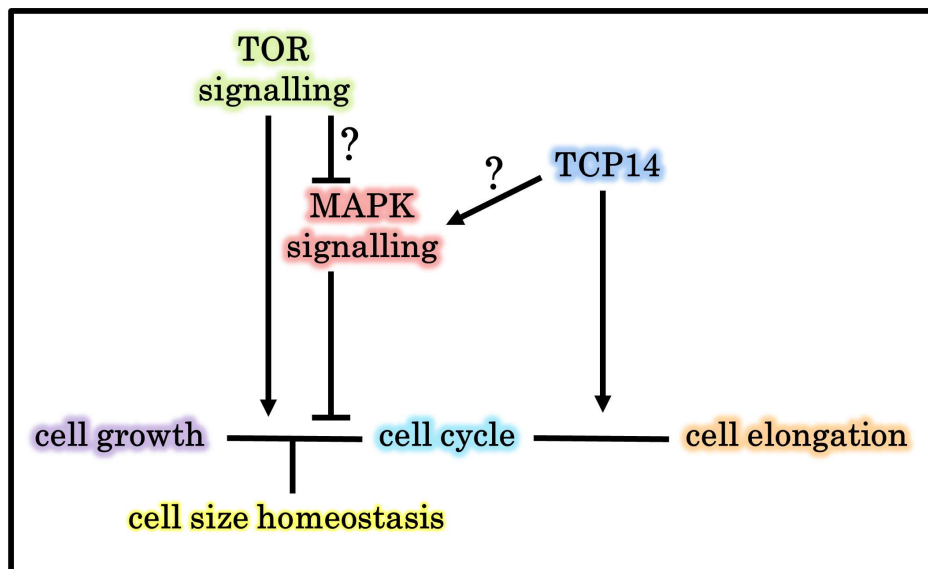
Declaration – some of the ideas presented in this chapter appear in:

Ahmad Z, Magyar Z, Bogre L, Papdi C (2019) Cell cycle control by the target of rapamycin signalling pathway in plants. *J Exp Bot.* 70: 2275-2284b

Rossana Henriques, Csaba Papdi, **Zaki Ahmad**, László Bögre (2018) Circadian Regulation of Plant Growth. *Annual Plant Reviews Online*
<https://doi.org/10.1002/9781119312994.apr0655>

General discussion, conclusions, and future perspectives

In this final chapter, I summarise main findings of the thesis and how it may fit with other working models and make a few suggestions for future work.



Molecular control of cellular processes driving root growth

In a nutshell

- Primary root growth is dependent on the proper execution of cell cycle progression and exit to cell elongation
- Light/sugar induced high TOR activity drives cell cycle during the day and supposedly reduced TOR activity at night limits cell cycle
- TOR signalling might work antagonistically to MAPK signalling cascade
- Diurnal rhythm of cell cycle may have an underlying circadian rhythm
- Down-tuning of cell cycle is actively controlled and might be driven by CDK inhibitors SMRs and KRPs
- Connection between TCP14 and a MAP kinase is discussed

Plant organ growth relies on continuous production and growth of cells in meristematic tissues, both of these processes (cell division cycle and cell growth) are extremely energy consuming and thus must only occur when nutrients are in abundant supply (Henriques *et al.*, 2014; Lastdrager *et al.*, 2014). Whilst root meristem is extensively used as a model system and much is known about hormonal and environmental control and some of the underlying genetic regulatory networks that shape root growth (Jung and McCouch, 2013; Kitagawa and Jackson, 2019), there is still a lack of complete understanding of cellular and molecular root biology, especially in relation to diel dynamics and sugar signalling. In this thesis I aimed to contribute in filling this gap by characterising cell cycle and cell size in relation to different growth conditions.

In chapter 3, I discovered the fluidity and rapid adjustment to light and sugar availability as well as diurnal rhythm of cell cycle- and cell size-driven root meristem growth. This followed the findings in chapter 4 that TOR signalling pathway likely regulates both G1-to-S phase and G2-to-M phase transition points, the former involves phosphorylation of RBR which is regulated upstream by TOR kinase. These novel findings suggest that cell cycle-driven root growth is tightly regulated and connected to cellular nutrient status which is continuously monitored both at the start of (G1/S) and throughout (G2/M) the cell cycle and is centred on TOR signalling.

In chapter 5, we defined MKK7, a MAP kinase kinase, as a negative regulator of cell cycle that may be involved in coupling cell cycle with cell growth. Finally, in chapter 6, we found that induced overexpression of *TCP14* transcription factor suppresses cells exiting the meristem region. The following discussion focuses on how these findings fill in the knowledge gap to advance current understanding of meristem growth dynamics.

Prolonged inhibition of TOR signalling severely reduces primary root growth as a result of blockage of S phase and onset of mitosis (Figures 4.3, 4.4, 4.7, 4.13). Long-term induction of *TCP14* overexpression also leads to strong root growth inhibition, due to suppression of cell cycle but additionally we noted that cell elongation is spatially delayed (Figures 6.3, 6.5). Elevated MKK7 amount strongly inhibits root growth due to loss of cell cycle in the meristem (Figures 5.1, 5.2, 5.4). By noting these observations in conjunction, we suggest that progression through and exit from the cell cycle to enter cell elongation are equally critical to sustain root growth, an imbalance between any of the two cellular events (namely, cell cycle entry and cell cycle exit coupled to cell elongation) can result in organ fatality as seen from near-complete inhibition of primary root growth upon overexpression of *MKK7* and *TCP14* and chemical inhibition of TOR.

Cell elongation is often accompanied with endocycle, an alternative form of cell cycle in which repeated rounds of DNA replication occurs without mitosis (de Veylder *et al.*, 2011; Bhosale *et al.*, 2018), whilst diel dynamics of endocycle has not yet been investigated, our observation of differential accumulation of E2FA and E2FB (Figure 3.7) suggests endocycle may have an underlying time-of-the-day dependent rhythm. This is based on previous reports that RBR-bound E2FA complex suppresses endocycle genes such as *CELL-CYCLE SWITCH 52 A 1* (*CCS52A*) and *CCS52A2* and E2FA is also mildly detectable in elongation zone (Magyar *et al.*, 2012), given the observation that E2FA protein is high during the morning and starts to decrease towards the end-of-day (Figure 3.7), this would presumably de-repress endocycle genes and promote onset of endocycle (Figure 7.1). This could be experimentally tested by carry out flow cytometry analysis of whole-root, collecting samples during mid-day and mid-night for a longer time period as supposed to our two-day

timecourse, as ploidy level increases as plants progress through developmental stages (Magyar *et al.*, 2012).

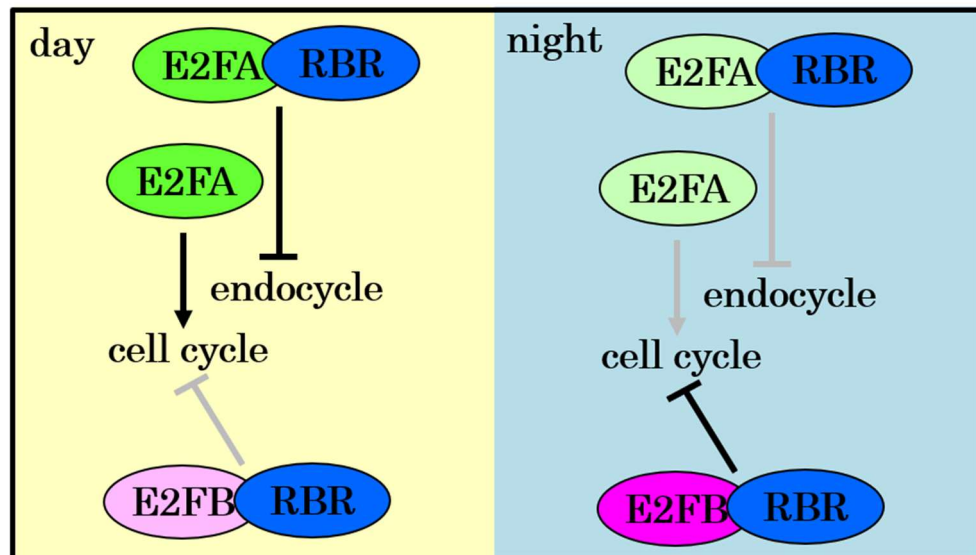


Figure 7.1 A proposed model of daily control of cell cycle and endocycle.

E2FA and E2FB largely have non-overlapping temporal pattern of protein accumulation such that E2FA level is high during the day whilst E2FB accumulates at night. RBR-bound E2FA complex is known to inhibit endocycle genes (Magyar *et al.*, 2012), reduced amount E2FA towards the end-of-day supposedly lifts this suppression and allows onset of endocycle. E2FB in complex with RBR acts as a negative regulator of cell cycle (Oszi *et al.*, 2019) and increased E2FB level during the night would increase formation of E2FB-RBR complex which subsequently prevents cell cycle. Thus, these three proteins (E2FA, E2FB, RBR) form a central regulatory network to tune cellular processes (cell proliferation and cell elongation) driving plant growth on a daily basis.

A major challenge for plants is to find the optimal balance between energy expenditure and energy production, and thus energy-consuming processes namely cell division and cell growth should optimally occur when nutrient supply is high. For plants, light/day period (photosynthesis-derived sugar availability) represents a nutrient-rich condition and dark/night period represents a low-nutrient condition (Mohammed *et al.*, 2018). Consistent with this notion, we found that overwhelmingly high number of cell division events occur during the day and cells divided less frequently and at smaller size during the dark hours (Figures 3.4, 3.5). Given that

diurnal rhythm of plant growth is largely regulated by the circadian clock which serves to harmonise growth-related processes with fluctuating environment (Smith and Stitt, 2007; Creux and Harmer, 2019); it is plausible that the diurnal rhythm of cell cycle we observed is under the control of the circadian clock.

Circadian regulation of cell proliferation is widespread in animals (Henriques *et al.*, 2018) and has also been reported in *Arabidopsis* where the evening clock component TOC1 binds to *CDC6* and constrains its transcription and thereby limits onset of cell cycle (Fung-Uceda *et al.*, 2018). Whether diel changes in cell cycle that we observed are clock-driven can be explored by timecourse EdU labelling experiment in circadian mutants and/or overexpression lines as well as free-running experiments, if cell cycle in the root meristem has a circadian rhythm then the diel changes should continue to occur in the absence of light-dark cycles.

TCP transcription factors have been implicated in regulation of circadian proteins, TCP20 and TCP22 was shown to bind to the TCP-binding site in the *CCA1* promoter (Wu *et al.*, 2016). Whether TCP14 is also capable of bind to *CCA1* promoter region needs to be investigated. *CCA1* is a transcription factor which is part of the core circadian network that accumulates in the morning (McClung, 2006), and its target genes include D-type cyclins (Nagel *et al.*, 2015). Thus, it seems plausible that TCP-circadian network works in parallel to E2FA to boost S phase gene expression in the morning (Figure 7.2).

The creation of diurnal rhythm of cell cycle likely requires active TOR signalling since we observed that chemical inhibition of TOR significantly reduces light and sugar-induced cell cycle count in the meristem (Figure 4.2). Phosphorylation pattern of RPS6, a TOR target, was shown to be disrupted in clock-deficient mutants (Enganti *et al.*, 2018). Zhang and co-workers (2019) found that TOR signalling is

required for nutrient-induced circadian period adjustment and cell proliferation in root meristem (N. Zhang *et al.*, 2019). In line with these two studies, we suggest that underlying circadian regulation of cell cycle diurnal rhythm might involve TOR signalling as means to integrate metabolic signals to catabolic processes. In relation to RPS6, it is worth noting that RPS6A has been identified as a target of MKK7-MPK3/6 cascade (Huck *et al.*, 2017), coupling our observation of cell cycle inhibition upon *MKK7* overexpression (Figure 5.4) with RPS6A as a well-known phospho-target of TOR kinase (Dobrenel, Mancera-Martínez, *et al.*, 2016), thus it seems likely that TOR and MAPK signalling work in antagonistic ways to tune cell cycle with cell growth. In support of this view, a recent phospho-proteomics screen identified at least three MPK6 phospho-peptides that were target of TOR phosphorylation (Van Leene *et al.*, 2019), the functional relevance of this has not been explored but it may contribute to TOR control of cell proliferation.

The two cell cycle transcription factors, that are TOR phospho-targets E2FA and E2FB (Wu *et al.*, 2019), have distinct protein accumulation (Figure 3.7) and corresponds differentially to cell cycle diel dynamics such that E2FA increase in level corresponds to increase in cell cycle count and high level of E2FB corresponds to reduced occurrence of cell cycle (Figures 3.6 and 3.7). We think that the down-tuning of cell cycle is actively controlled as supposed to reduced supply of nutrients. Dependent on its protein:protein interactions, E2FB can act both as a positive and negative regulator of cell proliferation (Oszi *et al.*, 2020), it would be of interest to explore diel changes in E2FB complex formation through Co-immunoprecipitation experiments under light-dark cycles.

In addition to E2Fs, CDK inhibitors KRPs and/or SMRs may play a role creating a diurnal rhythm of cell cycle. Accordingly, transcript level of *KRP2* and *KRP7* are low

during the day and increase during the night (Fung-Uceda *et al.*, 2018), a similar correlation with peaks and troughs of cell cycle we observed (Figure 3.6).

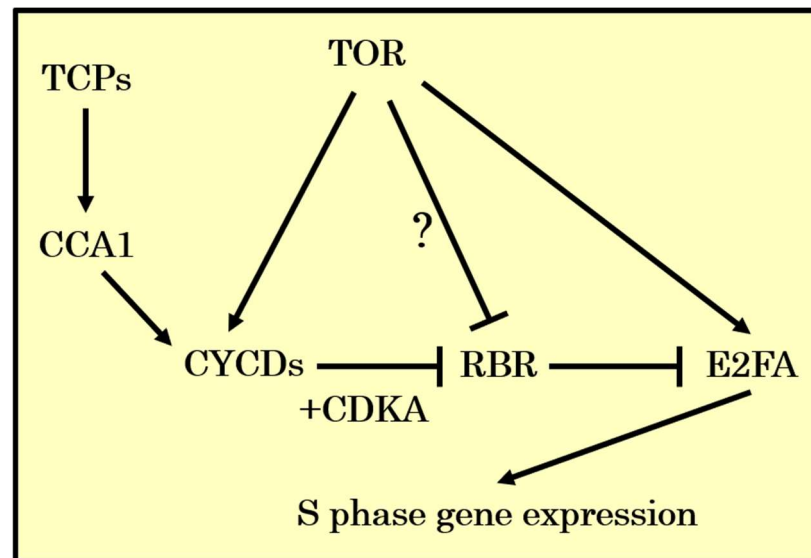


Figure 7.2 A proposed model of cell cycle control by TCP transcription factors and TOR signalling pathway.

TCP20 and TCP22 have been shown to bind to the promoter region of the circadian transcription factor CCA1 which accumulates in the morning (Wu *et al.*, 2016). CCA1 target genes include D-type CYCLINS (Nagel *et al.*, 2015), thus the TCP-CCA1 axis can potentially serve to connect circadian clock to the cell cycle. TOR signalling promotes CYCD2 protein level (Figure 4.9) and is required for phosphorylation of RBR (Figure 4.12) which results in “release” of E2FA to allow transcription of S phase genes. Whether these two branches work independently or cooperatively to boost S phase gene expression in the morning remains to be investigated.

Additionally, TOR phosphorylates and inhibits YAK1, a DYRK kinase which promotes transcription of *SMR4*, *SMR5* and *SMR7* (Barrada *et al.*, 2019; Forzani *et al.*, 2019). In conjunction with this observation, it is possible that reduced TOR activity towards the end-of-day derepresses YAK1 which subsequently results in *SMR* expression and reduced CDK activity.

Could TCPs and MAP kinase cascade work in the same pathway? Although exploring the connection between MAPK signalling and TCP transcription factors was not the scope of this thesis, long-term induction of overexpression of *MKK7* and *TCP14* phenocopy each other at the level of S phase count (Figures 5.4 and 6.4) suggests

they may act in cooperative ways. A recent study found MAP KINASE 8 (MPK8) and TCP14 to physically interact, and MPK8 was shown to *in vitro* phosphorylate TCP14 to work in a common pathway to promote dormancy-to-germination transition (W. Zhang *et al.*, 2019). Cell cycle genes such as *MCMs*, *PCNA*, *CDKB1;1*, *CYCDs* are among the down-regulated genes in imbibed seeds of *tcp14.4* and *mpk8.1* mutants (W. Zhang *et al.*, 2019), whether this interaction continues during post-embryonic growth needs to be investigated.

Plant growth is a combination of multiple cellular processes, each of which has an array of underlying molecular mechanisms. In this thesis, we focused on some of these events in the root meristem and found an adjustable cell cycle behaviour that is intricately connected with the cell's internal and external environment, namely light and sugar availability. We hope a better understanding of organ growth could be used to improve crop yield and productivity to ensure future food security.

Appendices

Supplemental figures presented below are biological repeats of selected experiments from chapter 3, see figure legends for specific cross-references.

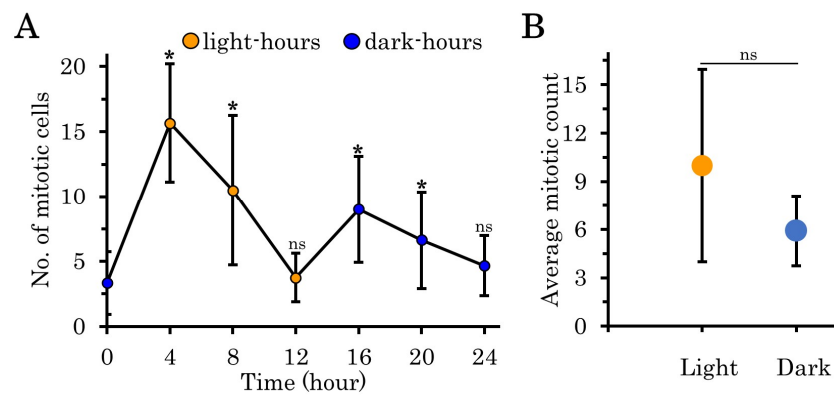


Figure S3.1 Mitotic count under light-dark cycles.

A. Number of mitotic cells at each timepoint during the course of experiment.

B. Number of mitotic cells in light-timepoints and dark-timepoints were averaged and plotted separately.

This figure supports Figure 3.4

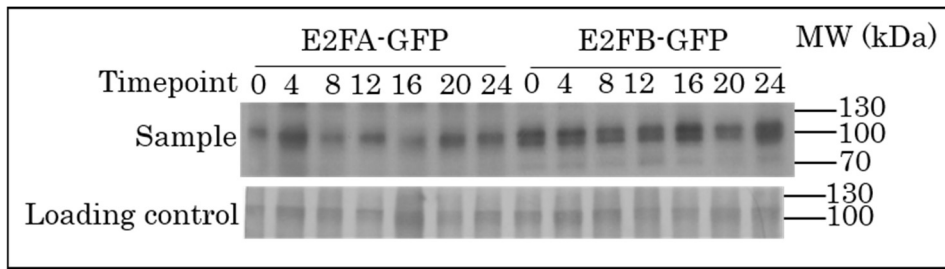


Figure S3.2 Differential accumulation of E2FA and E2FB proteins.
 This figure supports Figure 3.7. For antibody dilution, see Table 2.2.

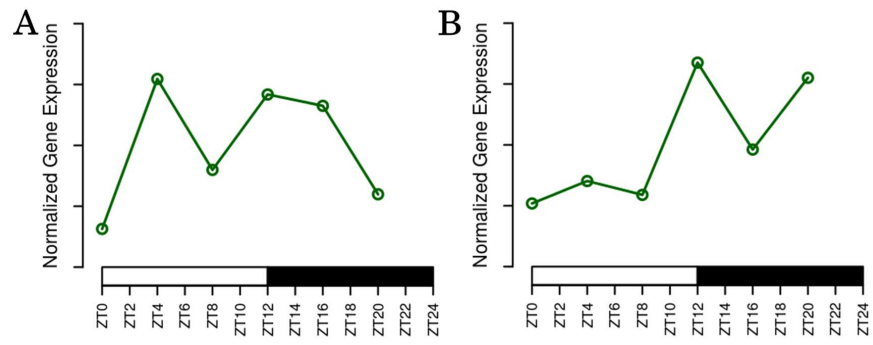


Figure S3.3 Diurnal changes in transcript level of *Arabidopsis E2Fs*.

A. Transcript dynamics of *E2FA*.

B. Transcript dynamics of *E2FB*.

Plots are obtained from CircadiaNet at the following weblink:

(<http://viridiplantae.ibvf.csic.es/circadiaNet/exploration/searchGene.html>)

List of references

- Aguilar-Martínez, J. A. and Sinha, N. (2013) 'Analysis of the role of arabidopsis class I TCP genes AtTCP7, AtTCP8, AtTCP22, and AtTCP23 in leaf development', *Frontiers in Plant Science*. doi: 10.3389/fpls.2013.00406.
- Ahmad, Z., Magyar, Z., Bögre, L. and Papdi, C. (2019) 'Cell cycle control by the target of rapamycin signalling pathway in plants', *Journal of Experimental Botany*. doi: 10.1093/jxb/erz140.
- Alonso-Blanco, C., Andrade, J., Becker, C., Bemm, F., Bergelson, J., Borgwardt, K. M. M., Cao, J., Chae, E., Dezaan, T. M. M., Ding, W., Ecker, J. R. R., Exposito-Alonso, M., Farlow, A., Fitz, J., Gan, X., Grimm, D. G. G., Hancock, A. M. M., Henz, S. R. R., Holm, S., *et al.* (2016) '1,135 Genomes Reveal the Global Pattern of Polymorphism in *Arabidopsis thaliana*', *Cell*. doi: 10.1016/j.cell.2016.05.063.
- Amodeo, A. A. and Skotheim, J. M. (2016) 'Cell-size control', *Cold Spring Harbor Perspectives in Biology*. doi: 10.1101/cshperspect.a019083.
- An, Z., Liu, Y., Ou, Y., Li, J., Zhang, B., Sun, D., Sun, Y. and Tang, W. (2018) 'Regulation of the stability of RGF1 receptor by the ubiquitin-specific proteases UBP12/UBP13 is critical for root meristem maintenance', *Proceedings of the National Academy of Sciences of the United States of America*. doi: 10.1073/pnas.1714177115.
- Aranda, S., Laguna, A. and Luna, S. de la (2011) 'DYRK family of protein kinases: evolutionary relationships, biochemical properties, and functional roles', *The FASEB Journal*. doi: 10.1096/fj.10-165837.
- Bailey, S., Walters, R. G., Jansson, S. and Horton, P. (2001) 'Acclimation of *Arabidopsis thaliana* to the light environment: The existence of separate low light and high light responses', *Planta*. doi: 10.1007/s004250100556.
- Barbet, N. C., Schneider, U., Helliwell, S. B., Stansfield, I., Tuite, M. F. and Hall, M. N. (1996) 'TOR controls translation initiation and early G1 progression in yeast.', *Molecular biology of the cell*. American Society for Cell Biology, 7(1), pp. 25–42. Available at: <http://www.ncbi.nlm.nih.gov/pubmed/8741837>.
- Barrada, A., Djendli, M., Desnos, T., Mercier, R., Robaglia, C., Montané, M. H. and

Menand, B. (2019) 'A TOR-YAK1 signaling axis controls cell cycle, meristem activity and plant growth in Arabidopsis', *Development (Cambridge, England)*. doi: 10.1242/dev.171298.

Barrada, A., Montané, M. H., Robaglia, C. and Menand, B. (2015) 'Spatial regulation of root growth: Placing the plant TOR pathway in a developmental perspective', *International Journal of Molecular Sciences*, pp. 19671–19697. doi: 10.3390/ijms160819671.

Beemster, G. T. S., De Veylder, L., Vercruyse, S., West, G., Rombaut, D., Van Hummelen, P., Galichet, A., Gruissem, W., Inzé, D. and Vuylsteke, M. (2005) 'Genome-wide analysis of gene expression profiles associated with cell cycle transitions in growing organs of Arabidopsis', *Plant Physiology*. doi: 10.1104/pp.104.053884.

Bennett, T. and Scheres, B. (2010) 'Root development-two meristems for the price of one?', in *Current Topics in Developmental Biology*. doi: 10.1016/S0070-2153(10)91003-X.

Berckmans, B., Lammens, T., van den Daele, H., Magyar, Z., Bögre, L. and de Veylder, L. (2011) 'Light-dependent regulation of DEL1 is determined by the antagonistic action of E2Fb and E2Fc', *Plant Physiology*. doi: 10.1104/pp.111.183384.

Berckmans, B., Vassileva, V., Schmid, S. P. C., Maes, S., Parizot, B., Naramoto, S., Magyar, Z., Lessa Alvim Kamei, C., Koncz, C., Bögre, L., Persiau, G., de Jaeger, G., Friml, J., Simon, R., Beeckman, T. and de Veylder, L. (2011) 'Auxin-Dependent cell cycle reactivation through transcriptional regulation of arabidopsis E2Fa by lateral organ boundary proteins', *Plant Cell*. doi: 10.1105/tpc.111.088377.

Berckmans, B. and De Veylder, L. (2009) 'Transcriptional control of the cell cycle', *Current Opinion in Plant Biology*. doi: 10.1016/j.pbi.2009.07.005.

Bhosale, R., Boudolf, V., Cuevas, F., Lu, R., Eekhout, T., Hu, Z., Van Isterdael, G., Lambert, G. M., Xu, F., Nowack, M. K., Smith, R. S., Vercauteren, I., De Rycke, R., Storme, V., Beeckman, T., Larkin, J. C., Kremer, A., Höfte, H., Galbraith, D. W., *et al.* (2018) 'A spatiotemporal dna endoploidy map of the arabidopsis root reveals roles for the endocycle in root development and stress adaptation', *Plant Cell*. doi: 10.1105/tpc.17.00983.

Biedermann, S., Harashima, H., Chen, P., Heese, M., Bouyer, D., Sofroni, K. and Schnittger, A. (2017) 'The retinoblastoma homolog RBR 1 mediates localization of the repair protein RAD 51 to DNA lesions in Arabidopsis', *The EMBO Journal*. doi: 10.15252/embj.201694571.

Bläsing, O. E., Gibon, Y., Günther, M., Höhne, M., Morcuende, R., Osuna, D., Thimm, O., Usadel, B., Scheible, W. R. and Stitt, M. (2005) 'Sugars and circadian regulation make major contributions to the global regulation of diurnal gene expression in Arabidopsis', *Plant Cell*. doi: 10.1105/tpc.105.035261.

Boniotti, M. B. and Gutierrez, C. (2001) 'A cell-cycle-regulated kinase activity phosphorylates plant retinoblastoma protein and contains, in Arabidopsis, a CDKA/cyclin D complex', *Plant Journal*, 28(3), pp. 341–350. doi: 10.1046/j.1365-313X.2001.01160.x.

Boudolf, V., Lammens, T., Boruc, J., van Leene, J., van den Daele, H., Maes, S., van Isterdael, G., Russinova, E., Kondorosi, E., Witters, E., de Jaeger, G., Inzé, D. and de Veylder, L. (2009) 'CDKB1;1 forms a functional complex with CYCA2;3 to suppress endocycle onset', *Plant Physiology*. doi: 10.1104/pp.109.140269.

Boudolf, V., Vlieghe, K., Beemster, G. T. S., Magyar, Z., Torres Acosta, J. A., Maes, S., Van Der Schueren, E., Inzé, D. and De Veylder, L. (2004) 'The plant-specific cyclin-dependent kinase CDKB1;1 and transcription factor E2Fa-DPa control the balance of mitotically dividing and endoreduplicating cells in Arabidopsis', *Plant Cell*. doi: 10.1105/tpc.104.024398.

Breuer, C., Ishida, T. and Sugimoto, K. (2010) 'Developmental control of endocycles and cell growth in plants', *Current Opinion in Plant Biology*. doi: 10.1016/j.pbi.2010.10.006.

Breyne, P., Dreesen, R., Vandepoele, K., De Veylder, L., Van Breusegem, F., Callewaert, L., Rombauts, S., Raes, J., Cannoot, B., Engler, G., Inzé, D. and Zabeau, M. (2002) 'Transcriptome analysis during cell division in plants', *Proceedings of the National Academy of Sciences of the United States of America*. doi: 10.1073/pnas.222561199.

Buck, S. B., Bradford, J., Gee, K. R., Agnew, B. J., Clarke, S. T. and Salic, A. (2008) 'Detection of S-phase cell cycle progression using 5-ethynyl-2'-deoxyuridine incorporation with click chemistry, an alternative to using 5-bromo-2'-deoxyuridine

antibodies', *BioTechniques*. doi: 10.2144/000112812.

Buckner, E., Madison, I., Chou, H., Matthiadis, A., Melvin, C. E., Sozzani, R., Williams, C. and Long, T. A. (2019) 'Automated Imaging, Tracking, and Analytics Pipeline for Differentiating Environmental Effects on Root Meristematic Cell Division', *Frontiers in Plant Science*. doi: 10.3389/fpls.2019.01487.

Bulavin, D. V., Higashimoto, Y., Popoff, I. J., Gaarde, W. A., Basrur, V., Potapova, O., Appella, E. and Fornace, A. J. (2001) 'Initiation of a G2/M checkpoint after ultraviolet radiation requires p38 kinase', *Nature*. doi: 10.1038/35075107.

Cai, W., Li, X., Liu, Y., Wang, Y., Zhou, Y., Xu, T. and Xiong, Y. (2017) 'COP1 integrates light signals to ROP2 for cell cycle activation', *Plant Signaling and Behavior*. doi: 10.1080/15592324.2017.1363946.

Caldana, C., Li, Y., Leisse, A., Zhang, Y., Bartholomaeus, L., Fernie, A. R., Willmitzer, L. and Giavalisco, P. (2013) 'Systemic analysis of inducible target of rapamycin mutants reveal a general metabolic switch controlling growth in *Arabidopsis thaliana*', *Plant Journal*. doi: 10.1111/tpj.12080.

Campos, M., Surovtsev, I. V., Kato, S., Paintdakhi, A., Beltran, B., Ebmeier, S. E. and Jacobs-Wagner, C. (2014) 'A constant size extension drives bacterial cell size homeostasis', *Cell*. doi: 10.1016/j.cell.2014.11.022.

Cardinale, F., Meskiene, I., Ouaked, F. and Hirt, H. (2002) 'Convergence and divergence of stress-induced mitogen-activated protein kinase signaling pathways at the level of two distinct mitogen-activated protein kinase kinases', *Plant Cell*. doi: 10.1105/tpc.010256.

Chen, H. Y., Huh, J. H., Yu, Y. C., Ho, L. H., Chen, L. Q., Tholl, D., Frommer, W. B. and Guo, W. J. (2015) 'The *Arabidopsis* vacuolar sugar transporter SWEET2 limits carbon sequestration from roots and restricts *Pythium* infection', *Plant Journal*. doi: 10.1111/tpj.12948.

Cheng, Y., Cao, L., Wang, S., Li, Y., Shi, X., Liu, H., Li, L., Zhang, Z., Fowke, L. C., Wang, H. and Zhou, Y. (2013) 'Downregulation of multiple CDK inhibitor ICK/KRP genes upregulates the E2F pathway and increases cell proliferation, and organ and seed sizes in *Arabidopsis*', *Plant Journal*. doi: 10.1111/tpj.12228.

Cheng, Y., Liu, H., Cao, L., Wang, S., Li, Y., Zhang, Y., Jiang, W., Zhou, Y. and Wang,

- H. (2015) ‘Down-regulation of multiple CDK inhibitor ICK/KRP genes promotes cell proliferation, callus induction and plant regeneration in arabidopsis’, *Frontiers in Plant Science*. doi: 10.3389/fpls.2015.00825.
- Choe, G. and Lee, J. Y. (2017) ‘Push–pull strategy in the regulation of postembryonic root development’, *Current Opinion in Plant Biology*. doi: 10.1016/j.pbi.2016.12.005.
- Creux, N. and Harmer, S. (2019) ‘Circadian rhythms in plants’, *Cold Spring Harbor Perspectives in Biology*. doi: 10.1101/cshperspect.a034611.
- Cristina, M., Petersen, M. and Mundy, J. (2010) ‘Mitogen-Activated Protein Kinase Signaling in Plants’, *Annual Review of Plant Biology*. doi: 10.1146/annurev-arplant-042809-112252.
- Cruz-Ramírez, A., Díaz-Triviño, S., Blilou, I., Grieneisen, V. A., Sozzani, R., Zamioudis, C., Miskolczi, P., Nieuwland, J., Benjamins, R., Dhonukshe, P., Caballero-Pérez, J., Horvath, B., Long, Y., Mähönen, A. P., Zhang, H., Xu, J., Murray, J. A. H., Benfey, P. N., Bako, L., *et al.* (2012) ‘A bistable circuit involving SCARECROW-RETINOBLASTOMA integrates cues to inform asymmetric stem cell division’, *Cell*. doi: 10.1016/j.cell.2012.07.017.
- Cruz-Ramírez, A., Díaz-Triviño, S., Wachsman, G., Du, Y., Arteága-Vázquez, M., Zhang, H., Benjamins, R., Blilou, I., Neef, A. B., Chandler, V. and Scheres, B. (2013) ‘A SCARECROW-RETINOBLASTOMA Protein Network Controls Protective Quiescence in the Arabidopsis Root Stem Cell Organizer’, *PLoS Biology*. Public Library of Science, 11(11), pp. e1001724–e1001724. doi: 10.1371/journal.pbio.1001724.
- Dahl, M., Meskiene, I., Bogre, L., Ha Dang-Thi-Cam, Swoboda, I., Hubmann, R., Hirt, H. and Heberle-Bors, E. (1995) ‘The D-type alfalfa cyclin gene cycMs4 complements G1 cyclin-deficient yeast and is induced in the G1 phase of the cell cycle’, *Plant Cell*. doi: 10.1105/tpc.7.11.1847.
- Dai, Y., Wang, H., Li, B., Huang, J., Liu, X., Zhou, Y., Mou, Z. and Li, J. (2006) ‘Increased expression of MAP KINASE KINASE7 causes deficiency in polar auxin transport and leads to plant architectural abnormality in Arabidopsis’, *Plant Cell*. doi: 10.1105/tpc.105.037846.
- Danisman, S. (2016) ‘TCP transcription factors at the interface between environmental challenges and the plant’s growth responses’, *Frontiers in Plant*

Science. doi: 10.3389/fpls.2016.01930.

Darzynkiewicz, Z., Halicka, H. D. and Zhao, H. (2010) 'Analysis of cellular DNA content by flow and laser scanning cytometry', *Advances in Experimental Medicine and Biology*. doi: 10.1007/978-1-4419-6199-0_9.

Davière, J. M., Wild, M., Regnault, T., Baumberger, N., Eisler, H., Genschik, P. and Achard, P. (2014) 'Class I TCP-DELLA interactions in inflorescence shoot apex determine plant height', *Current Biology*. doi: 10.1016/j.cub.2014.07.012.

Deprost, D., Yao, L., Sormani, R., Moreau, M., Leterreux, G., Bedu, M., Robaglia, C. and Meyer, C. (2007) 'The Arabidopsis TOR kinase links plant growth, yield, stress resistance and mRNA translation', *EMBO Reports*. doi: 10.1038/sj.embor.7401043.

Dewitte, W. and Murray, J. A. H. (2003) 'THE PLANT CELL CYCLE', *Annual Review of Plant Biology*. doi: 10.1146/annurev.arplant.54.031902.134836.

Dick, F. A., Goodrich, D. W., Sage, J. and Dyson, N. J. (2018) 'Non-canonical functions of the RB protein in cancer', *Nature Reviews Cancer*. doi: 10.1038/s41568-018-0008-5.

Dick, F. A. and Rubin, S. M. (2013) 'Molecular mechanisms underlying RB protein function', *Nature Reviews Molecular Cell Biology*. doi: 10.1038/nrm3567.

Dobrenel, T., Caldana, C., Hanson, J., Robaglia, C., Vincentz, M., Veit, B. and Meyer, C. (2016) 'TOR Signaling and Nutrient Sensing', *Annual Review of Plant Biology*. doi: 10.1146/annurev-arplant-043014-114648.

Dobrenel, T., Mancera-Martínez, E., Forzani, C., Azzopardi, M., Davanture, M., Moreau, M., Schepetilnikov, M., Chicher, J., Langella, O., Zivy, M., Robaglia, C., Ryabova, L. A., Hanson, J. and Meyer, C. (2016) 'The arabidopsis TOR kinase specifically regulates the expression of nuclear genes coding for plastidic ribosomal proteins and the phosphorylation of the cytosolic ribosomal protein S6', *Frontiers in Plant Science*. Frontiers Media SA, 7, p. 1611. doi: 10.3389/fpls.2016.01611.

Dóczi, R. and Bögre, L. (2018) 'The Quest for MAP Kinase Substrates: Gaining Momentum', *Trends in Plant Science*. doi: 10.1016/j.tplants.2018.08.002.

Doerner, P. (2008) 'Signals and mechanisms in the control of plant growth', *Plant Cell Monographs*. doi: 10.1007/7089_2007_142.

Doerner, P., Jørgensen, J. E., You, R., Steppuhn, J. and Lamb, C. (1996) 'Control of

root growth and development by cyclin expression', *Nature*. doi: 10.1038/380520a0.

Dolan, L., Janmaat, K., Willemsen, V., Linstead, P., Poethig, S., Roberts, K. and Scheres, B. (1993) 'Cellular organisation of the *Arabidopsis thaliana* root.', *Development (Cambridge, England)*. The Company of Biologists Ltd, 119(1), pp. 71–84. Available at: <http://www.ncbi.nlm.nih.gov/pubmed/8275865>.

Dong, P., Xiong, F., Que, Y., Wang, K., Yu, L., Li, Z. and Ren, M. (2015) 'Expression profiling and functional analysis reveals that TOR is a key player in regulating photosynthesis and phytohormone signaling pathways in *Arabidopsis*.' *Frontiers in plant science*. Frontiers Media SA, 6, p. 677. doi: 10.3389/fpls.2015.00677.

Donnelly, P. M., Bonetta, D., Tsukaya, H., Dengler, R. E. and Dengler, N. G. (1999) 'Cell cycling and cell enlargement in developing leaves of *Arabidopsis*', *Developmental Biology*. doi: 10.1006/dbio.1999.9443.

Dory, M., Hatzimasoura, E., Kállai, B. M., Nagy, S. K., Jäger, K., Darula, Z., Náday, T. V., Mészáros, T., López-Juez, E., Barnabás, B., Palme, K., Bögre, L., Ditengou, F. A. and Dóczi, R. (2018) 'Coevolving MAPK and PID phosphosites indicate an ancient environmental control of PIN auxin transporters in land plants', *FEBS Letters*. doi: 10.1002/1873-3468.12929.

Dubois, M., Selden, K., Bedié, A., Rolland, G., Baumberger, N., Noir, S., Bach, L., Lamy, G., Granier, C. and Genschik, P. (2018) 'SIAMESE-RELATED1 is regulated posttranslationally and participates in repression of leaf growth under moderate drought', *Plant Physiology*. doi: 10.1104/pp.17.01712.

Dvořáčková, M., Raposo, B., Matula, P., Fuchs, J., Schubert, V., Peška, V., Desvoyes, B., Gutierrez, C. and Fajkus, J. (2018) 'Replication of ribosomal DNA in *Arabidopsis* occurs both inside and outside the nucleolus during S phase progression', *Journal of Cell Science*. doi: 10.1242/jcs.202416.

Enganti, R., Cho, S. K., Toperzer, J. D., Urquidi-Camacho, R. A., Cakir, O. S., Ray, A. P., Abraham, P. E., Hettich, R. L. and von Arnim, A. G. (2018) 'Phosphorylation of ribosomal protein RPS6 integrates light signals and circadian clock signals', *Frontiers in Plant Science*. doi: 10.3389/fpls.2017.02210.

Evans, T., Rosenthal, E. T., Youngblom, J., Distel, D. and Hunt, T. (1983) 'Cyclin: A protein specified by maternal mRNA in sea urchin eggs that is destroyed at each cleavage division', *Cell*. doi: 10.1016/0092-8674(83)90420-8.

- Facchetti, G., Chang, F. and Howard, M. (2017) 'Controlling cell size through sizer mechanisms', *Current Opinion in Systems Biology*. doi: 10.1016/j.coisb.2017.08.010.
- Feng, W. and Michaels, S. D. (2015) 'Accessing the Inaccessible: The Organization, Transcription, Replication, and Repair of Heterochromatin in Plants', *Annual Review of Genetics*. doi: 10.1146/annurev-genet-112414-055048.
- Fingar, D. C., Richardson, C. J., Tee, A. R., Cheatham, L., Tsou, C. and Blenis, J. (2004) 'mTOR Controls Cell Cycle Progression through Its Cell Growth Effectors S6K1 and 4E-BP1/Eukaryotic Translation Initiation Factor 4E', *Molecular and Cellular Biology*. American Society for Microbiology (ASM), 24(1), pp. 200–216. doi: 10.1128/mcb.24.1.200-216.2004.
- Fischer, M. and Müller, G. A. (2017) 'Cell cycle transcription control: DREAM/MuvB and RB-E2F complexes', *Critical Reviews in Biochemistry and Molecular Biology*. doi: 10.1080/10409238.2017.1360836.
- Forzani, C., Duarte, G. T., Van Leene, J., Clément, G., Huguet, S., Paysant-Le-Roux, C., Mercier, R., De Jaeger, G., Leprince, A. S. and Meyer, C. (2019) 'Mutations of the AtYAK1 Kinase Suppress TOR Deficiency in Arabidopsis', *Cell Reports*. doi: 10.1016/j.celrep.2019.05.074.
- Fung-Uceda, J., Lee, K., Seo, P. J., Polyn, S., De Veylder, L. and Mas, P. (2018) 'The Circadian Clock Sets the Time of DNA Replication Licensing to Regulate Growth in Arabidopsis', *Developmental Cell*. doi: 10.1016/j.devcel.2018.02.022.
- Galinha, C., Hofhuis, H., Luijten, M., Willemsen, V., Blilou, I., Heidstra, R. and Scheres, B. (2007) 'PLETHORA proteins as dose-dependent master regulators of Arabidopsis root development', *Nature*. doi: 10.1038/nature06206.
- Gázquez, A. and Beemster, G. T. S. (2017) 'What determines organ size differences between species? A meta-analysis of the cellular basis', *New Phytologist*, 215(1), pp. 299–308. doi: 10.1111/nph.14573.
- Ginzberg, M. B., Kafri, R. and Kirschner, M. (2015) 'On being the right (cell) size', *Science*. doi: 10.1126/science.1245075.
- Gonzalez, N., Beemster, G. T. and Inzé, D. (2009) 'David and Goliath: what can the tiny weed Arabidopsis teach us to improve biomass production in crops?', *Current Opinion in Plant Biology*. doi: 10.1016/j.pbi.2008.11.003.

- Gonzalez, N., Vanhaeren, H. and Inzé, D. (2012) 'Leaf size control: Complex coordination of cell division and expansion', *Trends in Plant Science*. doi: 10.1016/j.tplants.2012.02.003.
- Gutierrez, C. (2009) 'The Arabidopsis cell division cycle.', in *The Arabidopsis book / American Society of Plant Biologists*. American Society of Plant Biologists, p. e0120. doi: 10.1199/tab.0120.
- Gutierrez, C., Ramirez-Parra, E., Castellano, M. M. and Del Pozo, J. C. (2002) 'G1 to S transition: More than a cell cycle engine switch', *Current Opinion in Plant Biology*. doi: 10.1016/S1369-5266(02)00301-1.
- Gutzat, R., Borghi, L., Fütterer, J., Bischof, S., Laizet, Y., Hennig, L., Feil, R., Lunn, J. and Gruissem, W. (2011) 'Retinoblastoma-related protein controls the transition to autotrophic plant development', *Development*. doi: 10.1242/dev.060830.
- Haga, N., Kato, K., Murase, M., Araki, S., Kubo, M., Demura, T., Suzuki, K., Müller, I., Voß, U., Jürgens, G. and Ito, M. (2007) 'R1R2R3-Myb proteins positively regulate cytokinesis through activation of KNOLLE transcription in Arabidopsis thaliana', *Development*. doi: 10.1242/dev.02801.
- Haga, N., Kobayashi, K., Suzuki, T., Maeo, K., Kubo, M., Ohtani, M., Mitsuda, N., Demura, T., Nakamura, K., Jurgens, G. and Ito, M. (2011) 'Mutations in MYB3R1 and MYB3R4 cause pleiotropic developmental defects and preferential down-regulation of multiple G2/M-specific genes in Arabidopsis', *Plant Physiology*. doi: 10.1104/pp.111.180836.
- Halford, N. G. and Hey, S. J. (2009) 'Snf1-related protein kinases (SnRKs) act within an intricate network that links metabolic and stress signalling in plants', *Biochemical Journal*. doi: 10.1042/BJ20082408.
- Harashima, H., Dissmeyer, N. and Schnittger, A. (2013) *Cell cycle control across the eukaryotic kingdom*, *Trends in Cell Biology*. doi: 10.1016/j.tcb.2013.03.002.
- Hayashi, K., Hasegawa, J. and Matsunaga, S. (2013) 'The boundary of the meristematic and elongation zones in roots: Endoreduplication precedes rapid cell expansion', *Scientific Reports*. doi: 10.1038/srep02723.
- Healy, J. M. S., Menges, M., Doonan, J. H. and Murray, J. A. H. (2001) 'The Arabidopsis D-type Cyclins CycD2 and CycD3 both Interact in Vivo with the

PSTAIRES Cyclin-dependent Kinase Cdc2a but are Differentially Controlled', *Journal of Biological Chemistry*. doi: 10.1074/jbc.M009074200.

Heitman, J., Movva, N. R. and Hall, M. N. (1991) 'Targets for cell cycle arrest by the immunosuppressant rapamycin in yeast.', *Science (New York, N.Y.)*. American Association for the Advancement of Science, 253(5022), pp. 905–909. doi: 10.1126/SCIENCE.1715094.

Heldt, F. S., Lunstone, R., Tyson, J. J. and Novák, B. (2018) 'Dilution and titration of cell-cycle regulators may control cell size in budding yeast', *PLoS Computational Biology*. doi: 10.1371/journal.pcbi.1006548.

Henriques, R., Bögre, L., Horváth, B. and Magyar, Z. (2014) 'Balancing act: matching growth with environment by the TOR signalling pathway', *Journal of Experimental Botany*, 65(10), pp. 2691–2701. doi: 10.1093/jxb/eru049.

Henriques, R., Papdi, C., Ahmad, Z. and Bögre, L. (2018) 'Circadian Regulation of Plant Growth', in *Annual Plant Reviews online*. doi: 10.1002/9781119312994.apr0655.

Hoffmann, M. H. (2002) 'Biogeography of *Arabidopsis thaliana* (L.) Heynh. (Brassicaceae)', *Journal of Biogeography*. doi: 10.1046/j.1365-2699.2002.00647.x.

Horiguchi, G. and Tsukaya, H. (2011) 'Organ size regulation in plants: Insights from compensation', *Frontiers in Plant Science*. doi: 10.3389/fpls.2011.00024.

Horvath, B. M., Kourova, H., Nagy, S., Nemeth, E., Magyar, Z., Papdi, C., Ahmad, Z., Sanchez-Perez, G. F., Perilli, S., Blilou, I., Pettkó-Szandtner, A., Darula, Z., Meszaros, T., Binarova, P., Bogre, L. and Scheres, B. (2017) 'Arabidopsis RETINOBLASTOMA RELATED directly regulates DNA damage responses through functions beyond cell cycle control.', *The EMBO journal*. European Molecular Biology Organization, 36(9), pp. 1261–1278. doi: 10.15252/emboj.201694561.

Horváth, B. M., Magyar, Z., Zhang, Y., Hamburger, A. W., Bakó, L., Visser, R. G. F., Bachem, C. W. B. and Bögre, L. (2006) 'EBP1 regulates organ size through cell growth and proliferation in plants', *EMBO Journal*. doi: 10.1038/sj.emboj.7601362.

Huang, T. and Irish, V. F. (2015) 'Temporal Control of Plant Organ Growth by TCP Transcription Factors', *Current Biology*. doi: 10.1016/j.cub.2015.05.024.

Huck, N. V., Leissing, F., Majovsky, P., Buntru, M., Aretz, C., Flecken, M., Müller,

- J. P. J., Vogel, S., Schillberg, S., Hoehenwarter, W., Conrath, U. and Beckers, G. J. M. (2017) 'Combined ^{15}N -labeling and tandemmoac quantifies phosphorylation of map kinase substrates downstream of MKK7 in Arabidopsis', *Frontiers in Plant Science*. doi: 10.3389/fpls.2017.02050.
- Ichimura, K., Shinozaki, K., Tena, G., Sheen, J., Henry, Y., Champion, A., Kreis, M., Zhang, S., Hirt, H., Wilson, C., Heberle-Bors, E., Ellis, B. E., Morris, P. C., Innes, R. W., Ecker, J. R., Scheel, D., Klessig, D. F., Machida, Y., Mundy, J., *et al.* (2002) 'Mitogen-activated protein kinase cascades in plants: A new nomenclature', *Trends in Plant Science*. doi: 10.1016/S1360-1385(02)02302-6.
- Inzé, D. and De Veylder, L. (2006) 'Cell Cycle Regulation in Plant Development', *Annual Review of Genetics*. doi: 10.1146/annurev.genet.40.110405.090431.
- Dello Ioio, R., Linhares, F. S., Scacchi, E., Casamitjana-Martinez, E., Heidstra, R., Costantino, P. and Sabatini, S. (2007) 'Cytokinins Determine Arabidopsis Root-Meristem Size by Controlling Cell Differentiation', *Current Biology*. doi: 10.1016/j.cub.2007.02.047.
- Jia, W., Li, B., Li, S., Liang, Y., Wu, X., Ma, M., Wang, J., Gao, J., Cai, Y., Zhang, Y., Wang, Yingchun, Li, J. and Wang, Yonghong (2016) 'Mitogen-Activated Protein Kinase Cascade MKK7-MPK6 Plays Important Roles in Plant Development and Regulates Shoot Branching by Phosphorylating PIN1 in Arabidopsis', *PLoS Biology*. doi: 10.1371/journal.pbio.1002550.
- Johnson, K. and Lenhard, M. (2011) 'Genetic control of plant organ growth', *New Phytologist*. doi: 10.1111/j.1469-8137.2011.03737.x.
- Jones, A. R., Band, L. R. and Murray, J. A. H. (2019) 'Double or Nothing? Cell Division and Cell Size Control', *Trends in Plant Science*. doi: 10.1016/j.tplants.2019.09.005.
- Jones, A. R., Forero-Vargas, M., Withers, S. P., Smith, R. S., Traas, J., Dewitte, W. and Murray, J. A. H. (2017) 'Cell-size dependent progression of the cell cycle creates homeostasis and flexibility of plant cell size', *Nature Communications*. doi: 10.1038/ncomms15060.
- Jun, S. E., Okushima, Y., Nam, J., Umeda, M. and Kim, G. T. (2013) 'Kip-related protein 3 is required for control of endoreduplication in the shoot apical meristem and leaves of Arabidopsis', *Molecules and Cells*. doi: 10.1007/s10059-013-2270-4.

- Jung, J. K. H. and McCouch, S. (2013) 'Getting to the roots of it: Genetic and hormonal control of root architecture', *Frontiers in Plant Science*. doi: 10.3389/fpls.2013.00186.
- Kawade, K., Horiguchi, G. and Tsukaya, H. (2010) 'Non-cell-autonomously coordinated organ size regulation in leaf development', *Development*. doi: 10.1242/dev.057117.
- Kieffer, M., Master, V., Waites, R. and Davies, B. (2011) 'TCP14 and TCP15 affect internode length and leaf shape in Arabidopsis', *Plant Journal*. doi: 10.1111/j.1365-313X.2011.04674.x.
- Kitagawa, M. and Jackson, D. (2019) 'Control of Meristem Size', *Annual Review of Plant Biology*. doi: 10.1146/annurev-arplant-042817-040549.
- Klepikova, A. V., Logacheva, M. D., Dmitriev, S. E. and Penin, A. A. (2015) 'RNA-seq analysis of an apical meristem time series reveals a critical point in Arabidopsis thaliana flower initiation', *BMC Genomics*. doi: 10.1186/s12864-015-1688-9.
- Kobayashi, K., Suzuki, T., Iwata, E., Magyar, Z., Bögre, L. and Ito, M. (2015) 'MYB3Rs, plant homologs of Myb oncoproteins, control cell cycle-regulated transcription and form DREAM-like complexes', *Transcription*. Taylor & Francis, 6(5), pp. 106–111. doi: 10.1080/21541264.2015.1109746.
- Kobayashi, K., Suzuki, T. T., Iwata, E., Nakamichi, N., Suzuki, T. T., Chen, P., Ohtani, M., Ishida, T., Hosoya, H., Müller, S., Leviczky, T., Pettkó-Szandtner, A., Darula, Z., Iwamoto, A., Nomoto, M., Tada, Y., Higashiyama, T., Demura, T., Doonan, J. H., *et al.* (2015) 'Transcriptional repression by MYB3R proteins regulates plant organ growth.', *The EMBO journal*. European Molecular Biology Organization, 34(15), pp. 1992–2007. doi: 10.15252/embj.201490899.
- Koornneef, M. and Meinke, D. (2010) 'The development of Arabidopsis as a model plant', *Plant Journal*. doi: 10.1111/j.1365-313X.2009.04086.x.
- Kosetsu, K., Matsunaga, S., Nakagami, H., Colcombet, J., Sasabe, M., Soyano, T., Takahashi, Y., Hirt, H. and Machida, Y. (2010) 'The MAP kinase MPK4 Is required for cytokinesis in Arabidopsis thaliana', *Plant Cell*. doi: 10.1105/tpc.110.077164.
- Kumar, N., Harashima, H., Kalve, S., Bramsiepe, J., Wang, K., Sizani, B. L., Bertrand, L. L., Johnson, M. C., Faulk, C., Dale, R., Simmons, L. A., Churchman, M.

L., Sugimoto, K., Kato, N., Dasanayake, M., Beemster, G., Schnittger, A. and Larkin, J. C. (2015) 'Functional conservation in the SIAMESE-RELATED family of cyclin-dependent kinase inhibitors in land plants', *Plant Cell*. doi: 10.1105/tpc.15.00489.

Kumar, N. and Larkin, J. C. (2017) 'Why do plants need so many cyclin-dependent kinase inhibitors?', *Plant Signaling and Behavior*. doi: 10.1080/15592324.2017.1282021.

Lampard, G. R., Lukowitz, W., Ellis, B. E. and Bergmann, D. C. (2009) 'Novel and expanded roles for MAPK signaling in Arabidopsis Stomatal cell fate revealed by cell type-specific manipulations', *Plant Cell*. doi: 10.1105/tpc.109.070110.

Lampard, G. R., Wengier, D. L. and Bergmann, D. C. (2014) 'Manipulation of mitogen-activated protein kinase signaling in the arabidopsis stomatal lineage reveals motifs that contribute to protein localization and signaling specificity', *Plant Cell*. doi: 10.1105/tpc.114.127415.

Lastdrager, J., Hanson, J. and Smeekens, S. (2014) 'Sugar signals and the control of plant growth and development', *Journal of Experimental Botany*, 65(3), pp. 799–807. doi: 10.1093/jxb/ert474.

Van Leene, J., Han, C., Gadeyne, A., Eeckhout, D., Matthijs, C., Cannoot, B., De Winne, N., Persiau, G., Van De Slijke, E., Van de Cotte, B., Stes, E., Van Bel, M., Storme, V., Impens, F., Gevaert, K., Vandepoele, K., De Smet, I. and De Jaeger, G. (2019) 'Capturing the phosphorylation and protein interaction landscape of the plant TOR kinase', *Nature Plants*. doi: 10.1038/s41477-019-0378-z.

Van Leene, J., Hollunder, J., Eeckhout, D., Persiau, G., Van De Slijke, E., Stals, H., Van Isterdael, G., Verkest, A., Neiryneck, S., Buffel, Y., De Bodt, S., Maere, S., Laukens, K., Pharazyn, A., Ferreira, P. C. G., Eloy, N., Renne, C., Meyer, C., Faure, J. D., *et al.* (2010) 'Targeted interactomics reveals a complex core cell cycle machinery in Arabidopsis thaliana', *Molecular Systems Biology*. doi: 10.1038/msb.2010.53.

Leviczky, T., Molnár, E., Papdi, C., O Szi, E., Horváth, G. V., Vizler, C., Nagy, V., Pauk, J., Bögre, L. and Magyar, Z. (2019) 'E2FA and E2FB transcription factors coordinate cell proliferation with seed maturation', *Development (Cambridge)*. doi: 10.1242/dev.179333.

Li, C., Potuschak, T., Colón-Carmona, A., Gutiérrez, R. A. and Doerner, P. (2005)

‘Arabidopsis TCP20 links regulation of growth and cell division control pathways’, *Proceedings of the National Academy of Sciences of the United States of America*. doi: 10.1073/pnas.0504039102.

Li, S. (2015) ‘The Arabidopsis thaliana TCP transcription factors: A broadening horizon beyond development’, *Plant Signaling and Behavior*. doi: 10.1080/15592324.2015.1044192.

Li, X., Cai, W., Liu, Y., Li, H., Fu, L., Liu, Z., Xu, L., Liu, H., Xu, T. and Xiong, Y. (2017) ‘Differential TOR activation and cell proliferation in Arabidopsis root and shoot apices’, *Proceedings of the National Academy of Sciences of the United States of America*. National Academy of Sciences, 114(10), pp. 2765–2770. doi: 10.1073/pnas.1618782114.

Li, Y., Van Den Ende, W. and Rolland, F. (2014) ‘Sucrose induction of anthocyanin biosynthesis is mediated by della’, *Molecular Plant*. doi: 10.1093/mp/sst161.

Li, Z. Y., Li, B. and Dong, A. W. (2012) ‘The arabidopsis transcription factor AtTCP15 regulates endoreduplication by modulating expression of key cell-cycle genes’, *Molecular Plant*. doi: 10.1093/mp/ssr086.

Liu, S., Ginzberg, M. B., Patel, N., Hild, M., Leung, B., Li, Z., Chen, Y. C., Chang, N., Wang, Y., Tan, C., Diena, S., Trimble, W., Wasserman, L., Jenkins, J. L., Kirschner, M. W. and Kafri, R. (2018) ‘Size uniformity of animal cells is actively maintained by a p38 MAPK-dependent regulation of G1-length’, *eLife*. doi: 10.7554/eLife.26947.

Lloyd, A. C. (2013) ‘The regulation of cell size’, *Cell*. doi: 10.1016/j.cell.2013.08.053.

Lokdarshi, A., Papdi, C., Pettkó-Szandtner, A., Dorokhov, S., Scheres, B., Magyar, Z., von Arnim, A. G., Bögre, L. and Horváth, B. M. (2020) ‘ErbB-3 binding protein 1 regulates translation and counteracts retinoblastoma related to maintain the root Meristem1[CC-by]’, *Plant Physiology*. doi: 10.1104/pp.19.00805.

López-Bucio, J. S., Dubrovsky, J. G., Raya-González, J., Ugartechea-Chirino, Y., López-Bucio, J., De Luna-Valdez, L. A., Ramos-Vega, M., León, P. and Guevara-García, A. A. (2014) ‘Arabidopsis thaliana mitogen-activated protein kinase 6 is involved in seed formation and modulation of primary and lateral root development’, *Journal of Experimental Botany*. doi: 10.1093/jxb/ert368.

- López-Juez, E., Dillon, E., Magyar, Z., Khan, S., Hazeldine, S., De Jager, S. M., Murray, J. A. H., Beemster, G. T. S., Bögre, L. and Shanahan, H. (2008) 'Distinct light-initiated gene expression and cell cycle programs in the shoot apex and cotyledons of Arabidopsis', *Plant Cell*. doi: 10.1105/tpc.107.057075.
- Ma, L., Li, J., Qu, L., Hager, J., Chen, Z., Zhao, H. and Deng, X. W. (2001) 'Light Control of Arabidopsis Development Entails Coordinated Regulation of Genome Expression and Cellular Pathways', *The Plant Cell*. doi: 10.1105/tpc.010229.
- Magyar, Z., Bögre, L. and Ito, M. (2016) *DREAMs make plant cells to cycle or to become quiescent*, *Current Opinion in Plant Biology*. Elsevier Current Trends. doi: 10.1016/j.pbi.2016.10.002.
- Magyar, Z., Horváth, B., Khan, S., Mohammed, B., Henriques, R., De Veylder, L., Bakó, L., Scheres, B. and Bögre, L. (2012) 'Arabidopsis E2FA stimulates proliferation and endocycle separately through RBR-bound and RBR-free complexes', *EMBO Journal*. doi: 10.1038/emboj.2012.13.
- Magyar, Z., Mészáros, T., Miskolczi, P., Deák, M., Fehér, A., Brown, S., Kondorosi, É., Athanasiadis, A., Pongor, S., Bilgin, M., Bakó, L., Koncz, C. and Dudits, D. (1997) 'Cell cycle phase specificity of putative cyclin-dependent kinase variants in synchronized alfalfa cells', *Plant Cell*. doi: 10.1105/tpc.9.2.223.
- Magyar, Z., De Veylder, L., Atanassova, A., Bakó, L., Inzé, D. and Bögre, L. (2005) 'The role of the Arabidopsis E2FB transcription factor in regulating auxin-dependent cell division', *Plant Cell*. doi: 10.1105/tpc.105.033761.
- Mahfouz, M. M., Kim, S., Delauney, A. J. and Verma, D. P. S. (2006) 'Arabidopsis TARGET of RAPAMYCIN interacts with RAPTOR, which regulates the activity of S6 kinase in response to osmotic stress signals', *Plant Cell*. doi: 10.1105/tpc.105.035931.
- Marshall, W. F., Young, K. D., Swaffer, M., Wood, E., Nurse, P., Kimura, A., Frankel, J., Wallingford, J., Walbot, V., Qu, X. and Roeder, A. H. K. (2012) 'What determines cell size?', *BMC Biology*. doi: 10.1186/1741-7007-10-101.
- Martín-Trillo, M. and Cubas, P. (2010) 'TCP genes: a family snapshot ten years later', *Trends in Plant Science*. doi: 10.1016/j.tplants.2009.11.003.
- Martin, S. G. and Berthelot-Grosjean, M. (2009) 'Polar gradients of the DYRK-family

- kinase Pom1 couple cell length with the cell cycle', *Nature*. doi: 10.1038/nature08054.
- Martins, B. M. C., Tooke, A. K., Thomas, P. and Locke, J. C. W. (2018) 'Cell size control driven by the circadian clock and environment in cyanobacteria', *Proceedings of the National Academy of Sciences of the United States of America*. doi: 10.1073/pnas.1811309115.
- Matsuzaki, Y., Ogawa-Ohnishi, M., Mori, A. and Matsubayashi, Y. (2010) 'Secreted peptide signals required for maintenance of root stem cell niche in Arabidopsis', *Science*. doi: 10.1126/science.1191132.
- McClung, C. R. (2006) 'Plant circadian rhythms', *Plant Cell*. doi: 10.1105/tpc.106.040980.
- Menand, B., Desnos, T., Nussaume, L., Berger, F., Bouchez, D., Meyer, C., Robaglia, C., Bergert, F., Bouchez, D., Meyer, C. and Robaglia, C. (2002) 'Expression and disruption of the Arabidopsis TOR (target of rapamycin) gene', *Proceedings of the National Academy of Sciences of the United States of America*. National Academy of Sciences, 99(9), pp. 6422–6427. doi: 10.1073/pnas.092141899.
- Meng, L. and Feldman, L. J. (2010) 'CLE14/CLE20 peptides may interact with CLAVATA2/CORYNE receptor-like kinases to irreversibly inhibit cell division in the root meristem of Arabidopsis', *Planta*. doi: 10.1007/s00425-010-1236-4.
- Menges, M., De Jager, S. M., Gruissem, W. and Murray, J. A. H. (2005) 'Global analysis of the core cell cycle regulators of Arabidopsis identifies novel genes, reveals multiple and highly specific profiles of expression and provides a coherent model for plant cell cycle control', *Plant Journal*. doi: 10.1111/j.1365-313X.2004.02319.x.
- Menges, M., Samland, A. K., Planchais, S. and Murray, J. A. H. (2006) 'The D-type cyclin CYCD3;1 is limiting for the G1-to-S-phase transition in Arabidopsis', *Plant Cell*. doi: 10.1105/tpc.105.039636.
- Mishra, Y., Johansson Jänkänpää, H., Kiss, A. Z., Funk, C., Schröder, W. P. and Jansson, S. (2012) 'Arabidopsis plants grown in the field and climate chambers significantly differ in leaf morphology and photosystem components', *BMC Plant Biology*. doi: 10.1186/1471-2229-12-6.
- Mohammed, B., Biloei, S. F., Dóczy, R., Grove, E., Railo, S., Palme, K., Ditengou, F. A., Bögre, L. and López-Juez, E. (2018) 'Converging light, energy and hormonal

signaling control meristem activity, leaf initiation, and growth', *Plant Physiology*. American Society of Plant Biologists, 176(2), pp. 1365–1381. doi: 10.1104/pp.17.01730.

Montané, M.-H. H. and Menand, B. (2013) 'ATP-competitive mTOR kinase inhibitors delay plant growth by triggering early differentiation of meristematic cells but no developmental patterning change', *Journal of Experimental Botany*. Oxford University Press, 64(14), pp. 4361–4374. doi: 10.1093/jxb/ert242.

Montané, M. H. and Menand, B. (2019) 'TOR inhibitors: From mammalian outcomes to pharmacogenetics in plants and algae', *Journal of Experimental Botany*. doi: 10.1093/jxb/erz053.

Moseley, J. B., Mayeux, A., Paoletti, A. and Nurse, P. (2009) 'A spatial gradient coordinates cell size and mitotic entry in fission yeast', *Nature*. doi: 10.1038/nature08074.

Murashige, T. and Skoog, F. (1962) 'A Revised Medium for Rapid Growth and Bio Assays with Tobacco Tissue Cultures', *Physiologia Plantarum*. doi: 10.1111/j.1399-3054.1962.tb08052.x.

Nagel, D. H., Doherty, C. J., Pruneda-Paz, J. L., Schmitz, R. J., Ecker, J. R. and Kay, S. A. (2015) 'Genome-wide identification of CCA1 targets uncovers an expanded clock network in *Arabidopsis*', *Proceedings of the National Academy of Sciences of the United States of America*. doi: 10.1073/pnas.1513609112.

Nakagami, H., Kawamura, K., Sugisaka, K., Sekine, M. and Shinmyo, A. (2002) 'Phosphorylation of retinoblastoma-related protein by the cyclin D/cyclin-dependent kinase complex is activated at the G1/S-phase transition in tobacco', *Plant Cell*. American Society of Plant Biologists, 14(8), pp. 1847–1857. doi: 10.1105/tpc.002550.

Nakai, T., Kato, K., Shinmyo, A. and Sekine, M. (2006) 'Arabidopsis KRPs have distinct inhibitory activity toward cyclin D2-associated kinases, including plant-specific B-type cyclin-dependent kinase', *FEBS Letters*. doi: 10.1016/j.febslet.2005.12.018.

Nicolai, M., Roncato, M. A., Canoy, A. S., Rouquié, D., Sarda, X., Freyssinet, G. and Robaglia, C. (2006) 'Large-scale analysis of mRNA translation states during sucrose starvation in *Arabidopsis* cells identifies cell proliferation and chromatin structure as targets of translational control', *Plant Physiology*. doi: 10.1104/pp.106.079418.

- Nieuwland, J., Maughan, S., Dewitte, W., Scofield, S., Sanz, L. and Murray, J. A. H. (2009) 'The D-type cyclin CYCD4;1 modulates lateral root density in Arabidopsis by affecting the basal meristem region', *Proceedings of the National Academy of Sciences of the United States of America*. doi: 10.1073/pnas.0906354106.
- Norbury, C. and Nurse, P. (1992) 'Animal Cell Cycles and Their Control', *Annual Review of Biochemistry*. doi: 10.1146/annurev.bi.61.070192.002301.
- Nowack, M. K., Harashima, H., Dissmeyer, N., Zhao, X., Bouyer, D., Weimer, A. K., De Winter, F., Yang, F. and Schnittger, A. (2012) 'Genetic Framework of Cyclin-Dependent Kinase Function in Arabidopsis', *Developmental Cell*. doi: 10.1016/j.devcel.2012.02.015.
- Nurse, P. (1990) 'Universal control mechanism regulating onset of M-phase', *Nature*. doi: 10.1038/344503a0.
- O'Leary, B. M., Khim Oh, G. G., Lee, C. P. and Harvey Millar, A. (2020) 'Metabolite regulatory interactions control plant respiratory metabolism via target of rapamycin (TOR) kinase activation[open]', *Plant Cell*. doi: 10.1105/tpc.19.00157.
- Oszi, E., Papdi, C., Mohammed, B., Petkó-Szandtner, A., Leviczky, T., Molnár, E., Galvan-Ampudia, C., Khan, S., Juez, E. L., Horváth, B., Bögre, L. and Magyar, Z. (2020) 'E2FB interacts with RETINOBLASTOMA RELATED and regulates cell proliferation during leaf development', *Plant Physiology*. doi: 10.1104/pp.19.00212.
- Otero, S., Desvoves, B., Peiró, R. and Gutierrez, C. (2016) 'Histone H3 dynamics reveal domains with distinct proliferation potential in the arabidopsis root', *Plant Cell*. doi: 10.1105/tpc.15.01003.
- Pavelescu, I., Vilarrasa-Blasi, J., Planas-Riverola, A., González-García, M., Caño-Delgado, A. I. and Ibañez, M. (2018) 'A Sizer model for cell differentiation in Arabidopsis thaliana root growth', *Molecular Systems Biology*. doi: 10.15252/msb.20177687.
- Peng, L., Skylar, A., Chang, P. L., Bisova, K. and Wu, X. (2014) 'CYCP2;1 integrates genetic and nutritional information to promote meristem cell division in Arabidopsis', *Developmental Biology*. Academic Press, 393(1), pp. 160–170. doi: 10.1016/J.YDBIO.2014.06.008.
- Peng, Y., Chen, L., Lu, Y., Wu, Y., Dumenil, J., Zhu, Z., Bevan, M. W. and Lia, Y.

- (2015) 'The Ubiquitin receptors DA1, DAR1, and DAR2 redundantly regulate endoreduplication by modulating the stability of TCP14/15 in arabidopsis', *Plant Cell*. doi: 10.1105/tpc.114.132274.
- Perrot-Rechenmann, C. (2010) 'Cellular responses to auxin: division versus expansion.', *Cold Spring Harbor perspectives in biology*. doi: 10.1101/cshperspect.a001446.
- Petersen, J. and Nurse, P. (2007) 'TOR signalling regulates mitotic commitment through the stress MAP kinase pathway and the Polo and Cdc2 kinases', *Nature Cell Biology*. doi: 10.1038/ncb1646.
- Poorter, H., Niinemets, Ü., Ntagkas, N., Siebenkäs, A., Mäenpää, M., Matsubara, S. and Pons, T. L. (2019) 'A meta-analysis of plant responses to light intensity for 70 traits ranging from molecules to whole plant performance', *New Phytologist*. doi: 10.1111/nph.15754.
- Popescu, S. C., Popescu, G. V., Bachan, S., Zhang, Z., Gerstein, M., Snyder, M. and Dinesh-Kumar, S. P. (2009) 'MAPK target networks in Arabidopsis thaliana revealed using functional protein microarrays', *Genes and Development*. doi: 10.1101/gad.1740009.
- Del Pozo, J. C., Boniotti, M. B. and Gutierrez, C. (2002) 'Arabidopsis E2Fc functions in cell division and is degraded by the ubiquitin-SCFAtSKP2 pathway in response to light', *Plant Cell*. doi: 10.1105/tpc.006791.
- Del Pozo, J. C., Diaz-Trivino, S., Cisneros, N. and Gutierrez, C. (2006) 'The balance between cell division and endoreplication depends on E2FC-DPB, transcription factors regulated by the ubiquitin-SCFAtSKP2A pathway in Arabidopsis', *Plant Cell*. doi: 10.1105/tpc.105.039651.
- Ren, H., Santner, A., Pozo, J. C. Del, Murray, J. A. H. and Estelle, M. (2008) 'Degradation of the cyclin-dependent kinase inhibitor KRP1 is regulated by two different ubiquitin E3 ligases', *Plant Journal*. doi: 10.1111/j.1365-313X.2007.03370.x.
- Riou-Khamlichi, C., Huntley, R., Jacquard, A. and Murray, J. A. H. (1999) 'Cytokinin activation of Arabidopsis cell division through a D-type cyclin', *Science*. doi: 10.1126/science.283.5407.1541.

- Riou-Khamlichi, C., Menges, M., Healy, J. M. S. and Murray, J. A. H. (2000) 'Sugar Control of the Plant Cell Cycle: Differential Regulation of Arabidopsis D-Type Cyclin Gene Expression', *Molecular and Cellular Biology*. doi: 10.1128/mcb.20.13.4513-4521.2000.
- Rivero, L., Scholl, R., Holomuzki, N., Crist, D., Grotewold, E. and Brkljacic, J. (2014) 'Handling arabidopsis plants: Growth, preservation of seeds, transformation, and genetic crosses', *Methods in Molecular Biology*. doi: 10.1007/978-1-62703-580-4_1.
- Rossignol, P., Stevens, R., Perennes, C., Jasinski, S., Cella, R., Tremousaygue, D. and Bergounioux, C. (2002) 'AtE2F-a and AtDP-a, members of the E2F family of transcription factors, induce Arabidopsis leaf cells to re-enter S phase', *Molecular Genetics and Genomics*. doi: 10.1007/s00438-001-0624-7.
- Roukos, V., Pegoraro, G., Voss, T. C. and Misteli, T. (2015) 'Cell cycle staging of individual cells by fluorescence microscopy', *Nature Protocols*. doi: 10.1038/nprot.2015.016.
- Sadasivam, S. and DeCaprio, J. A. (2013) 'The DREAM complex: master coordinator of cell cycle-dependent gene expression.', *Nature reviews. Cancer*. NIH Public Access, 13(8), pp. 585–595. doi: 10.1038/nrc3556.
- Salvi, E., Di Mambro, R. and Sabatini, S. (2020) 'Dissecting mechanisms in root growth from the transition zone perspective', *Journal of Experimental Botany*. doi: 10.1093/jxb/eraa079.
- Sanz, L., Dewitte, W., Forzani, C., Patell, F., Nieuwland, J., Wen, B., Quelhas, P., de Jager, S., Titmus, C., Campilho, A., Ren, H., Estelle, M., Wang, H. and Murray, J. A. H. (2011) 'The Arabidopsis D-Type Cyclin CYCD2;1 and the Inhibitor ICK2/KRP2 Modulate Auxin-Induced Lateral Root Formation', *Plant Cell*. doi: 10.1105/tpc.110.080002.
- Sasabe, M., Boudolf, V., De Veylder, L., Inzé, D., Genschik, P. and Machida, Y. (2011) 'Phosphorylation of a mitotic kinesin-like protein and a MAPKKK by cyclin-dependent kinases (CDKs) is involved in the transition to cytokinesis in plants', *Proceedings of the National Academy of Sciences of the United States of America*. doi: 10.1073/pnas.1110174108.
- Schepetilnikov, M., Dimitrova, M., Mancera-Martínez, E., Geldreich, A., Keller, M. and Ryabova, L. A. (2013) 'TOR and S6K1 promote translation reinitiation of uORF-

- containing mRNAs via phosphorylation of eIF3h.', *The EMBO journal*. European Molecular Biology Organization, 32(8), pp. 1087–1102. doi: 10.1038/emboj.2013.61.
- Schmoller, K. M. (2017) 'The phenomenology of cell size control', *Current Opinion in Cell Biology*. doi: 10.1016/j.ceb.2017.11.011.
- Schmoller, K. M., Turner, J. J., Kõivomägi, M. and Skotheim, J. M. (2015) 'Dilution of the cell cycle inhibitor Whi5 controls budding-yeast cell size', *Nature*. doi: 10.1038/nature14908.
- Schommer, C., Debernardi, J. M., Bresso, E. G., Rodriguez, R. E. and Palatnik, J. F. (2014) 'Repression of cell proliferation by miR319-regulated TCP4', *Molecular Plant*. doi: 10.1093/mp/ssu084.
- Schumann, T., Paul, S., Melzer, M., Dörmann, P. and Jahns, P. (2017) 'Plant growth under natural light conditions provides highly flexible short-term acclimation properties toward high light stress', *Frontiers in Plant Science*. doi: 10.3389/fpls.2017.00681.
- Shen, L., Zhuang, B., Wu, Q., Zhang, H., Nie, J., Jing, W., Yang, L. and Zhang, W. (2019) 'Phosphatidic acid promotes the activation and plasma membrane localization of MKK7 and MKK9 in response to salt stress', *Plant Science*. doi: 10.1016/j.plantsci.2019.110190.
- Shimotohno, A., Heidstra, R., Blilou, I. and Scheres, B. (2018) 'Root stem cell niche organizer specification by molecular convergence of PLETHORA and SCARECROW transcription factor modules', *Genes and Development*. doi: 10.1101/gad.314096.118.
- Shulze, C. N., Cole, B. J., Ciobanu, D., Lin, J., Yoshinaga, Y., Gouran, M., Turco, G. M., Zhu, Y., O'Malley, R. C., Brady, S. M. and Dickel, D. E. (2019) 'High-Throughput Single-Cell Transcriptome Profiling of Plant Cell Types', *Cell Reports*. doi: 10.1016/j.celrep.2019.04.054.
- Shultz, R. W., Tatineni, V. M., Hanley-Bowdoin, L. and Thompson, W. F. (2007) 'Genome-wide analysis of the core DNA replication machinery in the higher plants *Arabidopsis* and rice1[W][OA]', *Plant Physiology*. doi: 10.1104/pp.107.101105.
- Sizani, B. L., Kalve, S., Markakis, M. N., Domagalska, M. A., Stelmaszewska, J., Abdelgawad, H., Zhao, X., De Veylder, L., De Vos, D., Broeckhove, J., Schnittger, A. and Beemster, G. T. S. (2019) 'Multiple mechanisms explain how reduced KRP

expression increases leaf size of *Arabidopsis thaliana*’, *New Phytologist*. doi: 10.1111/nph.15458.

Skylar, A., Sung, F., Hong, F., Chory, J. and Wu, X. (2011) ‘Metabolic sugar signal promotes *Arabidopsis* meristematic proliferation via G2.’, *Developmental biology*. NIH Public Access, 351(1), pp. 82–89. doi: 10.1016/j.ydbio.2010.12.019.

Slovak, R., Setzer, C., Roiuk, M., Bertels, J., Göschl, C., Jandrasits, K., Beemster, G. T. S. and Busch, W. (2020) ‘Ribosome assembly factor Adenylate Kinase 6 maintains cell proliferation and cell size homeostasis during root growth’, *New Phytologist*. doi: 10.1111/nph.16291.

Smékalová, V., Luptovčíak, I., Komis, G., Šamajová, O., Ovečka, M., Doskočilová, A., Takáč, T., Vadovič, P., Novák, O., Pechan, T., Ziemann, A., Košútová, P. and Šamaj, J. (2014) ‘Involvement of YODA and mitogen activated protein kinase 6 in *Arabidopsis* post-embryogenic root development through auxin up-regulation and cell division plane orientation’, *New Phytologist*. doi: 10.1111/nph.12880.

Smith, A. M. and Stitt, M. (2007) ‘Coordination of carbon supply and plant growth’, *Plant, Cell and Environment*. doi: 10.1111/j.1365-3040.2007.01708.x.

Soni, R., Carmichael, J. P., Shah, Z. H. and Murray, J. A. (1995) ‘A family of cyclin D homologs from plants differentially controlled by growth regulators and containing the conserved retinoblastoma protein interaction motif’, *Plant Cell*. doi: 10.1105/tpc.7.1.85.

Soppa, U. and Becker, W. (2015) ‘DYRK protein kinases’, *Current Biology*. doi: 10.1016/j.cub.2015.02.067.

Sormani, R., Lei, Y., Menand, B., Ennar, N., Lecampion, C., Meyer, C. and Robaglia, C. (2007) ‘*Saccharomyces cerevisiae* FKBP12 binds *Arabidopsis thaliana* TOR and its expression in plants leads to rapamycin susceptibility’, *BMC Plant Biology*. doi: 10.1186/1471-2229-7-26.

Sozzani, R., Maggio, C., Varotto, S., Canova, S., Bergounioux, C., Albani, D. and Cella, R. (2006) ‘Interplay between *Arabidopsis* activating factors E2Fb and E2Fa in cell cycle progression and development’, *Plant Physiology*. American Society of Plant Biologists, 140(4), pp. 1355–1366. doi: 10.1104/pp.106.077990.

Stegmann, M. (2018) ‘EBP1: A crucial growth regulator downstream of receptor

- kinases across kingdoms’, *PLoS Biology*. doi: 10.1371/journal.pbio.3000056.
- Street, I. H., Aman, S., Zubo, Y., Ramzan, A., Wang, X., Shakeel, S. N., Kieber, J. J. and Eric Schaller, G. (2015) ‘Ethylene inhibits cell proliferation of the arabidopsis root meristem’, *Plant Physiology*. doi: 10.1104/pp.15.00415.
- Stumpf, C. R., Moreno, M. V., Olshen, A. B., Taylor, B. S. and Ruggero, D. (2013) ‘The translational landscape of the mammalian cell cycle’, *Molecular Cell*. doi: 10.1016/j.molcel.2013.09.018.
- Takatsuka, H. and Umeda, M. (2014) ‘Hormonal control of cell division and elongation along differentiation trajectories in roots’, *Journal of Experimental Botany*. doi: 10.1093/jxb/ert485.
- Tamura, K. and Hara-Nishimura, I. (2011) ‘Involvement of the nuclear pore complex in morphology of the plant nucleus’, *Nucleus*. doi: 10.4161/nucl.2.3.16175.
- Tatematsu, K., Nakabayashi, K., Kamiya, Y. and Nambara, E. (2008) ‘Transcription factor AtTCP14 regulates embryonic growth potential during seed germination in *Arabidopsis thaliana*’, *Plant Journal*. doi: 10.1111/j.1365-313X.2007.03308.x.
- Trolet, A., Baldrich, P., Criqui, M. C., Dubois, M., Clavel, M., Meyers, B. C. and Genschik, P. (2019) ‘Cell cycle–dependent regulation and function of ARGONAUTE1 in plants’, *Plant Cell*. doi: 10.1105/tpc.19.00069.
- Uhrig, R. G., Schläpfer, P., Roschitzki, B., Hirsch-Hoffmann, M. and Gruissem, W. (2019) ‘Diurnal changes in concerted plant protein phosphorylation and acetylation in *Arabidopsis* organs and seedlings’, *Plant Journal*. doi: 10.1111/tpj.14315.
- Umbrasaite, J., Schweighofer, A., Kazanaviciute, V., Magyar, Z., Ayatollahi, Z., Unterwurzacher, V., Choopayak, C., Boniecka, J., Murray, J. A. H., Bogre, L. and Meskiene, I. (2010) ‘MAPK phosphatase AP2C3 induces ectopic proliferation of epidermal cells leading to stomata development in *Arabidopsis*’, *PLoS ONE*. doi: 10.1371/journal.pone.0015357.
- Umen, J. G. and Goodenough, U. W. (2001) ‘Control of cell division by a retinoblastoma protein homolog in *Chlamydomonas*’, *Genes and Development*. doi: 10.1101/gad.892101.
- Usadel, B., Bläsing, O. E., Gibon, Y., Retzlaff, K., Höhne, M., Günther, M. and Stitt, M. (2008) ‘Global transcript levels respond to small changes of the carbon status

- during progressive exhaustion of carbohydrates in arabidopsis rosettes', *Plant Physiology*. doi: 10.1104/pp.107.115592.
- Vandepoele, K., Raes, J., De Veylder, L., Rouzé, P., Rombauts, S. and Inzé, D. (2002) 'Genome-wide analysis of core cell cycle genes in Arabidopsis', *Plant Cell*. doi: 10.1105/tpc.010445.
- Vandepoele, K., Vlieghe, K., Florquin, K., Hennig, L., Beemster, G. T. S., Gruissem, W., Van De Peer, Y., Inzé, D. and De Veylder, L. (2005) 'Genome-wide identification of potential plant E2F target genes', *Plant Physiology*. doi: 10.1104/pp.105.066290.
- Vercruyssen, J., Baekelandt, A., Gonzalez, N. and Inzé, D. (2020) 'Molecular networks regulating cell division during Arabidopsis leaf growth', *Journal of Experimental Botany*. doi: 10.1093/jxb/erz522.
- Verkest, A., Manes, C. L. D. O., Vercruyssen, S., Maes, S., Van Der Schueren, E., Beeckman, T., Genschik, P., Kuiper, M., Inzé, D. and De Veylder, L. (2005) 'The cyclin-dependent kinase inhibitor KRP2 controls the onset of the endoreduplication cycle during Arabidopsis leaf development through inhibition of mitotic CDKA;1 kinase complexes', *Plant Cell*. doi: 10.1105/tpc.105.032383.
- De Veylder, L., Beeckman, T., Beemster, G. T. S., Krols, L., Terras, F., Landrieu, I., Van Der Schueren, E., Maes, S., Naudts, M. and Inzé, D. (2001) 'Functional analysis of cyclin-dependent kinase inhibitors of Arabidopsis', *Plant Cell*. doi: 10.1105/tpc.13.7.1653.
- De Veylder, L., Beeckman, T., Beemster, G. T. S. S., De Almeida Engler, J., Ormenese, S., Maes, S., Naudts, M., Van der Schueren, E., Jacquard, A., Engler, G. and Inzé, D. (2002) 'Control of proliferation, endoreduplication and differentiation by the Arabidopsis E2Fa-DPa transcription factor', *EMBO Journal*. European Molecular Biology Organization, 21(6), pp. 1360–1368. doi: 10.1093/emboj/21.6.1360.
- de Veylder, L., Larkin, J. C. and Schnittger, A. (2011) 'Molecular control and function of endoreplication in development and physiology', *Trends in Plant Science*. doi: 10.1016/j.tplants.2011.07.001.
- Wallden, M., Fange, D., Lundius, E. G., Baltekin, Ö. and Elf, J. (2016) 'The Synchronization of Replication and Division Cycles in Individual E. coli Cells', *Cell*. doi: 10.1016/j.cell.2016.06.052.

Wang, G., Kong, H., Sun, Y., Zhang, X., Zhang, W., Altman, N., DePamphilis, C. W. and Ma, H. (2004) 'Genome-wide analysis of the cyclin family in arabidopsis and comparative phylogenetic analysis of plant cyclin-like proteins', *Plant Physiology*. doi: 10.1104/pp.104.040436.

Wang, L. and Ruan, Y. L. (2013) 'Regulation of cell division and expansion by sugar and auxin signaling', *Frontiers in Plant Science*. doi: 10.3389/fpls.2013.00163.

Wang, M. Y., Zhao, P. M., Cheng, H. Q., Han, L. B., Wu, X. M., Gao, P., Wang, H. Y., Yang, C. L., Zhong, N. Q., Zuo, J. R. and Xia, G. X. (2013) 'The cotton transcription factor TCP14 functions in auxin-mediated epidermal cell differentiation and elongation1', *Plant Physiology*. doi: 10.1104/pp.113.215673.

Wang, S., Gu, Y., Zebell, S. G., Anderson, L. K., Wang, W., Mohan, R. and Dong, X. (2014) 'A noncanonical role for the CKI-RB-E2F cell-cycle signaling pathway in plant effector-triggered immunity', *Cell Host and Microbe*. doi: 10.1016/j.chom.2014.10.005.

Weimer, A. K., Biedermann, S., Harashima, H., Roodbarkelari, F., Takahashi, N., Foreman, J., Guan, Y., Pochon, G., Heese, M., Van Damme, D., Sugimoto, K., Koncz, C., Doerner, P., Umeda, M. and Schnittger, A. (2016) 'The plant-specific CDKB 1-CYCB 1 complex mediates homologous recombination repair in Arabidopsis', *The EMBO Journal*. doi: 10.15252/embj.201593083.

Wen, B., Nieuwland, J. and Murray, J. A. H. (2013) 'The Arabidopsis CDK inhibitor ICK3/KRP5 is rate limiting for primary root growth and promotes growth through cell elongation and endoreduplication', *Journal of Experimental Botany*. doi: 10.1093/jxb/ert009.

West, G., Inzé, D. and Beemster, G. T. S. (2004) 'Cell cycle modulation in the response of the primary root of Arabidopsis to salt stress', *Plant Physiology*. doi: 10.1104/pp.104.040022.

Wingler, A. (2017) 'Transitioning to the next phase: the role of sugar signaling throughout the plant life cycle', *Plant Physiology*. doi: 10.1104/pp.17.01229.

Wood, E. and Nurse, P. (2013) 'Pom1 and cell size homeostasis in fission yeast', *Cell Cycle*. doi: 10.4161/cc.26462.

Wu, J. F., Tsai, H. L., Joanito, I., Wu, Y. C., Chang, C. W., Li, Y. H., Wang, Y., Hong,

- J. C., Chu, J. W., Hsu, C. P. and Wu, S. H. (2016) 'LWD-TCP complex activates the morning gene CCA1 in Arabidopsis', *Nature Communications*. doi: 10.1038/ncomms13181.
- Wu, Y., Shi, L., Li, L., Fu, L., Liu, Y., Xiong, Y. and Sheen, J. (2019) 'Integration of nutrient, energy, light, and hormone signalling via TOR in plants', *Journal of Experimental Botany*. doi: 10.1093/jxb/erz028.
- Wullschleger, S., Loewith, R. and Hall, M. N. (2006) 'TOR signaling in growth and metabolism', *Cell*. doi: 10.1016/j.cell.2006.01.016.
- Xiong, Y., McCormack, M., Li, L., Hall, Q., Xiang, C. and Sheen, J. (2013) 'Glucose-TOR signalling reprograms the transcriptome and activates meristems', *Nature*. NIH Public Access, 496(7444), pp. 181–186. doi: 10.1038/nature12030.
- Xiong, Y. and Sheen, J. (2012) 'Rapamycin and glucose-target of rapamycin (TOR) protein signaling in plants', *Journal of Biological Chemistry*. doi: 10.1074/jbc.M111.300749.
- Xiong, Y. and Sheen, J. (2014) 'The role of target of rapamycin signaling networks in plant growth and metabolism', *Plant Physiology*. doi: 10.1104/pp.113.229948.
- Yi, D., Kamei, C. L. A., Cools, T., Vanderauwera, S., Takahashi, N., Okushima, Y., Eekhout, T., Yoshiyama, K. O., Larkin, J., Van den Daele, H., Conklin, P., Britt, A., Umeda, M. and De Veylder, L. (2014) 'The Arabidopsis SIAMESE-RELATED cyclin-dependent Kinase Inhibitors SMR5 and SMR7 Regulate the DNA damage checkpoint in response to reactive oxygen species', *Plant Cell*. doi: 10.1105/tpc.113.118943.
- Yin, K., Ueda, M., Takagi, H., Kajihara, T., Aki, S. S., Nobusawa, T., Umeda-Hara, C. and Umeda, M. (2014) 'A dual-color marker system for in vivo Visualization of cell cycle progression in Arabidopsis', *Plant Journal*. doi: 10.1111/tpj.12652.
- Zatulovskiy, E., Berenson, D. F., Topacio, B. R. and Skotheim, J. M. (2018) 'Cell growth dilutes the cell cycle inhibitor Rb to trigger cell division', *bioRxiv*. doi: 10.1101/470013.
- Zhang, N., Meng, Y., Li, X., Zhou, Y., Ma, L., Fu, L., Schwarzländer, M., Liu, H. and Xiong, Y. (2019) 'Metabolite-mediated TOR signaling regulates the circadian clock in Arabidopsis', *Proceedings of the National Academy of Sciences of the United*

States of America. doi: 10.1073/pnas.1913095116.

Zhang, T. Q., Xu, Z. G., Shang, G. D. and Wang, J. W. (2019) 'A Single-Cell RNA Sequencing Profiles the Developmental Landscape of Arabidopsis Root', *Molecular Plant*. doi: 10.1016/j.molp.2019.04.004.

Zhang, T., Qu, Y., Wang, H., Wang, J., Song, A., Hu, Y., Chen, S., Jiang, J. and Chen, F. (2017) 'The heterologous expression of a chrysanthemum TCP-P transcription factor CmTCP14 suppresses organ size and delays senescence in Arabidopsis thaliana', *Plant Physiology and Biochemistry*. doi: 10.1016/j.plaphy.2017.03.026.

Zhang, W., Cochet, F., Ponnaiah, M., Lebreton, S., Matheron, L., Pionneau, C., Boudsocq, M., Resentini, F., Huguet, S., Blázquez, M., Bailly, C., Puyaubert, J. and Baudouin, E. (2019) 'The MPK8-TCP14 pathway promotes seed germination in Arabidopsis', *Plant Journal*. doi: 10.1111/tpj.14461.

Zhang, X., Dai, Y., Xiong, Y., DeFraia, C., Li, J., Dong, X. and Mou, Z. (2007) 'Overexpression of Arabidopsis MAP kinase kinase 7 leads to activation of plant basal and systemic acquired resistance', *Plant Journal*. doi: 10.1111/j.1365-313X.2007.03294.x.

Zhou, F., Roy, B., Dunlap, J. R., Enganti, R. and von Arnim, A. G. (2014) 'Translational Control of Arabidopsis Meristem Stability and Organogenesis by the Eukaryotic Translation Factor eIF3h', *PLoS ONE*. doi: 10.1371/journal.pone.0095396.

Zuo, J., Niu, Q. W. and Chua, N. H. (2000) 'An estrogen receptor-based transactivator XVE mediates highly inducible gene expression in transgenic plants', *Plant Journal*. doi: 10.1046/j.1365-313X.2000.00868.x.